Carl Howell, 731

FINAL REPORT
FOR THE
NIMBUS-D HIGH DATA RATE STORAGE SYSTEM

Contract No. NAS5-10396

Prepared by

RCA | Defense Electronic Products
Astro-Electronics Division | Princeton, New Jersey

for

Goddard Space Flight Center
National Aeronautics and Space Administration
Greenbelt, Maryland

FINAL REPORT
FOR THE
NIMBUS-D HIGH DATA RATE STORAGE SYSTEM

Contract No. NAS5-10396

Prepared by

RCA | Defense Electronic Products
Astro-Electronics Division | Princeton, New Jersey

AED R-3548-F

Issued: April 17, 1970

INTENTIONALLY

LEFT

BLANK

PREFACE

This report summarizes the work performed by the Astro-Electronics Division of the RCA Corporation for the Goddard Space Flight Center of the National Aeronautics and Space Administration under Contract NAS5-10396. The work was performed during the period starting April 28, 1967 and ending February 6, 1970.

SUMMARY AND CONCLUSIONS

The HDRSS-D program required the development of a new two-frame center connected multiplexer, a slightly modified electronics module, and a modified tape transport. The last two items are basically the same as those used on the HDRSS-B program. The multiplexer, qualified at prototype levels, contains improved crystal mounts, new adder and telemetry circuits, a modified IRIS channel, and a new VIP channel similar to the IRIS channel. The electronics module was modified to include a new VIP channel and a widened IRIS channel. The tape transport, operational during launch, contains a new brake mechanism, an optical end-of-tape sensor, and a method for cleaning the magnetic heads (Serial No. 08 only).

Analysis of the test data from the prototype multiplexer and the flight model systems show conformance with the performance specifications contained in Section 2. The use of the widened IRIS channel did not have pronounced effects on the test results; however, analytical and empirical measurements on inter-symbol interference shows that detection of data transmitted from the satellite and via the long lines will be improved. Bit Error rate tests of the VIP and IRIS channels using the worst-case word pattern produced test results well below specifications. Linearity, signal-to-noise and amplitude response of the THIR and ID channels were far better than the specified levels. The time code channel valley-to-peak ratio was more stringently controlled than specified by tailoring the adjustment to a specific multiplexer prior to system tests. A complete data summary is contained in Section 8.

A number of improvements applicable to the basic tape transport are recommended for future programs; specifically, high inertia idlers, abrasive head cleaner, a two-speed bi-directional motor, and development of a new method to anchor the tape to the reels.

During the Nimbus-III mission a significant 3400 Hz flutter component appeared on the VIP channel data. Tests conducted at RCA have shown that high inertia idlers will reduce the 3400 Hz flutter component below the inherent noise level of the tape transport.

An abrasive oxide, formulated during prototype life tests, was added to a section of the magnetic tape between the optical end-of-tape and the mechanical end-of-tape switches. With a special command sequence, the abrasive can be commanded over the heads at controlled intervals. Tests conducted on a tape-life test setup at RCA have increased the usefulness of the tape recorder by 30 percent. The time interval between cleanings was 30 days.

A two-speed bi-directional motor is presently under development at RCA. The use of this motor would eliminate the entire planetary assembly. This will increase reliability as ten bearings and four mylar drivebelts would be eliminated. This change will not affect the physical size of the tape transport.

Development of a new method to anchor the magnetic tape is recommended to eliminate tape splice imprinting. Tape splice imprinting was detected by the Illinois Institute of Technology and Research Institute (IITRI) under an independent study contract issued by NASA.

TABLE OF CONTENTS

TABLE OF CONTENTS (Cont'd)

TABLE OF CONTENTS (Cont'd)

TABLE OF CONTENTS (Cont'd)

LIST OF ILLUSTRATIONS

LIST OF ILLUSTRATIONS (Continued)

LIST OF TABLES

SECTION 1

INTRODUCTION

A. PURPOSE OF REPORT

This report presents technical discussions on the fabrication and flight qualification of the spacecraft subsystem of the High Data Rate Storage System (HDRSS) for use on the Nimbus-D Meteorological Satellite.

B. CONTRACT OBJECTIVES

The primary contract objectives were to provide the following services:

- Modify and test three engineering model tape recorder systems. Two systems were supplied as GFE from previous contracts, one consisted of piece parts supplied as GFE from a previous contract.
- Design and fabricate a new multiplexer and qualify at prototype test levels.
- Fabricate and acceptance test two flight model tape recorder systems and to modify and acceptance test one flight model tape recorder system supplied GFE from the previous program.
- Design, fabricate, and acceptance test modification kits for three Bench Check Units (BCU); two at the RCA Corporation, one at the General Electric Co.
- Design, fabricate, and acceptance test modification kits for four ground stations; one at the Goddard Space Flight Center (GSFC), one at the General Electric Co., one at the Western Test Range, and one at the receiving station in Alaska.

C. HDRSS HISTORICAL DATA

A complete description of the tape recorder system design and development is contained in the final reports for contracts NAS5-3772* and NAS5-10205**. Contract NAS5-10396, awarded April 28, 1968 is described by GSFC specification S-731-P-40 and addendum dated July 13, 1966, an errata sheet dated April 10, 1967, 28 contract modifications, and 38 technical directives.

---

*RCA Astro-Electronics Division, Final Report for the High Data Rate Storage System (Engineering Models EM-1 and EM-2), Contract NAS5-3772, Princeton, New Jersey, May 3, 1968.

**RCA, Astro-Electronics Division, Final Report for the Nimbus-D High Data Rate Storage System (Prototype and Flight Models F-1 through F-3), Contract NAS5-10205, Princeton, New Jersey, June 27, 1968.

1. Contract Modifications

Contract modifications define equipment modifications, schedule changes, and additional funding of the program. Equipment changes authorized by Contract modifications are itemized in chronological order; the remaining modifications describe financial adjustments that occurred as a result of the equipment modifications.

a. Modification 2

Modification 2 (issued Sept. 6, 1967) addended the "Quality and Reliability Provisions for Nimbus-D Procurements," GSFC Specification S-450-P-1A.

b. Modification 3

Modification 3 (issued Aug. 23, 1967) changed the GSFC environmental specification from S-320-N1-2 to S-320-N1-3.

c. Modification 4

Modification 4 (issued Nov. 7, 1967) re-identified the High Resolution Radiometer (HRR) signal as the 11-micron Thermal Humidity Infra-red Radiometer (THIR-11) signal and changed the bandwidth from 3 dB at 630 Hz to 3 dB at 360 Hz.

This modification also described the 6-micron Thermal Humidity Infra-red Radiometer (THIR-6) signal that could be recorded on the Image Dissector (ID) channel when commanded on. The design of the tape recorder system was not affected by the addition of the THIR-6 signal; the description was required to determine system test and data processing considerations.

d. Modification 7

Modification 7 (issued April 15, 1968) provided for the addition of optical end-of-tape sensors redundant to the mechanical end-of-tape switches, and the addition of disk brakes to replace the drum and shoe brakes.

e. Modification 8

Modification 8 (issued May 2, 1968) provided for the design and fabrication of a breadboard model of a HDRSS real-time multiplexer and conduct feasibility tests. The modification also directed that the tape transport would be capable of recording data on all channels during launch.

f. Modification 9

Modification 9 (issued June 20, 1968) directed that the prototype tape-transport life test would be continued under the subject contract and all costs accrued to date would be transferred from Contract NAS5-10196 (HDRSS-B Integration Support) to the subject contract. Continuation of the life test was authorized.

g. Modification 12

Modification 12 (issued July 28, 1968) authorized the following tasks:

- Provide a-c erase heads for the engineering model tape transports.
- Widen the Biphase channel bandwidths in the multiplexer and demultiplexer link.
- Conduct an S-band transmitter requirement study.

The modification directed that two engineering model tape transports would be equipped with externally controlled a-c erase heads instead of permanent-magnet, zero-remanant erase heads. In conjunction with the externally controlled erase heads, a test device that provided for tape transfer from reel-to-reel at the play-back speed during the record mode was designed, fabricated, and tested.

The modification also directed that the biphase channels (IRIS and VIP) have bandwidths that would ensure repeatable bit-error-rates (BER) less than 1×10^{-5} and have an upper cutoff in excess of 1.3 X the bit rate. The IRIS channel bandwidth was widened from 120 kHz to 168 kHz as a result of this modification; the VIP channel was satisfactory.

In conjunction with the biphase channels, modifications a study to determine the S-band transmitter requirements with respect to the biphase channels modifications was performed.

h. Modification 18

Modification 18 (issued Feb. 7, 1969) authorized a study to analyze and define an add-on multiplexer providing four coincident signal bands each containing seven 50 kHz signals with a duty cycle of 0.4 to 0.7. The four signal bands are to be multiplexed into a common output for wide-band recording. The results of this study were submitted in a letter report issued under separate cover.

j. Modification 20

Modification 20 (issued March 25, 1969) changed the thermal-vacuum temperature requirements for tape transport flight acceptance tests from 40°C to 35°C.

k. Modification 22

Modification 22 (issued May 27, 1969) directed RCA to deliver the GSFC and Alaska Ground Station modification kits to the General Electric Co. instead of NASA-GSFC.

l. Modification 24

Modification 24 (issued July 30, 1969) modified GSFC specification S-731-P-40 by adding the THIR-6 signal to the ID channel. Refer to Modification 4.

m. Modification 26

Modification 26 (issued September 16, 1969) added the following GFE to the work statement.

- Beckman Frequency Counter
- Tektronics Plug-in Unit
- Phased Computer AD-YU

n. Modification 27

Modification 27 (issued August 25, 1969) changed the contractor's name from the Radio Corporation of America to the RCA Corporation.

2. Technical Directives

Technical directives define tasks deemed necessary to the program by the GSFC contract officer and the RCA Corp. project manager. These tasks, not readily defined at the start of the program, are approved as the need arises. A summary of the technical directives issued as of this report date are contained in Table 1.

TABLE 1. SUMMARY OF TECHNICAL DIRECTIVES

Directive No.	Description
1	Modified the addendum to GSFC specification S-731-P-40, Par. 3.3.1.2 as follows: Operation of the tape recorder during vibration shall be limited to the tape transport.
2	Performance Study of VIP channel data quality using a wide band Ampex Recorder, Model FR-1400. The analysis was completed and the data was supplied to NASA.
3	Transfer one Bit Error Rate Checker to GSFC for three weeks from date of receipt at GSFC.
4 & 5	Review and approve the HDRSS interface agreement with the General Electric Co.
6 & 9	Engineering evaluation, rework, and retest of the F-3B tape transport to correct a 3500 Hz flutter problem. The flutter, traced to the lower bearing on the planetary shaft, the bearing was replaced and the objectionable flutter was eliminated. Unit tests of the tape transport were completed and the system test required prior to vibration of the tape transport is in progress.

TABLE 1. SUMMARY OF TECHNICAL DIRECTIVES (Continued)

Directive No.	Description
7	Investigate the effect of the Mincom tape recorder on the quality of the IRIS channel data and define the required equalization.
8	Rework the slow-time time code demodulator to facilitate monitoring of the time code at the 10 kHz rate at ground station No. 7 (GSFC).
10	Assist the GSFC in the generation of a long-line specification. RCA recommendations for the long-line specification were presented to NASA on June 28, 1968.
11	Prepare a test tape containing Image Disector (ID) and Thermal-Humidity Infrared (THIR) data for ground station check out at the GSFC.
12	Design and fabricate a demultiplexer test set for use on the HDRSS-D program.
13	Design and fabricate a matching line amplifier for use in ground station No. 7.
14	Investigate flutter and wow compensation in the ground station No. 1 kinescope. Assistance provided at GE.
15	Eliminate the drift in the HRIR outputs (2) of the HRIR demodulator drawers received from ground station No. 7 (GSFC).
16	Perform integration tests of the IRIS/HDRSS S-band link using the equalizer at GE.
17	Check the signal-to-noise ratio of the time code channel with and without noise (clock and link) for flight F-3 at GE.
18	Supply parts and instructions to eliminate the drift in the HRIR outputs of the HRIR demodulator drawers located at ground station No. 1 and bench check unit No. 1 at the General Electric Co., ground station No. 2 at the Pacific Missile Range, and the spare unit at ground station No. 7 (GSFC).
19	Perform phase measurements of the IRIS channel of the Bench Check Unit at the General Electric Co.
20	Set up special test equipment at GSFC for HDRSS tape transport tests and provide modifications to measure dropouts at 80 and 60 percent of peak.

TABLE 1. SUMMARY OF TECHNICAL DIRECTIVES (Continued)

Directive No.	Description
21	Perform support tests of the widened IRIS channel for the Multiplexer/Demultiplexer link at the General Electric Company.
22	Revise the HRIR demodulator and output amplifier and add a THIR-6 filter to the gridding equipment in ground station No. 7 at GSFC.
23	Examine engineering model EM-2 tape transport, received from GE, to determine reason for failure of unit to switch from playback to record automatically.
24	Exchange demultiplexer (serial no. 03 located at RCA) with a demultiplexer from ground station no. 7 at GSFC and repair the latter.
25	Perform thermal-vacuum tests of the F1-D tape transport with the chamber pressure at 2×10^{-5} mm Hg (the specified pressure value is 1×10^{-5} mm Hg).
26	Supply two spare transformers (RCA 1840971-501) for the HDRSS motor drive assemblies.
27	Provide a breadboard feasibility model for cross-strapping two HDRSS multiplexers and S-band transmitters.
28	Evaluate a preventive head-cleaning mode for chronic oxide on RCA-MPE 617 magnetic tape on the APT breadboard tape transport in life test.
29	Determine circuit values for a linear demodulation slope between 41 and 50.5 kHz. The THIR demodulator from Ground Station No. 7 was provided for this study.
30	Deliver the following spares to GSFC to support the HDRSS Special Test Equipment: Item — Quantity Transistor 2N2049 — 4 Transistor 2N2907A — 4 Transistor 2N1893 — 8 Transistor 2N1488 — 12

TABLE 1. SUMMARY OF TECHNICAL DIRECTIVES (Continued)

Directive No.	Description
31	Assemble the following circuit boards into a box with input and output connectors and deliver to GSFC: 1769479-501 Time Code Separator 1706472-503 Time Code Mixer 1769483-501 Time Code Translator 1849420-502 IRIS Channel Separator 1977421-501 IRIS Channel Phase Connector 1849438-501 IRIS Channel Output Amplifier
32	Prepare Z-axis correction circuits for IDCS and THIR.
33	Rework the F-1D tape transport to repair the end-of-tape switch telemetry problem, perform a workmanship vibration, and an electrical performance test.
34	Fabricate and supply one record/playback amplifier circuit (RCA 1843758) for the VIP and IDCS circuits. Conformal coating is not required; the use of substitute parts (non-flight quality) is permitted. These circuits are scheduled for electrical tests only.
35	Rework and prepare one HRIR tape recorder for delivery to the Illinois Institute of Technology and Research Institute. The unit will be used for magnetic tape evaluation tests.
36	Repair a connector stud on a HDRSS flight multiplexer at the General Electric Co. VFSTC.
37	Prepare and apply a chromic oxide (green tape) to the magnetic tape on the F-3D tape transport.
38	Expand the bandwidth of the Dynatronics signal conditioner to provide for decoding IRIS and VIP data if the HDRSS tape transport flutter increases to the levels shown by Nimbus III equipment.

3. Equipment Transfers and Delivery Dates

a. General

Failure of the Nimbus-B launch and the subsequent destruction of the Nimbus-B spacecraft in April 1968 delayed the HDRSS-D program as a backup spacecraft was assembled from existing spares and follow-up programs. Consequently, HDRSS-D equipment was transferred to the Nimbus-B2 program and the contract delivery dates were severely impacted.

b. Equipment Transfers

The HDRSS-D contract provided for the fabrication of three engineering models (tape transport, electronics module and multiplexer), three flight models, and a prototype multiplexer. Refer to Table 2 for subsystem designations and serial numbers for each unit.

Three subsystems and some piece parts were designated as GFE to the program for refurbishment and test. When the Nimbus-B spacecraft was lost, three tape transports and two electronics modules were diverted to the HDRSS-B2 program and the HDRSS-D program was delayed until additional parts or GFE were available.

c. Delivery Dates

The contractual delivery dates specified by the contract and the actual delivery dates of the subsystems as affected by the HDRSS-B2 program are listed in Table 3.

D. HDRSS OPERATIONAL DESCRIPTION

The Spacecraft Subsystem of the HDRSS was designed for use on the Nimbus-D Meteorological Satellite, an earth-stabilized spacecraft designed to circle the earth in a 600-nmi, near-polar, sun-synchronous orbit with an orbital period of approximately 107 minutes. The television and infrared sensors provide complete coverage of every point on the earth's surface once in daylight and once in darkness every 24 hours. During each orbital revolution, continuous infrared mappings and 31 single-frame television photographs are made. To provide the capability both for real-time transmission to local stations and complete orbital readout at the CDA station, a tape recorder speed-up concept was adopted. The HDRSS-D Subsystem shown on Figure 1 was specifically designed for use on Nimbus D (Nimbus IV).

Two command and data-acquisition (CDA) stations provide for transmission of data obtained from 93 percent of the Nimbus orbital passes at an altitude of 600 nmi. The Alaska station (GS-3) is located at Gilmore Creek near Fairbanks, Alaska; the other, Rosman, is located at Rosman, North Carolina. The Alaska station acquires the spacecraft output signal on an average of 10 out of 14 orbital passes each day. Two of the passes missed by the Alaska station are acquired by the Rosman station. The remaining passes are stored on the redundant HDRSS subsystem.

S-band data received at the Alaska station is detected, demultiplexed and transmitted as VLF data via long lines to the data processing center at the Goddard Space Flight Center (GS-7) in Greenbelt, Maryland. S-band data received at the Rosman station is transmitted to the data processing center via a wideband microwave link. Additional ground stations are located at the integration contractor's site (GS-1) and the Western Test Range (GS-2). The ground stations were originally designed for the Nimbus I and II programs, modified for HDRSS-B operation on the Nimbus III program (GS-1 and GS-2 on contract NAS5-3772, GS-3 and GS-7 on contract NAS5-10205), and modified for HDRSS-D on the Nimbus-D (Nimbus IV) program.

TABLE 2. HDRSS-D EQUIPMENT DESIGNATIONS AND TRANSFERRED EQUIPMENT

HDRSS-D Contract Definitions			Equipment Transferred to HDRSS-B2	Replacement Name, Serial No., and Source	Final Subsystem Configurations as Delivered
Subsystem Designations	Unit* and Serial No.	Source			
EM-1D	TT-01 EM-01 MUX-01D	EM-1B Subsystem, GFE From Contract NAS5-10205	None	None	TT-02 EM-04 MUX-02D
EM-2D	TT-04 EM-04 MUX-02D	EM-4B Subsystem, GFE From Contract NAS5-10205	TT-04 transferred to Contract 028-G-20373 (GE Co.)	TT replaced with TT-02 from EM-2B subsystem, GFE from Contract NAS5-10205.	TT-01 EM-02 MUX-03D
EM-3D	TT-09 EM-09 MUX-03D	Piece Parts, GFE From Contract NAS5-10205	TT-09 transferred to Contract 028-G-20373 (GE Co.)	TT replaced with TT-03 from EM-3B subsystem, GFE from Contract NAS5-10205.	Never refurbished to HDRSS-D configuration, diverted to tape qualification test.
Prototype Multiplexer	MUX-04D	New Fabrication	None	None	MUX-04D
F-1D	TT-10 EM-10 MUX-05D	New Fabrication	EM-10 transferred to Contract 028-G-20373 (GE Co.)	EM replaced with EM-09 from EM-3D	TT-10 EM-09 MUX-05D
F-2D	TT-11 EM-11 MUX-06D	New Fabrication	None	None	TT-11 EM-11 MUX-06D
F-3D	TT-08 EM-08 MUX-07D	F-3B Subsystem, GFE From Contract NAS5-10205	EM-08 and TT-08 transferred to Contract 028-G-20373 (GE Co.)	EM and TT replaced with EM-08 and TT-08 from F-3B2 subsystem GFE from Contract 028-G-20373.	TT-08 EM-08 MUX-07D

*TT = Tape Transport, EM = Electronics Module, MUX = Multiplexer

TABLE 3. HDRSS-D SUBSYSTEM DELIVERY DATES

Subsystem Designation	Contractual Delivery Date	Actual Delivery Date
EM-1D	February 28, 1968	July 24, 1968
EM-2D	May 1, 1968	February 3, 1969
EM-3D	May 15, 1968	See Note 1
Prototype Multiplexer	July 28, 1968	December 27, 1968
F-1D	August 28, 1968	May 16, 1969
F-2D	October 28, 1968	July 16, 1969
F-3D	December 31, 1968	January 6, 1970
Note: 1. Delivery of tape transport deleted, unit diverted to tape test program.		

1. Spacecraft Equipment

The Spacecraft Equipment contains a 5-channel tape recorder (electronics module and tape transport), and a multiplexer as shown on Figure 1. The tape recorder records and reproduces digital data and analog video signals for transmission as the spacecraft passes over a Nimbus ground station. All the data is played back at 32 times the record rate, frequency multiplexed, and transmitted to earth via an S-band F-M communications link (see Figure 2). During orbital revolution, the signals from the ID and THIR sensors are also transmitted to local weather stations in real time, and are analyzed for local weather conditions.

2. Ground Station Equipment

S-band data received at the GSFC ground station is detected, demultiplexed, and passed to the respective processing circuits for further processing and to a tape recorder for storage (see Figure 2). VHF data received at the GSFC ground station is applied directly to the processing circuits and to the tape recorder.

The ID subcarrier is demodulated and applied to the horizontal sync detector and the kine complex for display. Horizontal sync and vertical sync is detected from the analog video and applied to the deflection generator in conjunction with a flutter and wow signal. Thus, the video signal is displayed on a kinescope and projected onto the 70-mm film in the film processor with unity magnification. The picture size is approximately 2 by 2 inches with a vertical sweep period of 6.5 seconds and a horizontal sweep rate of 128 lines per second, 800 lines per picture. At the end of the picture, a decimal readout from the ID index computer is illuminated and focused onto the film below the video display. At the end of each decimal readout, the film is automatically advanced, developed, fixed, dried in approximately one minute, and displayed on a viewer.

Tape Transport

Electronics Module

TAPE RECORDER

MULTIPLEXER

Figure 1. Nimbus-D High Data Rate Storage Subsystem

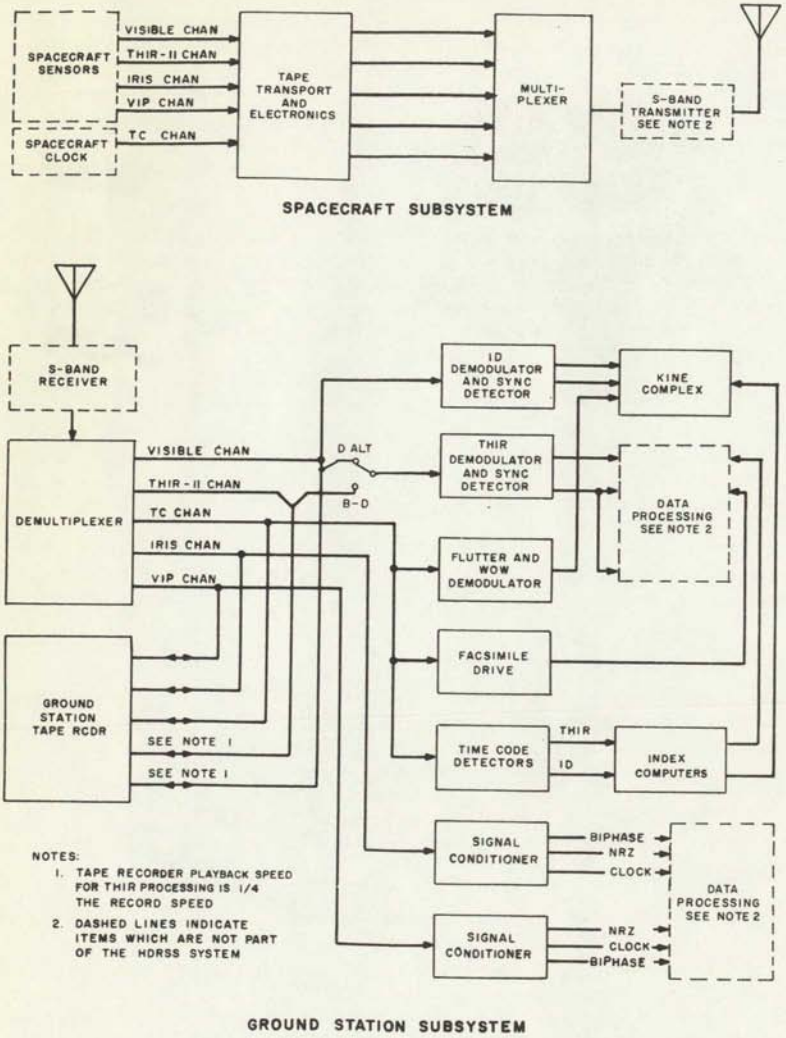

Figure 2. High Data Rate Storage System (HDRSS), Block Diagram

The THIR signals (-6 and -11) received from the demultiplexer cannot be processed until the frequency is reduced by a factor of 4. Therefore, the THIR signals, along with the timing signal, is recorded on a ground station tape recorder. When THIR-6 data, located on the ID channel, is transmitted, an alarm is set off and the operator records the data. Either signal (THIR-11 or THIR-6) is then played back at 1/4 the record speed. The slow-rate THIR is demodulated and then displayed on a Westrex facsimile recorder. The slow-rate THIR timing signal is envelope detected, and used to drive the facsimile recorder motor. At the beginning of each picture, a decimal readout from the THIR index computer is illuminated and focused onto the picture.

The time code signal is applied to envelope detectors that recover the 100-bit per second minitrack time code and supplies a PWM time code to the index computers that drive the decimal displays for the THIR or ID video pictures. The PWM time codes are also applied to gridding computers (not shown in Figure 2) that supply latitude and longitude data for superimposition on the ID and THIR video subcarrier by means of grid mixers. The time code is also supplied to a flutter and wow demodulator to provide a correction signal that modifies the sweep rate to coincide with speed variations introduced by the spacecraft subsystem tape recorder.

The two biphase digital signals (IRIS and VIP) are applied to signal conditioners where they are converted to a non-return-to-zero (NRZ) by a sampling detector. A clock signal, a biphase signal, and the NRZ signal are detected and applied to data processing circuits for analysis and display.

Two additional stations (one at the Western Test Range (WTR), the other at the integration contractor's site) provide for spacecraft subsystem verification.

3. Test Equipment

Spacecraft subsystem performance is verified with a bench check unit at the system level. This unit simulates all spacecraft interfaces, including signal inputs, commands, power, and telemetry, and provides quantitative measurement of all specified parameters. All subsystem interfaces are routed to breakout boxes to facilitate fault isolation to the unit level. The bench check unit includes a link simulator in which shaped noise is added to simulate the noise of the FM communication link. In addition, noise is added to each of the signal inputs and the power supply to verify spacecraft subsystem operation under realistic noise conditions.

Spacecraft subsystem operation is demonstrated by recording simulated analog and digital signals on the tape recorder and processing the signals on equipment similar to that contained in the ground stations. Photographic copies of all signal outputs are made for reference purposes. Quantitative measurements of the ID and THIR signals are made to determine system linearity, drift, frequency response, transient response, and signal-to-noise ratio. The time code is checked for an acceptable bit-error rate and for a flutter correction capability which is observed on the ID pictures. The IRIS and VIP signals are compared with a reference signal to determine the bit-error rate.

SECTION 2

SYSTEM PERFORMANCE OBJECTIVES

Each HDRSS Spacecraft Subsystem consists of a five-track tape recorder and a five-channel, frequency-division multiplexer. Two tape recorder tracks record biphase digital data; two tracks record FM subcarriers containing analog video data, and one track records an amplitude-modulated signal containing a minitrack time code that is also used for flutter correction.

The digital portions of the system are designed for a maximum bit-error-rate (BER) of 1×10^{-5}. The analog and flutter channels of the HDRSS system were designed to duplicate the performance of the Nimbus-I and -II AVCS and HRIR systems.

The AVCS and HRIR channel performance requirements, summarized at the conceptual design review, are as follows:

AVCS

Signal-to-Noise Ratio	30 dB p-p/rms
Frequency Response	-10 dB @ 800 TV lines
Linearity (% Black-to-White)	±2.7% (black), ±5.4% (white)
Drift	±2.7% (black), ±5.4% (white)
Flutter Correction	±1/2 TV element

HRIR

Signal-to-Noise	30 dB (p-p/rms)
Linearity	±2.7% (black), ±5.4% (white)
Drift	±2.7% (black), ±5.4% (white)
Frequency Response	-12 dB @ 360 Hz

In certain cases, actual Nimbus-I and -II designs were used; in addition, certain design constraints changed during the course of the program and these objectives evolved into a firm set of performance specifications. These specifications are tabulated in Paragraphs A, B, C, and D.

For the ID channel the performance is specified exclusive of the Mincom recorders. For the THIR (HRIR on Nimbus-I, -II and III) channel, the Mincom recorder amplitude response and amplitude linearity are included in the overall system specification.

The performance of the biphase data channels is specified in terms of a bit error rate and a bit rate stability observed at the output of the ground station bit synchronizer.

A. ID CHANNEL

The performance on the ID channel, measured between the tape recorder input and the ID demodulator output is:

Amplitude Response:	Within -12 dB at 1600 Hz (relative to the low frequency response).
Signal-to-Noise:	30 dB B-W/rms (including 18.1 dB link CNR and 34.0 dB B-W/rms sensor SNR).
Linearity:	(deviation from best straight line) At Black, ±2.6% of B-W range At White, ±5.2% of B-W range
Drift:	At Black, ±5.0% of B-W range At White, ±6.6% of B-W range
Flutter Correction:	Displacement of two vertically aligned elements on adjacent horizontal lines shall be less than ±1/2 TV element.

B. THIR CHANNEL

The performance of the THIR channel, measured from the HDRSS recorder input to the THIR demodulator output is given below:

Amplitude Response:	Within -8 dB at 360 Hz (relative to the low frequency response).
Signal-to-Noise Ratio:	30 dB B-W/rms (including 18.1 dB link CNR and 35 dB B-W/rms sensor SNR).
Linearity:	At Black, ±3.1% of B-W range At White, ±5.1% of B-W range
Drift:	At Black, ±6% of B-W range At White, ±7.9% of B-W range
Sync Jitter:	±0.8 millisecond

C. TIME CODE CHANNEL

The signal to noise ratio at the output of the wow and flutter demodulator will be 20 dB rms/rms minimum, including simulated link noise.

D. BIPHASE CHANNELS

The performance on the biphase digital channels measured between the tape recorder input and the bit synchronizer (decoder) output will be:

(1) Data Bit Error Rate: 10^{-5} maximum, excluding bits lost during acquisition

(2) Data Bit Stability: within ±0.6 percent of nominal bit rate

(3) The output clock waveform delay variation relative to the data output will be within ±25 percent of the bit period.

The output data format is NRZ level and the clock waveform is a squarewave at the instantaneous bit rate of the NRZ output.

SECTION 3
SPACECRAFT EQUIPMENT

A. GENERAL

The Spacecraft Subsystem of the HDRSS consists of a tape recorder and a multiplexer (see Figure 1). As shown, the Spacecraft Subsystem weighs 30 lb. and requires 10 watts (max) record power and 16 watts (max) playback power. Detailed descriptions are contained in the spacecraft instruction manual.*

B. TAPE RECORDER ASSEMBLY

The tape recorder (see Figure 3) consists of an electronics module and a tape transport assembly. The tape recorder electronics module contains twelve 5.75 by 4.6-inch circuit-boards which plug into respective receptacles on a harness-board. A thirteenth circuit-board, containing the inverter bridge amplifiers, is rigidly mounted at the end of the assembly and connects electrically to the harness-board, by means of a plug and cable arrangement. The latter circuit-board provides a heat sink for the inverter bridge amplifier transistors and a mounting surface for the thermal transducer of the assembly. A harness board provides a mounting surface for a surge limiter, miscellaneous electrical components, and the cabling that connects the 14 circuit boards to the six connectors on the end of the assembly.

The tape transport assembly consists of an enclosure assembly, the tape transport mechanism, and a baseplate. The enclosure assembly consists of a spun magnesium cover which is sealed to a base by means of a V-band coupling and is pressurized to 17 psia with a gas mixture consisting of 78 percent nitrogen, 12 percent oxygen, and 10 percent helium, with a relative humidity of 30 percent at a temperature of 25°C. The tape transport mechanism contains two coaxial reels that contain 950 feet of 1/2-inch mylar-base tape, a five-track record head, a five-track playback head, a permanent-magnet erase-head, eight circuit boards and a planetary drive mechanism. The planetary drive mechanism contains two 8,000 rpm motors which employ mylar-belt drives and pulleys to move the tape. The record motor and planetary drive provides a tape speed of 1.34 inches-per-second: the playback motor and planetary drive move the tape in a reverse direction at 42.88 inches-per-second. The tape passes over both the record and playback head in each mode of operation; however, only one is active. On the flight models, erasure is performed by a permanent magnet after playback and again before recording to ensure complete data removal; on two engineering models, the erase head is an ac controlled device that provides an erase signal of approximately 30 kHz. Controls for the ac erase head also provide for a high speed record cycle that reduces test time by a factor of 1/30th. Power and control signals for the tape transport are supplied by the tape recorder electronics. Five output signals are applied to the multiplexer via the tape recorder electronics.

*RCA, Astro-Electronics Division, Instruction Manual, Nimbus-D High Data Rate Storage System, Spacecraft Equipment, Contract NAS5-10396 Princeton, New Jersey, March 21, 1969.

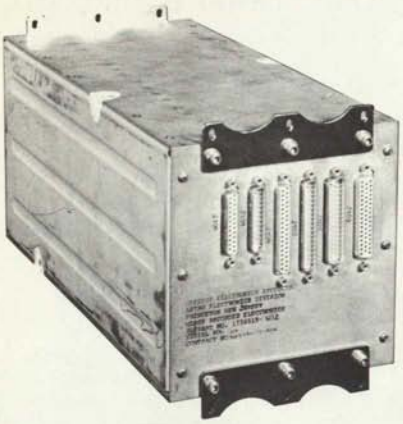

A. Tape Recorder Electronics

B. Tape Transport Assembly

Figure 3. HDRSS Tape Recorder Assemblies

Tape recorder operation consists of two modes (record and playback) which are controlled by the end-of-tape switches (mechanical and optical) and ground station commands. Initially, the tape recorder is commanded on (power on) and then commanded to record. Operation continues until the record end-of-tape switch is actuated (recorder reverts to off). Playback is initiated by the playback-on command and continues until the playback end-of-tape switch is actuated (reverts to record). This cycle continues until the off command is received.

Five signals are processed and recorded on the tape recorder: the ID or THIR-6 video signal (0 to 1,600 Hz); the THIR signal (0 to 360 Hz); the IRIS signal, a biphase 3,750-bit/sec data signal; the VIP signal, a biphase 4,000-bit/sec data signal; and a time code signal, a 2,500-Hz carrier amplitude modulated by the pulse width modulated (PWM) 100-bit Minitrack time code.

The ID video signal is applied to a voltage controlled oscillator (see Figure 4) that converts the analog signal to an FM signal (2.5 to 3.67 kHz) suitable for recording. During playback, the ID signal is reproduced at 32 times the record frequency (72 to 117.6 kHz), amplified, limited, and applied to the multiplexer. The THIR-11 signal is processed in the same manner as the ID signal except for the frequency. The record frequency is 2.3 to 3.16 kHz; the reproduced frequency is 73.6 to 101.12 kHz. The time code signal (2.5 kHz) is amplified and recorded. During playback, the frequency is increased to 80.0 kHz and frequency modulated with flutter data introduced by speed variations of the tape transport during the record and playback modes. The time code is then applied to the multiplexer. The VIP signal, a 4.0 kb/sec biphase digital signal is limited, amplified and recorded. During playback the reproduced signal is increased to 128 kb/sec, equalized to minimize phase and amplitude distortion, limited to reduce amplitude variations, and applied to the multiplexer. The IRIS signal is processed in the same manner as the VIP signal except for the bit rate. The input signal bit is 3.75 kb/sec; the reproduced bit rate is 120.0 kb/sec.

C. MULTIPLEXER ASSEMBLY

The Multiplexer assembly shown in Figure 5 contains six circuit boards. Power is supplied by the spacecraft via the Tape Recorder Electronics: control signals are supplied by the Tape Recorder Electronics. The ID, THIR, VIP and time code signals applied to the multiplexer where they are frequency shifted to a specific bandpass (see Figure 6) and applied to a summing amplifier. The summing amplifier combines the heterodyned signals with the IRIS signal and the pilot tone (the 355 kHz frequency of the local oscillator) to form a 1.2-to 786-kHz subcarrier that is applied to an S-band transmitter (see Figure 7). The nominal output amplitude of the output signal is 0.660 V rms.

The IRIS signal, a 120-kb biphase signal, is filtered to provide a 0-to 165-kHz signal. Since heterodyning is not required, the signal is applied directly to the summing amplifier.

The time code signal, an 80-kHz carrier amplitude modulated by a PWM data stream with a pulse repetition rate of 3.2 kHz, is heterodyned with an 850-kHz frequency. The output frequency is filtered to provide a 754-to 786-kHz output signal that is applied to the summing amplifier.

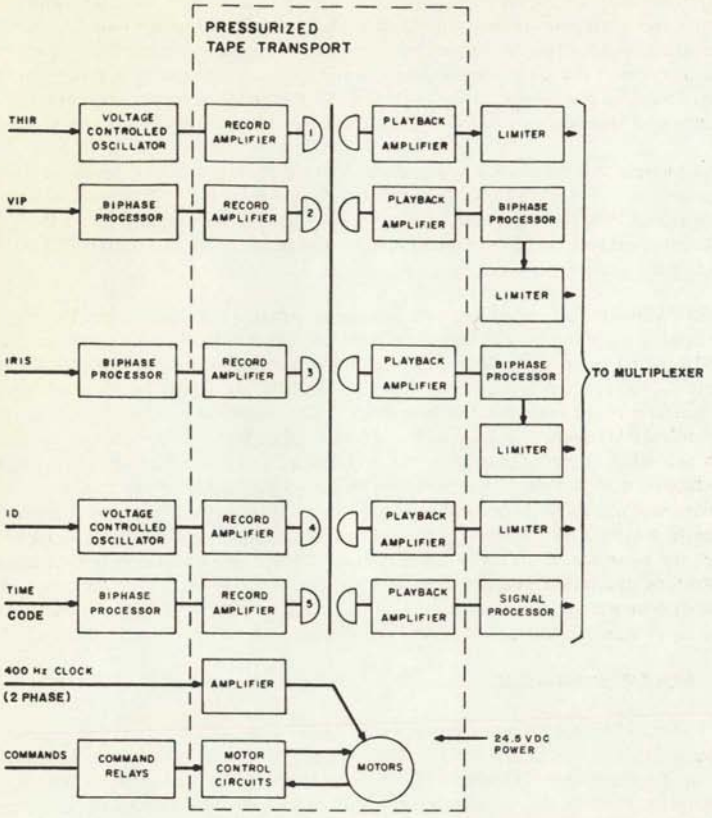

Figure 4. HDRSS-Tape Recorder, Block Diagram

The VIP signal, a 128-kb biphase signal, is bandpass limited from 0 to 360 kHz and heterodyned with a 355 kHz frequency to provide a double-side band AM signal. The output signal is bandpass limited from 175 to 343 kHz and is applied to the summing amplifier.

A pilot tone, the 355-kHz frequency of the local oscillator, is also applied to the summing amplifier.

The ID signal, an FM signal from 72 to 117.6 kHz, is frequency doubled and heterodyned with a 640-kHz frequency. The output frequency is filtered to provide a 400-to 530-kHz

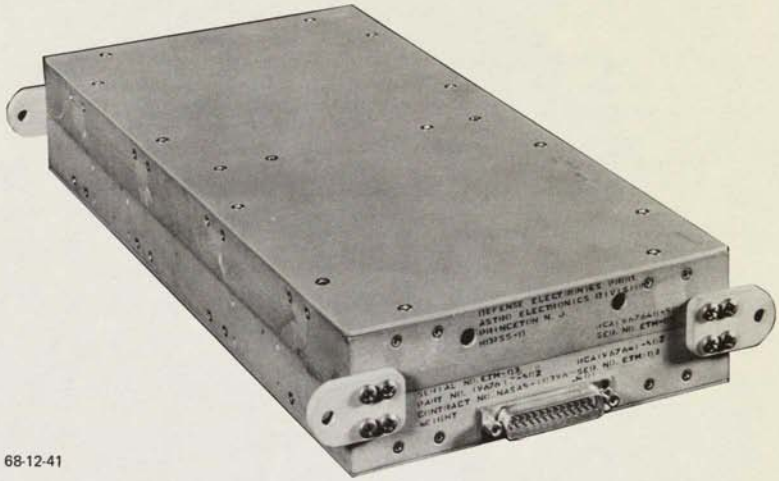

Figure 5. Multiplexer Assembly

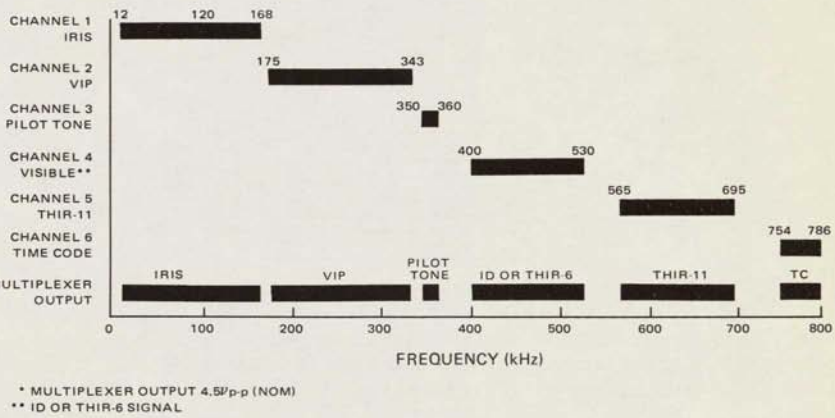

Figure 6. Multiplexer Output Frequency Spectrum

output that is applied to the summing amplifier. The bandwidth is such that the signalling received at the ground station is a "single-sideband" FM carrier for certain combinations of peak deviation and modulating frequencies. For example, video signals superimposed on a

white (120 kHz) average field, become an SSB-FM for any modulating frequency, since all upper sidebands corresponding to the video signal are removed by the multiplexer filter which cuts off at 400 kHz.

The THIR signal, an FM signal from 73.6 to 101.12 kHz, is frequency doubled and heterodyned with a 805-kHz frequency. The output frequency is filtered to provide a 565-to 695-kHz output signal that is applied to the summary amplifier. The composition of the output signal is similar to the ID signal previously described.

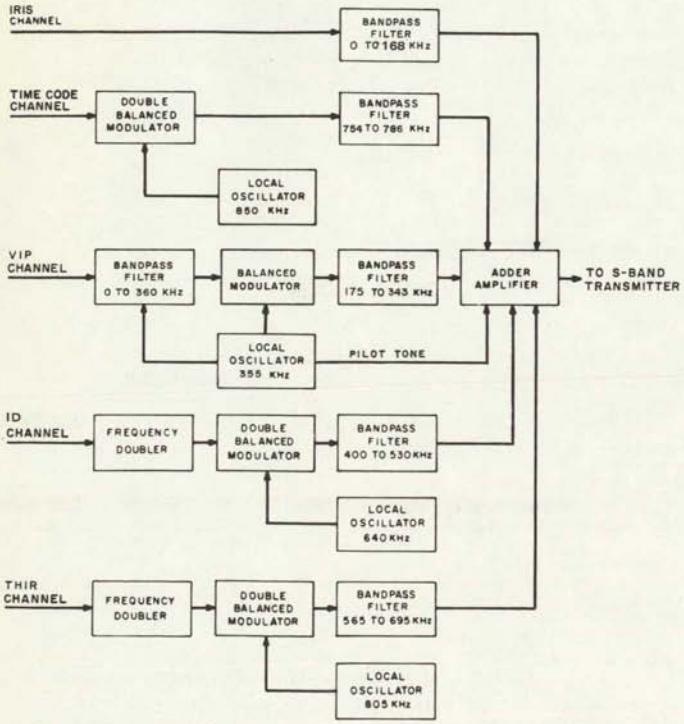

Figure 7. Multiplexer Block Diagram

SECTION 4
DESIGN CHANGES

A. INTRODUCTION

The basic HDRSS-B Configuration was changed significantly during the HDRSS-D program. The multiplexer design was changed extensively to meet the requirements of GSFC specification S-731-P-40. The tape recorder changes consist of design improvements authorized by contract modifications. Design improvements are the results of investigations resulting from test anomalies or equipment malfunctions, the results of new technology developed on other programs, or the results of independent research and development programs. Detailed descriptions are contained in the spacecraft subsystem instruction manual.*

Ground station and bench check unit modifications are the direct result of the changes made to the spacecraft tape recorder and multiplexer. Detailed descriptions are contained in the ground station** and bench check unit instruction manual.***

B. TAPE RECORDER CHANGES

1. Balanced Disk Brake

Operation of the HDRSS during the launch of the Nimbus-D spacecraft is specified in GSFC specification S-731-P-40. The balanced disk brake, designed to operate without slippage during the launch mode, is shown on Figure 8. The balanced disk brake consists of a fiberglass yoke with a set of counter weights attached to maintain a constant brake action. Attached to the fiberglass yoke is a silicone rubber disk that makes contact with the flat surface of the ferrite gear. When the brake is engaged (solenoid deenergized) the rubber disk rests against the ferrite gear and stops all motor rotation. During motor operation the brake is released (solenoid energized).

In addition to the modified brake configuration, the brake solenoid control circuit was modified to provide a high current through the pull-in coil during the

---

*RCA, Astro-Electronics Division, Instruction Manual, Nimbus-D High Data Rate Storage System, Spacecraft Equipment, Contract NAS5-10396, Princeton, New Jersey, March 21, 1969.

**RCA, Astro-Electronics Division, Instruction Manual, Nimbus-D High Data Rate Storage System Modifications for the HDRSS-B Ground Stations, Contract NAS5-10396, Princeton, New Jersey, January 9, 1970.

***RCA, Astro-Electronics Division, Instruction Manual, Nimbus-D Modifications of the Bench Check Unit of the HDRSS, Contract NAS5-10396, Princeton, New Jersey, September 3, 1968.

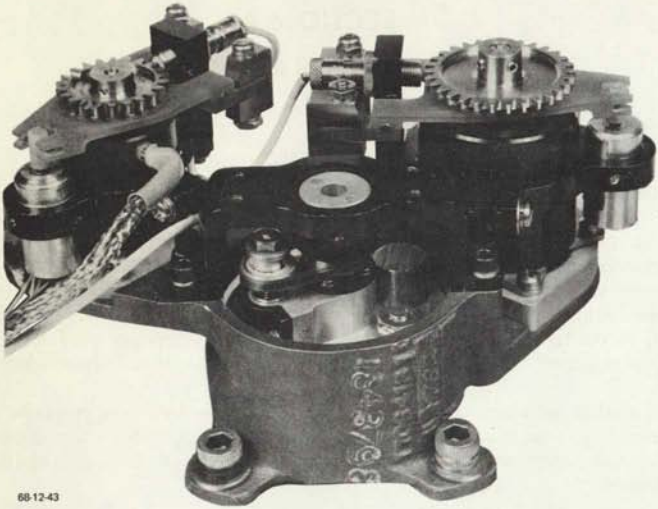

Figure 8. Planetary Pulley Assembly With Balanced Disk Brake

start mode, and a constant reduced current during the run mode. To insure a high impedance during the run mode, a series resistor is inserted into the circuit by means of the start-run relay.

2. End-of-Tape Sensors

The HDRSS-D tape transport contains an optical end-of-tape sensor not used on the HDRSS-B program, and modified mechanical end-of-tape sensors.

a. Optical End-of-Tape Sensors

The optical end-of-tape sensor consists of two optical sensors, an amplifier/relay control (board A-11) and two relays as shown on Figure 9. At the beginning of each record cycle, record power is applied to the bias circuits, the record-light emitter diode, charge controller Q4, and the drive circuits of the tape recorder via relay K1. When the transparent 10-inch window in the magnetic tape passes under the light emitter, photo transistor Q1 is biased on, and an input signal is applied to the integration network (R3, R4, C1, and C2). The resultant charge on capacitors C1 and C2 drives current amplifier Q1, Q2 (a modified Darlington circuit) and relay driver Q3 conducts. Conduction of Q3 completes a ground for relay K1 and record power is removed from the record circuits and electronics module. Closure of relay K1 also provides a self-latch to relay driver Q3, and simultaneously discharges the integration circuit through the second set of contacts.

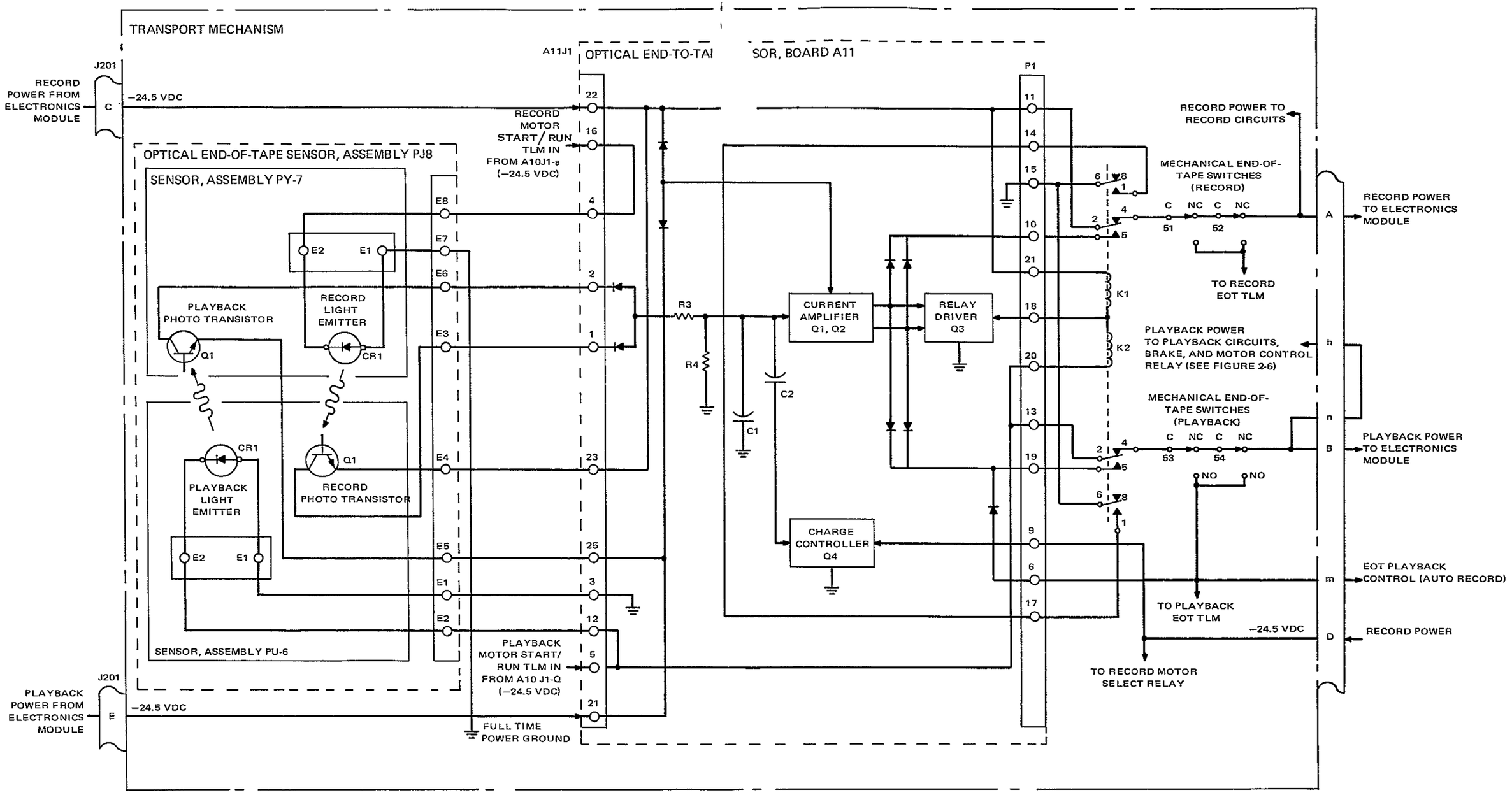

FOLDOUT FRAME 1

FOLDOUT FRAME 2

Figure 9. End-of-Tape Sensors, Block Diagram

Discharge of the integration circuit provides for instant response to a playback command initiated during or after the record cycle. The self latch feature insures power cutoff even if the transparent window moves beyond the light emitter due to transport inertia.

Charge controller Q4 allows for random pin holes that may occur in the iron oxide coating of the magnetic tape. During the record mode, charge controller Q4 is energized and the RC time constant is increased (insertion of C1 and C2 into the integration network) to compensate for possible pin holes and the slow tape speed. During playback, charge controller Q4 is inactive and the RC time constant is decreased (removal of capacitor C2) to allow for possible pin holes and the high tape speed.

End-of-tape operation during playback is identical to that described for the record mode except for the control of playback power, the operation of charge controller Q4, and the provisions for a end-of-tape command that initiates automatic record at the end of the playback cycle.

b. Mechanical End-of-Tape Sensors

The mechanical end-of-tape switches in the original design had silver plated contacts. These proved to be inadequate as the current level was insufficient to clean the contacts. This problem was complicated when the atmosphere was changed from a dry nitrogen/helium gas to a nitrogen/helium/oxygen mixture with a 30-percent relative humidity that increased corrosion of the contacts. In addition to the atmosphere charge, the installation of the optical end-of-tape sensor further deteriorated the situation as the number of switch actuations was decreased even more. As a result of these conditions, the contacts of the mechanical end-of-tape switches were changed from silver to gold plate.

3. Tape/Head Configuration Changes

a. Tape/Head Cleaner

The primary failure mode of the prototype tape transport life test was accumulation of binder residue on the magnetic heads. As the accumulation increased, the output signal levels deteriorated. As a result of these manifestations, a chromic oxide was placed on the magnetic tape and commanded over the heads at regular intervals. This technique demonstrated that the life of the tape transport could be increased substantially and the last flight model (F-3D) was equipped with the chromic oxide formulation.

b. Magnetic Tape

The RCA-617 magnetic tape, qualified for use on the HDRSS-B and -D program, is no longer available as existing stocks were depleted by the Nimbus-B2 and prototype life tests. RCA 765, a direct replacement, was installed on the F 3-D tape transport and flight qualified. The test results were excellent.

c. Acceptance Temperature Levels

Investigations disclosed that oxide accumulation on the heads was directly related to the temperature exposures (especially high) experienced during environmental test. As a result of these investigations the high temperature exposure was reduced from 45°C to 35°C.

4. AC Erase Head

During engineering model design and test, an a-c erase head was designed and installed on two engineering models. The use of an a-c erase head instead of the permanent magnet erase head eliminated erasure after each playback cycle. Combined with the use of the a-c erase interface assembly, a high speed rewind was substituted for the slow speed record cycle. This capability substantially reduces the time required for system troubleshooting and spacecraft integration tests.

C. MULTIPLEXER CHANGES

A summary of the multiplexer changes for HDRSS-D are as follows:

- The MRIR signal (53.33 kb/sec) was replaced by a VIP signal (128 kb/sec)
- The time code channel was relocated in the frequency spectrum (see Figure 6) to provide the additional bandwidth required by the VIP signal.
- A pilot tone for synchronous ground station demodulation of the VIP signal was added.
- Provision for transmitting an infrared signal on the ID channel was investigated.
- The overall bandwidth of the multiplexer output signal was increased from 1.2 to 695 kHz to 1.2 to 786 kHz to allow for the VIP and time code channel changes.
- The effect of the multiplexer output signal bandwidth on the S-band transmitter was investigated.

These changes are reflected in the description and configuration described in Section 3. Systems studies of the VIP, ID, and TC channels (multiplexer, S-band link, and demultiplexer - see Figure 2) as contained in Section 5. The VIP channel, completely re-designed, required a complete analysis; the TC channel required a minimum study effort, the ID channel analysis was limited to the effect of the infrared (THIR-6) signal recorded and transmitted on the ID channel. The THIR-11 (HRIR on Nimbus B) and ID channel were not changed.

D. GROUND STATION CHANGES

1. General

The ground station equipment was modified from the HDRSS-B configuration to the HDRSS-D configuration. The major changes were in the demultiplexer and the switching circuits. These changes were based on the following spacecraft equipment design changes;

- The MRIR signal (53.33 kb/sec) was replaced by the VIP signal (128 kb/sec).
- The time code channel was relocated to provide the additional bandwidth required by the VIP signal.
- A pilot tone for synchonous ground station demodulation of the VIP signal was added.
- Provisions for transmitting an infrared signal on the ID channel was added.
- The overall bandwidth of the multiplexer output signal was changed to allow for the VIP and TC changes.

A detailed description of the ground station changes is contained in the ground station modifications instruction manual*.

2. Demultiplexer

Modification of the demultiplexer for HDRSS-D operation required the removal of the MRIR circuits, design and installation of VIP circuits, and modification of the TC circuits. Mechanically, the HDRSS-B demultiplexer (RCA-1849418-502) and the HDRSS-D demultiplexer (RCA-1967618-502) are compatible with all the ground stations and bench check units. Electrically, the two demultiplexers are not interchangable as the MRIR signal was replaced with a VIP signal, a pilot tone (VIP oscillator frequency) was placed on channel 3, the IRIS bandpass filter was widened, and the time code was assigned to channel 6. The ID and THIR-11 (HRIR on HDRSS-B) channels are unchanged. Circuit similarities between the two demultiplexers are listed in Table 4.

*RCA, Astro-Electronics Division, Nimbus-D High Data Rate Storage System Modifications for the HDRSS-B Ground Stations, Contract NAS5-10396, Princeton N.J. January 9, 1970.

TABLE 4. HDRSS-B AND -D DEMULTIPLEXER CIRCUIT SIMILARITIES

Circuit Board Nomenclature	Circuit Designation for	
	HDRSS-B	HDRSS-D
IRIS Channel Separator	NA	A1
IRIS Channel Phase Corrector	NA	A2
IRIS Channel Output Amplifier	A2	A3
TC Channel Separator	NA	A4
TC Channel Mixer	NA	A5
TC Channel Post Translator	NA	A6
VIP Channel Separator, Phase Corrector	NA	A7
VIP Channel Synchronous Detector, Filter, and Output Amplifier	NA	A8
Pilot Tone	NA	A9
Phase Detector Drive	NA	A9A2
Separator, Limit Phase Detector	NA	A9A1
VCO, DC Amp, Filter, and Phase Shift	NA	A10
6-Volt DC Power Supply	NA	A19
Visible* (ID on HDRSS-B) Channel Separator	A9	A11
Visible Channel Mixer	A8	A12
Visible Channel Low Pass Filter	A7	A13
Visible Channel Phase Corrector	NA	A14
THIR-11 (HRIR on HDRSS-B) Channel Separator	A12	A15
THIR-11 Channel Mixer	A11	A16
THIR-11 Channel Low Pass Filter	A10	A17
THIR-11 Channel Phase Corrector	A15	A18

* ID or THIR-6 on HDRSS-D

NA - Not Applicable

3. THIR Demodulator Drawers

Modification of the HRIR demodulator drawers from the HRIR to THIR configuration for HDRSS-D at all the ground stations required the following changes and additions:

- Add a low pass filter for the THIR-6 video and change the chassis wiring.
- Add a switch to select the proper video filter.
- Add a sync squelch circuit.
- Change the video and sync filter frequency and amplitude responses.
- Change the output amplifier impedance to obtain the correct output voltage range.

4. Balanced Line Amplifier

Modification of the Balanced Line Amplifier drawer for HDRSS-D operation at GS-7 required the following changes and additions:

- Add a low pass filter for the THIR-6 video and change the chassis wiring.
- Add a switch to select the proper video filter.
- Change the video and sync filter frequency and amplitude response.

5. Monitor Circuits

Modification of the monitor circuits for HDRSS-D operation at GS-3 and GS-7 required the following changes.

- Provide output bandwidth filters for the monitor circuits to display the THIR-11 signal during Real Time and Slow Time data transmission.
- Modify a ST FM demodulator to process the HDRSS-D time code during Slow Time data transmission.

6. THIR-6 Detector and Control Circuit

Two analog signals, IDCS (Image Dissector Camera Subsystem) and THIR-6 (Temperature-Humidity Infrared: 6 micron wavelength), are transmitted alternately on the visible channel of the HDRSS system. At GS-7, these signals must be processed separately; IDCS by the Kine Complex, and THIR-6 by THIR equipment. When THIR-6 data, incompatible to the Kine Film Processor, is received, random start and stop pulses are generated and applied to the Index Computer. Index

Computer operation during THIR-6 signal reception was incompatible with ground station requirements. To eliminate this condition, a THIR-6 Detector and Control Circuit was designed and fabricated. Upon detection of the THIR-6 signal, the start and stop pulses are inhibited and the index computer is disabled.

E. BENCH CHECK UNIT CHANGES

1. General

The following modifications were made to the bench check units at the RCA Astro-Electronics Division. Modification of the bench check unit at the General Electric Company, treated as part of Ground Station No. 1, consisted of changing the demultiplexer as described in Paragraph D.2. A complete description of the bench check unit modifications are contained in the BCU instruction manual*.

2. Signal Selector Chassis

The ID signal selector was modified to allow for selection and data processing on the ID or THIR-6 data signal. The time code signal selector was modified to provide for selection of the 80-kHz or 187-kHz time code signal from the TC simulator. The 80-kHz signal is required for HDRSS-D operation and tape transport tests, the 187-kHz signal is required for HDRSS-B operation.

3. Demultiplexer

The demultiplexer changes are identical to the changes described for the ground station demultiplexer (refer to Par D.2.). The HDRSS-B and -D multiplexers are mechanically interchangeable to allow for testing of either configuration; electrically the two units are incompatible.

4. THIR Demodulator Drawer

The only modification to the THIR demodulator drawer is the addition of the a low pass filter to the THIR demodulator.

The low pass filter (0-960 Hz) is used for THIR-6 data processing. Selection of the low pass filter for THIR-11 or THIR-6 is controlled by a selector switch in the time code simulator.

*RCA Astro-Electronics Division, Instruction Manual, for Nimbus-D Modifications of the Bench Check Units of the HDRSS, NAS5-10396. Princeton, New Jersey, September 3, 1968.

5. RF Link Simulator

The r-f link simulator was modified to provide the following:

- the proper coupling capacitor for HDRSS-B (MRIR) or HDRSS-D (VIP) data processing
- an isolation amplifier to provide for the addition of VIP channel noise
- a relay, controlled from the clock simulator, to select the circuits required for VIP or MRIR operation.

6. Clock Simulator

The clock simulator was modified to provide the following:

- a VCO network with an external frequency control for flutter and wow simulation
- a counter network to provide a VIP bit rate
- a switch and relay to control all the switching (VIP or MRIR) for the entire bench check unit.

7. THIR Simulator

The THIR simulator was modified to provide the following THIR-6 signals:

- an analog video signal
- an fm subcarrier (fm)
- a double subcarrier (2 fm)

8. 400-Hz Phase Detector

During tape transport operation, a two phase 400-Hz square wave drive signal is supplied by the clock simulator. Phase A must lead Phase B by 90°. If the phase relationship is incorrect, a relay driver is energized and power is removed from the tape transport to prevent operation in the playback direction with a record command or record direction with a playback command. In either case, the end-of-tape switches are not applicable and the magnetic tape is dumped thereby causing severe damage and delays.

9. A-C Erase Interface Assembly

The a-c erase interface assembly, used in conjunction with an a-c erase head (engineering models only) eliminated the erase function after playback and provided for a fast rewind instead of a slow speed record. This capability reduces test time by a factor of 128/4 or $\approx$ 32.

SECTION 5
VIP, TC, AND ID CHANNEL ANALYSIS

A. INTRODUCTION AND SUMMARY

1. HDRSS-D Signal Characteristics and Performance Objectives

The HDRSS-D signal characteristics are listed in Table 5; the performance objectives are listed in Section 2. The analysis in this section was performed for an IRIS bandwidth of 132 kHz and a frequency deviation of 100 kHz. The IRIS bandwidth was subsequently changed to 168 kHz and a frequency deviation of 200 kHz per contract modification No. 12. This modification improved IRIS performance above the levels shown in the study and had no effect on the remaining channels.

2. HDRSS-D Frequency Division Multiplexed Spectrum, Frequency Deviation, and RF In-band Power.

The HDRSS-D Frequency Division Multiplexed (FDM) spectrum is shown on Figure 6. The frequency deviation of each channel as compared to HDRSS-B is listed in Table 6. The specified S-band transmitter has a frequency deviation of ±1.5 MHz with a ±1.0 percent linearity. The rms deviation is 405 kHz and the peak deviation of the transmitter is 1244 kHz. For a 3.0 MHz bandwidth, the percentage of the time the instantaneous deviation exceeds the maximum deviation allowed by Carsons rule is approximately 5 percent. This amount of over deviation is negligible and is confirmed by the calculated RF in-band energy. The over deviation, bandwidth, and worst-case in-band power for two values of bandwidth are listed in Table 7.

A computer calculation was performed on the RCA-601 computer to determine the amount of in-band energy in the RF channel. The Frequency-Division Multiplexed Spectrum in Figure 6 was simulated by 6 sinusoidal waveforms. The frequency of the waveforms was assigned values within the bandwidth of each subcarrier channel in order to determine the frequencies yielding the smallest in-band energy. Each waveform was assigned the maximum frequency deviation of the corresponding channel. A very small amount of energy is spilled outside the RF bandwidth, refer to Table 7. This indicates that the frequency deviation assignments of Table 6 will not "overdeviate" the link, by any appreciable amount.

3. Summary of S-band Link Characteristics.

a. Doppler

Maximum relative doppler shift (5-degree elevation at a 550 n m orbital altitude) is $\pm 2.1 \times 10^{-5}$. Maximum absolute doppler shift (at 1707.5 MHz) is ±35.7 kHz. The Nimbus-D spacecraft will orbit at an altitude of 600 ± 50 n m.

TABLE 5. HDRSS-D TAPE RECORDER INPUT/OUTPUT SIGNAL CHARACTERISTICS

Channel	Signal Description	Input Signal (Record)	Output Signal (Playback)
IRIS	Infra-red Interferometer Spectrometer, Digital Data, Biphase Format	Data Rate: 3.75 k b/sec	Data Rate: 120 k b/sec Subcarrier-NA
VIP	Versatile Information Processor, Digital Data, Biphase Format	Data Rate: 4.0 k b/sec	Data Rate: 128 k b/sec Subcarrier-NA
TC	NASA-Minitrack Time Code	2.5 kHz ± 0.0001% AM with 100 bits/sec; PWM Time Code Ones = 6 m sec Zeros = 2 m sec Valley-to-Peak ratio = 0.3 + 5% −0%	3.2 k b/sec Pulse duration Ones = 187.5 u sec Zeros = 62.5 u sec Valley to Peak Ratio = 0.30 to 0.54 Subcarrier - 80 kHz
THIR-11	Temperature-Humidity Infra-red 11-Micron Range	Baseband: 0 to 360 Hz Black Level = 0 V White Level = -6 V	Baseband: 0 to 11.52 kHz Black Level Freq. 73.6 kHz White Level Freq. 101.12 kHz Subcarrier - None, Single Side band
ID	Image-Dissector Camera Subsystem	Baseband: 0 to 1600 Hz Sync Level: -8.0 V Black Level: -6.5 V White Level: -2.3 V	Baseband: 0 to 51.2 kHz Sync Level Freq: 72 kHz Black Level Freq: 84 kHz White Level Freq: 117.6 kHz
THIR-6	Temperature Humidity Infra-red 6-Micron Range	Baseband: 0 to 120 Hz Black Level: -7.8 V White Level: -4.36 V	Baseband: 0 to 3.84 kHz Black Level Freq: 73.6 kHz White Level Freq: 101.12 kHz

TABLE 6. HDRSS-B AND -D FREQUENCY DEVIATIONS

HDRSS-B		HDRSS-D	
Channel	Deviation (kHz)	Channel	Deviation (kHz)
IRIS	100	IRIS	100*
TC	75	VIP	300
MRIR	400	PT	44
ID	300	ID	300
HRIR	200	THIR	200
		TC	300
TOTAL 1075 kHz		TOTAL 1244 kHz	
* Changed to 200 kHz per Contract Mod No. 12, refer to Par A.1.			

TABLE 7. HDRSS-D IN-BAND POWER

System	Bandwith (MHz)	Worst Case In-Band Power (%)
HDRSS-D	3.0	99.75
HDRSS-D	3.4	99.91

b. Crosstalk and Intermodulation Distortion

Figure 10 shows the approximate pass bands and rejection characteristics of the multiplexer and demultiplexer filters. Table 8 shows the calculated Signal-to-Distortion (S/D) ratios at the demultiplexer, i.e. in the subcarrier domain. For the VIP and IRIS channels, the S/D ratios are also the baseband S/D ratios. For the ID and THIR channels, the baseband S/D is obtained from the subcarrier S/D by increasing the latter by the fm improvement from subcarrier to baseband. The derivations are contained in Appendix I.

c. Signal-to-Noise Ratio (Link Noise Only)

(1) RF Link. The link calculation obtained from the HDRSS Engineering Model final report* shows that the worst-case carrier-to-noise ratio in the 3-MHz bandwidth is 18.1 dB rms/rms. A summary of the calculations are contained in Appendix II. These calculations assume the use of a 5-watt S-band transmitter, a 650 n m orbit, and a maximum receiving antenna elevation of 5 degrees.

*RCA Astro-Electronics Division, Final Report for the High Data Rate Storage System (Engineering Models EM-1 and EM-2), Appendix IV, NASA 5-3772, Princeton, New Jersey, May 3, 1968.

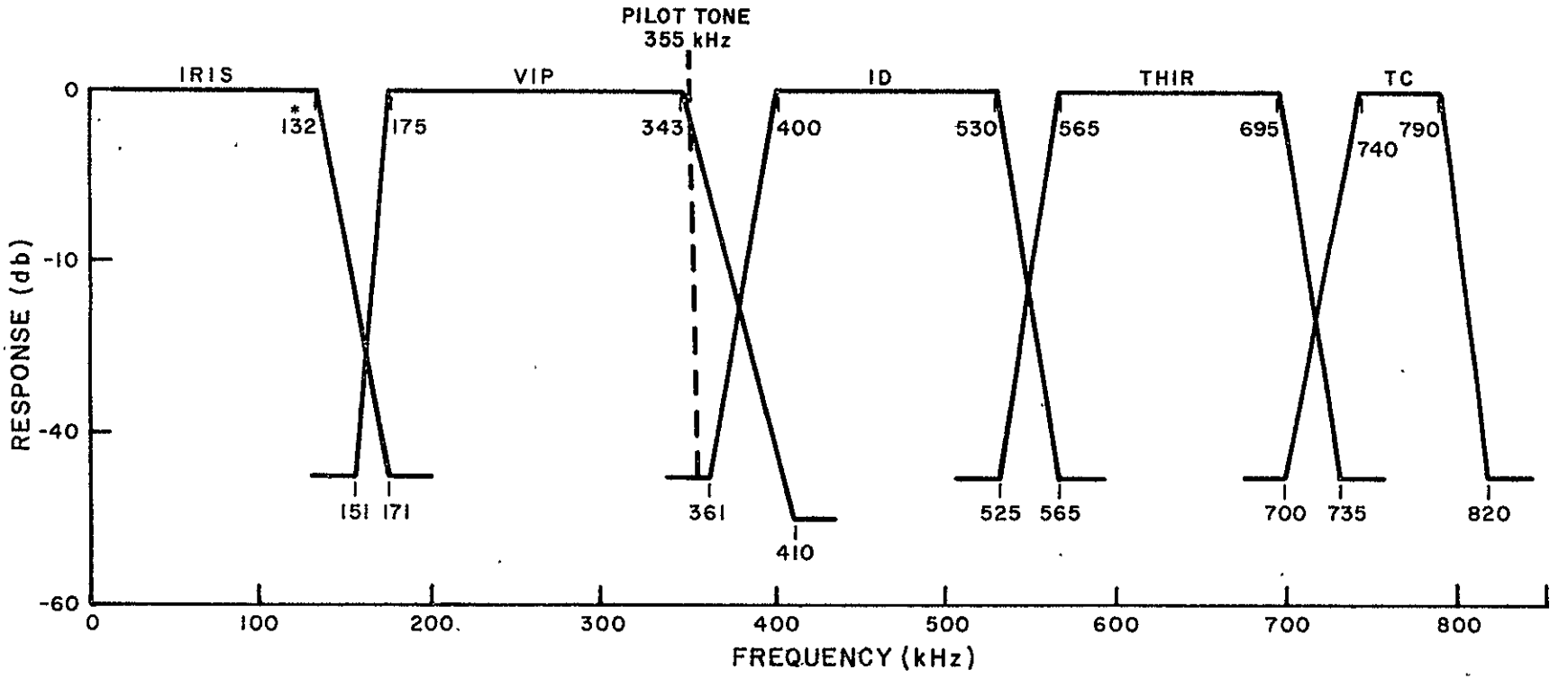

*Expanded to 168 kHz (1.4 x the bit rate) by Contract Model No. 12, refer to Par. A.1.

Figure 10. HDRSS-D Multiplexer/Demultiplexer Characteristics

TABLE 8. HDRSS-D SIGNAL-TO-DISTORTION RATIO AT THE DEMULTIPLEXER OUTPUT

Channel	Gain, System Non-Linearity (dB)	Linear Crosstalk (dB)	IF Phase Non-Linearity (dB)	IF Bandwidth at 3 MHz (≈dB)	Resultant Signal-to-Distortion Ratio (dB)
IRIS**	19.4*	28.9*	42.1*	30.0	18.6*
VIP	28.5*	32.2*	39.8*	30.0	25.8*
ID	30.0	36.8	35.8	30.0	26.1
THIR	27.4	34.3	30.2	30.0	24.0
TC	31.7	38.8	32.8	30.0	26.3

*Same values at base band. ** Refer to Par. A.1.

(2) Baseband. The baseband signal-to-noise ratio for the VIP channel is summarized in Table 9. The THIR-6 signal-to-noise ratio is 64.7 dB black-to-white rms (refer to Section 5, Paragraph D). Analysis of the time code channel signal-to-noise ratios, unchanged from HDRSS-B, are listed in Table 10 (refer to Section 5, Paragraph C).

B. VIP CHANNEL ANALYSIS

1. Introduction

The VIP channel carries a high data rate (128 kilo bits/sec) digital signal that replaces the MRIR signal (55.33 kilo bits/sec) used on HDRSS-B. The substantial increase in data rate precludes the transmission of VIP data on the channel originally allocated to the MRIR signal.

2. Channel Analysis Trade-offs

Figure 11 shows the HDRSS-D and HDRSS-B channel allocations and three possible alternatives considered prior to hardware. The baseband required for the VIP signal is 180 kHz (1.4 x the bit rate). This baseband, obtained through a computer simulation of the channel, produces a well behaved response to the square-pulse biphase input signal. If the bandwidth is reduced, the channel response will suffer from excessive zero-crossing errors and increased signal loss due to intersymbol interference.

A direct substitution of the VIP signal in the MRIR channel (Figure 10, plan A) was rejected as the MRIR channel bandwidth was 1.02 x the VIP bit rate, not 1.4 x the bit rate as required.

TABLE 9. VIP CHANNEL SIGNAL-TO-NOISE RATIO SUMMARY

Parameter and Values		Reference
Carrier-to-Noise Ratio	18.1 dB rms/rms	Section 5, Par A.3.c
FM Improvement	10.7 dB rms/rms	Table 17
TOTAL:	28.8 dB rms/rms	
Pilot Tone SNR at Demultiplexer Band pass filter (Bandwidth of 15.0 kHz)	20.0 dB rms/rms	
Signal Loss Due to Component Tol	-9.8	Table 17
Signal Loss Due to Crosstalk and Intermodulation Distortion	-2.0	Section 5, Par B.7.b.(2)
TOTAL LOSSES:	11.8 dB rms/rms	
Net VIP SNR in baseband (no dropouts) (28.8 dB - 11.8 dB)=	17.0 dB rms/rms	Table 17
SNR Requirements for BER of $1X10^{-6}$ (no dropouts)	13.0 dB rms/rms	Table 17
Margin	4.0 dB rms/rms	
Maximum BER with Tape Recorder Dropouts	7.2×10^{-6}	Table 18
System Specification	1.0×10^{-5}	

TABLE 10. TIME CODE SIGNAL-TO-NOISE RATIOS

Subcarrier-to Noise Ratio (dB rms/rms)	Flutter & Wow Output Signal to Noise Ratio (dB rms/rms)	Time Code Demod Output Signal to Noise Ratio (dB rms/rms)
26.9	30.2	15.4

In plan B, the TC channel was moved to the upper end of the spectrum to yield more space for the VIP channel. This approach would provide a bandwidth of 183 kHz (182 to 365 kHz) with the pilot tone located at 182 kHz. While essentially the same as the HDRSS-D allocations, this plan required the transmission of the upper side band. This was not acceptable as there was a possibility of interference due to baseband feed-through.

The ID and THIR channels were shifted upwards in plan C and the VIP signal, designated as a double sideband AM signal, utilized the ID and MRIR channel allocations. This approach was not selected for two reasons.

- It required extensive changes to the multiplexer/demultiplexer circuits.
- It required increased frequency deviations for the ID and THIR channels.

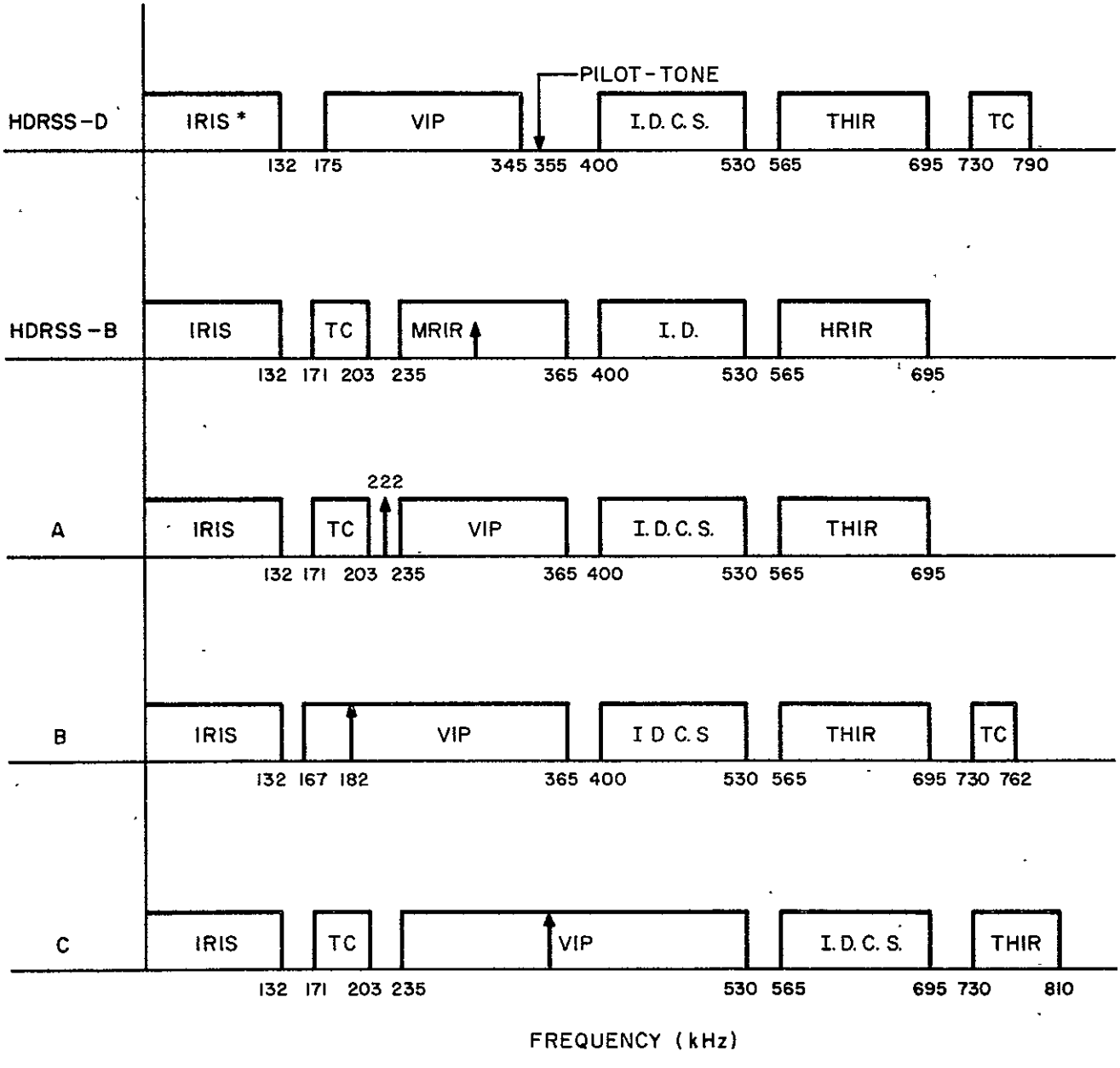

*Expanded to 168 kHz by Modification No. 12, refer to Par. A.1.

Figure 11. Possible Frequency-Division Multiplexed Channel Allocations

The increased frequency deviations would have increased the RF bandwidth, which was limited to 1.2.

The selected HDRSS-D channel allocations have the following advantages.

- Adequate bandwidth
- Efficient use of transmitter power and RF bandwidth due to single sideband modulation
- Relocation of the TC channel

Since the TC channel is narrow band, the increased frequency deviation was reasonable and well within the present transmitter capabilities.

The only complexity was the addition of the pilot tone and the phase locked loop filter in the demultiplexer. The design of the phase locked loop presented no difficulties and the pilot tone was located in the low energy region of the biphase spectrum.

3. Circuit Description

The biphase digital data (see Figure 12) from the Versatile Information Processor (VIP) is recorded on one track of the tape recorder at the rate of 4 kilo bits/sec. During playback the biphase digital data becomes a quasi-sinusoid waveform due to the bandwidth limitations of the tape recorder. This waveform is applied to a wideband hard limiter internal to the tape recorder. The subsequent output is a square-pulse biphase signal at 128 kilo bits/second. Waveform distortion caused by intersymbol interference and the effect of noise prior to the limiter will show up at the limiter output in the form of zero-crossing error.

The square-pulse biphase data from the Tape Recorder is applied to the HDRSS-D Multiplexer (see Figure 13). The waveform is first prefiltered in a low-pass filter where the high-frequency components which might produce spectrum fold-over (aliasing) during the modulation process are removed. The effect of spectrum fold-over is signal distortion in the transmitted waveform. The filtered waveform is modulated in a double balanced modulator (DBM) on a 355 kHz subcarrier. A bandpass filter eliminates the upper sideband frequency and passes components from 175 kHz to 343 kHz; the subcarrier is suppressed by the DBM. The subcarrier, reinserted as a pilot tone, has an amplitude 16.7 dB smaller than the VIP signal amplitude.

The VIP and pilot tone signals, along with the ID, THIR, TC, and IRIS signals, are summed-up and then applied to the S-band transmitter. At the Command and Data Aquisition (CDA) station, the FDM spectrum is recovered by the receiver and applied to the demultiplexer where the six signals are separated by appropriate bandpass filters. After separation, the VIP signal is applied to an

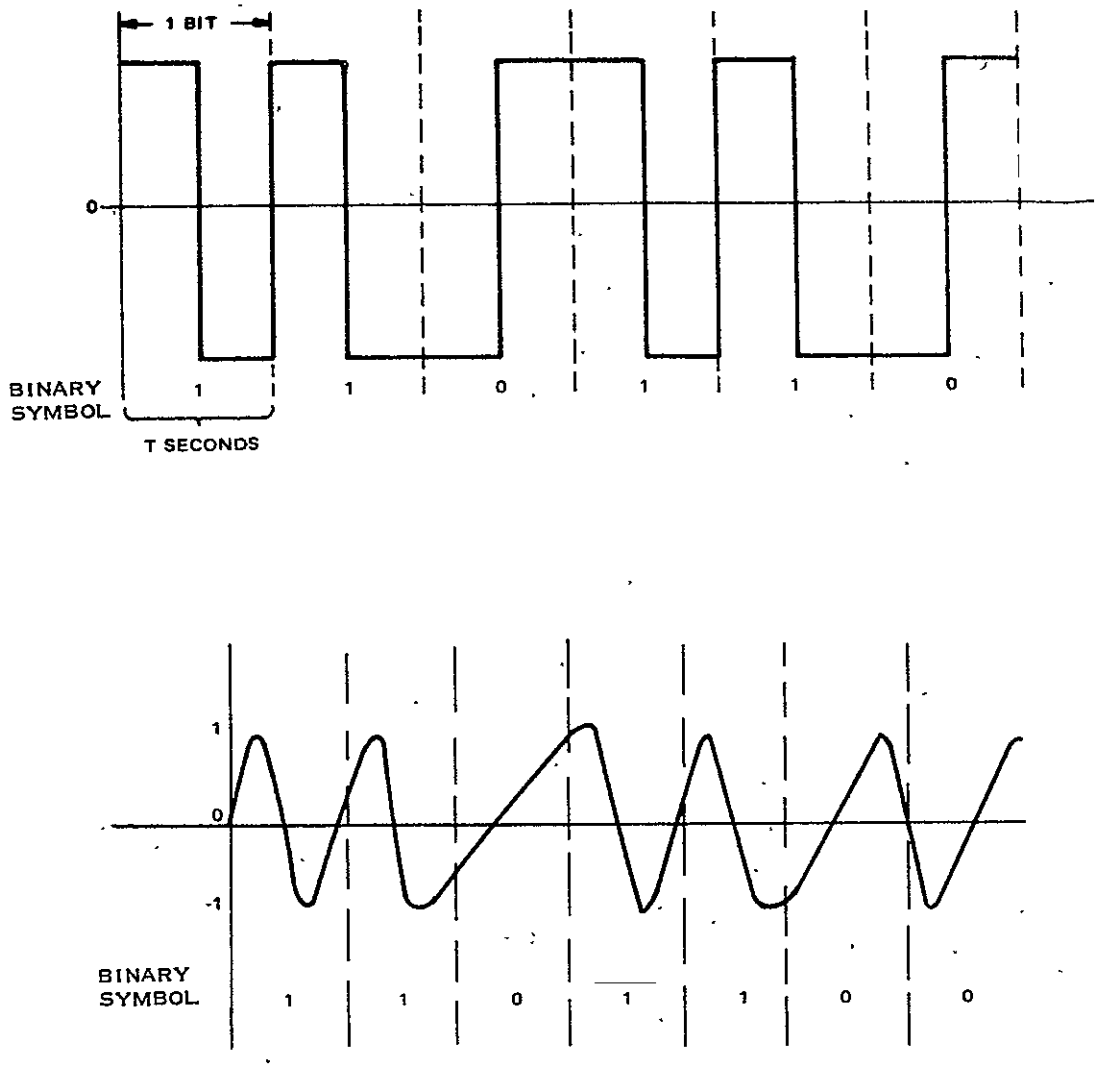

Figure 12. Biphase Signal Format

equalizer that corrects the combined phase distortion of both the multiplexer and demultiplexer filters. After equalization, the single-sideband signal is synchronously demodulated by processing it with the recovered pilot tone in a product demodulator. A final low pass filter rejects the unwanted products. The recovered VIP signal from an engineering model breadboard is shown in Figure 14, a computer simulation is shown in Figure 15, The simulation approximates the actual phase distortion of the breadboard by a quarter of a sine-wave (refer to Appendix III). The breadboard differential time delay distortion (see Figure 16) is well within the specified limits. The reason that Figure 15 appears as a mirror image of Figure 14 is the effective sign reversal in the baseband phase response of the VIP channel resulting from the transmission of the lower sideband spectrum.

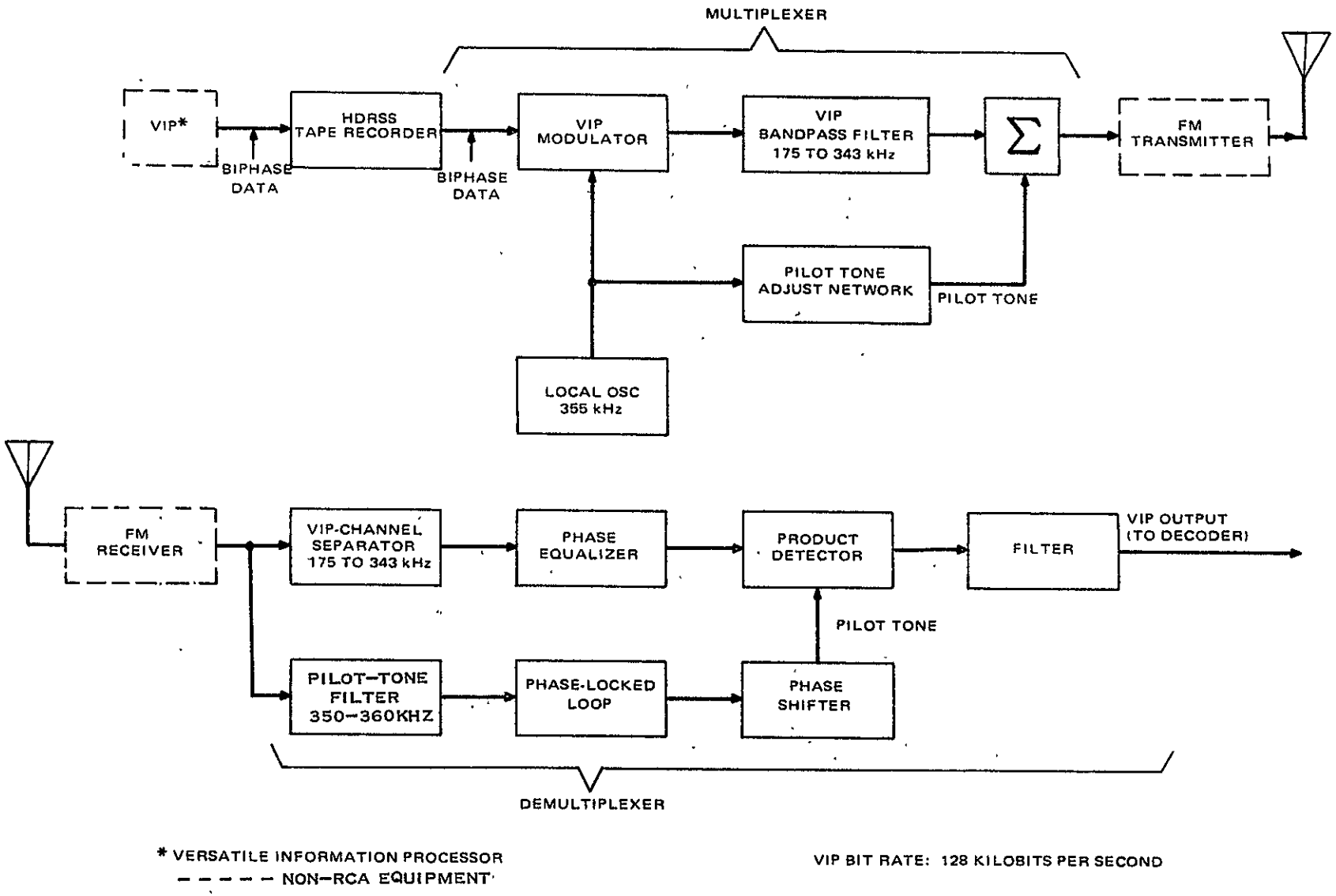

Figure 13. VIP Channel, Block Diagram

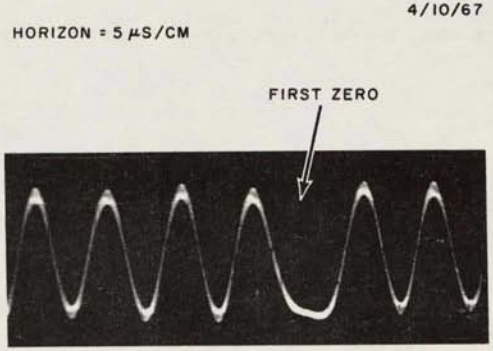

Figure 14. VIP Breadboard Response to Binary Word 11111000001111100000111110000

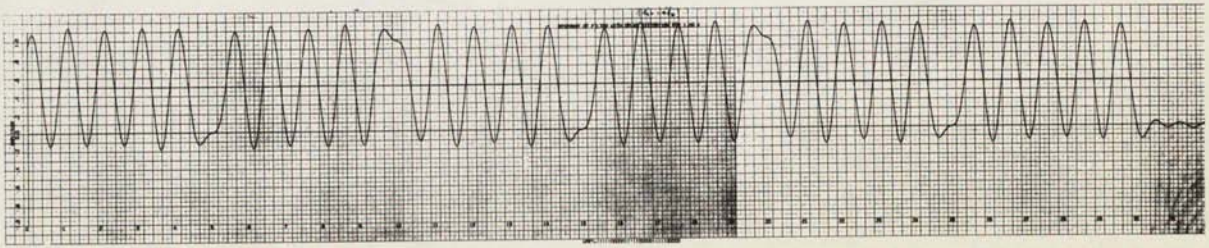

Figure 15. Calculated Response Binary Word 11111000001111100000111110000

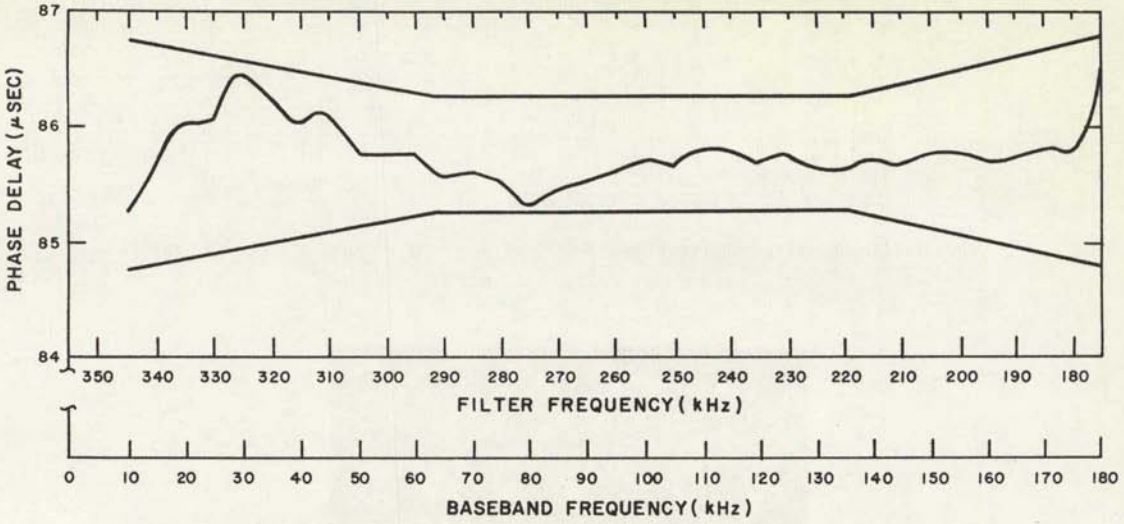

Figure 16. Measured Phase Delay Versus Computer Evaluated Filters

The pilot tone is extracted from the FDM spectrum by a 350- to 360-kHz filter that limits the amount of interference from the VIP spectrum into the phase-locked loop (PPL). A 90-degree phase shifter corrects the phase shift introduced by the PPL and any phase differential between the VIP and pilot tone signals.

4. Theoretical Considerations For Single-Sideband Amplitude Modulation

a. Introduction

The VIP subcarrier spectrum is essentially single-sideband. A pilot tone, used as a reference subcarrier for synchronous demodulation at the receiving station, is extracted from the FDM spectrum by a phase-locked loop. A functional block diagram of the VIP circuit is shown on Figure 17. A summary of Single Sideband Amplitude Modulation (SSB-AM) characteristics are contained in the following paragraphs; analytical derivations are contained in Appendix IV.

b. Effect of Pilot Tone Static Phase Error

The subcarrier reference used in the synchronous demodulation will have a static phase error (ϕ_o). The effect of ϕ_o is a distortion of the output signal Y (t). The distortion component Q (t) has an amplitude proportional to (sin ϕ_o); the undistorted component P (t) of Y (t) is attenuated by (cos ϕ_o). As a result the maximum output signal occurs when ϕ_o equals zero. The output signal is written as:

$$Y(t) = P(t) + Q(t) \qquad (1)$$

where

$$P(t) = kf(t) \cos \phi_o$$

$$Q(t) = k\hat{f}(t) \sin \phi_o, \text{ and}$$

$k\hat{f}(t)$ = the Hilbert transform for k (f).

When f (t) is even, $\hat{f}(t)$ will be odd and waveform Y (t) will display a skew. When a small phase error (ϕ_o) is present, the effect of $\hat{f}(t)$ introduces a timing error.

c. Overall Phase Versus Frequency Response

The effect of the static phase error ϕ_o on the overall frequency response is a constant phase shift ϕ_o at all baseband frequencies (see Figure 18). The effects of ϕ_o, evaluated by computer simulation, are described in Paragraph 6,d, "Effects of Static Phase Shift and Bandwidth Truncation or VIP Channel Performance."

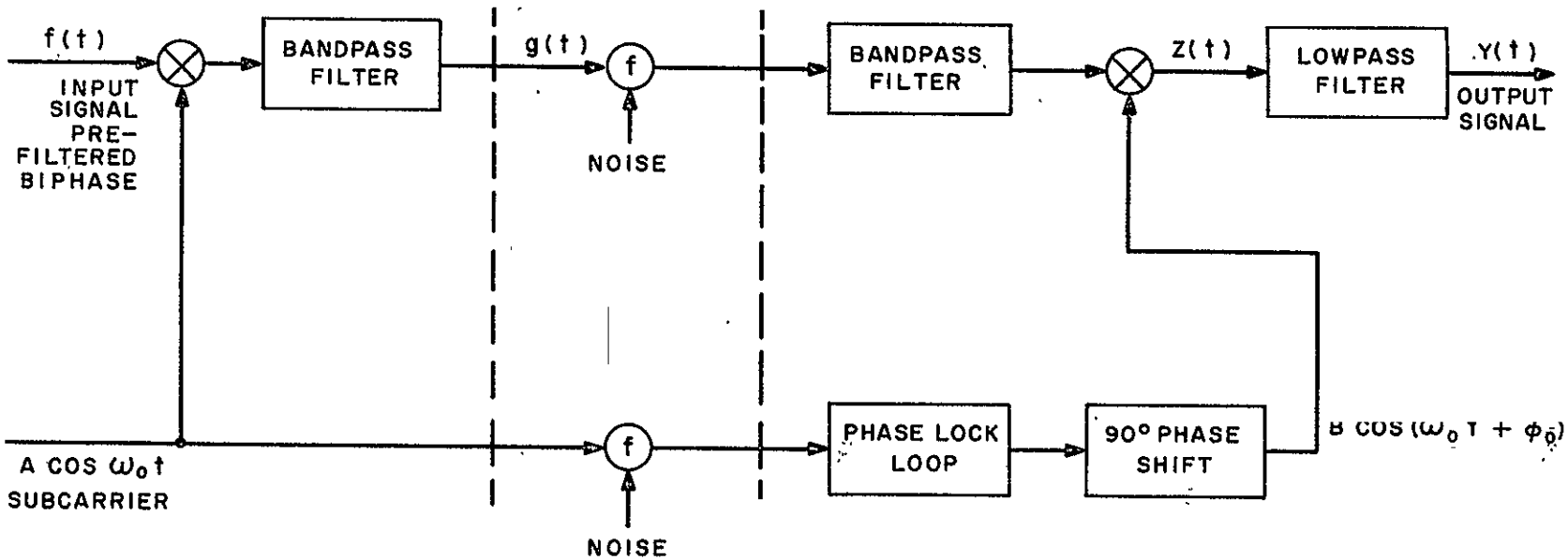

Figure 17. VIP Channel, Functional Block Diagram

d. Subcarrier Peaking

The SSB-AM signal g(t) at the demultiplexer output exhibits peaking when the modulation f(t) is not sinusoidal. The SSB-AM signal is defined as:

$$g(t) = f(t) \cos W_o t + \hat{f}(t) \sin W_o t$$

The Hilbert transform f(t) usually has sharp peaks. For example, if f(t) is a square wave, $\hat{f}(t)$ will have infinitely large peaks at time locations corresponding to the sharp edges of the square wave. In the VIP channel, the waveform, f(t) does not have sharp edges; they are QUASI-sinusoids. Consequently the peaks of f(t) are not excessive. Measurements performed on the VIP breadboard indicated that peaking was about 3 dB when various binary patterns were transmitted. When 3 dB peaking occurs, the VIP channel deviation will exceed the nominal 300 kHz deviation by 127 kHz. The total peak deviation of the transmitter is subsequently increased by approximately 10 percent. This is not expected to produce any significant increase in intermodulation distortion.

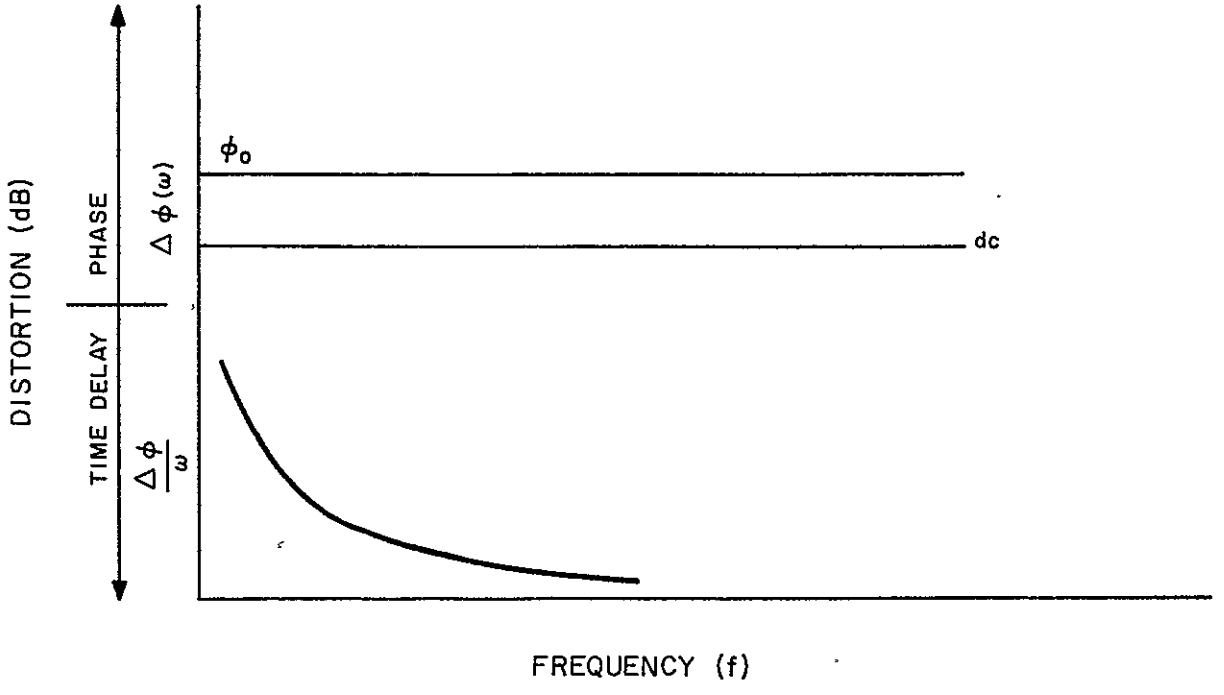

Figure 18. Phase and Time Delay Distortion Versus Phase Locked Loop Static Phase Error

e. Pilot Tone Channel Noise

Pilot Tone Channel noise produces phase jitter in the extracted pilot tone. The rms phase error (θ rms) is related to the signal-to-noise ratio (in the phase-locked-loop bandwidth) by the following formula.

$$\theta_{rms} = \sqrt{\frac{N}{2S}} \quad \text{(radians)}$$

where

$\frac{S}{N}$ = signal-to-noise power ratio.

In general, when the input is cos $W_o t$, the output of the phase-locked loop is:

$$B \sin \left[W_o t + \varphi_o + \hat{\theta}(t)\right]$$

where

φ_o = the static phase error

$\hat{\theta}(t)$ = is the phase jitter due to noise and VCO jitter.

The effect of the total phase error $\bar{\psi} = \varphi_o + \hat{\theta}(t)$ is to produce an attenuation of the desired signal $\hat{f}(t)$ equal to cos $(\varphi_o + \hat{\theta}(t))$ and to introduce a distortion term proportional to $\hat{f}(t)$ Sin $(\varphi_o + \hat{\theta}(t))$ where $\hat{f}(t)$ is the Hilbert transform of $\hat{f}(t)$.

The rate of variation of $\hat{\theta}(t)$ is slow relative to the bit rate since the noise bandwidth of the phase-locked-loop is order of magnitudes smaller than the bit rate. In the VIP channel $\hat{\theta}(t)$ is much smaller than φ_o and the loss is essentially cos φ_o.

5. Bit Synchronizer SNR Requirements

The signal-to-noise ratio requirements were calculated for a sinusoidal waveform into the bit-synchronizer. The noise and signals coming from the demultiplexer occupy a bandwidth of 1.4 f_b with a bit rate (f_b) of 128 kilobits/sec. The peak amplitude of the sinusoid is A volts. The noise power in the demultiplexer filter bandwidth of 1.4 f_b is N_1 (watts in 1 ohm reference). The dotted line curve on Figure 19 shows the calculated probability of error versus $\frac{A}{\sqrt{N_o}}$ dB for the Dynatronics BSC-7B bit synchronizer. The Dynatronics BSC-7B, a reset - integrator decoder, was used in the IRIS channel of HDRSS-B.

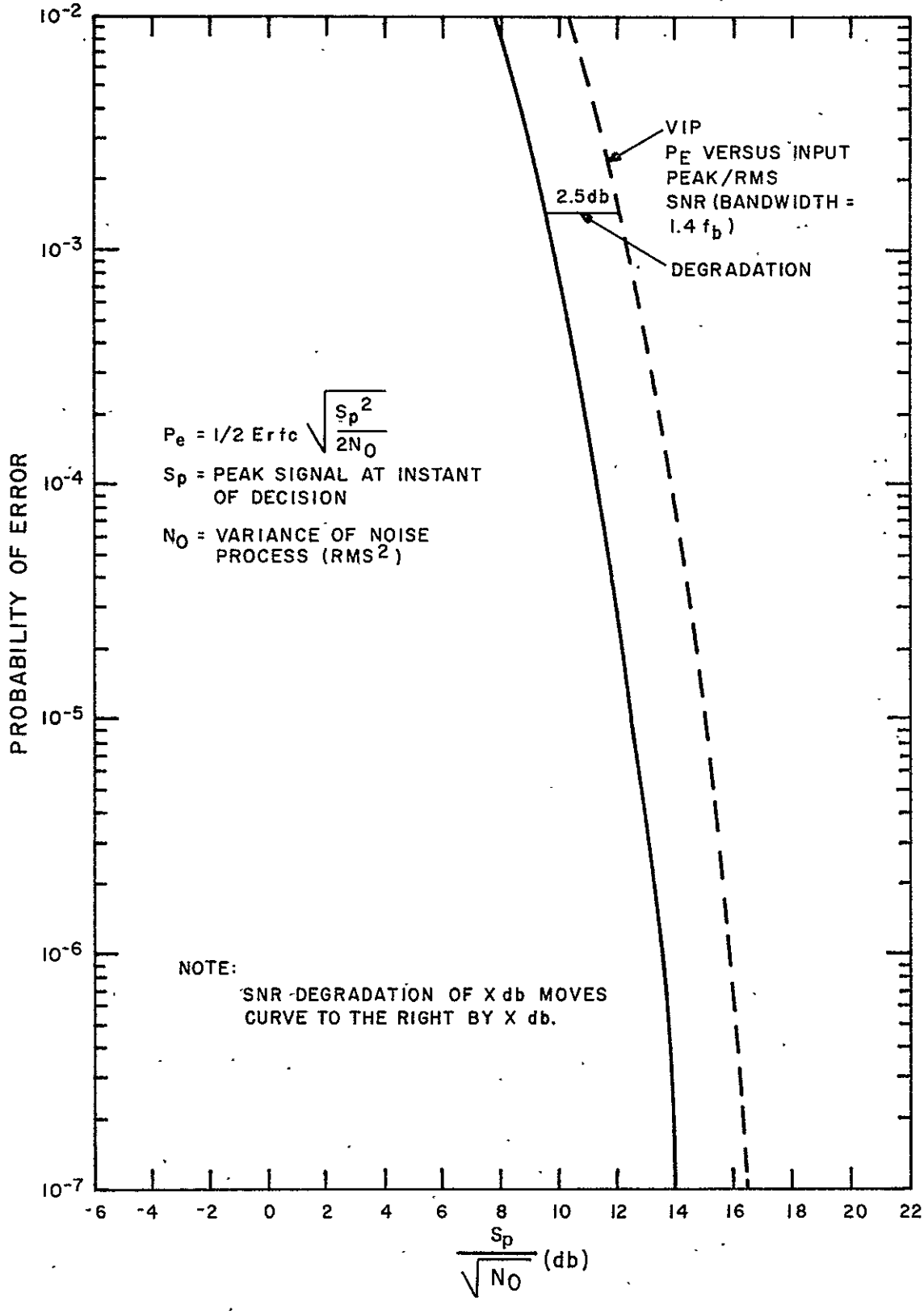

Figure 19. Probability of Error at a Threshold Detector (Bipolar Signal)

The solid curve on Figure 19, is the Probability of Error curve versus the peak signal-to-rms noise ratio required at the threshold detector at sampling instants. The relationship between the input peak-signal-to rms noise ratio ($A/\sqrt{N_1}$) to the peak signal to the peak signal-to-rms noise ($S/\sqrt{N_0}$) at the threshold detector is defined in Appendix VII. For VIP, the ratio is 2.5 db; this takes parabolic distribution of noise into account.

For a Bit-Error-Rate (BER) of 1×10^{-6}, the signal-to-noise requirement in the VIP channel bandwidth is 16.0 dB peak/rms (13.0 db rms/rms). When the data pattern is either a long string of binary ones, binary zeros or binary continuation of zero/one, the patterns produced are sinusoidal output waveform and the multiplexer output level is adjusted to yield the assigned peak deviation.

Where random data is transmitted, there will be an effective signal-to-noise ratio degradation due to intersymbol interference caused by bandwidth limitation and phase non-linearity. The signal loss occurs in a few bits in a given word and it is sensitive to word pattern. Nevertheless, in order to maintain a low BER, the link SNR must be increased accordingly. Other factors contributing to signal loss are discussed in Paragraph 6, Design Considerations.

6. System Design Considerations

a. Introduction

The system is designed with the following objectives:

- The BER rate would be 1×10^{-6} in the absence of tape recorder dropouts.
- The bandwidth of the VIP channel would provide a well behaved response, i.e., the output waveform would not exhibit excessive zero-crossing jitter or excessive signal loss due to intersymbol interference. Sensitivity to word pattern variations would be minimal.
- The maximum acceptable phase delay distortion would be determined.
- Minimize the fold-over energy by proper pre-filtering.
- Minimize the amount of signal interference into the pilot tone and limit the phase jitter to a small value.
- Minimize crosstalk into adjacent channels.

The system performance was evaluated in order to determine the impact of degrading factors not directly controllable in the design of the multiplexer/demultiplexer. Among the most important factors are tape recorder flutter and dropouts. The system performance analysis is given in tabular form. The overall performance objective is a maximum Bit-Error-Rate of 1×10^{-5}.

The Bit-Synchronizer considered in the analysis was the Dynatronics BSC-7B, a reset integrater type, used in the IRIS channel of HDRSS-B.

b. Prefiltering of VIP Data

The power spectral density of random biphase data is shown on Figure 20. Due to bandwidth limitations, the frequency spectrum will be truncated above a frequency equal to 182 kHz or 1.4 times the bit rate. This filtering is done in the multiplexer after frequency translation with a 355 KHz local oscillator. The filtered biphase signal is frequency shifted in a double-balanced modulator and applied to a 175 to 343-kHz bandpass filter that rejects the upper sideband frequencies.

A frequency 2.78 times the bit rate (355 kHz) corresponds to the d-c component after the mixing process. Any components avove 2.78 times the bit rate will be folded over, and any frequency 4.2 to 5.6 times the bit rate will overlap the useful spectrum. Since the overlap occurs, before the bandpass filter, filtering from 4.2 to 5.6 times the bit rate (538 to 720 kHz) is needed. An attenuation of 40 dB or more over that range will maintain the level of interference to less than 50 dB below the power in the useful spectrum.

c. Bandwidth and Phase Linearity Requirements

(1) Introduction. A computer simulation was performed to determine the relationship of signal loss to bandwidth and phase non-linearity for sharp-cut-off channels (Refer to Appendix III). The result of the computer simulation indicated that the minimum bandwidth relative to the bit rate should be about 1.4 to produce a reasonably well behaved response, i.e., a response which is fairly insensitive to word patterns. The behavior is not too strongly dependent on phase nonlinearity, however, signal loss increases with the amount of phase nonlinearity. A peak-to-peak group delay distortion equal to 0.59 times the bit duration was found acceptable when signal loss and equalizer complexity requirements were considered.

Figures 21 and 22 show the specified values of amplitude and time delay, and the approximate curves used in the analysis. The time delay $T_d(\omega)$ is defined as $\phi(\omega)/\omega$.

(2) Signal Loss Calculations by Computer Simulation. During the simulation, the amplitude response was assumed flat from dc to cut-off frequency. The channel actually suppresses signal energy below 12 kHz. This was done in order to provide sufficient attenuation of the upper sideband of the subcarrier spectrum. Note that all signal filtering is done in the bandpass filters of the multiplexer and demultiplexer. The purpose of the lowpass input and output filter is to remove frequency components that would result in a fold-over spectrum, and to remove intermodulation products during the synchronous demodulation process. The channel baseband bandwidth is completely determined by the band-pass filters; the phase nonlinerity contribution of the low-pass filters is negilgible since those filters are not required to have steep attenuation slopes.

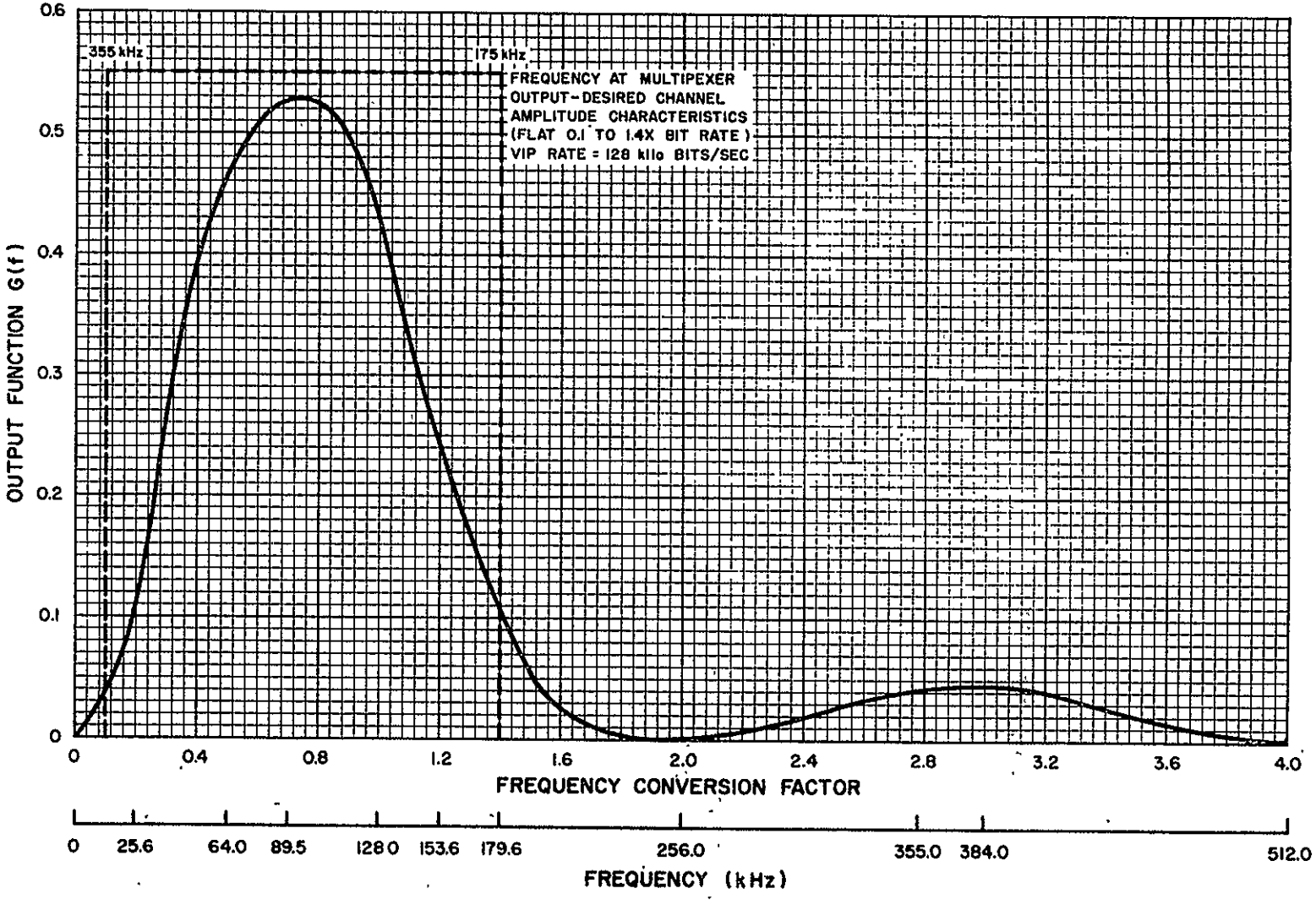

Figure 20. Power Spectral Density for Random Biphase Data

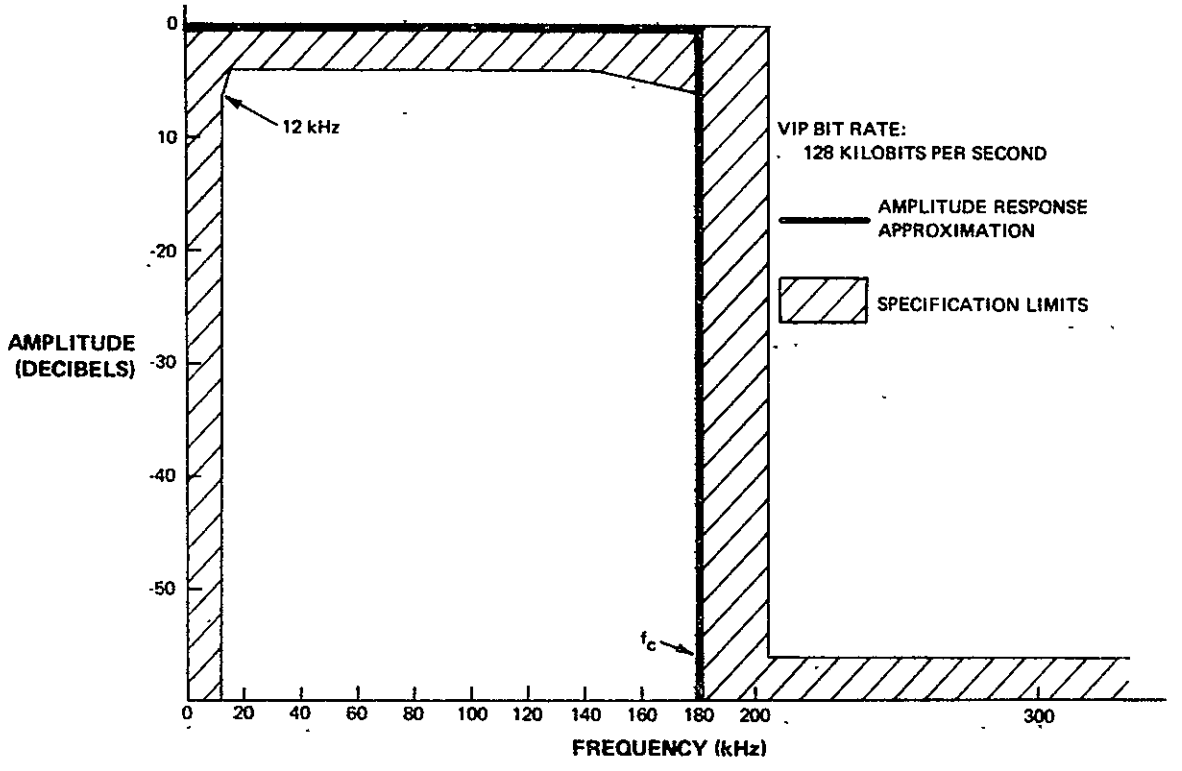

Figure 21. Approximation of Amplitude Response

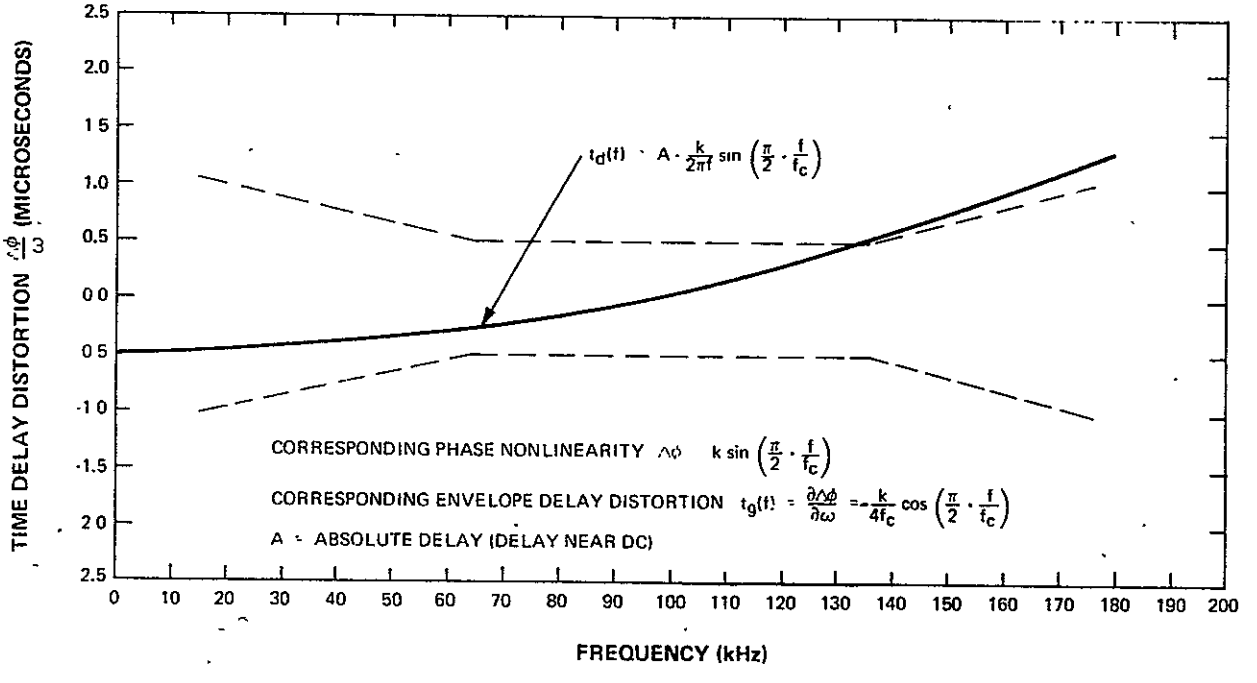

Figure 22. Approximation of Nonlinear Phase Component

The effect of suppression energy below 12 kHz has been investigated separately and, together with the effect of the state phase error in the pilot tone. The analysis has shown that the amount of signal loss is not significantly different from the values obtained with the approximations of Figures 21 and 22.

The phase nonlinearity is approximated by a quarter of a sine wave from d-c to the cutoff frequency. This is a fairly good assumption when a sharp cutoff filter is used. When an equalizer is used in addition, the phase linearity becomes more sinusoidal and more ripples appear in the passband.

For a fixed, peak-to-peak, time-delay variation, the pulse distortion is reduced when the number of ripples is increased. This fact can be easily verified by the paired-echo analysis.* Approximating the phase non-linearity by a quarter of a sine wave will produce greater pulse distortion than that obtained in an equalized channel. This fact was verified by comparing calculated waveforms with waveforms produced by the HDRSS Multiplexer/Demultiplexer breadboard; the calculated waveforms showed greater distortion than the actual waveforms from the equalized channel of the multiplexer/demultiplexer.

Analytical studies** indicate that the worst case of phase distortion for a sharp cutoff channel is close to sinusoidal.

(3) Binary Words. The response of the VIP channel was calculated for the following biphase words:

Word A (27 bits): 111111111100011011000101010

Word B (28 bits): 1111111110111111111110000000

Word C (30 bits): 111110000011111000001111100000

(4) Bit Integration. The reset integrator of the Dynatronics BSC-7B Bit Synchronizer, under the timing control of the clock, first integrates the area under the first half of a bit and then the area under the second half. The second integration is subtracted from the first. The net result is the peak voltage appearing at the decision device at the end of the integration period.

The presence of intersymbol interference results in a net integrated area that is smaller than the area obtained from the sinusoidal reference signal at bit-rate frequency (an input sequence of "ones" into the channel). The ratio of integrated

*H. A. Wheeler, "The Interpretation of Amplitude and Phase Distortion in Terms of Paired Echos," Procedings of the IRE, Vol. 27 pp 359-385, June 1939

**R. W. Lucky, "Analysis Relating Delay Variation and Intersymbol Interference", Bell System Technical Journal Volume 42, pp. 2247-2484 September 1963

area to reference area is the amount of intersymbol interference. The signal power must be increased by that factor to maintain a sufficient margin against noise.

The reference voltage level can be calculated easily. When a periodic sequence of "ones" is applied to the band-limited channel, all harmonics are filtered out and only the fundamental appears at the decoder input. For the sinusoidal signal, the wave function f(t) is given by

$$f(t) = A \sin 2\pi f_b t \tag{1}$$

where

A is the peak sine-wave voltage at the decoder input, and

f_b is the bit-rate frequency

The peak signal voltage S_p appearing at the threshold device at the end of the integration period is

$$S_p = \int_0^{T/2} f(t)dt - \int_{T/2}^{T} f(t)dt \tag{2}$$

For the sinusoidal signal,

$$S_p = \frac{4A}{\omega_b} = \frac{2A}{\pi} T \tag{3}$$

where

$\omega_b = 2\pi f_b$, and

T is the bit duration

The voltage given by equation 3 is the reference voltage level.

The amount of intersymbol interference is a function of the word pattern. When the word pattern is not periodic, there will be interference between adjacent bi-phase bits. The waveform will be distorted and the integrated area will be smaller than $4A/\omega_b$ for some bits in the particular word tested. This effect is illustrated in Figures 23 and 24.

(5) Results of Integration Program. A computer program was used to perform the integration of equation 2 for the waveforms of words A, B, and C. The results of the program are shown in Table 11.

The greatest intersymbol interference was found to be 2.8 dB, which is the value used in the system performance evaluation of the VIP channel. This interference occurred in word B at bit No. 11, which is the "one" following the first "zero." This "zero" is preceded and followed by a long string of "ones."

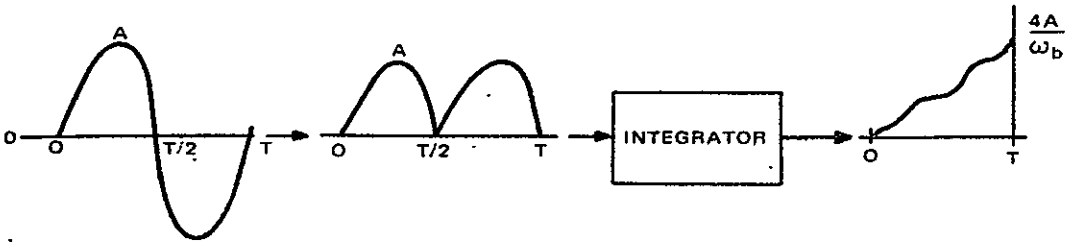

Figure 23. Operation of Reset-Integrator Decoder on a Sinewave

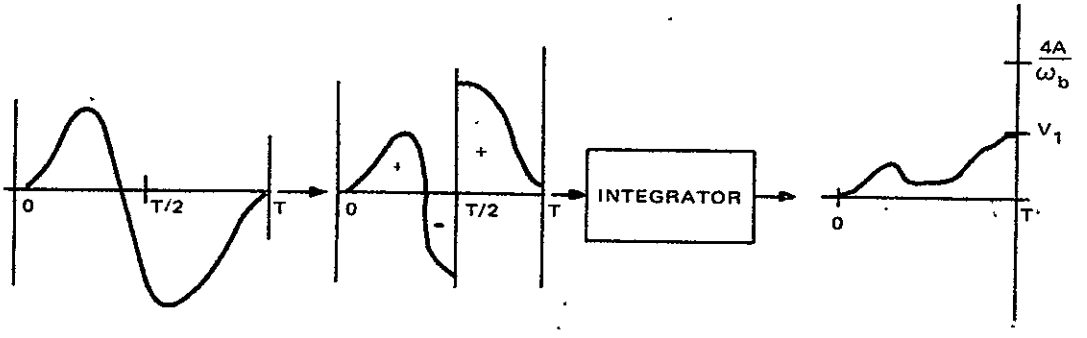

Figure 24. Operation of Reset-Integrator Decoder on a Bit Distorted by Intersymbol Interference

TABLE 11. RESULTS OF INTEGRATION PROGRAM

Word	Intersymbol Interference (decibels)	Bit No.*	Binary Symbol	Remarks
A	-2.4	19	"zero"	
B	-2.8	11	"one"	
C	-2.4	6,11,16...		Repeated every five bits
*Bit number where worst interference occurred.				

(6) Timing Errors. Intersymbol interference also disturbs the zero-crossings of the filtered biphase waveform. In the "square-pulse" biphase format, there is a zero-crossing in the middle of each bit. "One" bits are negative-going at the zero-crossing; "zero" bits are positive-going. The presence of intersymbol interference shifts the crossing from its ideal position in the middle of the bit. The largest timing shift usually occurs at, or in the vicinity of, the bit suffering the worst intersymbol interference. The peak timing shift ΔT is expressed as the percentage of the duration of a single bit.

The words A, B, and C start with a number of binary "ones" establishing a steady-state, sinusoidal reference. It was assumed that (1) the phase-locked loop (PLL) of the decoder is locked to this reference and (2) the PLL bandwidth is sufficiently narrow so that the timing will stay synchronized to the sinusoidal reference for an appreciable number of bits after the transition from the periodic sequence of "ones."

The timing shifts that were obtained in this fashion are greater than those that will be experienced during actual operation of the system. In the real situation, the data are more likely to be some random combination of "ones" and "zeros," rather than a long string of "ones" followed by random data followed by another string of "ones", etc. Consequently, the phase-lock loop will produce a timing waveform that is "centered" on the average positions of the zero-crossing. The peak timing shift ΔT on either side of this extracted timing-clock signal will be less than the peak ΔT obtained in the simulation.

The signal loss due to timing shifts is not an additional loss, but is an intrinsic part of the signal loss due to the integrated-area reduction produced by intersymbol interference. However, large timing shifts resulting from intersymbol interference, when combined with other timing shifts in the system, might have a detrimental effect on overall system performance. For that reason, channel bandwidth and phase equalization should be selected to minimize timing shifts. The maximum timing shifts of the VIP channel are listed in Table 12.

TABLE 12. VIP CHANNEL TIMING SHIFTS

Word	Maximum Peak Timing Shift (percentage of single-bit duration)
A	-3.0
B	-4.0
C	-3.0

The minus sign indicates that the zero-crossing in the filtered word is early with respect to the ideal position.

(7) Conclusions. In calculating the intersymbol interference of the VIP channel, the greatest degradation was obtained for word B, where a "zero" is preceded and followed by a long string of "ones." The selected bandwidth ($f_c = 1.4f_b$) can be considered almost optimum, since a further increase in bandwidth does not produce any substantial reduction of signal degradation. (Refer to Appendix III). At this bandwidth, system performance does not vary significantly with different word patterns, and zero-crossing shifts are small. (Refer to Tables 11 and 12). Conversely, the curves in Appendix III show that for normalized bandwidths less than 1.3 the system becomes very pattern-sensitive, and zero-crossing shifts are fairly large as intersymbol interference increases rapidly with decreasing bandwidth. The analysis of the VIP channel revealed that for best performance the normalized bandwidth of the sharp-cutoff biphase channels should be between 1.3 and 1.4.

d. Effect of Static Phase Shift and Bandwidth Truncation on VIP Channel Performance

The demultiplexer pilot-tone phase-lock loop of the VIP channel will have a static phase error ϕ_{ss} due to uncertainties in the pilot-tone and VCO frequencies. The maximum phase error specified for the multiplexer/demultiplexer is 0.12 radian rms (6.9 degrees rms). This phase error includes noise-induced jitter, VCO jitter, and static phase error. For the VIP channel, the phase jitter is negligible with respect to the static phase error; therefore, a maximum static phase shift of close to 6.9 degrees is allowed. (Note: the static value is equal to the rms value.)

The paired-echo method of analysis, used to gain insight into the relationship between phase distortion and intersymbol interference, cannot be used conveniently to obtain the effect of static phase shifts. A new program was written which essentially calculates the Fourier Spectrum of a repetitive biphase word and modifies the phase and amplitude of the components by the phase and amplitude characteristics for the filter of interest. The "Fourier program" was run with various amounts of positive and negative phase shifts superimposed on the

sinusoidal phase-distortion component. The total phase error ϕ_{total} is given by

$$\phi(f)_{total} = -\left[k \sin\left(\frac{\pi}{2} \cdot \frac{f}{f_c}\right) + \phi_{ss}\right]$$

Most of the computer runs were performed with the channel amplitude response assumed flat from d-c to the cutoff frequency. Some runs were performed with a low-frequency cutoff of 0.1 times the bit-rate frequency. The main effect of the bandwidth truncation and of the static phase shift was an increase in the timing shifts for positive phase shifts. The signal level was virtually unchanged. The signal losses and timing shifts obtained are listed in Table 13.

TABLE 13. EFFECT OF STATIC SHIFT AND BANDWIDTH TRUNCATION

Static Phase Shift (degrees)	Relative Bandwidth	Loss (dB)	Zero-Crossing Shift (% of bit)	Word	Remarks
0	d-c to 1.4	2.8	4.0	B	Bandwidth is relative to bit rate.
+5	d-c to 1.4	2.8	6.0	B	
-5	d-c to 1.4	2.7	2.5	B	
+10	d-c to 1.4	3.5	7.5	B	
+10	0.1 to 1.4	2.8	7.5	B	Bandwidth truncated
-10	0.1 to 1.4	2.2	1.0	B	
-10	0.1 to 1.4	2.7	3.8	A	
-10	d-c to 1.4	2.6	2.5	B	
+15	d-c to 1.4	3.5	11.0	B	
+20	d-c to 1.4	3.5	11.0	B	
-20	d-c to 1.4	3.5	2.5	B	

e. Signal Interference Into the Pilot Tone

(1) Random Signals. Figure 25 shows a plot of the power spectral density and the cumulative power of the cumulative power in a random biphase signal*. The biphase signal is not filtered, i.e the waveform is a square wave. The total average power is normalized to unity (the square pulses take values +1 or -1).

*J. C. Springett, Telemetry and Command Techniques for Planetary Spacecraft, Jet Propulsion Laboratory, January 15, 1965.

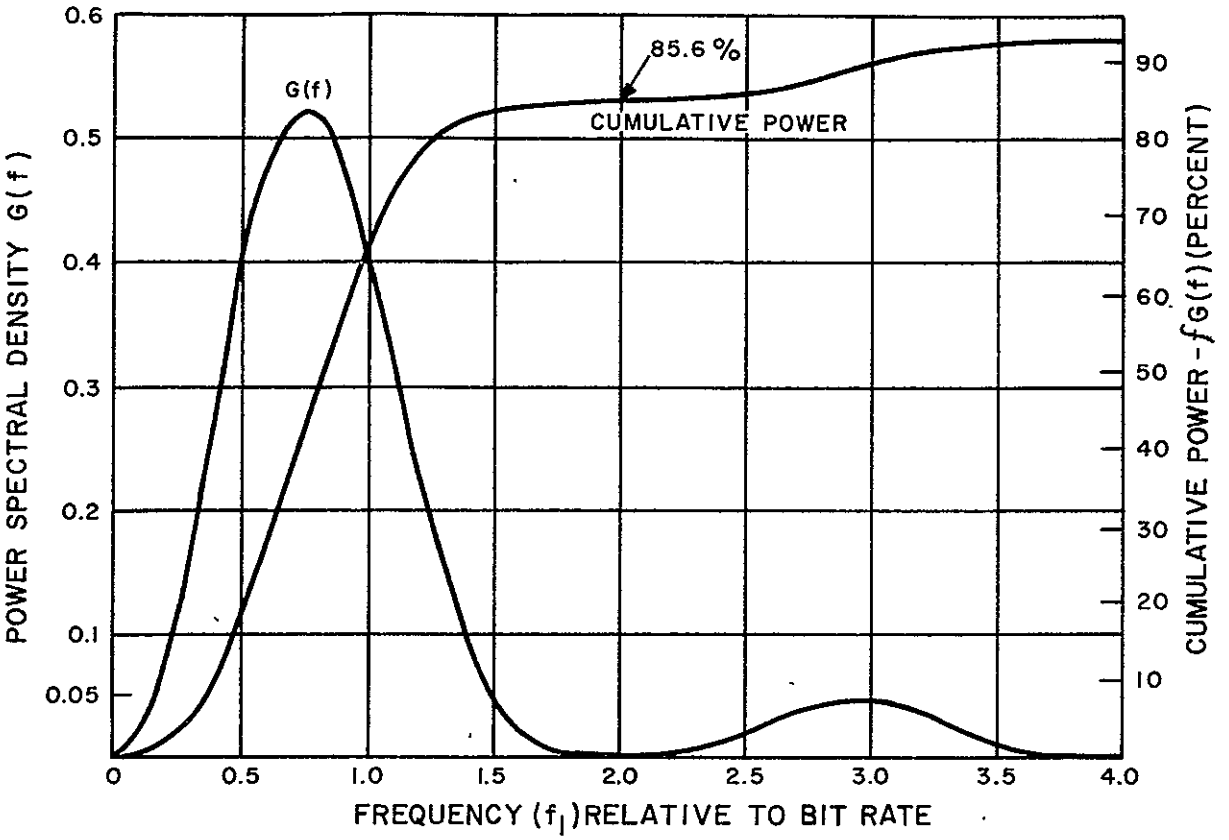

Figure 25. Power Spectral Density and Cumulative Power for Random Biphase Data

Around DC, the power spectral density G(f) is parabolic, $G(f) = k_f^2$. The cumulative from DC to frequency (f_1) is a cubic given by $P_{(f1)} = K_{f1}^3/3$.

According to Figure 25, the power below 0.1 x bit rate is about 1 percent of the total square wave power. This corresponds to 1.2 percent of the power in the bit rate sinusoidal signal (the reference signal). The bandpass filter has an equivalent low pass cutoff of approximately 7.5 kHz or 0.06 of the bit rate.

The signal power appearing in the filter bandwidth is then:

$$P_I\% \approx 2 \times 1.2 \times (0.6)^3 = 0.53\% \ (-22.8 \text{ db})$$

The factor of (2) in the calculation of $P_I\%$ takes care of the signal energy appearing on both sides of the subcarrier frequency (355 kHz - which corresponds to dc after demodulation). Actually the VIP demultiplexer filter rapidly attenuates the upper sidebands above 355 kHz so that the value of P_I is pessimistic.

(2) Non random Signal. As an added verification of the interference level into the bandpass filter, the calculations were performed for a repetitive word made up 1 "zero" imbedded in m "ones". The results listed in Table 14 show that the level

TABLE 14. VIP PILOT TONE-TO-INTERFERENCE RATIO

Word "ones"/"zeros"	Sideband Freq: Nearest Pilot Tone (kHz)	Sideband Level* (dB)	Sideband Pair* (dB)	Pilot* (dB)	Pilot/Interference Ratio (dB)	Minimum Filter Attenuation (dB)	Pilot/Interference Ratio After Filtering (dB)
9/1	±12.8	-26.2	-20.2	-16.7	+ 3.5	40.0	43.5
12/1	± 9.8	-30.4	-24.4	-16.7	+ 7.7	15.0	22.7
19/1	± 6.4	-37.7†	-31.7	-16.7	+15.0	6.0	21.0**
19/1	±12.8	-31.7††	-25.7		+ 8.0	40.0	

*Sidebands and Pilot Tone Levels are referenced to the bit rate signal level
†First Harmonic
††Second Harmonic
**Two Sideband pairs

of interference is about 21 dB when the bandpass filter meets the minimum attenuation limits of Figure 26. Figure 26 also shows the measured value of the breadboard model and the predicted computer model used in the analysis. The derivations supporting the spectrum is contained in Appendix V.

f. RMS Jitter in Extracted Pilot Tone

The signal-to-noise ratio due to leak noise in the input bandpass filter is 20 dB rms/rms in 15 kHz under worst case limit conditions (Refer to Table 9). The pilot tone amplitude is 16.7 dB smaller than the VIP signal. The parabolic nature of the noise was taken into account in the calculation.

The signal-to-interference ratio due to the VIP signal was shown to be about 21.0 dB rms/rms in the bandpass filter bandwidth. Combining the two numbers results in a signal-to-noise ratio of 17.5 dB rms/rms. Combining these numbers consists of adding the noise and interference powers.

The rms phase jitter θ_{rms} equals $= \sqrt{N/2S}$ where S/N is the signal-to-noise ratio of the noise bandwidth of the phase lock loop.

This bandwidth is not specified directly in the multiplexer/demultiplexer performance specification.

For a 1000-Hz bandwidth, the rms jitter would be 0.095 radians rms. However, in the breadboard, the bandwidth is smaller than this value. The measured rms jitter (not including static phase shift) is about 0.006 radians (0.3 degrees rms).

g. Timing Errors

(1) Introduction. The biphase signal at the demultiplexer output is degraded by timing jitter from various sources.

- Asymmetry in input data to tape recorder
- Clock Jitter
- Jitter caused by flutter
- Jitter caused by noise at the input to the tape recorder limiter
- Drift in the VIP bit rate, decoder VCO frequency, and tape recorder speed (These produce a static phase error in the clock extracting phase lock loop of the bit synchronizer)
- Waveform distortion due to intersymbol interference.

*The performance specification, RCA drawing PS-1967617, defines the maximum rms phase error as 0.2 radians rms with an input SNR of 18 dB rms/rms in the bandpass filter. The static phase error is included into the rms phase error.

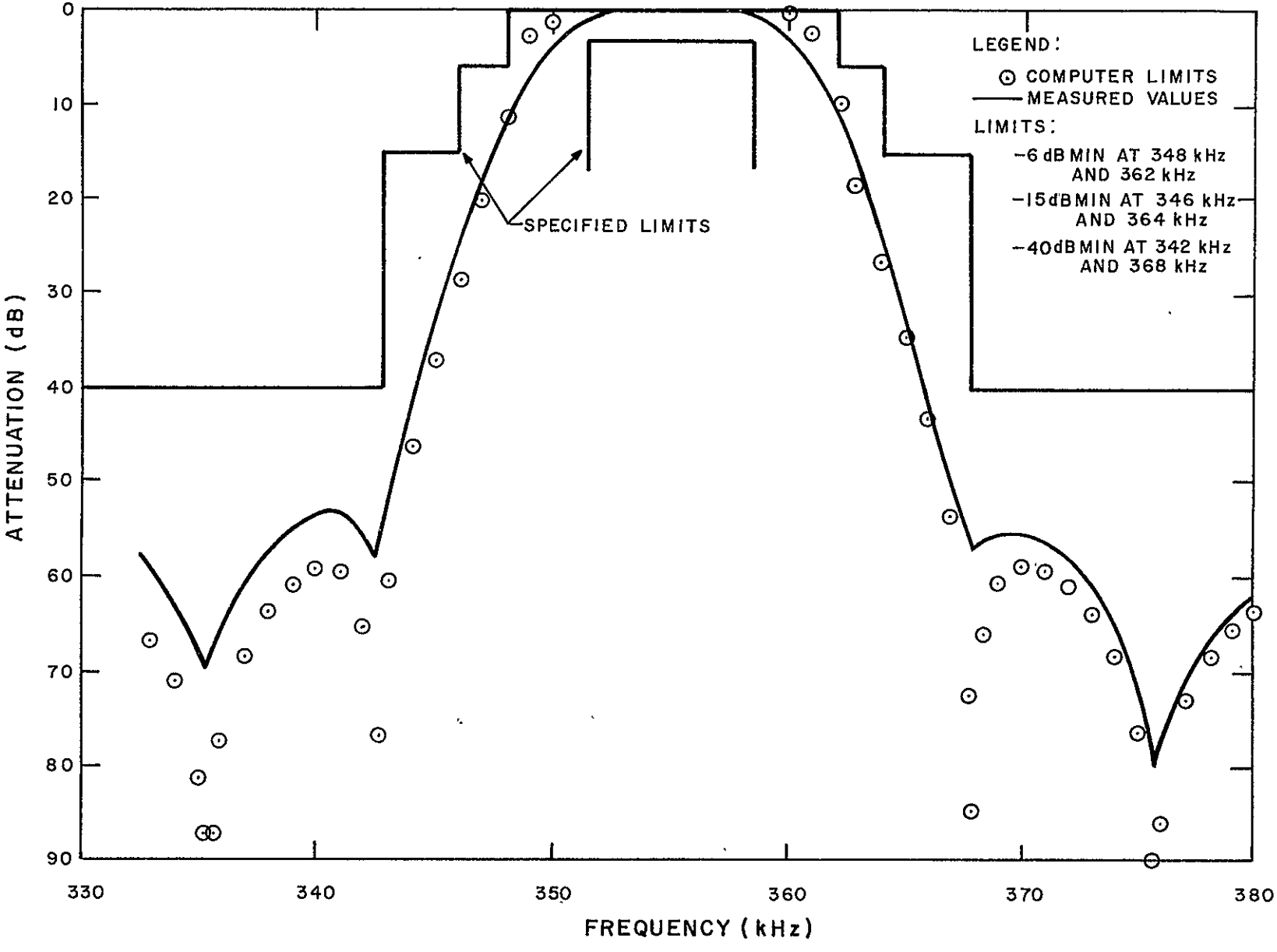

Figure 26. Measured VIP Carrier Filter-Attenuation With Specified Limits and Computer Evaluation Comparison

These timing jitters cause signal loss because they introduce a phase error in the extracted clock. The Dynatronics BSC-7B Bit Synchronizer (considered in this study) is of the reset integrator type.

Figure 27 shows a simplified block diagram of a reset integrator decoder. The phase-locked loop extracts the timing signal from the incoming data. This timing signal is used to invert the second half of any bit before applying it to the reset integrator. In an actual decoder this inversion is accomplished by appropriately gating one of two data channels into the integrator. The data in both channels are identical except for a polarity change. During the time interval corresponding to the first half of the bit, the biphase data is connected to the integrator with no polarity inversion. During the second half of the bit the second channel carrying the inverted data is connected to the integrator. In Figure 27, this inverting operation is represented by a multiplication of the incoming data by the square-wave clock signal from the phase-locked loop. The filtered biphase "1" is shown as it appears at the decoder input and at the reset integrator. A biphase "0" would be treated the same but all waveforms along the decoder would have the opposite polarity.

A timing error ΔT will result in the situation where the start of a bit integration is either too early or too late. The exact calculation of signal loss is rather involved. An approximate calculation, based on the assumption that a periodic sequence of binary ones or zeros is transmitted, indicates that the demux output will be a sinewave at the bit-rate frequency (fb), since only the fundamental is transmitted. When other patterns are transmitted, intersymbol interference will distort the waveforms and produce signal loss. This loss is due to both a waveform attenuation and a timing shift introduced by intersymbol interference. Consequently, for the purpose of calculating signal loss, the timing shift due to intersymbol interference will not be combined with the other timing errors. The remaining timing errors are combined as an rms sum (ΔT_{rms}) since they originate from independent sources. The corresponding rms phase error ϕ_{rms} is equal to $2\pi \Delta T/T$ where T is the bit duration.

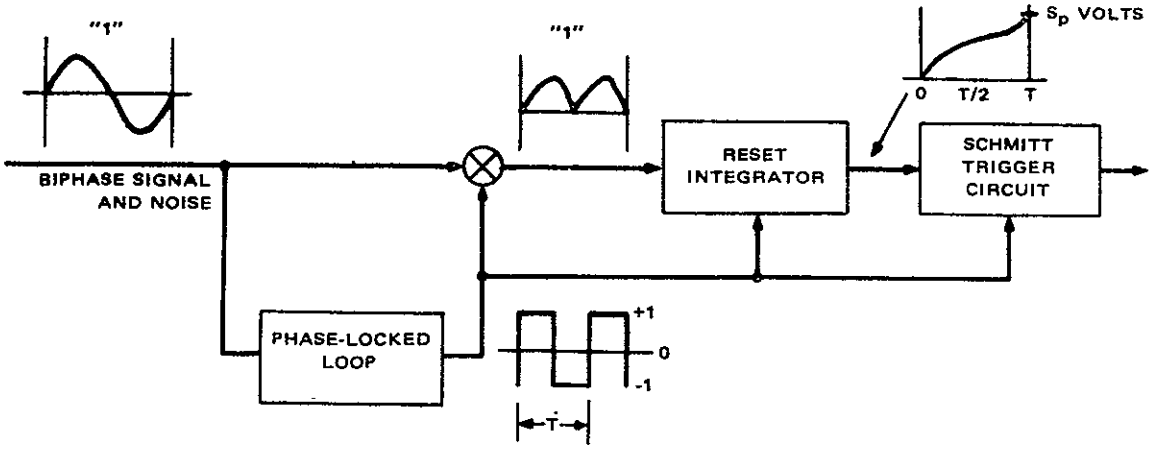

Figure 27. Simplified Block Diagram of Reset Integrator Decoder

For a 1111 ... pattern, the signal loss would, in general, be cos $\hat{\phi}$, where $\hat{\phi}$ is the phase error at a given bit. The phase error (cos $\hat{\phi}$) is random with an rms value (ϕ_{rms}). In the link analysis, the calculated loss for $\hat{\phi}$ is 3 ϕ_{rms}.

When a bit is distorted by intersymbol interference, the additional loss due to timing errors is given by the same formula [cos (3 ϕ_{rms})] used for a sinusoidal waveform. For small timing errors, as in the VIP channel, this is a reasonable assumption. For other systems which exhibit large timing shifts induced by intersymbol interference, the approximate calculations might not be valid.

(2) Tabulation of Timing Errors. The various peak timing errors are first converted to rms by dividing by a crest factor of 4 which is a commonly used value for such conversions. The total rms timing error (σ) is calculated and the signal loss is calculated for the 3σ value. The approximate loss (L) is defined as

$$\cos 2\pi (3\sigma)$$

The timing errors are tabulated in Table 15.

The tape recorder contributes most of the timing errors. The tape recorder cumulative timing error of 1.3 percent rms is the contribution due to flutter components which are not tracked by the decoder phase lock loop for a bandwidth setting of 2.8% of bit rate ($\approx$ 3600 Hz). The bandwidth setting is the frequency at which the Dynatronics Decoder has an open-loop gain of 0 dB, and corresponds loosely to the maximum frequency the loop will track. The "cumulative flutter jitter" specification of the tape recorder is 0.1 microseconds rms or 1.3 percent of 1 bit for components in the band of 3.0 kHz to 60 kHz (those not tracked by the loop). The tape recorder prelimiter SNR of 26 dB p-p/rms produces an rms jitter of 1.6 percent at the limiter output. Jitter is related to the rms/rms SNR by $\Delta T/T = 1/2\pi \sqrt{N/2S}$.

The static phase error due to frequency drifts is given by the formula

$$\frac{\Delta T}{T} = \frac{1}{2\pi} \frac{\Delta f}{G/2\pi} = \frac{\Delta f}{G}$$

where

Δf is the total frequency shifts (data, VCO, and Tape Recorder) and

G is the dc loop gain of the decoder 2nd order tracking loop.

For a 2.8 percent bandwidth, the dc loop gain has been calculated to be $G = \pi$ n x 1.41×10^4 based on open-loop characteristics of the Dynatronics Bit Synchronizer.

The total (3σ) loss due to timing errors is 1.2 dB.

TABLE 15. VIP TIMING ERRORS

	Peak (%)	RMS (%)	Reference	Remarks
I. Static Asymmetry				
Tape Recorder + Input Source	±1.5	0.375	See Note 1	Crest factor of four
Multiplexer/Demultiplexer	±1.0	0.250		
RMS Sum		0.450		
II. Bit-to-Bit Jitter (Due to clock jitter and pattern shift).				
Input Source	±0.5	0.125	See Note 2	
Tape Recorder	±6.0	1.5	See Note 1	
Multiplexer/Demultiplexer	N/A	N/A		Included in inter-symbol interference.
RMS Sum		≈1.5		
III. Cumulative Timing Error				
(Due to Tape Recorder Flutter into Dynatronics Decoder at 2.8% bandwidth setting).		1.3	See Note 1	
IV. Timing Jitter (due to prelimiter SNR of 26 db p-p/rms)		1.6	See Note 1	
V. Static Phase Shift				
of Dynatronics Decoder at 2.8% Bandwidth setting.		0.8		
Static Phase Shift is Caused By:				
VIP Data Drift:		±0.02	See Note 2	D.C. Loop
VCO Drift (Assumed):		±0.02		gain $\approx 2\pi \times 1.41 \times 10^4$
T/R Drift:		±0.5	See Note 1	
Total RMS Sum (σ)		2.7		
3σ Value		8.1		

Note 1. Refer to HDRSS Tape Recorder Performance specification, RCA Dwg. PS-1967674

Note 2. GSFC Specification S-731-P-40 dated July 13, 1966; Modified May 17, 1967. High Data Rate Storage System of the Nimbus D Meteorological Satellite.

7. VIP System Performance Analysis

a. Introduction

The performance objective for the VIP channel is a maximum bit-error-rate of 1×10^{-5}. The system is designed to have a bit-error-rate of 1×10^{-6} in the absence of tape drop-outs and the presence of all the other degrading factors listed below.

Some statistical information exists about the amplitude distribution of the playback signal where a drop-out occurs. Using this information in a simple analysis shows that the system performance will be met in the presence of drop-outs.

b. Factors Degrading the Received Signal-to-Noise Ratio

The block diagram of the HDRSS-D VIP channel is shown on Figure 13. The minimum value of the signal-to-noise ratio at the input to the decoder was shown to be 16.0 dB peak-to-RMS (13.0 dB rms/rms) in 180 kHz bandwidth (refer to Paragraph B.5.).

The amplitude of the VIP signal at the multiplexer output is adjusted to deviate the transmitter by ±300 kHz (nom.) with a square wave input to the multiplexer. Under these conditions the transmitted signal is a sinewave at the bit-rate frequency. The received signal-to-noise ratio is calculated for this condition and under the assumption of worst-case carrier-to-noise ratio at the receiver. This calculation yields a margin above the required SNR. The calculation is further refined by calculating the additional losses introduced by the following factors.

(1) Dynamic Signal Variations. This includes drift in the multiplexer output level, effective amplitude response tolerance of the multiplexer, intersymbol interference, pilot-tone phase error, and timing errors. A summary of dynamic signal variations are listed in Table 16.

(2) Crosstalk from Adjacent Channels. The crosstalk consists of a linear component due to the finite attenuation slopes of the multiplexer filters; and a non linear component due to transmitter and multiplexer amplitude non-linearity, the finite IF bandwidth of the FM receiver and the IF phase nonlinearity.

The losses due to crosstalk were calculated for the condition where the transmitted signal is a sinewave i.e. in the absence of intersymbol interference. The VIP signal-to-noise ratio for a bandwidth/1.4 x the bit rate is 28.8 dB. Removing the effects of multiplexer amplitude loss (2 dB) and the long term signal losses (3.2 dB) yields a signal-to-random noise ratio of 23.6 dB. The signal-to-crosstalk ratio is 25.8 dB (refer to Table 8). This yields a net SNR of 21.6 under these conditions or a loss of 2 dB. The assumption that the loss is approximately unchanged in the presence of intersymbol interference was used.

TABLE 16. VIP DYNAMIC SIGNAL VARIATIONS

	Losses (dB)	Reference	Remarks
I - Multiplexer Amplitude Response	-2.0	Refer to Note 1	
II - Mux/Demux Intersymbol Interference (Due to bandwidth limitation and phase nonlinearity)	-2.8	Table 11	
III - Long-Term Signal Amplitude Variation (Voltage level, impedance variation, transmitter sensitivity)	-3.2	Refer to Appendix VII and Notes 1 and 2	
IV - Pilot Tone Phase Error			
σ = 0.12 rad. rms (6.9°)		Refer to Note 1	
3σ = 0.36 rad. rms	-0.6		cos (3σ)
Loss Due to Timing Shift	-1.2 dB	Section 5 Par. B.6.g.(2).	
Total Dynamic Signal Variation	-9.8 dB		

Note 1. RCA Astro-Electronics Division, Performance Specification, Multiplexer/Demultiplexer RCA PS-1967617.

Note 2. NASA-GSFC, Specification, High Data Rate Storage System for the Nimbus D Meteorological Satellite July 13, 1966, Modification dated May 17, 1967.

(3) Conclusions. A summary of the link analysis, including the effect of crosstalk is listed in Table 17.

c. Tape Recorder Limiter Output SNR

The specified tape recorder output SNR, 46 dB p-p/rms minimum in the limiter bandwidth, corresponds to 37 dB rms/rms. This SNR is measured in a limiter bandwidth which is an order of magnitude larger than the overall channel bandwidth. As a result, the channel bandwidth will be better than 37 dB, and the effect on the overall channel bandwidth is negligible.

TABLE 17. SUMMARY OF SNR CALCULATIONS

Parameter and Calculated Values		Reference
1. CNR in 3 mHz IF Bandwidth	18.1 dB rms/rms	Refer to Note 1
2. VIP Channel FM Improvement (I)		
Deviation = ± 300 kHz		
Lowest Subcarrier Frequency = 177 kHz (F1)		
Highest Subcarrier Frequency = 343 kHz (Fu)		
$I = 3/2 \frac{(\Delta f)^2 \times B\ IF}{(fu)^3 - (f_L)^3} =$	10.7 dB rms/rms	
3. VIP Baseband SNR (No losses for bandwidth of 1.4 x bit rate) (1 and 2)	28.8 dB rms/rms	
Total Dynamic Signal Variation	- 9.8 dB rms/rms	Table 16
4. Net VIP Baseband SNR (No crosstalk)	19.0 dB rms/rms	
Loss due signal-to-cross-talk ratio (For S/C-T = 25.8 dB rms/rms).	2.0 dB rms/rms	Para. B.7.b(2)
5. Net VIP SNR (Including cross-talk)	17.0 dB rms/rms	
Reset Integrator Decoder requirement for BER = 1×10^{-6} =	13.0 dB rms/rms	Para. B.7.b
VIP Margin	4.0 dB rms/rms	

Note 1. RCA Astro-Electronics Division, Final Report for the High Data Rate Storage System (Engineering Models EM-1 and EM-2 Appendix IV, NAS5-3772, Princeton, New Jersey, May 3, 1968

d. Effect of Tape Recorder Drop-outs

(1) Introduction. The effect of tape recorder dropouts on the final bit error rate is based on the worst case SNR of 17 dB rms/rms without dropouts (Refer to Table 17) and the cumulative distribution of drop outs (See Figure 28). The final probability of error is based on the cumulative drop-out distribution shown on curve 3, which is based on curves 1 and 2. Curves 1 and 2 are based on a HDRSS-B tape recorder study that predicted a family of curves that are essentially straight line on a logarithmic scale and parallel. The VIP channel requirements* state that the maximum number of dropouts (number of bits whose amplitude drops 40 dB or more) is 2 bits in 10^6. This point was plotted on Figure 28 and a curve was drawn on the basis of the study

*RCA Astro-Electronics Division, Performance Specification, HDRSS-D Tape Transport, PS-1967674, Contract NAS5-1D396

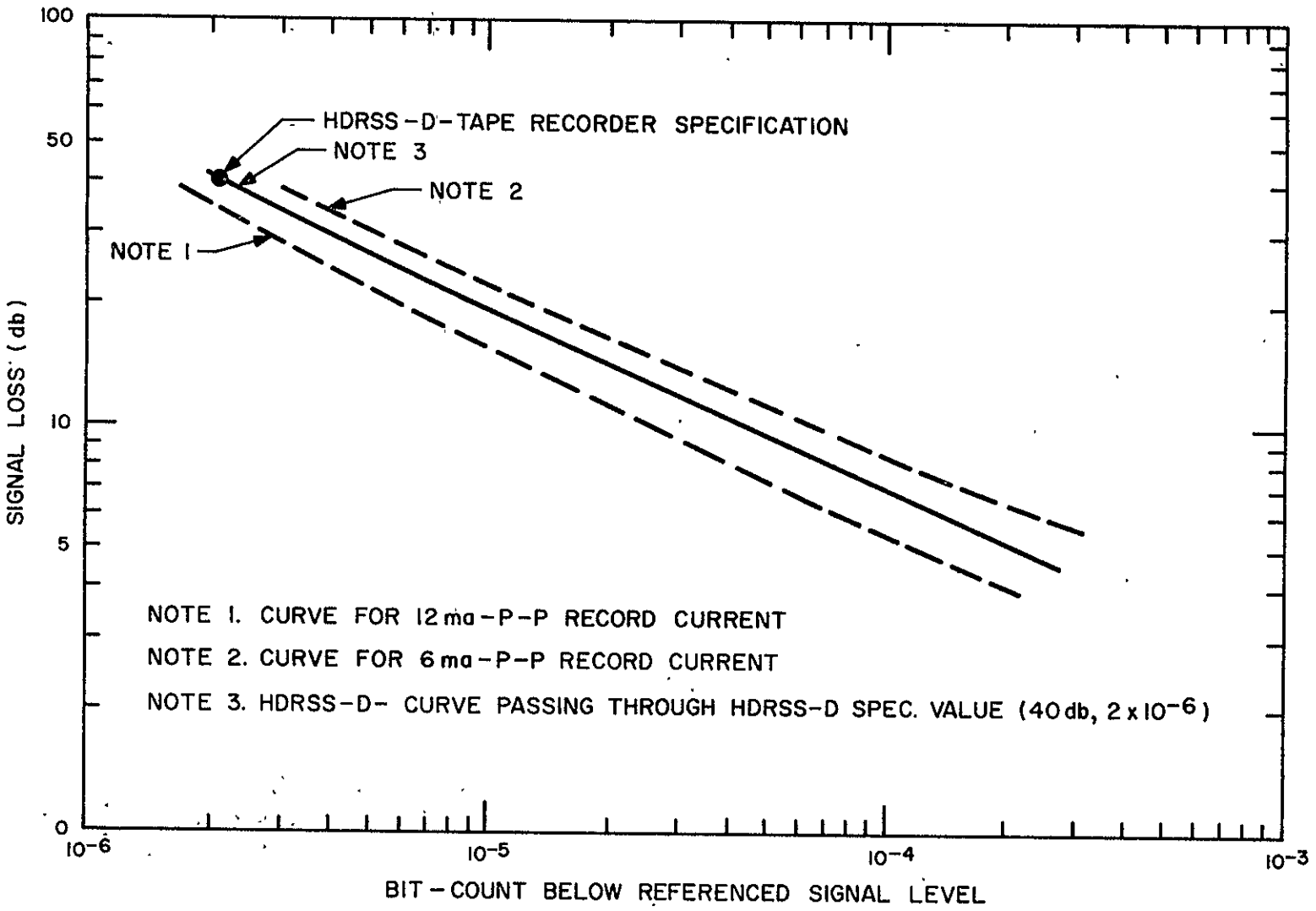

Figure 28. Predicted End-of-Life For Biphase Channel

(2) Calculation. The differential probability of making an error $dP_T(y)$ is due to two causes: Tape drop-outs and random noise. The differential probability of error is:

$$dP_T(y) = P_e(y) \times dP_d(y) \quad (1)$$

where

$P_e(y)$ is the probability of error (assuming that the signal level has dropped to (y) volts)

$dP_d(y)$ is the signal drop between (y) and (y + dy)

The probability of error $[P_e(y)]$ for the region of interest, calculated for the reset-integrator decoder for the bandpass parabolic noise spectrum of the VIP channel, is plotted on Figure 29. The total probability of error $P_T(y)$, an itegral of equation (1), is written as:

$$P_T \leq P_e(o)\,\Delta P_c(y_1) + P_e(y_1)\,\Delta P_c(y_2) + \ldots + P_e(y_{n-1}) + \Delta P_c(y_n) \ldots \quad (2)$$

Where

$\Delta P_c(y_n)$ = the probability that y lies between y_n and y_{n-1}

y_N = the no dropout level

Then

$$\Delta P_c(y_n) = \int_{y_{n-1}}^{y_n} dP_d(y)\, d_y \quad (3)$$

$P_c(y)$ is the drop-out characteristics shown on Figure 28.

Table 18 shows the calculations obtained from equation (2). This formula yields an upper-boundary on the overall probability of error. Column 2 is the probability $\Delta P_c(X_n)$ that the signal loss be anywhere between X_n dB (column 4) and the signal loss on the previous row. Column 3 is the SNR into the decoder after all losses (except drop-out) have been taken into consideration. Column 5 gives the net SNR when the signal drops X_n dB, i.e., it gives the difference between Column 3 and Column 4. Column 5, together with the decoder characteristics of Figure 29, yields the probability of error $P_e(X_{n-1})$ in column 6. Column 7 is the product $P_e(X_{n-1}) \times \Delta P_c(X_n)$. The summation of column 7 yields the upper boundary on the total error probability P_T.

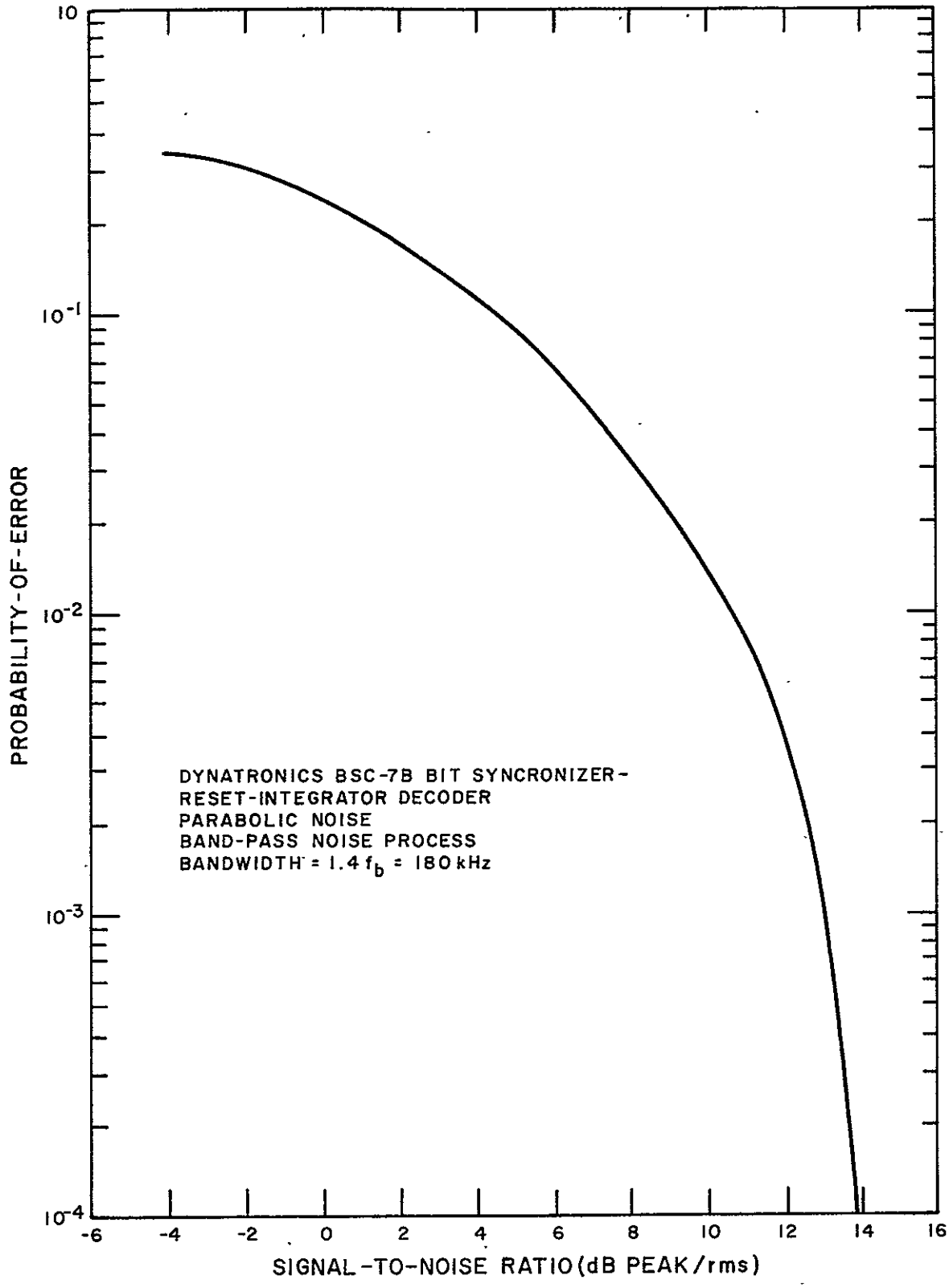

Figure 29. Calculated Probability of Error Versus Signal-to-Noise Ratio

TABLE 18. ERROR-RATE CALCULATION IN PRESENCE OF DROP-OUTS

N	A Differential Probability of Drop-Out Falling Between (X_ndB) and Preceding Values (See Figure 28, Curve 3) ($\times 10^{-6}$)	B SNR in Absence of Drop-Outs Refer to Table 17 (dBP/rms)	C Drop-Out Magnitude (x_ndB)	D Net SNR (dB P/rms)	E Probability of Error at Previous Level $Pe^{x}(n-1)$ (See Figure 29)	F Product A X E ($\times 10^{-6}$)	Remarks
1-	.2	20 (17 dB rms/ rms)	40	-20.0	0.5	1.0	2×10^{-6} = Prob. of drop-out between 40 dB and ∞ dB.
2-	0.4		36	-16.0	0.5	0.2	0.4×10^{-6} = Prob. of drop-out falling between 40 dB and 36 dB
3-	0.3		34	-14.0	0.5	0.15	
4-	0.5		32	-12.0	0.5	0.25	
5-	0.3		30	-10.0	0.45	0.13	
6-	0.7		28	- 8.0	0.45	0.31	
7-	0.8		26	- 6.0	0.41	0.32	
8-	1.0		24	- 4.0	0.40	0.40	
9-	1.0		22	- 2.0	0.35	0.35	
10-	2.0		20	0.0	0.30	0.60	
11-	2.0		18	2.0	0.24	0.48	
12-	4.0		16	4.0	0.14	0.56	
13-	5.0		14	6.0	0.12	0.60	
14-	8.0		12	8.0	0.08	0.64	
15-	16.0		10	10.0	0.04	0.64	
16-	26.0		8	12.0	0.015	0.39	
17-	30.0		7	14.0	0.005	0.15	
18-	40.0		6	12.9	0.001	0.04	
			Total Probability of error with Drop-Out ⟶			7.21×10^{-6}	

C. TIME CODE CHANNEL ANALYSES

The time code is an amplitude modulated subcarrier containing the pulse width modulated NASA Minitrack Time Code. The signal is recorded directly into the tape recorder, and has the following playback characteristics.

- Subcarrier Frequency — 80 kHz
- Data Rate — 3.2 k bits/sec
- Pulse Duration - Binary One — 187.5 μ sec
  - Binary Zero — 62.5 μ sec

The time code channel, located in the 171-to 203 kHz bandwidth on HDRSS-B, was moved to the 740- to 790 kHz bandwidth in HDRSS-D. The bandwidth of the multiplexer filter and the demultiplexer input filter was increased to take advantage of the additional space on the edge of the frequency spectrum. This does not affect the signal-to-noise ratio of the demodulated signal since the bandwidth of the demultiplexer output filter is practically unchanged. Figure 30 shows the amplitude response for both the HDRSS-D and HDRSS-B filters.

The signal-to-noise ratio remained unchanged as the frequency deviation, scaled to the respective center frequencies, was increased from 75 kHz (HDRSS-B) to 300 kHz (HDRSS-D).

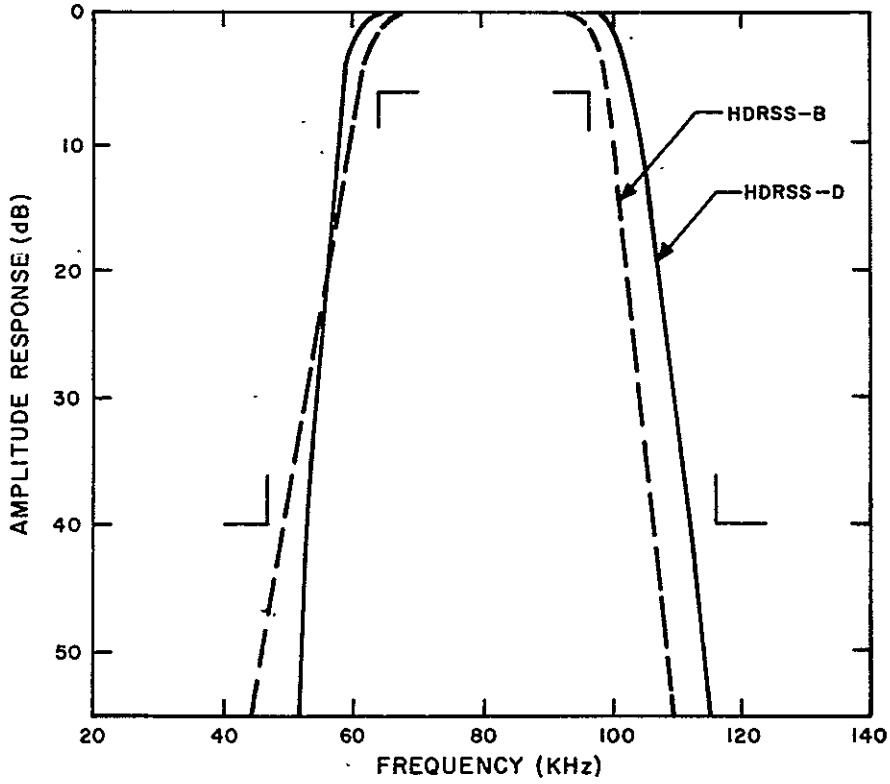

Figure 30. Amplitude Response of the Time Code Channel Bandpass Output Filter

D. ID CHANNEL ANALYSIS

1. Introduction

Provisions for storing one of two signals (ID or THIR-Visible) on the HDRSS-D tape recorder are contained on the Nimbus-D spacecraft. The THIR Visible signal, similar in format to the THIR-11 (HRIR on HDRSS-B) signal, originates from the 6 micron sensor (THIR-6). The THIR-6 signal has a baseband of 120 Hz; the THIR-11 has a baseband of 360 Hz. The THIR-6 signal is recorded on the ID track as on FM subcarrier. During playback, the subcarrier deviation limits are within the THIR-11 limits (73.6- to 101.1 kHz). In the multiplexer, the frequency deviations are doubled, while the baseband remains unchanged at 3.84 kHz. In the ground station the two signals, THIR-6 or THIR-11 are processed in the same circuits.

2. Signal-to-Noise Ratio

The signal-to-noise ratio due to link noise only is defined by the following formula:*

$$SNR = CNR \frac{3}{4} \frac{(\Delta f_{rf})^2 (\Delta f_{SC})^2 B_{IF}}{(f_m)^3 (f_{SC})^2 \left[1 + (3/5) (f_m/f_{SC})^2\right]}$$

where:

SNR = ratio of rms signal to rms noise, for sinusoidal modulation, at the output of the low-pass signal post detection filter.

f_m = the cutoff frequency of the low-pass post detection filter.

CNR = the ratio of rms signal to rms noise at the input to the RF discriminator.

B_{IF} = the bandwidth in which CNR is measured.

f_{SC} = the nominal center frequency of the subcarrier.

Δf_{SC} = the peak frequency deviation of the subcarrier.

Δf_{rf} = the peak frequency deviation of the RF carrier which is apportioned to this subcarrier.

---

*Radio Corporation of America, Test Log and Calibration Curve for HRIR Satellite Equipment, Prototype P1, Contract NAS 5-877, AED-1466, June 21, 1963.

The following values apply to the

Δf_{rf} = 300 kHz

Δf_{SC} = 27.5 kHz (after doubling)

f_m = 3.84 kHz

f_{SC} = 465 kHz

B_{IF} = 3.0 MHz*

CNR = 18.1 dB rms/rms (Refer to Appendix II.)

This expression assumes that the output circuit uses a zonal filter; the actual output circuit uses a 5th order Bessel filter. The Bessel baseband noise exceeds the zonal filter baseband noise by approximately 3.4 dB. Using the formula and subtracting 3.4 dB provides a SNR of 64.7 dB black-to-white to rms.

*International Telephone and Telegraph, Instruction Book, Solid State S-Band Transmitter, Contract NAS5 3392, Drawing No ITTD2339708

SECTION 6
BENCH CHECK UNIT AND TEST EQUIPMENT

A. BENCH CHECK UNITS

1. Purpose of Bench Check Units

The Bench Check Unit (BCU) is a self contained test facility that provides all the power, timing signals, and command signals for testing and exercising the spacecraft subsystems as separate entities or as a subsystem prior to installation in the spacecraft. The BCU has the following capabilities:

- Exercise the tape transport assembly, tape recorder electronics module, and the multiplexer module under operating conditions that approximate those in the spacecraft/ground station functional loop.
- Obtain quantitative and qualtitative data to determine if the HDRSS Spacecraft Subsystem meets established performance criteria.
- Localize malfunctions in the Spacecraft Subsystem under test whenever a performance anomaly is detected.
- Verify the functional integrity of the BCU by self-check features.

Interconnection between the BCU and the Spacecraft Subsystem for six separate conditions are provided by switching circuits. Two of the test conditions provide for complete subsystems tests. They are RECORD-MINCOM PLAYBACK and TAPE RECORDER + MUX playback. Switching for module or self test (BCU) are as follows:

- T/R P. B ONLY - for testing the spacecraft tape recorder without the multiplexer.
- MUX ONLY - for testing the spacecraft multiplexer without the tape recorder.
- TEST MODE - for BCU self-check.
- EXTERNAL - in which all simulator, spacecraft equipment, and processing equipment interfaces are open to permit manual interconnection of equipments for special tests.

For each of the test conditions, except the fourth item, the BCU provides complete circuit connections and controls the output signal rate of the simulators as required. Detailed descriptions are contained in the BCU Instruction Book. *

NOTE

The MRIR and HRIR designations on the equipment were not changed. When they appear on the equipment, they stand for VIP and THIR, respectively. Signal names have been changed in all the text of the reference document.

2. Spacecraft Test

Test of the Spacecraft Subsystem requires two modes of operation, record and playback. During the playback mode all the data except THIR signals can be processed for evaluation. THIR data must be recorded on the BCU tape recorder and played back at one-fourth the record speed before it can be processed and evaluated. A complete subsystem test requires that the Spacecraft Subsystem be operated in both the record and playback modes. A test device, the a-c erase interface assembly, that reduces the time between playback cycles from 135.5 minutes (full tape) to approximately 3.5 minutes can be utilized during test of the engineering models containing an a-c erase head (HDRSS-D only). This is accomplished by eliminating the erase function during playback and arranging for a high speed rewind. In this way, the tape can be shuttled to reduce the test time requirements during spacecraft and bench-test activities. A functional block diagram of the BCU and the Spacecraft Subsystem is shown in Figure 31.

a. Record Mode

When the record mode is selected, the clock simulator is set to record to provide 400 cps sync signals to the spacecraft tape recorder and timing pulses to the Image Dissector (ID), Time Code (TC), and Temperature Humidity Infrared (THIR) signal simulators. The timing pulses are also applied to the Bit Error Rate Checkers (BERC) where Infra-red Interferometer Spectrometer (IRIS) and Versatile Information Processor (VIP) signals are generated. The output of the signal simulators and BERC are then recorded on the spacecraft tape recorder at 1.34 ips. The frequency of the simulated signals controlled by the record switches on the switching equipment; data contained in each signal is selected on the front panel of the signal simulators and BERC.

---

*RCA, Astro-Electronics Division, Instruction Manual, Nimbus-D Modifications of the Bench Check Unit of HDRSS, Contract NAS5-10396, Princeton, New Jersey, September 3, 1968.

b. Playback Mode

When the playback mode is selected, the clock simulator is set at playback to provide 400 Hz sync signals to the spacecraft recorder, and timing pulses to the ID, TC, and THIR signal simulators. Timing pulses are also applied to the BERC where IRIS and VIP signals are generated. When the playback mode is in progress the switching equipment provides open circuits for the simulator and BERC outputs thereby eliminating input signal interference. During playback, the spacecraft tape recorder runs 32 times the record speed (42.9 ips) and the signals are applied directly to the multiplexer where four signals are applied to double-balanced modulators that shift each signal to a specific frequency, limited in bandpass filters, and applied to the summing amplifier. The fifth signal (IRIS) is applied directly to a bandpass filter and then the summing amplifier. The five signals plus the VIP channel oscillator output (pilot tone) are summed together to provide a 12- to 786 kHz subcarrier that is supplied to the RF link simulator. The RF link simulator attenuates the subcarrier to the level required by the demultiplexer, provides for the insertion of flat or triangular noise, and limits the bandpass to simulate signal degradation similar to that presented by the transmitter/receiver loop of the Nimbus system. Signal degradation is controlled by a switch and potentiometer on the front panel.

c. Signal Processing and Data Evaluation

In the demultiplexer, the 12- to 786 kHz subcarrier is applied to band-pass filters to provide six separate signals. Four signals (VIP, ID or THIR-6, THIR-11, and TC) are shifted to the proper processing frequencies and band-pass limited; the pilot tone is detected and applied to a phase-lock loop that controls the VIP output; and the IRIS signal is filtered and amplified. The outputs of the demultiplexer are then applied to the BCU tape recorder and the processing circuits. The ID signal is demodulated and applied to the kine complex, where the video is amplified and applied to the kinescope; and the horizontal sync is detected and used to generate horizontal sweep. Horizontal sync pulses are also applied to the vertical sync detector where vertical sync start and stop pulses are generated. The time code signal carrier is frequency demodulated to provide a flutter and wow signal that modifies the deflection generator sweep rate to reflect speed variations of the Spacecraft Subsystem tape recorder. The time code is also demodulated to provide binary data that can be recorded and analyzed to determine the time and quality of the signal. Processing of THIR signals requires playback of the BCU tape recorder at a speed reduction of four to one. When played back, the THIR-11 is demodulated and applied to the horizontal sync detector and facsimile recorder interface. The horizontal sync detector, keyed by the motor-drive circuit, provides sync pulses to the facsimile recorder interface. simultaneously, the time code is demodulated to provide a binary code that can be recorded and analyzed for time and quality. The time code demodulator also triggers the facsimile motor drive to provide a 2400 Hz signal to the facsimile recorder interface and the horizontal sync detector. The THIR-6 signal (recorder on the ID channel) is processed in the same manner as the THIR-11 signal

described. The only difference is the switching circuits. The IRIS and VIP signals are decoded and applied to the comparators where the input signal is compared to the signal from the pattern generator to provide a bit error count and a word frame count. The bit-error count is used to determine the quality of Spacecraft Subsystem operation.

B. DEMULTIPLEXER TEST SET

The demultiplexer test set, a self-contained unit designed to simulate a multiplexer output signals, has an electrical configuration identical to that used in the Spacecraft multiplexer. The test set is used to obtain the following quantitative information concerning electrical performance of a demultiplexer:

- VIP amplitude frequency response.
- IRIS channel phase delay.
- VIP channel phase delay.
- Time code and flutter and wow channel transmission delay.
- ID channel envelope delay.
- THIR channel envelope delay.

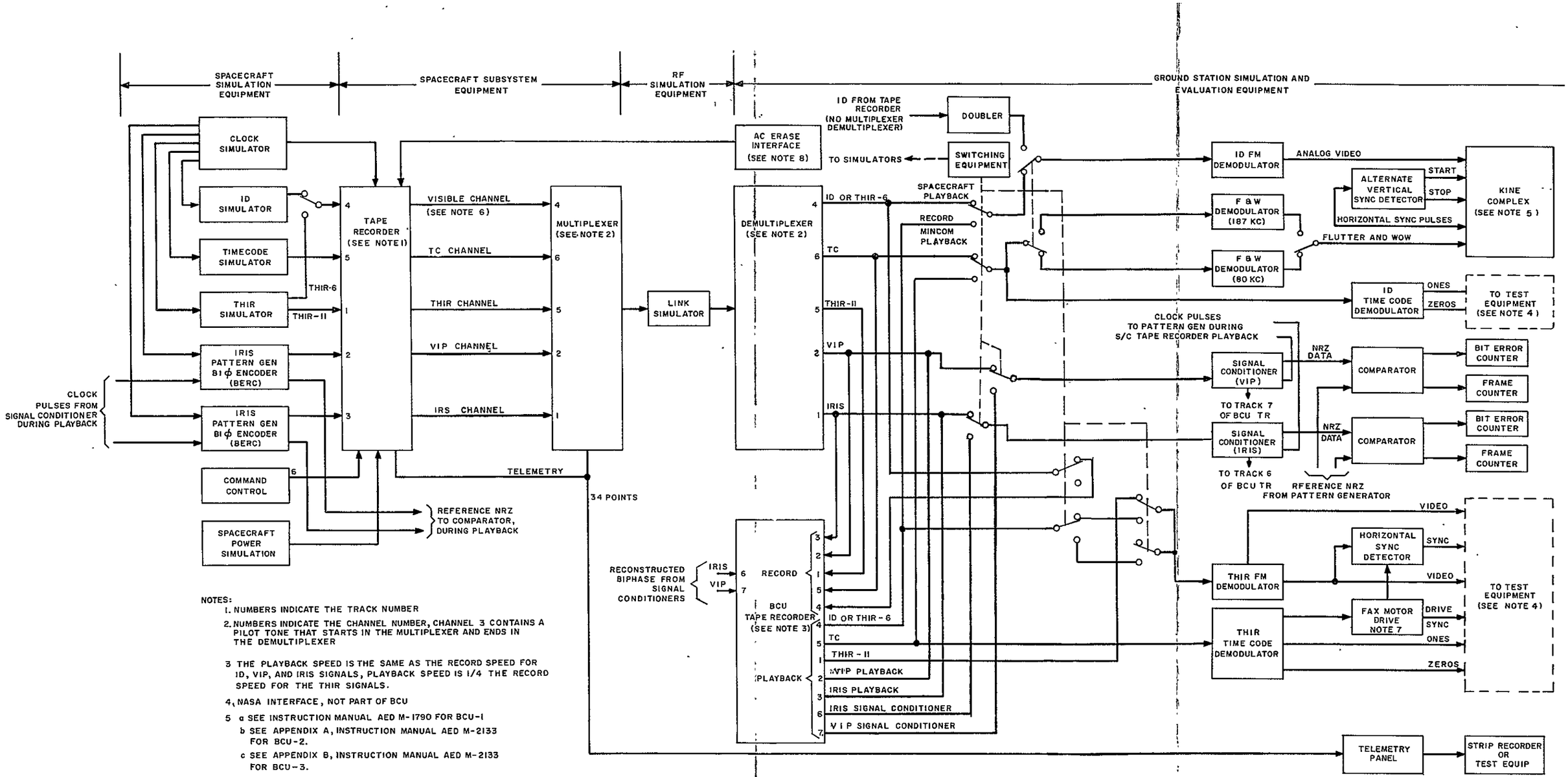

NOTES:

1. NUMBERS INDICATE THE TRACK NUMBER
2. NUMBERS INDICATE THE CHANNEL NUMBER, CHANNEL 3 CONTAINS A PILOT TONE THAT STARTS IN THE MULTIPLEXER AND ENDS IN THE DEMULTIPLEXER
3. THE PLAYBACK SPEED IS THE SAME AS THE RECORD SPEED FOR ID, VIP, AND IRIS SIGNALS, PLAYBACK SPEED IS 1/4 THE RECORD SPEED FOR THE THIR SIGNALS.
4. NASA INTERFACE, NOT PART OF BCU
5. a SEE INSTRUCTION MANUAL AED M-1790 FOR BCU-1
   b SEE APPENDIX A, INSTRUCTION MANUAL AED M-2133 FOR BCU-2.
   c SEE APPENDIX B, INSTRUCTION MANUAL AED M-2133 FOR BCU-3.
6. ID OR THIR -6 VIDEO SIGNAL
7. NOT CONTAINED IN BCU-3.
8. HDRSS-D ENGINERRING MODEL ONLY

FOLDOUT FRAME 1

Figure 31. HDRSS-D BCU Functional Block Diagram

FOLDOUT FRAME 2

SECTION 7
SYSTEM TEST DESCRIPTIONS

A. INTRODUCTION

The program test plan provided for three levels of testing: board level tests, module level tests, and system level tests. A brief description of each test level is supplied; details are contained in the system test plan, RCA drawing PN-1967674.

B. TEST PLAN

1. Board Level Tests

Board level tests were performed at various stages of assembly to ensure proper operation prior to module assembly. These tests provided for the selection of critical parameters, alignment, compensation of temperature sensitive circuits, and verification of all operating parameters after conformal coating. Tolerances and limits are included in the individual test procedures.

2. Module Level Tests

Module tests were performed after assembly of previously tested boards to ensure workmanship and the operating parameters outlined in the module performance specifications for the multiplexer and tape recorder, RCA drawing PS-1967617 and PS-1967674, respectively. The tests were performed during exposure to temperature extremes to ensure thermal stability, and after conformal coating to ensure that critical operating parameters have not changed. Selection of components, alignment, and operating tolerances are included in the test procedures. After module level tests, the engineering and flight modules were subjected to system tests. The prototype modules (multiplexer only) were subjected to prototype qualification tests. A summary of the tests conducted on each module (electronics module, tape transport, and multiplexer) as listed separately.

a. Electronic Module

Module tests for the engineering and flight quality electronics modules consisted of the following:

- Post Fabrication Operational Test
- Thermal Exposures and Electrical Test
- Conformal Coating
- Final Operational Test

b. Tape Transport

Module tests for the engineering and flight quality tape transports consisted of the following:

- Alignment (mechanical)
- Operational Test
- Thermal Exposure and Electrical Test
- Leak Rate Test

c. Multiplexer

Module tests for the engineering and flight quality multiplexers consisted of the following:

- Electrical Alignment
- Operational Test
- Thermal Exposures and Electrical Tests
- Conformal Coating
- Operational Test

Module tests of the prototype multiplexer consisted of the flight model tests and the following prototype qualification tests.

- Operational Test
- Vibration Exposure and electrical confidence test after exposure in each plane.
- Operational Test
- Acceleration and electrical confidence test after exposure
- Thermal Vacuum Exposure and electrical confidence tests
- Final Operational Test.

3. System Level Tests

System level tests include electrical and environmental tests for engineering and flight model systems.

a. Engineering Model Tests

System tests for the engineering models consisted of the following:

- Initial Operational Test
- 400 Hz Noise test (one system only)
- Thermal Exposure
- Thermal Exposure and Operational Test
- Final Operational Test.

b. Flight Model Tests

System tests for the flight models consisted of the following:

- Initial Operational Test
- Vibration Exposure - First Axis
- Leak Rate Test (tape transport only)
- Post Vibration Electrical Test (module or system)
- Vibration Exposure - Second Axis
- Leak Rate Test (tape transport only)
- Post Vibration Electrical Test (Module or System)
- Vibration Exposure (Third Axis)
- Leak Rate Test (tape transport only)
- Post Vibration Electrical Test (Module or System)
- Thermal Vacuum Exposure and Electrical Tests
- Leak Rate Test (Tape Transport only)
- Final Acceptance Test.

C. SPACECRAFT SUBSYSTEM PERFORMANCE TESTS

Electrical performance tests of the spacecraft subsystem outline the method of verifying system or module operation at various stages of the qualification acceptance test cycle. Each of the test procedures listed are performed with the bench check unit operating as a piece of test equipment. A summary of each test procedure is provided; refer to the applicable RCA drawing for specific details.

1. Operational Test

The operational test procedure (RCA drawing TP-OT-1967674) is a complete electrical performance test that verifies the system specifications outlined in the performance specification, RCA drawing PS-1769497. This test is performed prior to environmental tests and at customer acceptance. The operating parameters that constitute the minimum requirements are as follows:

- Commands
- Telemetry
- Power Supply Turn-on Transients
- Noise Feedback
- Power Profile
- Linearity and Drift (THIR & ID)
- Signal-to-Noise (THIR & ID)
- Frequency Response (THIR & ID)
- Transient Response (THIR & ID)
- Signal-to-Noise (Time Code)
- Flutter & Time Code Detection
- Sync Jitter (ID & THIR)
- Subjective Evaluation (ID)
- Acquisition Time (VIP & IRIS)
- Bit Error Rate (VIP & IRIS)

2. System Go No-Go Test

The system go no-go test (RCA drawing TP-SG-1967674) provides a complete confidence check of the spacecraft subsystem in a short period of time. This test is performed while the subsystem is in the thermal vacuum chamber or when a confidence check is required. The parameters tested during this procedure are as follows:

- Commands
- Telemetry
- Power Profile and Switching Transients
- Signal-to-Noise Ratio (ID & THIR)
- Flutter and Bit Error Rate
- Linearity (THIR & ID)
- ID, THIR, and Time Code Pictures

3. Transport Go No-Go Test

The tape transport go no-go test (RCA drawing TP-TG-1967674) provide an abbreviated performance check of the tape transport as a module. This test, conducted after vibration, acceleration, humidity tests, and during temperature transitions of the thermal-vacuum tests, consists of the following:

- Commands
- Telemetry
- Power Profile
- Flutter and Wow
- Bit Error Rate (VIP & IRIS)
- ID, THIR, and Time Code Pictures

4. Module Go No-Go Tests

The module go no-go test (RCA drawing TP-MG-1967674) provides an abbreviated performance check of the electronics module and multiplexer. This test, conducted after the first two single axes vibrations, consists of the following:

- Commands
- Telemetry
- Power Profile
- Bit Error Rate (IRIS)
- ID, THIR, and Time Code Pictures

5. Leak Rate Test

The leak rate test (RCA drawing TP-LC-1759765) checks the condition of the tape transport can assembly pressure seal before and after vibration, acceleration, and during thermal vacuum exposures.

D. BENCH CHECK UNIT TESTS

Performance of the bench check unit is verified by a self test feature that permits circuit operation without the use of a spacecraft subsystem. Calibration data for the following circuits is contained in the spacecraft subsystem operational test procedure (TP-OT-1967674).

- ID FM Demodulator
- Flutter and Wow Demodulator
- HRIR FM Demodulator

- ID Horizontal Sync Detector
- BCU Tape Recorder
- THIR Simulator (Gray Scale)
- ID Simulator (Gray Scale)
- VIP and IRIS Self Test
- Kinescope Flutter and Wow Correction

Performance of the demultiplexer is verified by performing the tests outlined in RCA drawing TP-1967618. During this test, the demultiplexer test set (the circuits are similar to the spacecraft subsystem multiplexer) or a qualified flight model multiplexer was used as test equipment. This test procedure, used to confirm the performance of either the multiplexer or the demultiplexer, verifies the performance specifications outlined in RCA drawing PS-1967617.

E. GROUND STATION EQUIPMENT TESTS

Performance of equipment designed for the ground stations was checked with tests similar to those used for the bench check unit and delivered to the appropriate sites.

F. ENVIRONMENTAL TESTS

1. Multiplexer Qualification Tests

Prototype qualification tests were limited to the multiplexer configuration. The tape transport and electronics module were qualified on the HDRSS-B program.

Prototype qualification tests were conducted at levels greater than those anticipated during launch or shipment of the spacecraft subsystem. Prototype qualification tests include the following:

- Vibration Tests
- Acceleration Tests
- Thermal Vacuum Tests

Detailed environmental specifications, test conditions and equipment requirements are contained in the environmental test procedure, RCA drawing TP-Q-1967617.

a. Vibration Tests

The prototype multiplexer was vibrated in each of three axes, one of which was parallel to the thrust axis. The levels of vibration for the sinusoidal and random modes are listed in Tables 19 and 20, respectively. After vibration (random and sine) in each plane, the multiplexer was subjected to a visual examination and an abbreviated electrical test

TABLE 19. SINUSOIDAL VIBRATION LEVELS, PROTOTYPE QUALIFICATION

Direction	Frequency Band (Hz)	Acceleration Amplitude	Sweep Rate*
Thrust Axis	5-20	0.5 in. double amplitude	one octave per minute, each axis,
	20-2000	10 g (0 to peak)	
Transverse Axes	5-20	0.5 in. double amplitude	
	20-2000	10 g (0 to peak)	
*The vibration excitation shall be supplied by logarithmically sweeping at a rate of one octave per minute, once per axis, from the lowest to the highest frequency. A tracking filter shall be used in the servo accelerometer return loop.			

TABLE 20. RANDOM VIBRATION LEVEL, PROTOTYPE QUALIFICATION

Direction	Frequency Band (Hz)	Spectral Density (g^2/Hz)	RMS Level (g's)
Thrust Axis	20-2000	0.2	20
Transverse Axes	20-2000	0.2	20
Duration of the test shall be 4 minutes in each direction.			

(par 5.2.3 and 5.2.4 of TP-1967617). One failure was experienced during vibration exposures; the 355 kHz crystal in the pilot-tone local oscillator failed. The failure was attributed to a potting error.

b. Acceleration Tests

The prototype multiplexer was subjected to an acceleration of 30g along the thrust axis for a duration of 5 minutes. After the exposure the multiplexer was subjected to the same electrical tests outlined in Paragraph a, Vibration Tests. Operation after acceleration was satisfactory.

c. Thermal Vacuum Tests

The multiplexer was installed in the test chamber and subjected to an electrical test (par 5.2.3 and 5.2.4 of TP-1967617). After test setup verification, a pressure of 1×10^{-5} mm Hg or less was established and the temperature was cycled as shown on Figure 31.

Performance of the multiplexer, confirmed by the tests shown on Figure 31, were satisfactory - no failures were noted.

2. Engineering Model Environmental Tests

Environmental tests of the engineering models consisted of thermal exposure at 0 and 35°C. During each exposure, the operational test described in test procedure TP-OT-1967674 was performed.

3. Flight Model Environmental Tests

The environmental tests required for flight acceptance testing consist of vibration and thermal vacuum tests. These tests demonstrate successful reproduction of the qualified prototype model. Detailed environmental specifications, test conditions, and equipment requirements are contained in the environmental test procedure, TP-EQ-1967674. Electrical test requirements during environmental exposure are contained in the electrical acceptance test procedure TP-EA-1967674.

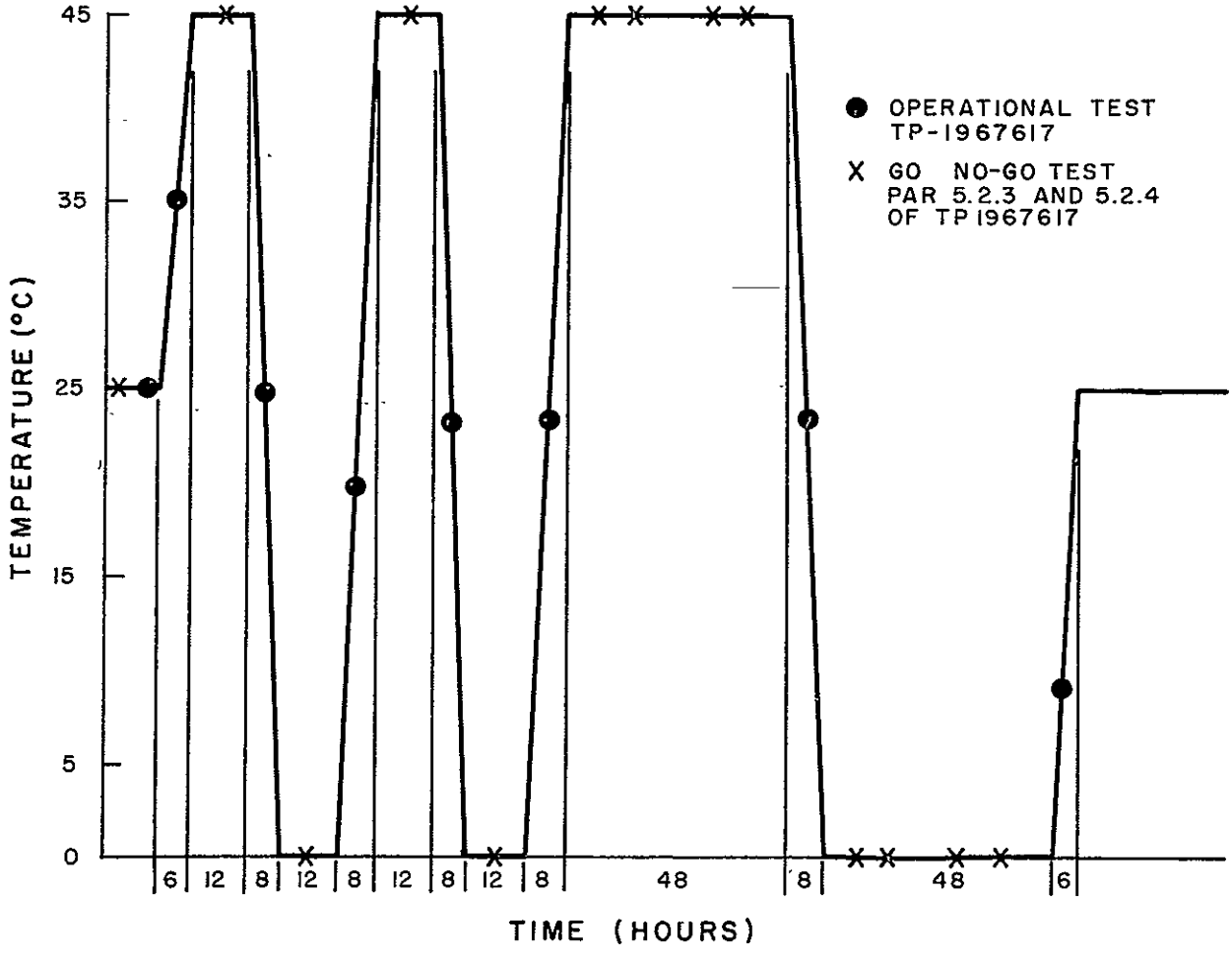

Figure 32. Thermal Vacuum Profile for Prototype Multiplexer

a. Vibration

Vibration procedures for the flight-model equipment are identical to the prototype tests except for the vibration levels. The vibration levels are listed in Tables 21 and 22.

Five failures were noted for the three flight model subsystems; four for the tape transport, one for the multiplexer. In each case, the failure was mechanical, namely, hardware.

b. Thermal Vacuum Tests

The thermal vacuum profile for the flight model acceptance tests are shown on Figure 33. Performance of the flight model subsystems, shown on Figure 33, were satisfactory.

TABLE 21. SINUSOIDAL VIBRATION LEVELS, FLIGHT ACCEPTANCE TESTS

Direction	Frequency Band (Hz)	Acceleration Amplitude	Sweep Rate*
Thrust Axis	5-14	0.5 in. double amplitude	two octaves per minute, each axis,
	14-2000	5g (0 to peak) (3.5g, rms)	
Transverse Axes	5-14	0.5 in. double amplitude	
	14-2000	5g (0 to peak) (3.5g, rms)	
*The vibration excitation shall be supplied by logarithmically sweeping at a rate of one octave per minute, once per axis, from the lowest to the highest frequency. A tracking filter shall be used in the servo accelerometer return loop.			

TABLE 22. RANDOM VIBRATION LEVELS, FLIGHT ACCEPTANCE TESTS

Direction	Frequency Band (Hz)	Spectral Density (g^2/Hz)	RMS Level (g's)
Thrust Axis	20-2000	0.07	11.7
Transverse Axes	20-2000	0.07	11.7
Duration of the test shall be 2 minutes in each direction.			

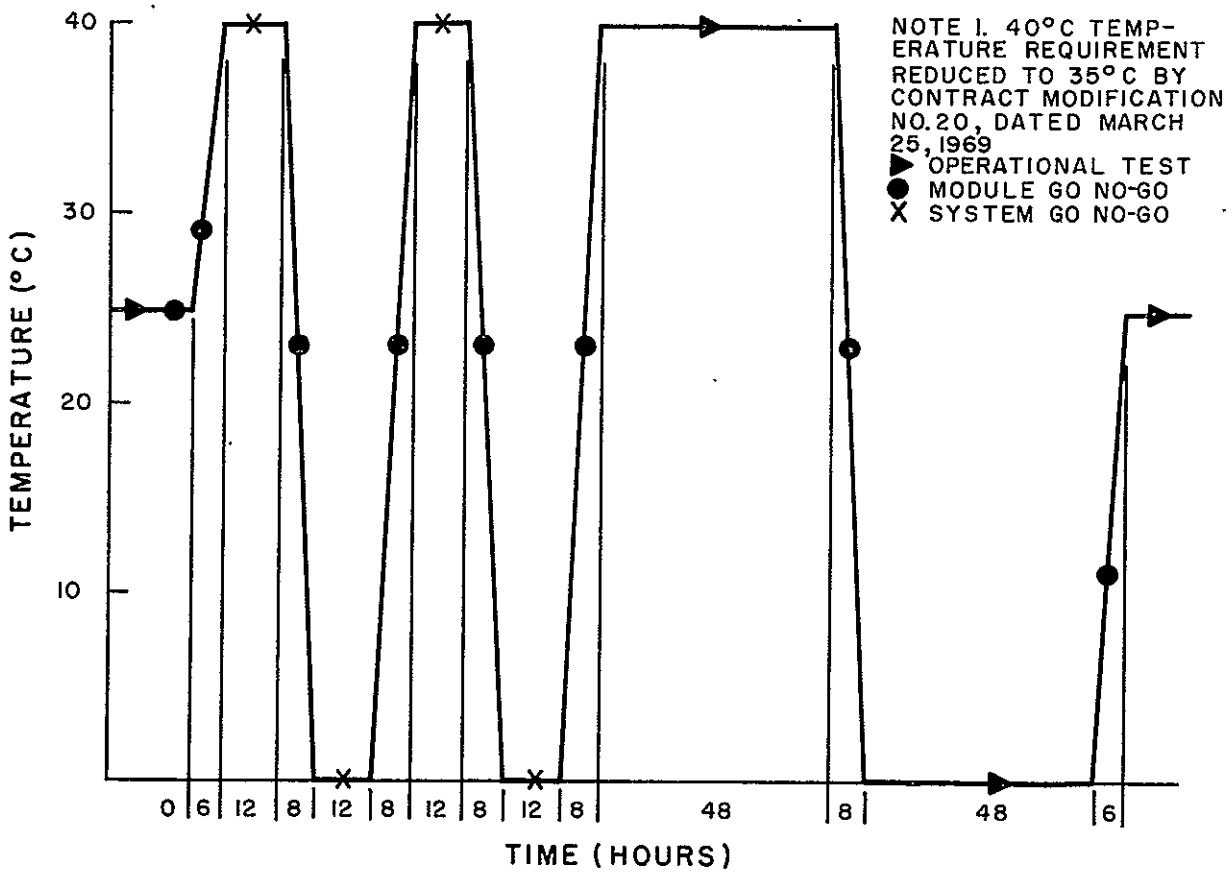

Figure 33. Thermal Vacuum Test Profile Subsystem Acceptance Test

SECTION 8
SYSTEM TEST DATA SUMMARY

A. INTRODUCTION

A summary of the critical operating parameters obtained during the final acceptance test of the prototype and flight model subsystems serve as a reference for all future tests. A brief description of the final acceptance test (RCA Drawing TP-OT-1967764) is contained in Section 7; a detailed summary of the data for each subsystem is contained in the following:

- "Test and Calibration Data for Engineering Model 1D of the Nimbus-D HDRSS", (AED-R-3370) issued October 17, 1968.
- "Test and Calibration Data for the Prototype Multiplexer of the Nimbus-D HDRSS", (AED-R-3416) issued January 27, 1969.
- "Test and Calibration Data for Engineering Model 2D of the Nimbus-D HDRSS", (AED-R-3441) issued April 9, 1969.
- "Test and Calibration Data for Flight Model 1 of the Nimbus-D HDRSS," (AED R-3464) issued June 16, 1969.
- "Test and Calibration Data for Flight Model 2 of the Nimbus-D HDRSS," (AED R-3476) issued August 14, 1969.
- "Test and Calibration Data for Flight Model 3 of the Nimbus-D HDRSS," (AED R-3540) issued February 6, 1970.
- THIR Channel Characteristics

  Signal-to-Noise
  Sync Jitter
  Transient Response
  Frequency Response
  Linearity

- VIP Channel Characteristics

  Bit Error Rate
  Tape Dropouts

- IRIS Channel Characteristics

  Bit Error Rate
  Tape Dropouts

- ID Channel Characteristics

  Signal-to-Noise
  Sync Jitter

Transient Response
Frequency Response
Linearity

- Time Code Channel Characteristics

  Valley-to-Peak Ratio

- Tape Speed and Flutter Data
- Power Supply Current Transients
- Multiplexer Deviation Schedule

B. DATA SUMMARY

Test data for the critical operating parameters of the engineering model subsystems, multiplexer, and flight model subsystems is presented in Table 23. All the data presented was obtained at room ambient temperature (approximately 25°C); the nominal operating temperature experienced on previous Nimbus satellites.

TABLE 23. SUMMARY OF CRITICAL OPERATING PARAMETERS, PROTOTYPE AND FLIGHT-MODEL SUBSYSTEMS

Operating Parameter	Required	Engineering Model 1	Prototype Multiplexer	Engineering Model 2	Flight Model 1	Flight Model 2	Flight Model 3
THIR Channel							
Signal-to-Noise Ratio	30 dB, min	34.0 dB		32.2 dB	33.7 dB	33.4 dB	33 4 dB
Sync Jitter	800 μsec, max	200.0 μsec		120.0 μsec	120.0 μsec	200.0 μsec	250.0 μsec
Transient Response - Pos Step Input							
Rise Time	Not Specified	180 0 μsec		200 0 μsec	200 0 μsec	200.0 μsec	200.0 μsec
Overshoot	Not Specified	0.0 %		0.0 %	0 0 %	0.0 %	0 0 %
Neg Step Input							
Fall Time	Not Specified	180.0 μsec		160.0 μsec	160.0 μsec	200.0 μsec	220.0 μ sec
Overshoot	Not Specified	0.0 %		0.0 %	0.0 %	9.0 %	10.0 %
Freq Response	<8 dB down at 360 Hz	-2.6 dB		-2.8 dB	-3.0 dB	-3.0 dB	-3.0 dB
Linearity and Drift							
White	18.6 ± 0.96 Vdc	See Figure 34		See Figure 35	See Figure 36	See Figure 37	See Figure 38
Black	0.0 ± 0.58 Vdc						
VIP Channel							
Bit Error Rate	1.0×10^{-5} min	6.7×10^{-6}		5.4×10^{-6}	8.23×10^{-6}	$0\ 97 \times 10^{-5}$	$5\ 3 \times 10^{-7}$
Tape Dropout between 10 and 240 sec	100 max	—		0	22	21	5
IRIS Channel							
Bit Error Rate	1.0×10^{-5} min	6.7×10^{-6}		5.8×10^{-6}	8.54×10^{-6}	2.83×10^{-6}	1.1×10^{-7}
Tape Dropouts between 10 and 240 sec	100 max	—		3	30	23	6
ID Channel							
Signal-to-Noise Ratio	30.0 dB min	33.6 dB		34.1 dB	32.6 dB	33 2 dB	33.2 dB
Sync Jitter	8.0 μsec	6.0 μsec		7 5 μsec	7.0 μsec	6.0 μsec	5 0 μsec
Transient Response - Pos Step Input							
Rise Time	Not Specified	15.0 μsec		30.0 μsec	18.0 μsec	10.0 μsec	18.0 μsec
Overshoot	Not Specified	0.0 %		0.0 %	0.0 %	0 0 %	7 0 %
Neg Step Input							
Fall Time	Not Specified	15 μsec		20.0 μsec	18.0 μsec	12.0 μsec	20.0 μsec
Overshoot	Not Specified	15.0 %		12.0 T	11.0 %	11.0 %	0.0 %
Freq Response	<12 dB down at 1600 Hz	7.0 dB		-9.2 dB	-10.0 dB	-10.0 dB	-10.0 dB
Linearity and Drift							
White	1.0 ± 0.043 Vdc	See Figure 39		See Figure 40	See Figure 41	See Figure 42	See Figure 43
Black	0.0 ± 0.027 Vdc						
Time Code Channel							
Valley-to-Peak Ratio	0.30 to 0.54	0.32		0.30	0.35	0 35	0 35
Tape Transport Speed and Flutter Data							
Record Time	≥ 120 minutes	125.2 minutes		121 0 minutes	123.6 minutes	122.1 minutes	122 1 minutes
Playback Time	≥ 223 seconds	236.0 sec		226.0 sec	233 0 sec	235.0 sec	234.0 sec
P-P Flutter, 1 kHz	≤ 0 8 %	0.64 %		0.45 %	0 26 %	0 75 %	0.6 %
P-P Flutter, 60 kHz	≤ 2.4 %	1.4 %		1.50 %	0.72 %	2.33 %	1 8 %
Speed Variation Ratio	≤ 0.50 %	0.37 %		0.32 %	0.33 %	0.30 %	0.34 %
Multiplexer Deviation							
IRIS Channel	0.840 ± 0.045 V p-p	0.426 V p-p	0.827 V p-p	0.849 V p-p	0.836 V p-p	0.853 V p-p	0.825 V p-p
Time Code Channel	1.260 ± 0.070 V p-p	1.268 V p-p	1.230 V p-p	1.242 V p-p	1.270 V p-p	1.275 V p-p	1.280 V p-p
VIP Channel	1.260 ± 0.070 V p-p	1.204 V p-p	1.250 V p-p	1.220 V p-p	1.243 V p-p	1.262 V p-p	1.200 V p-p
ID Channel	1.260 ± 0.070 V p-p	1.209 V p-p	1.260 V p-p	1.309 V p-p	1.290 V p-p	1.245 V p-p	1.274 V p-p
THIR Channel	0.840 ± 0.070 V p-p	0.846 V p-p	0.840 V p-p	0.810 V p-p	0. V p-p	0 810 V p-p	0.830 V p-p

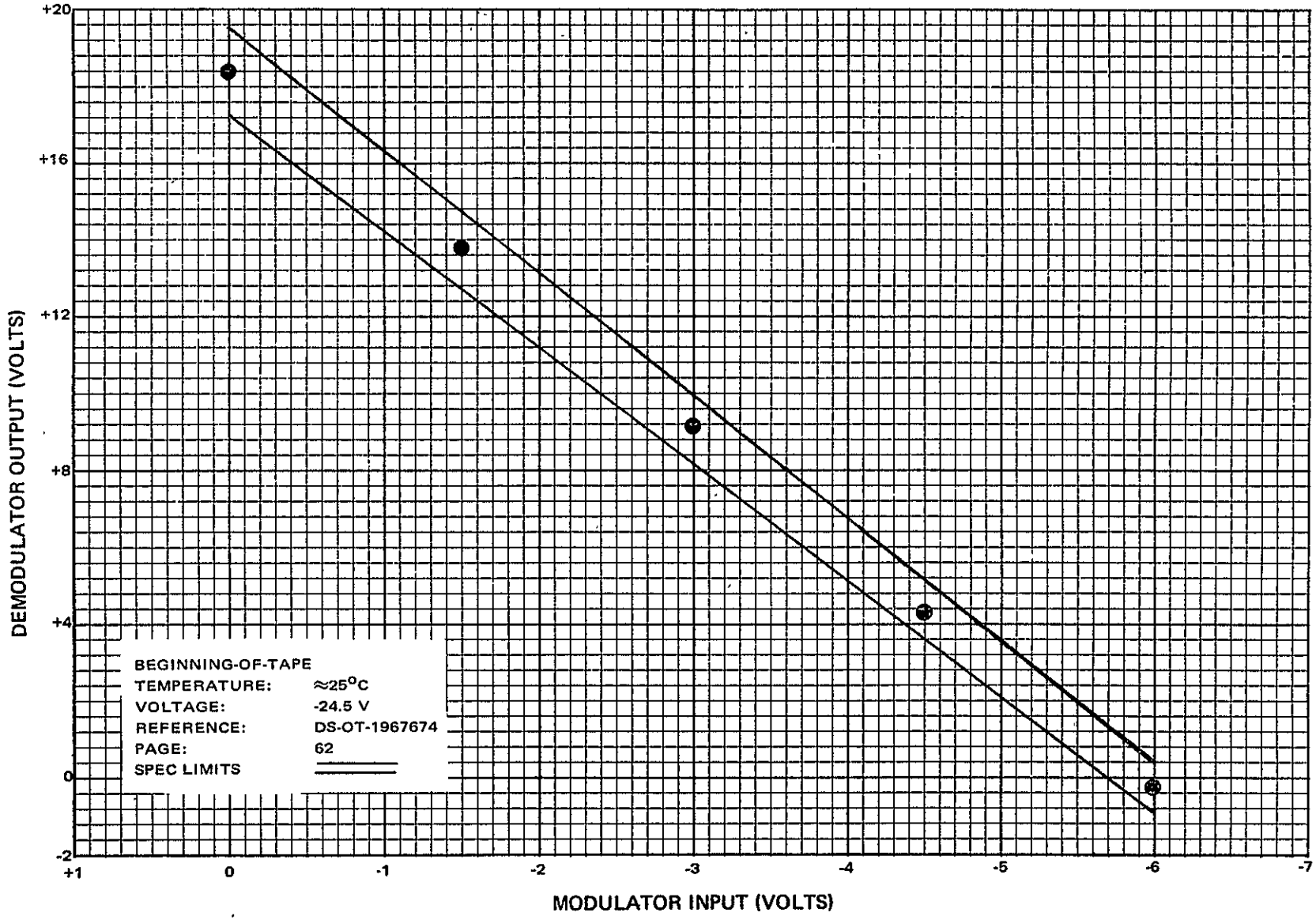

Figure 34. THIR Channel Linearity and Drift, Engineering Model 1 Subsystem (Sheet 1 of 2)

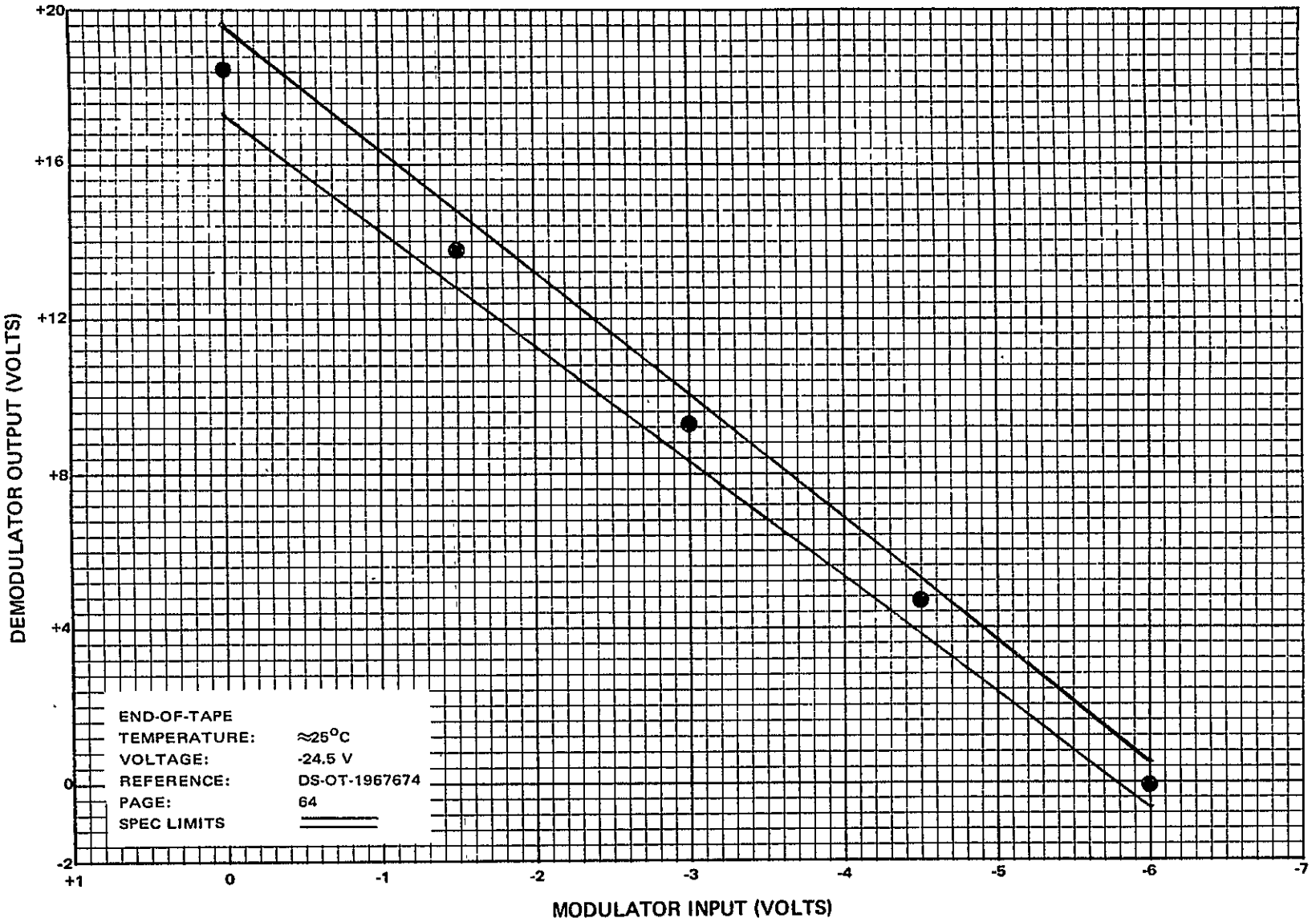

Figure 34. THR Channel Linearity and Drift, Engineering Model 1 Subsystem (Sheet 2 of 2)

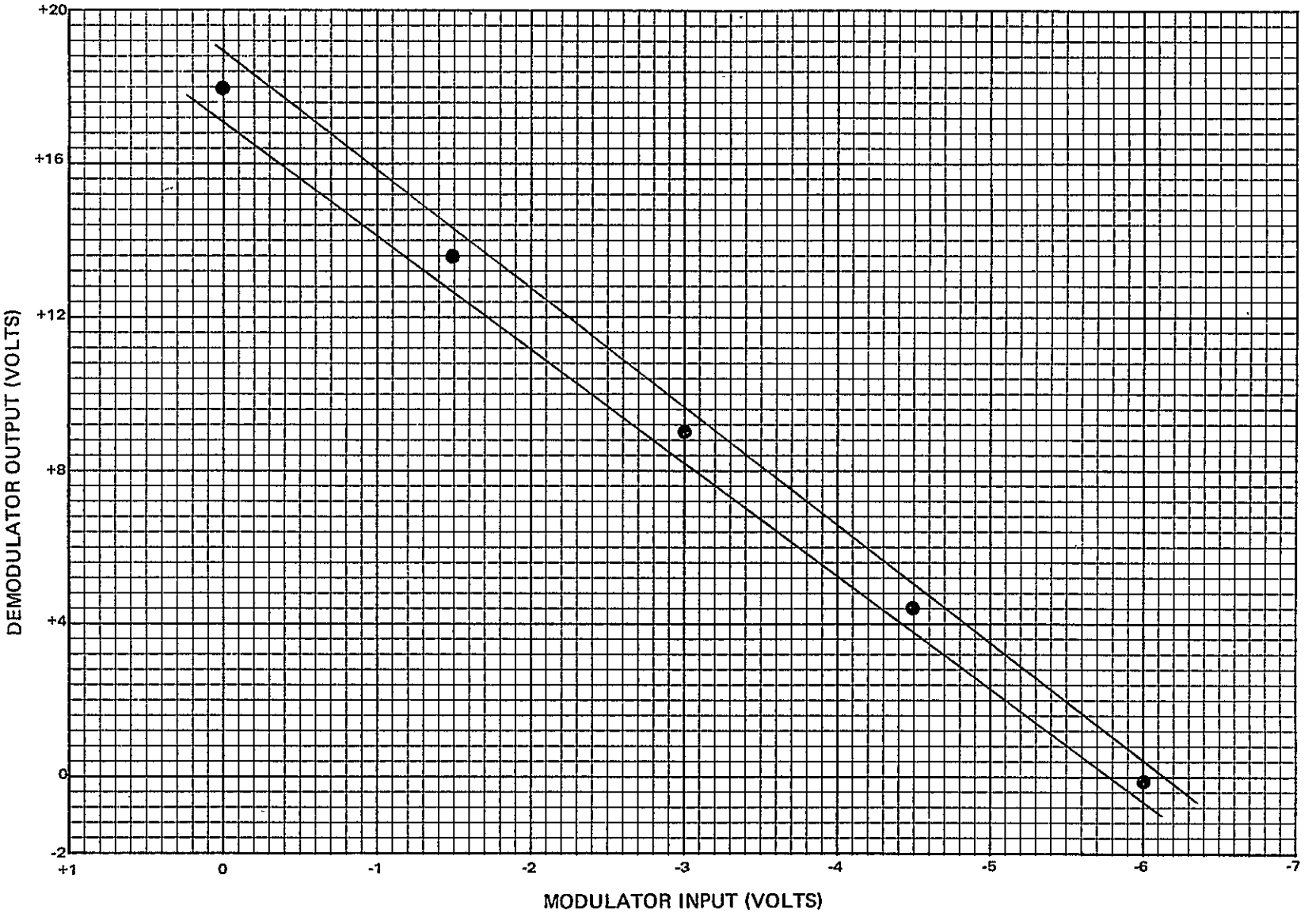

Figure 35. THIR Channel Linearity and Drift, Engineering Model 2 (Sheet 1 of 2)

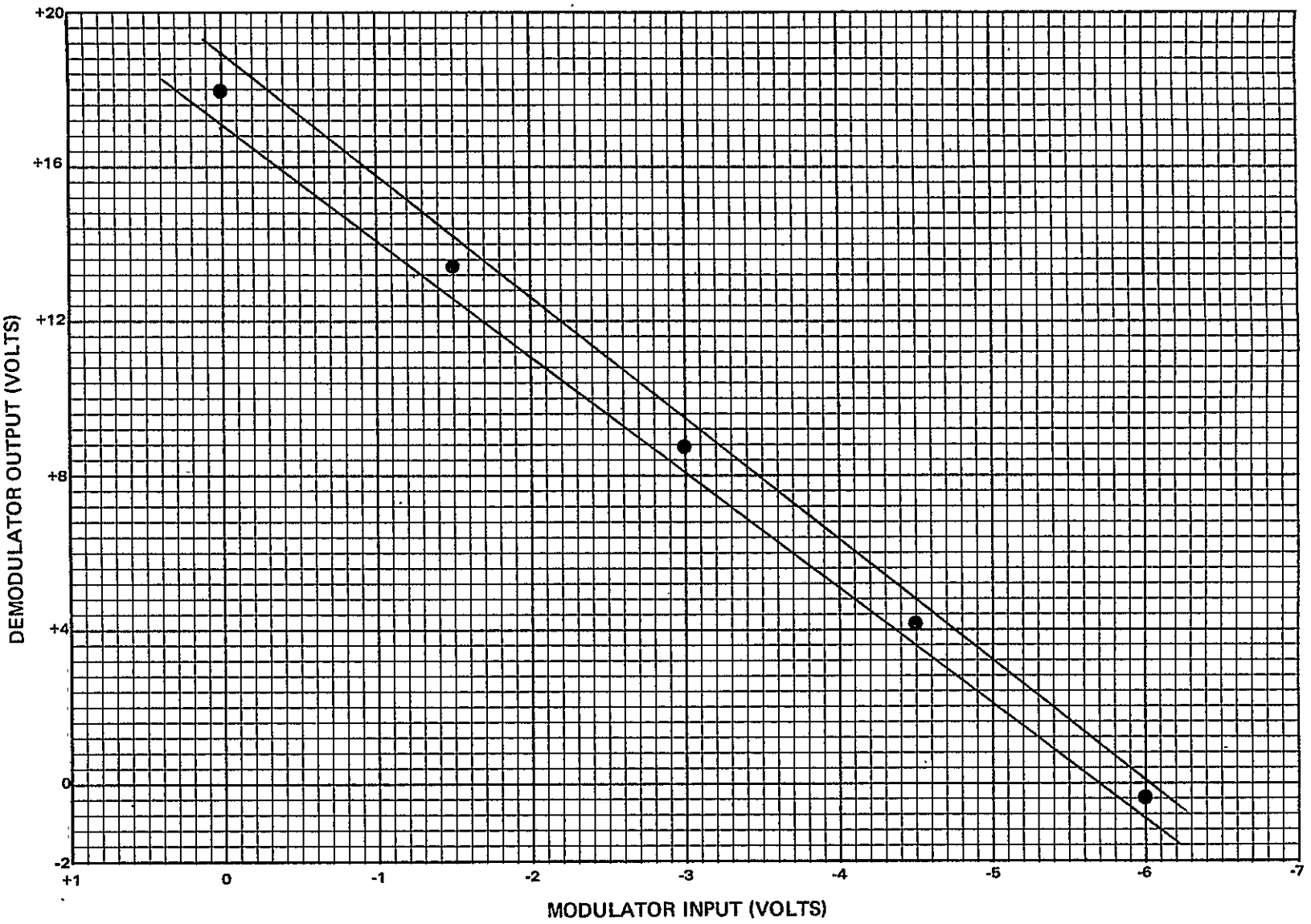

Figure 35. THIR Channel Linearity and Drift, Engineering Model 2 (Sheet 2 of 2)

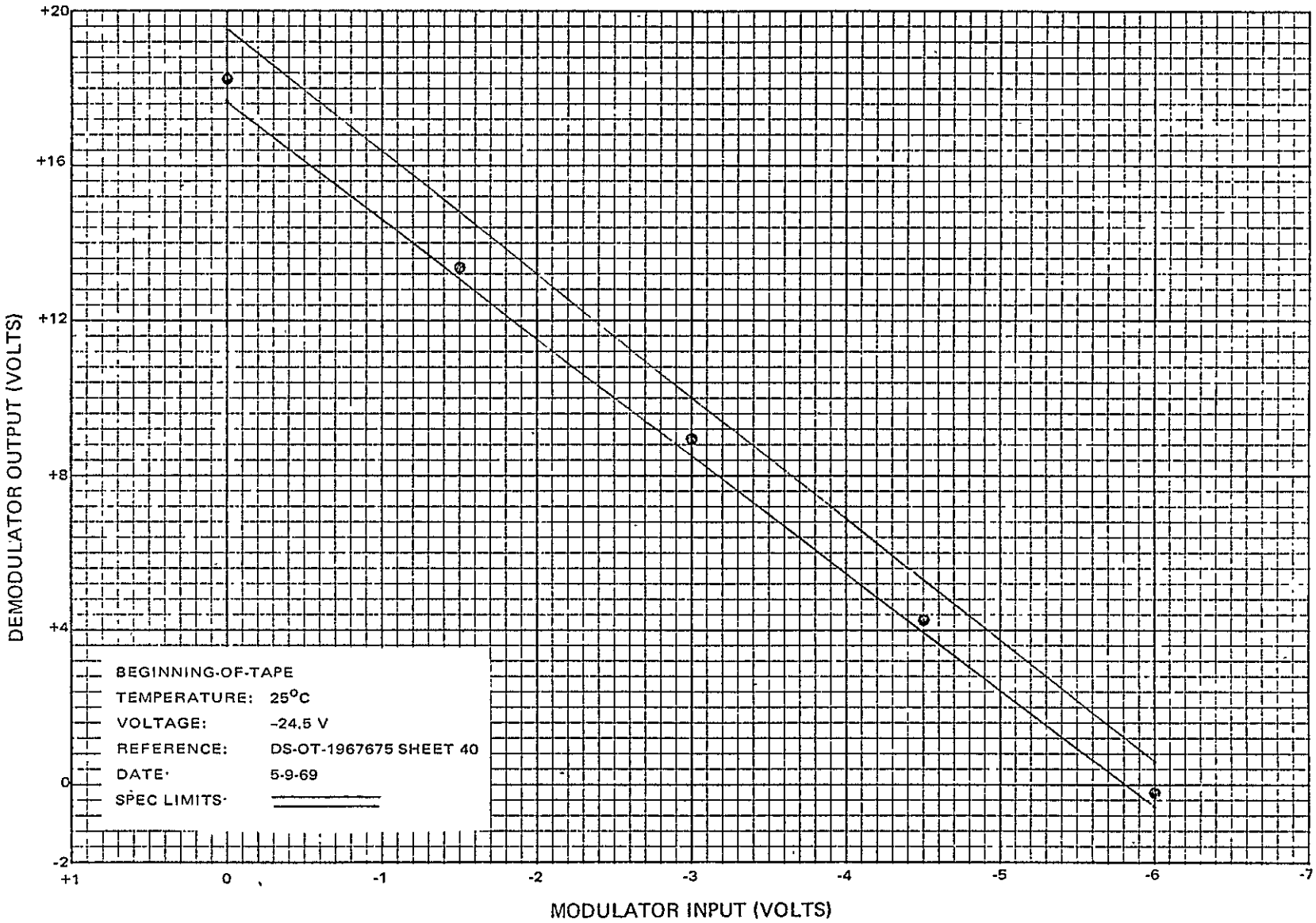

Figure 36. THIR Channel Linearity and Drift, Flight Model 1 (Sheet 1 of 2)

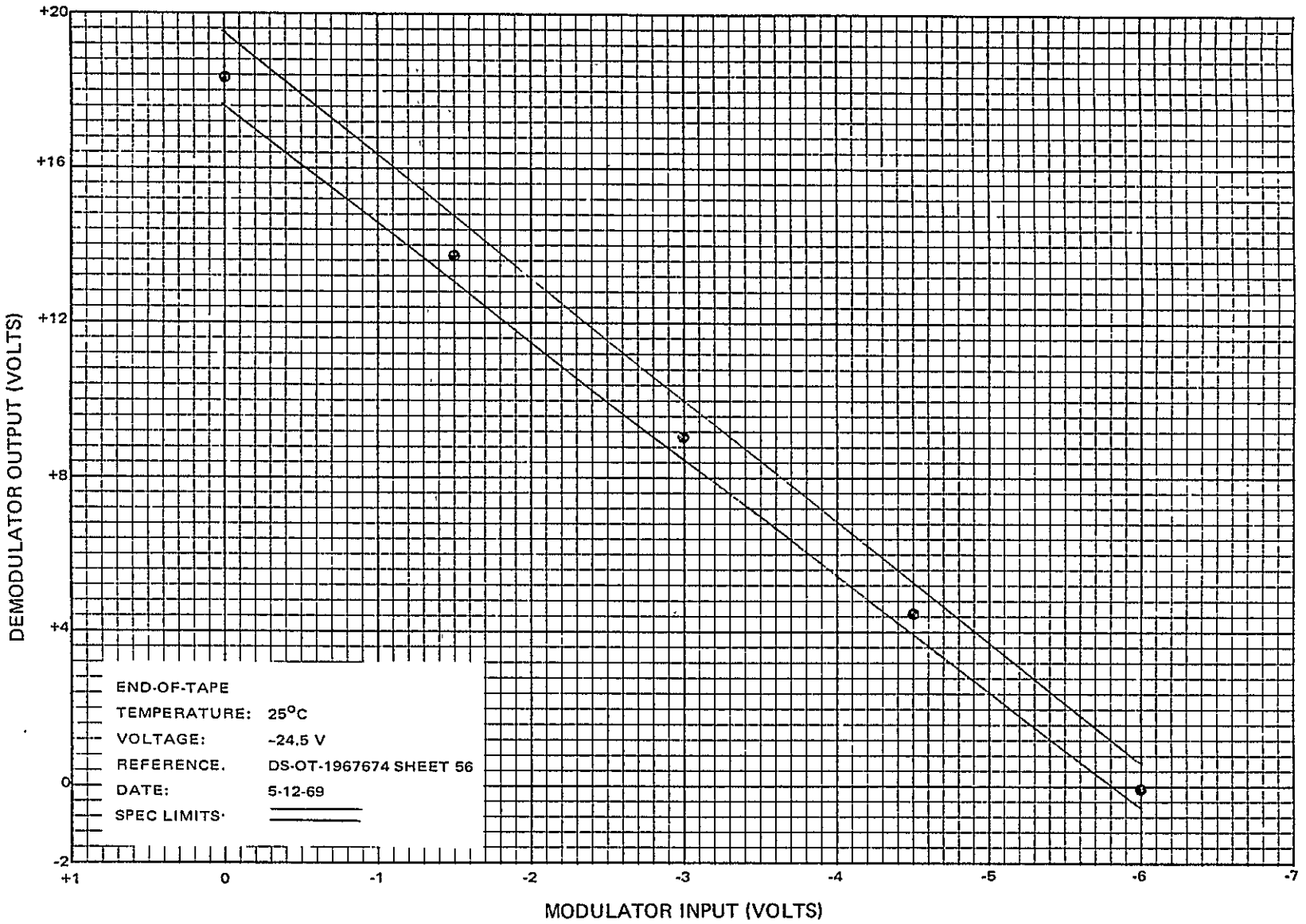

Figure 36. THIR Channel Linearity and Drift, Flight Model 1 (Sheet 2 of 2)

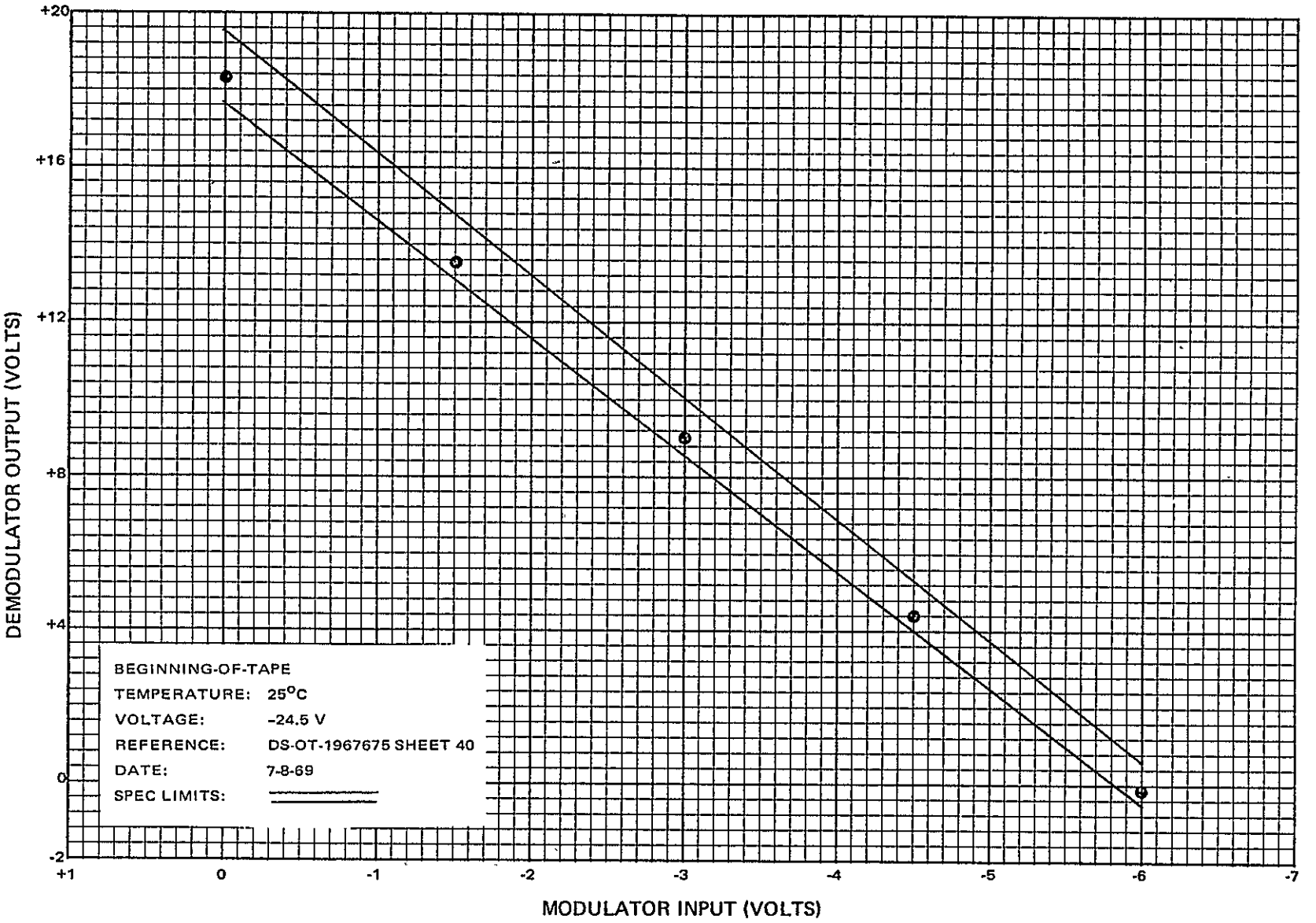

Figure 37. THIR Channel Linearity and Drift, Flight Model 2 (Sheet 1 of 2)

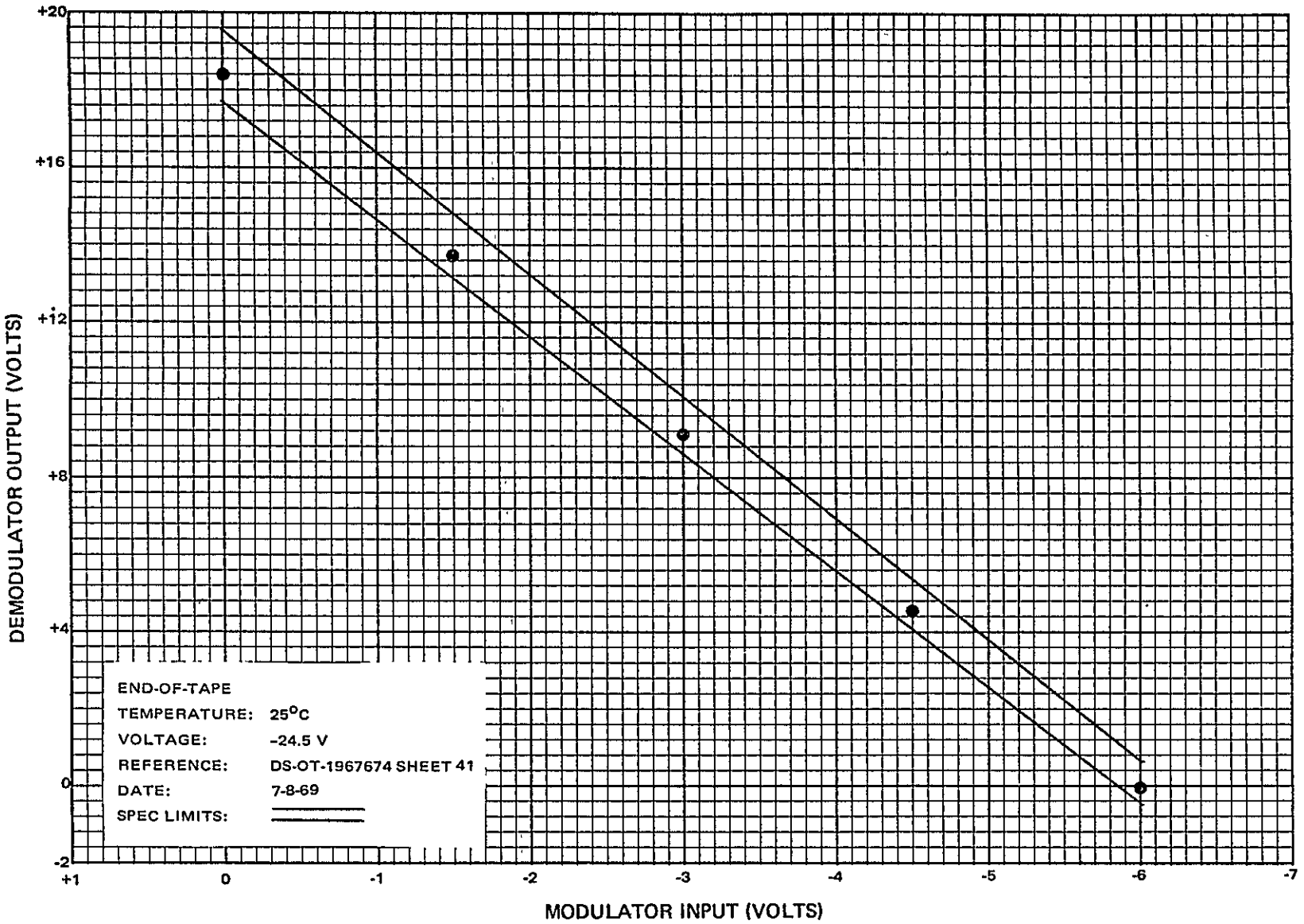

Figure 37. THIR Channel Linearity and Drift, Flight Model 2 (Sheet 2 of 2)

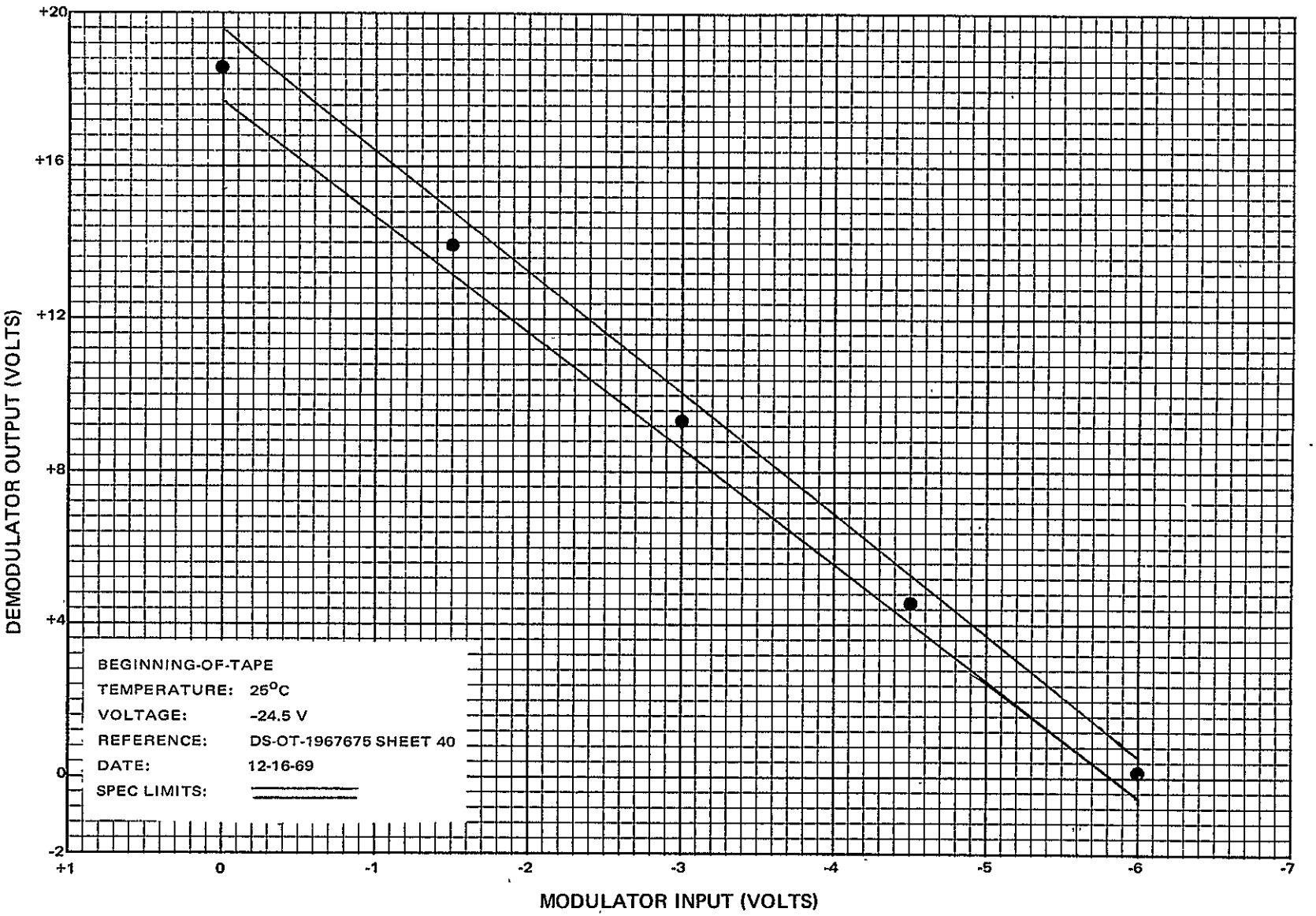

Figure 38. THIR Channel Linearity and Drift, Flight Model 3 (Sheet 1 of 2)

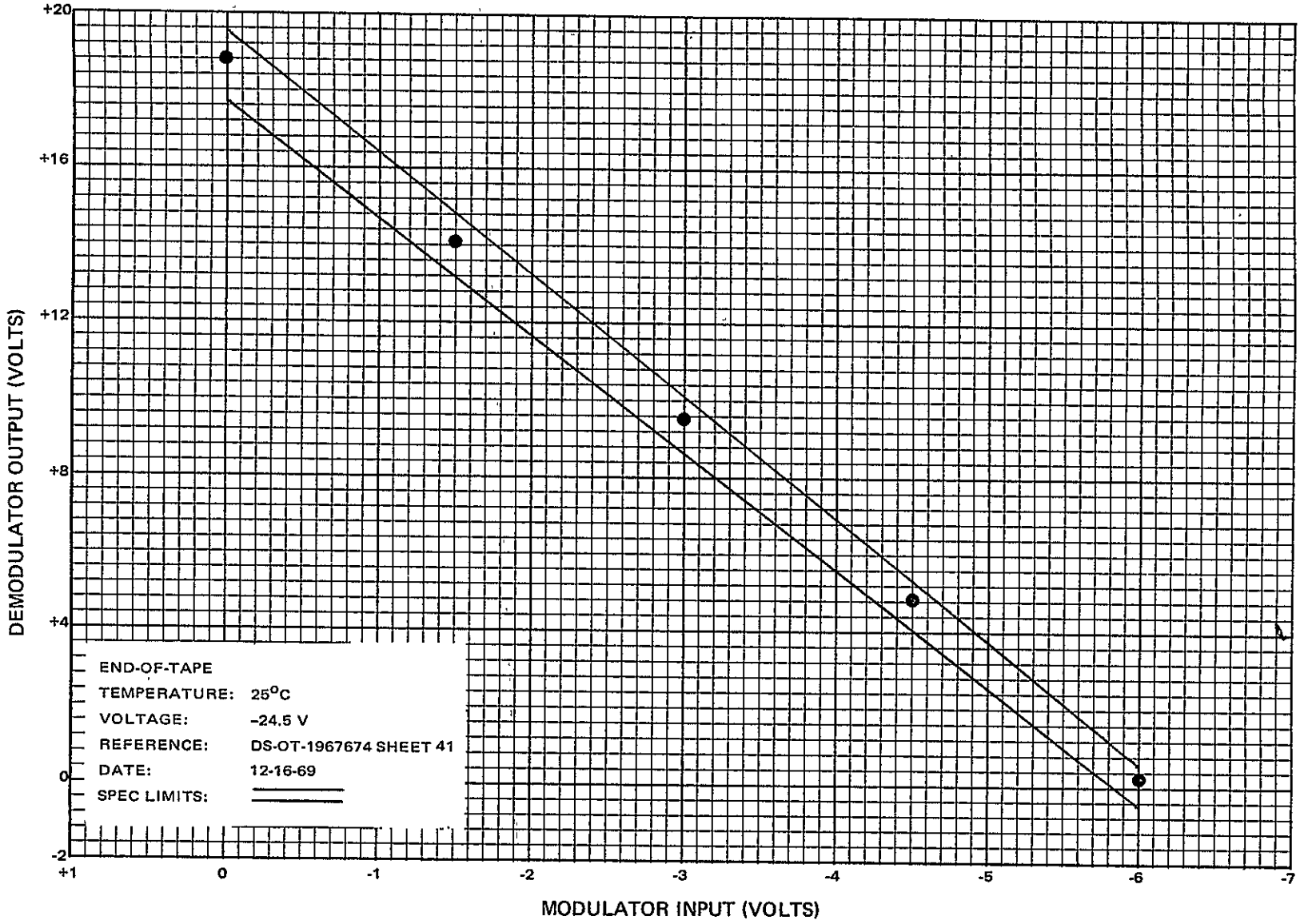

Figure 38. THIR Channel Linearity and Drift, Flight Model 3 (Sheet 2 of 2)

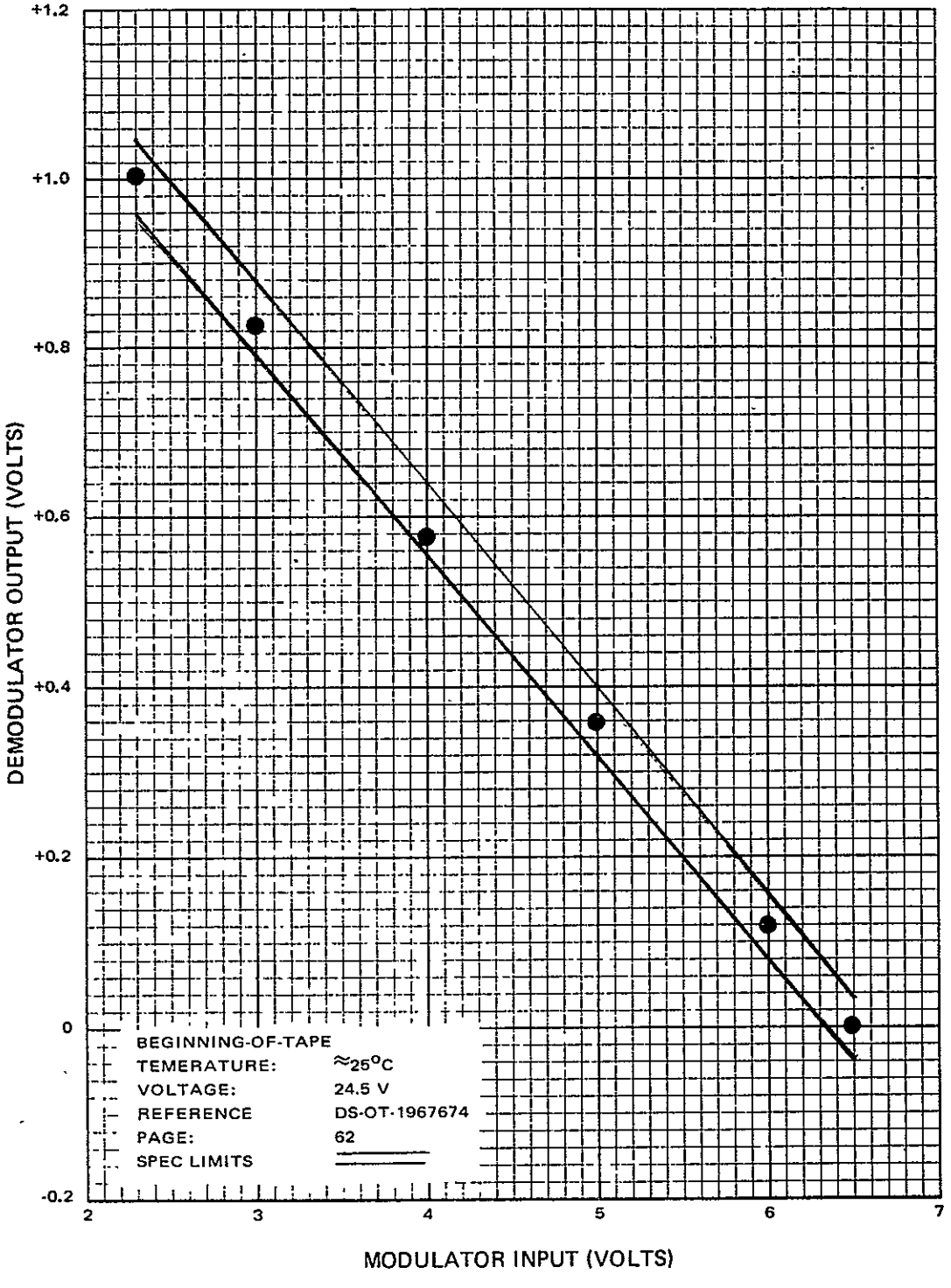

Figure 39. ID Channel Linearity and Drift, Engineering Model 1 Subsystem
(Sheet 1 of 2)

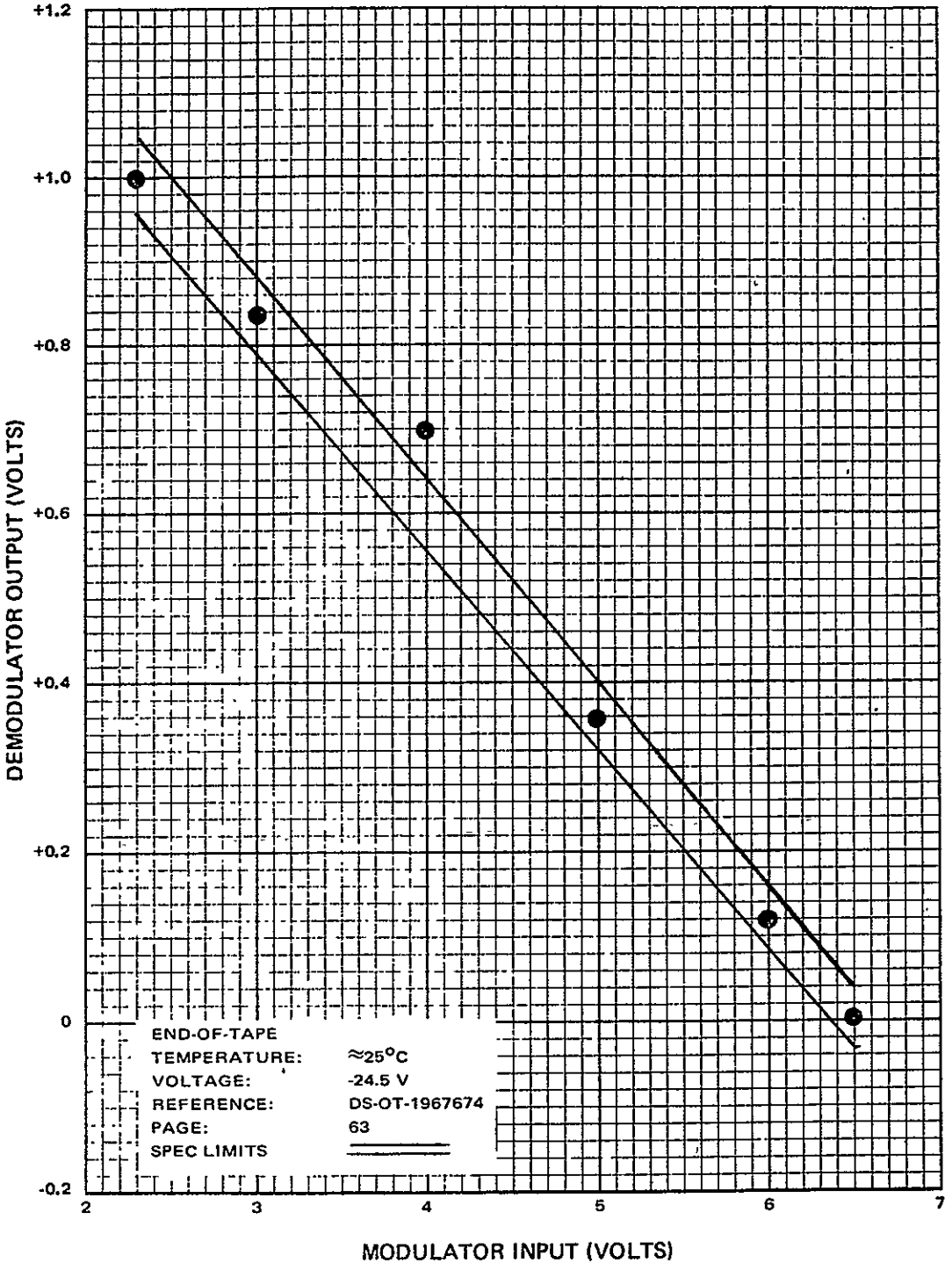

Figure 39. ID Channel Linearity and Drift, Engineering Model 1 Subsystem (Sheet 2 of 2)

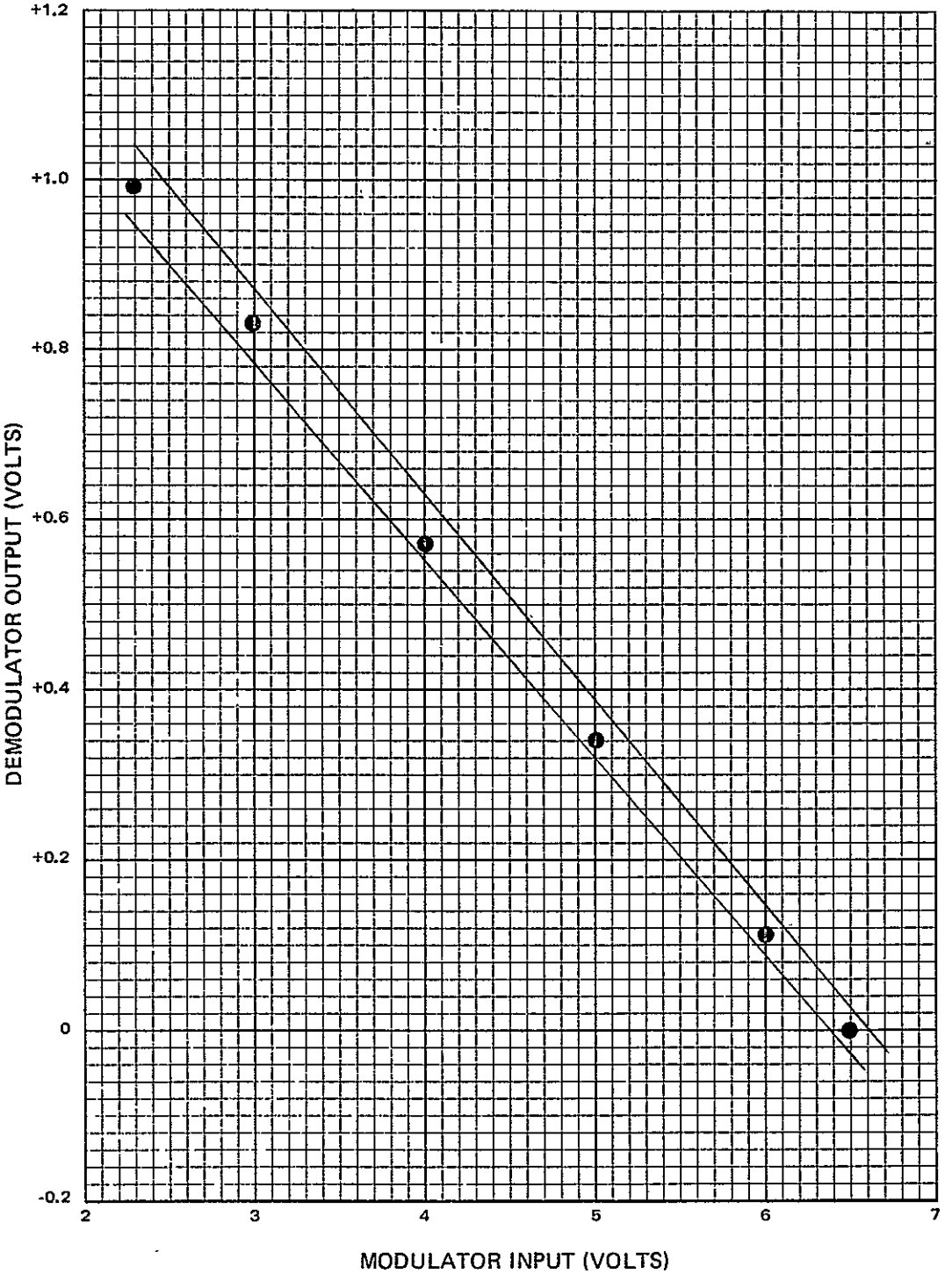

Figure 40. ID Channel Linearity and Drift, Engineering Model 2
(Sheet 1 of 2)

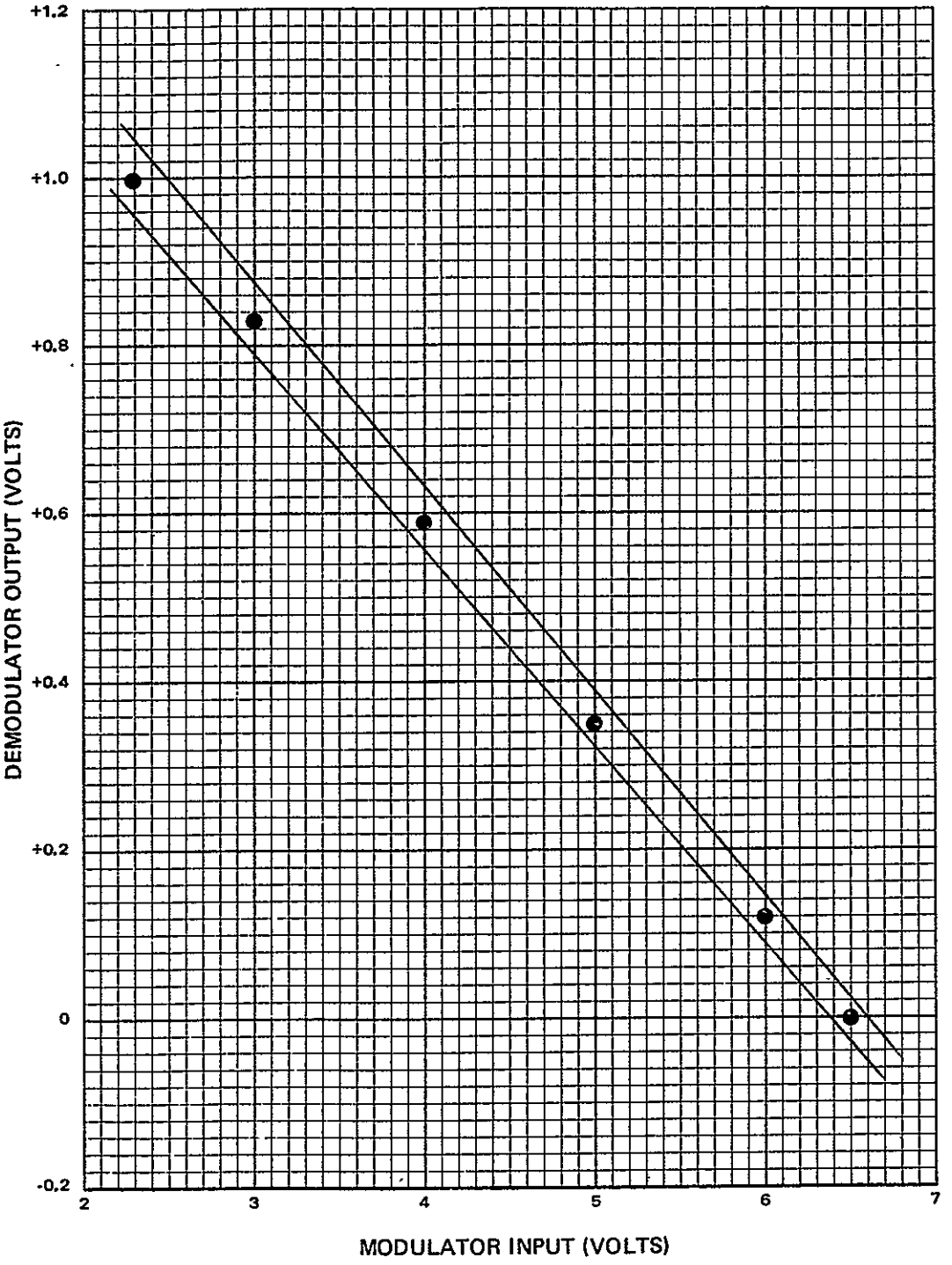

Figure 40. ID Channel Linearity and Drift, Engineering Model 2
(Sheet 2 of 2)

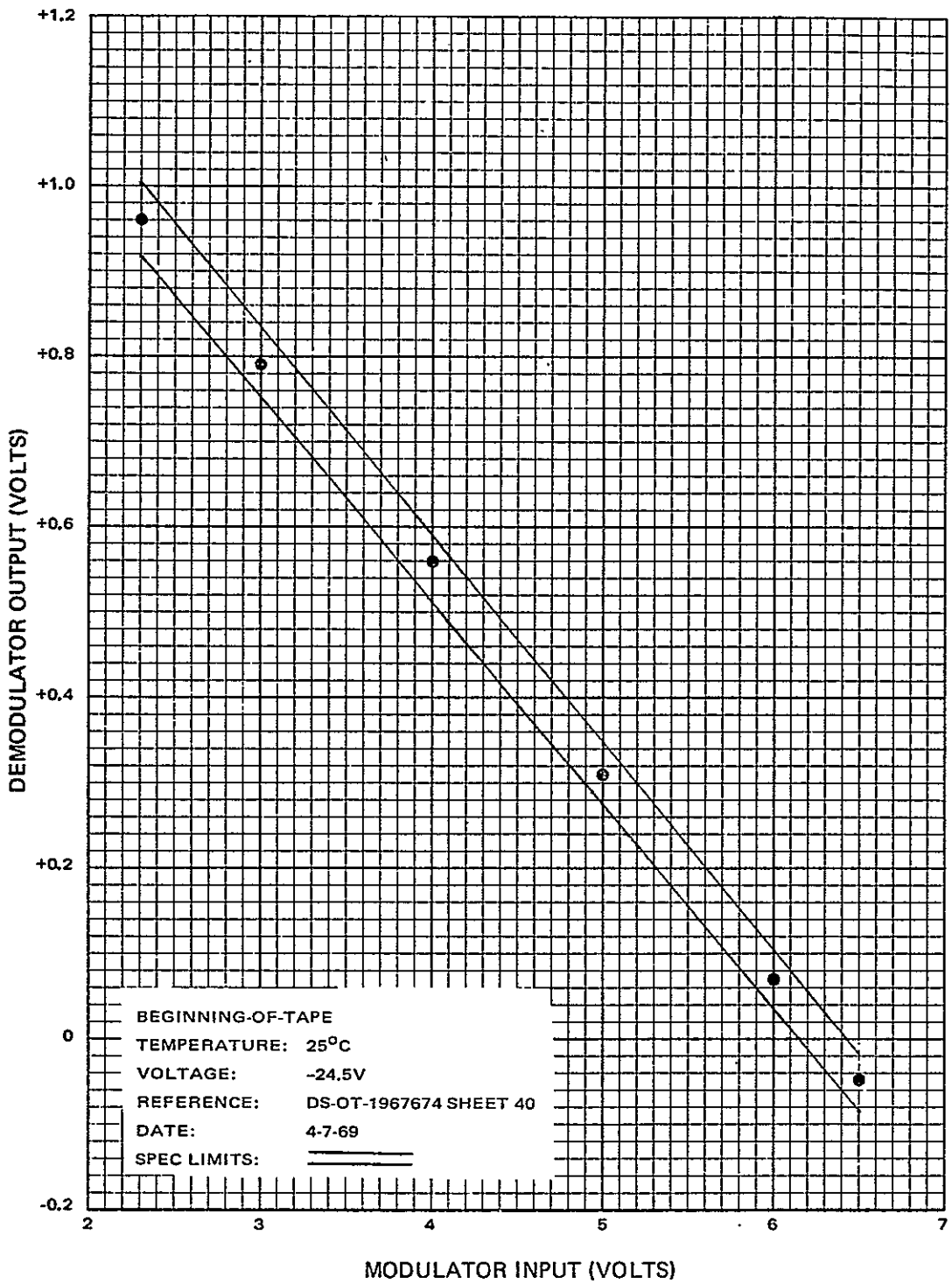

Figure 41. ID Channel Linearity and Drift, Flight Model 1
(Sheet 1 of 2)

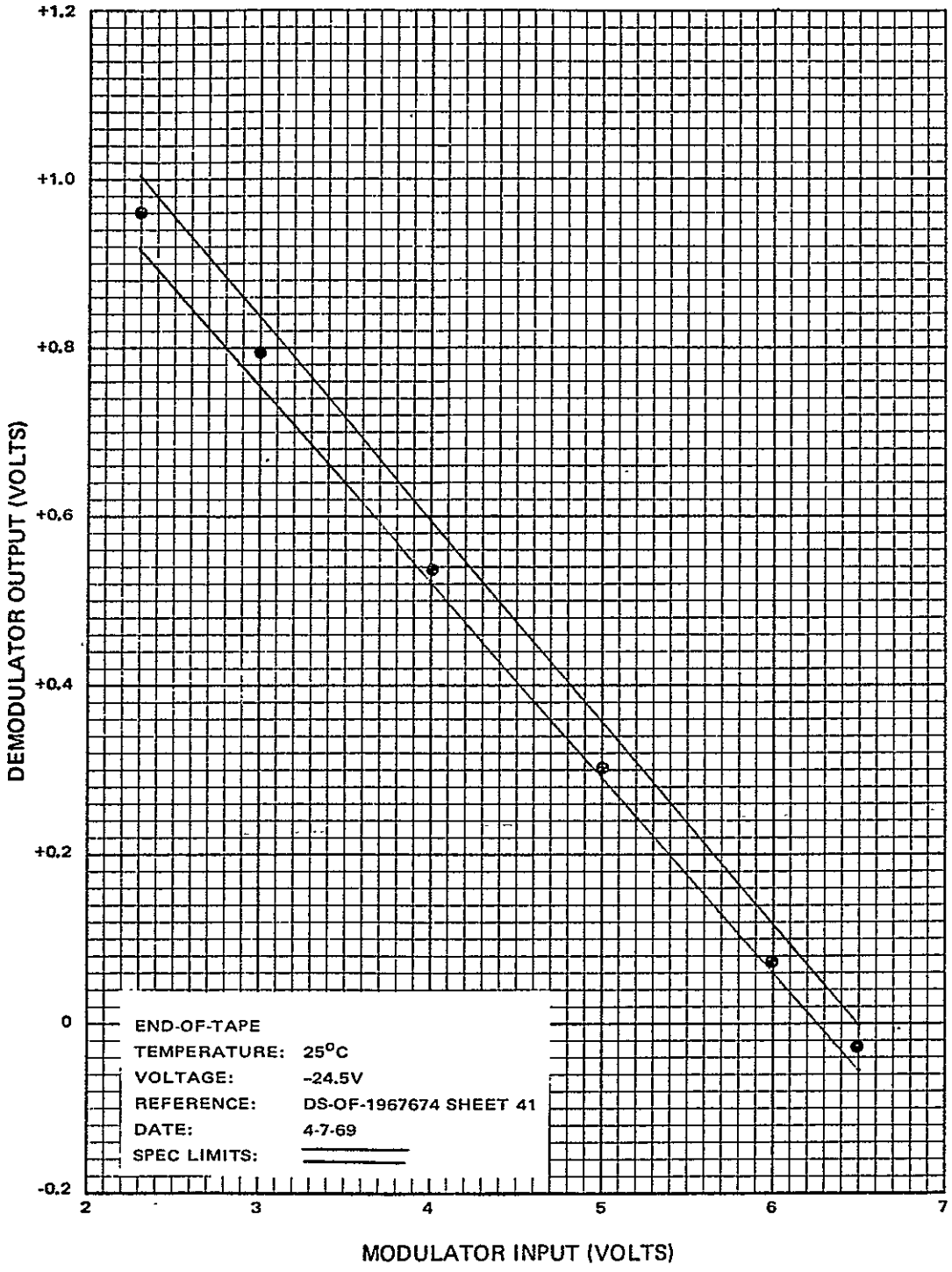

Figure 41. ID Channel Linearity and Drift, Flight Model 1
(Sheet 2 of 2)

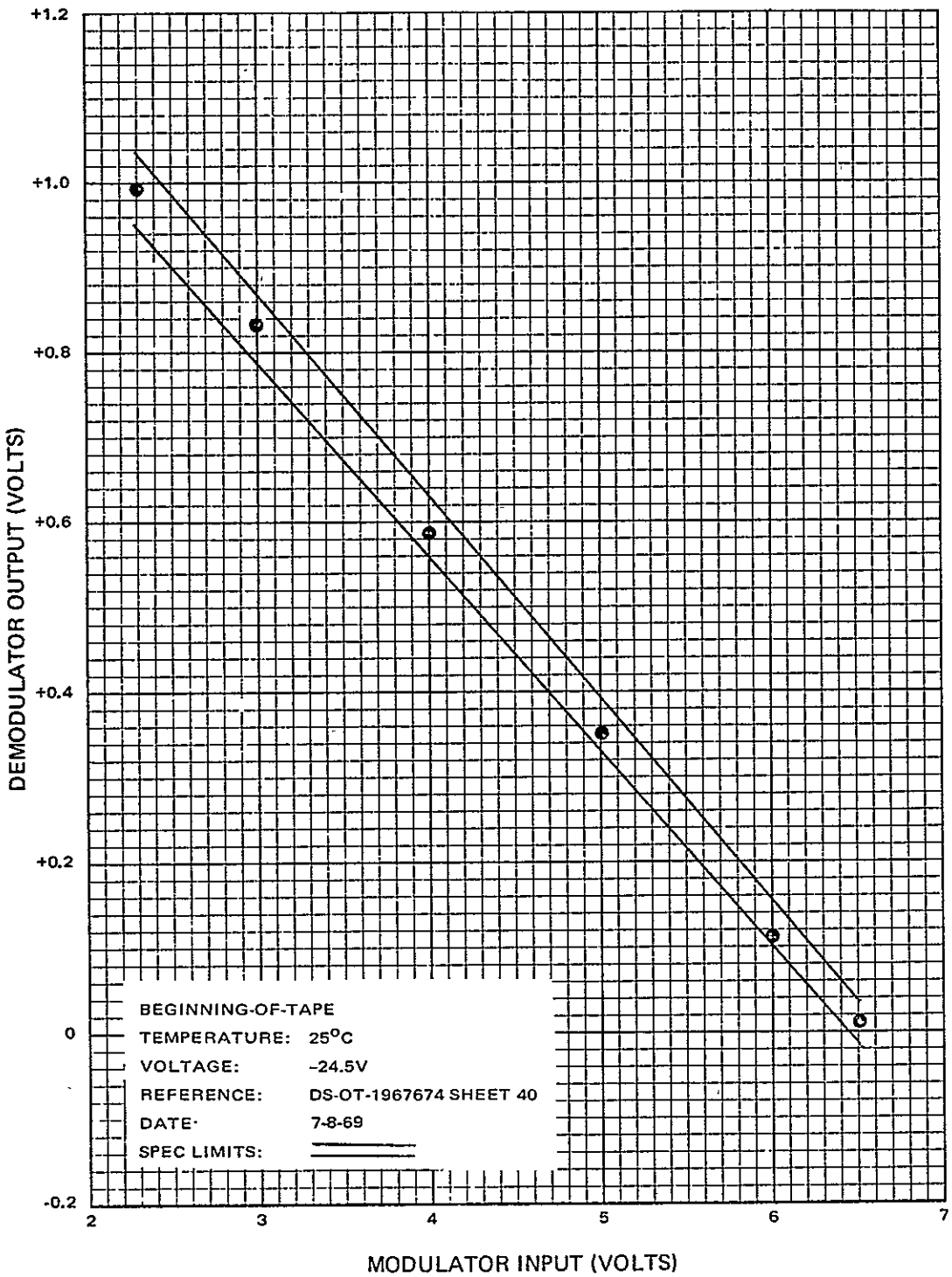

Figure 42. ID Channel Linearity and Drift, Flight Model 2
(Sheet 1 of 2)

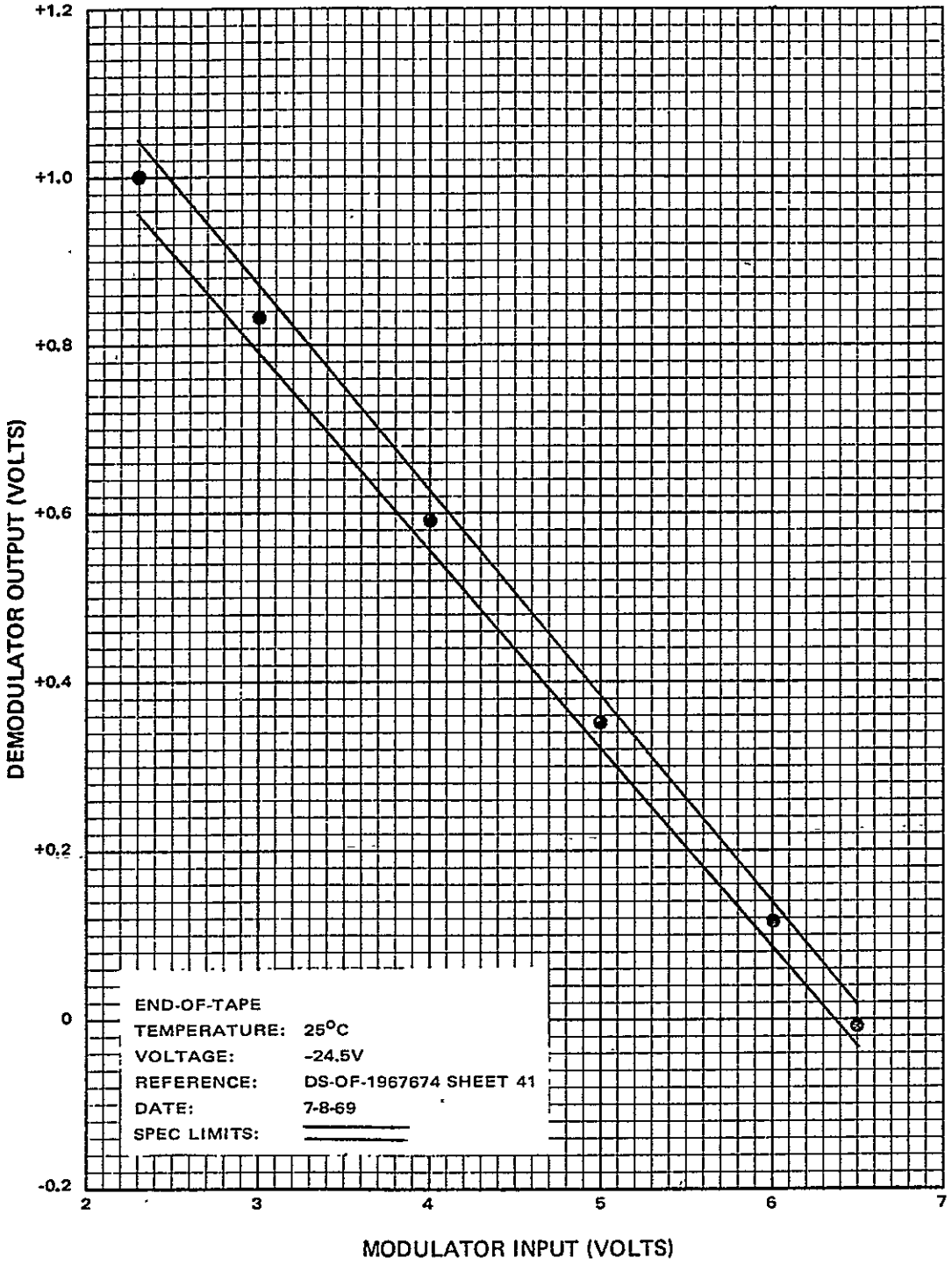

Figure 42. ID Channel Linearity and Drift, Flight Model 2
(Sheet 2 of 2)

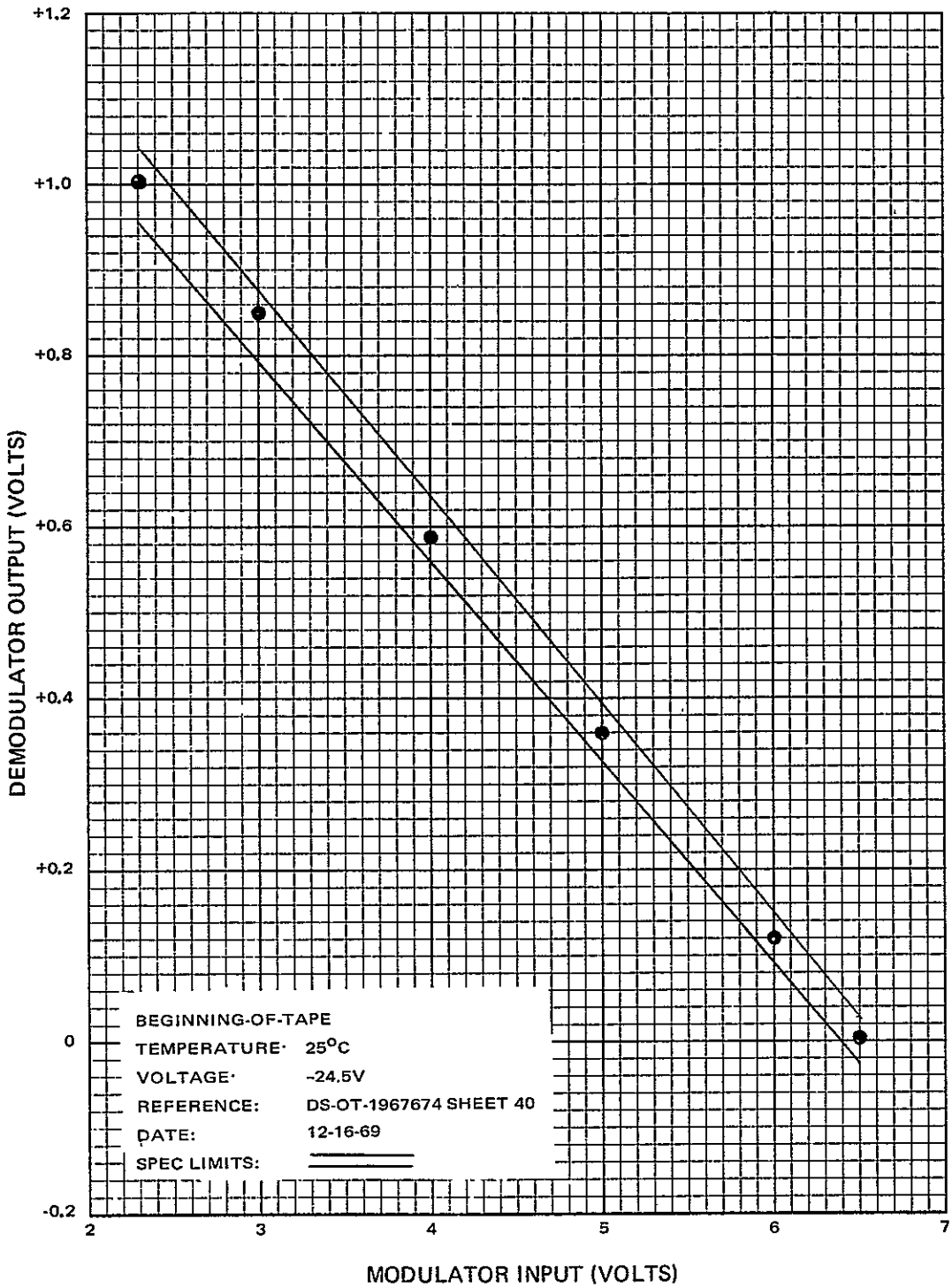

Figure 43. ID Channel Linearity and Drift, Flight Model 3
(Sheet 1 of 2)

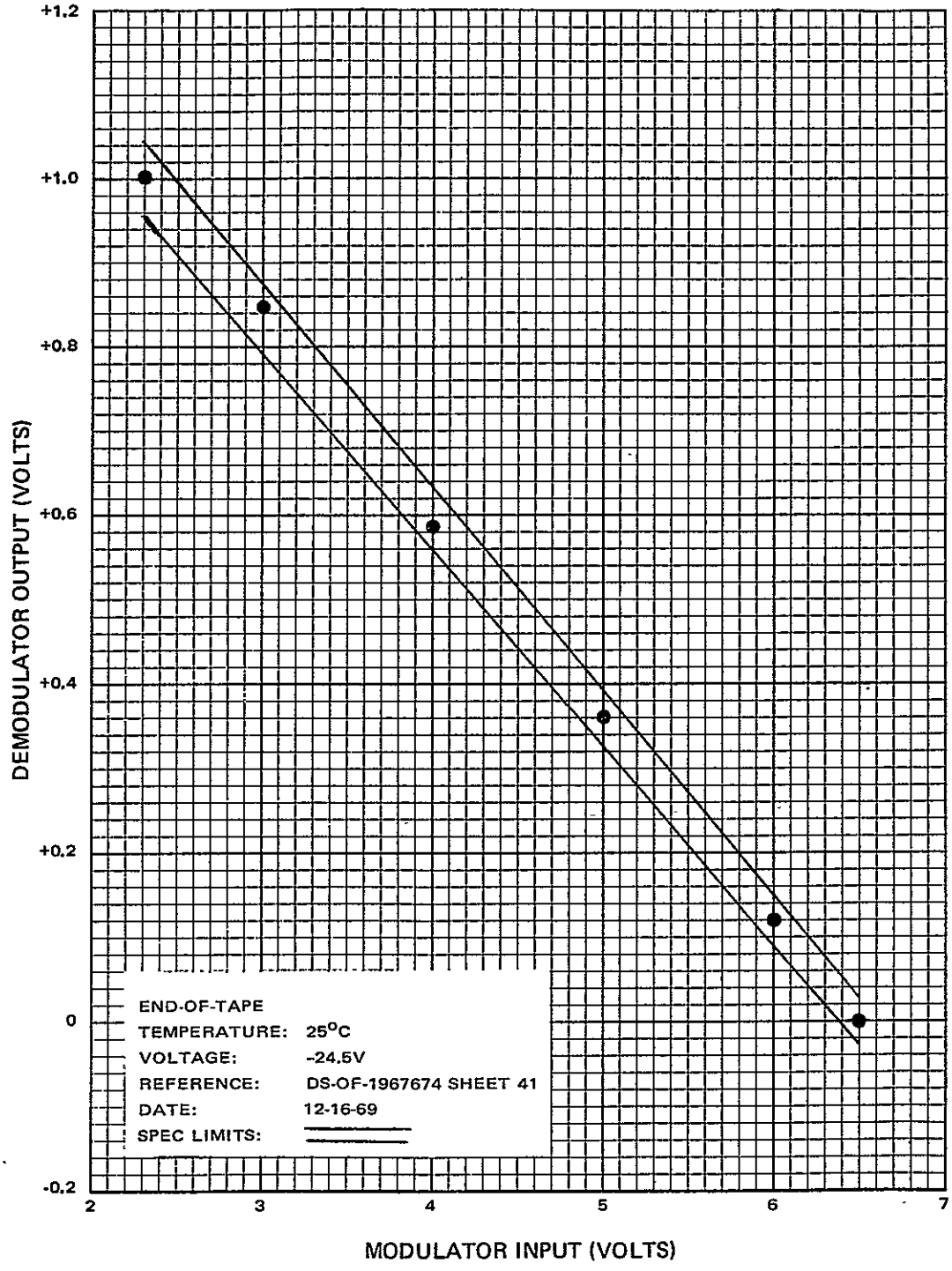

Figure 43. ID Channel Linearity and Drift, Flight Model 3
(Sheet 2 of 2)

SECTION 9
LIST OF REFERENCES

All the references cited in the text are tabulated in the order used in the text.

1. RCA, Astro-Electronics Division, Final Report for the High Data Rate Storage System (Engineering Models EM-1 and EM-2), Contract NAS5-3772, Princeton, New Jersey, May 3, 1968.

2. RCA, Astro-Electronics Division, Final Report for the Nimbus-B High Data Rate Storage System (Prototype and Flight Models F-1 through F-3), Contract NAS5-10205, Princeton, New Jersey, June 27, 1968.

3. RCA, Astro-Electronics Division, Instruction Manual, High Data Rate Storage System, Spacecraft Equipment, Contract NAS5-10396, Princeton, New Jersey, March 21, 1969.

4. RCA Astro-Electronics Division, Instruction Manual, Nimbus-D High Data Rate Storage System Modifications for the HDRSS-B Ground Stations, Contract NAS5-10396, Princeton, New Jersey, January 9, 1970.

5. RCA, Astro-Electronics Division, Instruction Manual, Nimbus-D Modifications of the Bench Check Unit of the HDRSS, Contract NAS5-10396, Princeton, New Jersey, September 3, 1968.

6. H.A. Wheeler, "The Interpretation of Amplitude and Phase Distortion Terms of Paired Echos," Procedings of the IRE, Volume 27, pp 353-385 June 1939.

7. R.W. Luchy, "Analysis Relating Delay Variation and Intersymbol Interference," Bell System Technical Journal, Volume 42, pp 2247-2484, September 1963.

8. RCA, Astro-Electronics Division, Performance Specification, HDRSS-D Tape Transport, PS-1967674, Contract NAS5-10396.

9. RCA, Astro-Electronics Division, Test and Calibration Curve for HRIR Satellite Equipment, Prototype P1, Contract NAS5-887, June 21, 1963.

10. RCA, Astro-Electronics Division, Operational Test, High Data Rate Storage System, TP-1967674, Contract NAS5-10396.

11. RCA, Astro-Electronics Division, Test Plan, High Data Rate Storage System, PN-1967674, Contract NAS5-10396.

APPENDIX I

HDRSS-D SIGNAL-TO- DISTORTION RATIO

A. INTRODUCTION

Signal distortion and crosstalk is due to the following:

- System Gain Non-Linearity - The intermodulation products which fall within the channel bandwidth appear as demodulated outputs. The gain non-linearity is contributed by the transmitter, multiplexer demultiplexer, and receiver non-linearity.
- I-F Bandwidth - The receiver IF filter bandwidth limits the received FM spectrum. The bandwidth limitation produces intermodulation products which fall in the subcarrier bandwidths. These products also appear as demodulated outputs.
- Phase Non-Linearity in the I-F Filters - Non-linear Phase in the IF filter of the receiver will produce intermodulation distortion which appear as demodulated outputs.
- Linear Crosstalk - Linear cross talk is the result of finite attenuations in the rejection bands of the multiplexer and demultiplexer.

B. DISTORTION DUE TO SYSTEM GAIN NON-LINEARITY

1. General

The various sources of amplitude non-linearity at a maximum deviation of ±1.5 MHz are as follows:

• Transmitter	± 1 percent
• Multiplexer/Demultiplexer	± 1 percent
• Receiver	± 2 percent
Total	± 4 percent

2. Problem

The output signal (e_1) passes through a non-linear amplifier whose transfer function is a polynominal function of the input (see Figure 1). The problem is to define the power in the important amplitude distortion terms.

3. Analysis

The auto correlation function of the amplifier output (e) was determined and the distortion components were identified. The spectra of the distortion components

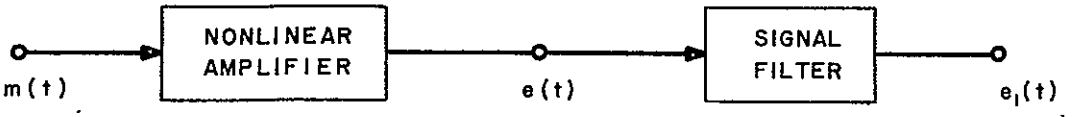

THE INPUT SIGNAL $m(t)$ = • GAUSSIAN DISTRIBUTED, MEAN VALUE = 0
• $S_m(\omega)$ = SPECTRUM OF m
• $\omega_m = 2\pi$ BANDWIDTH OF m

THE AMPLIFIER OUTPUT $e(t) = C_1 m + C_2 m^2 + C_3 m^3$

Figure I-1. Equivalent Circuit for System Gain Nonlinearity Analysis

were obtained by taking a Fourier transform of the autocorrelation function of the distortion components. The portion the power in each distortion component that passes through the signal filter adds to the distortion power.

a. Autocorrelation Function of the Amplifier Output

Let

$$m(t) = m_1 \quad m(t+\tau) = m_2$$
$$Rm(\tau) = E(m_1 m_2)$$
$$Rm(o) = E(m_1 m_1) = E(m_2 m_2) = \text{modulation power}$$

The autocorrelation function of e is

$$Re(\tau) = E\,(e(t)\,e\,(t+\tau))$$
$$= E\left[(C_1 m_1 + C_2 m_1^2 + C_3 m_1^3)(C_1 m_2 + C_2 m_2^2 + C_3 m_2^3)\right]$$
$$= C_1^2 E\,(m_1 m_2) + C_1 C_2 E\,(m_1 m_2 m_2) + C_1 C_3 E\,(m_1 m_2 m_2 m_2) + C_2 C_1 E\,(m_1 m_2)$$
$$+ C_1 C_2 E\,(m_1 m_1 m_2 m_2) + C_2 C_3 E\,(m_1 m_1 m_2 m_2 m_2) + C_3 C_1 E\,(m_1 m_1 m_1 m_2)$$
$$+ C_3 C_2 E\,(m_1 m_1 m_1 m_2 m_2) + C_3^2 E\,(m_1 m_1 m_1 m_2)$$
$$= C_1^2 E\,(m_1 m_2) + C_1 C_3 E\,(m_1 m_2 m_2 m_2) + C_2^2 E\,(m_1 m_1 m_2 m_2) + C_3 C_1 E\,(m_1 m_1 m_1 m_2)$$
$$+ C_3^2 E\,(m_1 m_1 m_1 m_2 m_2 m_2)$$

The expected value of the product of an odd number of gaussian distributed variables with zero mean value is zero.* The remaining five terms were evaluated separately. The method* of calculating the expected value of products of gaussian variables indicates that the terms which are linear functions of $Rm(\tau)$ contain undistorted signal. All the other terms are distorted terms.

Term 1: $c_1^2 E(m_1 m_2) = c_1^2 Rm(\tau)$

This term is an undistorted signal.

Term 2: $c_1 c_3 E(m_1 m_2 m_2 m_2) = 3 c_1 c_3 E(m_1 m_2) E(m_2 m_2)$

$$= 3 c_1 c_3 Rm(\tau) Rm(0)$$

This term is also an undistorted signal, ($Rm(0)$ is a constant).

Term 3: $c_2^2 E(m_1 m_1 m_2 m_2) = c_2^2 E(m_1 m_1) E(m_2 m_2)$

$$2 c_2^2 E(m_1 m_2) E(m_1 m_2)$$

$$= c_2^2 \left[Rm^2(0) + 2 Rm^2(\tau) \right]$$

This is a distortion term.

Term 4: $c_3 c_1 E(m_1 m_1 m_1 m_2) = 3 c_3 c_1 E(m_1 m_2) E(m_1 m_1)$

$$= 3 c_1 c_3 Rm(\tau) Rm(0)$$

This is undistorted signal.

Term 5: $c_3^2 E(m_1 m_1 m_1 m_2 m_2 m_2)$

$$= 2 c_3^2 E(m_1 m_1) E(m_1 m_2 m_2 m_2) + 3 c_3^2 E(m_1 m_2) E(m_1 m_1 m_2 m_2)$$

$$= 6 c_3^2 E(m_1 m_1) E(m_1 m_2) E(m_2 m_2)$$

$$+ 3 c_3^2 E(m_1 m_2) \left[E(m_1 m_1) E(m_2 m_2) + 2 E(m_1 m_2) E(m_1 m_2) \right]$$

$$= 9 c_3^2 Rm^2(0) Rm(\tau) + 6 c_3^2 Rm^3(\tau)$$

This first portion of this term is the signal; the second portion is the distortion.

---

*D. Middleton, Statistical Theory of Communications New York, McGraw Hill Book Co., Inc., 1960, p. 343.

The above results are summarized by the following equations:

Signal Terms =

$$\left[c_1^2 + 6\, c_1 c_3\, Rm(0) = 9\, c_3^2\, Rm^2(0) \right] Rm\ (\tau)$$

Distortion Terms =

$$c_2^2 \left[Rm^2(0) + 2\, Rm^2\ (\tau) \right] + 6\, c_3^2\, Rm^3\ (\tau)$$

If we assume ac coupling, then the dc term

$$c_2^2\, Rm^2\ (0)$$

can be ignored. In that case

$$R_2(\tau) = 2\, c_2^2\, Rm^2\ (\tau)$$

represents the 2nd order distortion and

$$R_3(\tau) = 6\, c_3^2\, Rm^3\ (\tau)$$

represents the 3rd order distortion.

b. Spectra of the Amplitude Distortion Terms

The spectra of the amplitude distortion terms are found by taking the Fourier Transform (FT) of the autocorrelation functions. Thus

$$S_2(\omega) = FT\Big(R_2(\tau)\Big) = FT\Big((2\, c_2^2\, Rm^2\ (\tau)\Big) = 2\, c_2^2\, S_m(\omega) * S_m\ (\omega)$$

and

$$S_3(\omega) = FT\ (R_3(\tau)) = FT\ (6\, c_3^2\, Rm^3\ (\tau)) = 6\, c_3^2\, S_m(\omega) * S_m(\omega) * S_m(\omega)$$

where

$$S_m(\omega) = FT\ (R_m(\tau))$$

* means convolution

c. Amplitude Distortion Power

The power due to the amplitude distortion terms at the output of the signal filter (e_1) may be computed by using the following equation:

$$Pi = \frac{1}{2\pi} \int_{-\infty}^{+\infty} |H_m(\omega)|^2 \, Si\,(\omega)\, d\omega$$

where Hm(w) is the transfer function of the signal filter

P_i = i-th order distortion power

(1) Second Order Signal-To-Distortion Ratio - Rectangular Spectrum. - Let

$$S_m(\omega) = \begin{cases} \pi R_m(0)/\omega_m, & |\omega| < \omega_m \\ 0, & |\omega| > \omega_m \end{cases}$$

i.e., the modulation has a rectangular spectrum.

Then

$$S_m(\omega) * S_m(\omega) = \begin{cases} \frac{\pi R_m^{\,2}(0)}{\omega_m} \left[1 - \frac{|\omega|}{2\omega_m}\right], & |\omega| < 2\omega_m \\ 0, & |\omega| > 2\omega_m \end{cases}$$

and

$$S_2(\omega) = \begin{cases} \frac{2\pi c_2^{\,2} R_m^{\,2}(0)}{\omega_m} \cdot \left[1 - \frac{|\omega|}{2\omega_m}\right], & |\omega| < 2\omega_m \\ 0, & |\omega| > 2\omega_m \end{cases}$$

The signal-to-second order amplitude distortion power ratio is

$$SDR_2 = \frac{R_m(0)}{\frac{2\pi c_2^2 R_m^2(0)}{\pi \omega_m} \int_0^{\omega_m} \left[1 - \frac{|\omega|}{2\omega_m}\right] d\omega}$$

$$SDR_2 = \frac{2}{3 c_2^2 R_m(0)}$$

(2) Third Order Signal-To-Distortion Ratio - Rectangular Spectrum. - Let

$$S_m(\omega) = \begin{cases} \pi R_m(0)/\omega_m , & |\omega| < \omega_m \\ 0 , & |\omega| > \omega_m \end{cases}$$

Again, we assume the modulation has a rectangular spectrum

Then

$$S_m(\omega) * S_m(\omega) * S_m(\omega)$$

$$= \frac{\pi R_m^3(0)}{4\omega_m} \left[3 - \frac{\omega^2}{\omega_m^2}\right], \quad |\omega| < \omega_m$$

The overall 3rd order signal-to-distortion power ratio is

$$SDR_3 = \frac{R_m(0)}{\frac{1}{\pi} \int_0^{\omega_m} \frac{6 c_3^2 \pi R_m^3(0)}{4\omega_m} \left[3 - \frac{\omega^2}{\omega_m^2}\right] d\omega}$$

$$SDR_3 = \frac{1}{4 c_3^2 R_m^2(0)}$$

d. Calculation of the Coefficients, c_1, c_2 and c_3. The coefficient c_1 is merely a gain factor and can be arbitrary. The coefficients c_2 and c_3 are chosen so that a certain percentage of non-linearity will be present when m is at its rms value.

Let E_2 = fractional deviation due to the 2nd order distortion at

$m = \sqrt{Rm^{(0)}}$

E_3 = fractional deviation due to the 3rd order distortion at

$m = \sqrt{Rm^{(0)}}$

Then

$$E_2 = \frac{c_2 m^2}{c_1 m}\Bigg|_{m = \sqrt{R_m^{(0)}}} = \frac{c_2}{c_1}\sqrt{R_m^{(0)}}$$

$$E_3 = \frac{c_3 m^3}{c_1 m}\Bigg|_{m = \sqrt{R_m(0)}} = \frac{c_3}{c_1} R_m(0)$$

and

$$c_2 = E_2 c_1 / \sqrt{R_m(0)}$$

$$c_3 = E_1 c_1 / R_m(0)$$

If we let $c_1 = CA_1$, $E_2 = \frac{CA_2}{CA_1}$, $E_3 = \frac{CA_3}{CA_1}$ then the transfer function of the non-linear amplifier is

$$e(t) = c_1 m + c_2 m^2 + c_3 m^3 = CA_1 m + \frac{CA_2 m^2}{\sqrt{R_m(0)}} + \frac{CA_3 m^3}{R_m(0)}$$

The calculations were performed on the RCA-601 computer; Figure I-2 shows the definition of non-linearity used in the computations.

For the calculation, the total non-linearity (±4%) is divided equally into 2nd order (±2%) and 3rd order (±2%) distortion. The 2nd order non-linearity is the term ($c_2 x^2$); the 3rd order is the term ($c_3 x^3$).

---

1. A Papoulis Probability, Random Variables, and Stochastic Processes, New York, McGraw-Hill Book Co. Inc., 1965.
2. D. Middleton, Statistical Theory of Communications, New York, McGraw-Hill Co. Inc. 1960, p.343

C. DISTORTION DUE TO IF BANDWIDTH

An approximate value of the signal-to-distortion ratio due to IF bandwidth was based on the curves of Figure 2*, modulation index (β) and the ratio RF bandwidth (BW) and the baseband (fm). The ratio

$$\frac{BW}{fm} = \frac{3.0\ MHz}{0.8\ MHz} = 3.7.$$

The modulation index

$$\beta rms = \frac{rms\ deviation}{maximum\ baseband\ freq.} = \frac{405\ kHz}{790\ kHz} = 0.5\ rms$$

The curves yielded a signal-to-distortion value of 30 dB. This value applies to an FM channel whose bandwidth extends from dc to fm. For the frequency multiplexed signal of Nimbus-D, the assumption that both signal power and distortion power are evenly distributed among the various subcarrier channels is made. Therefore, the signal to distortion for each channel is of the order of 30 dB.

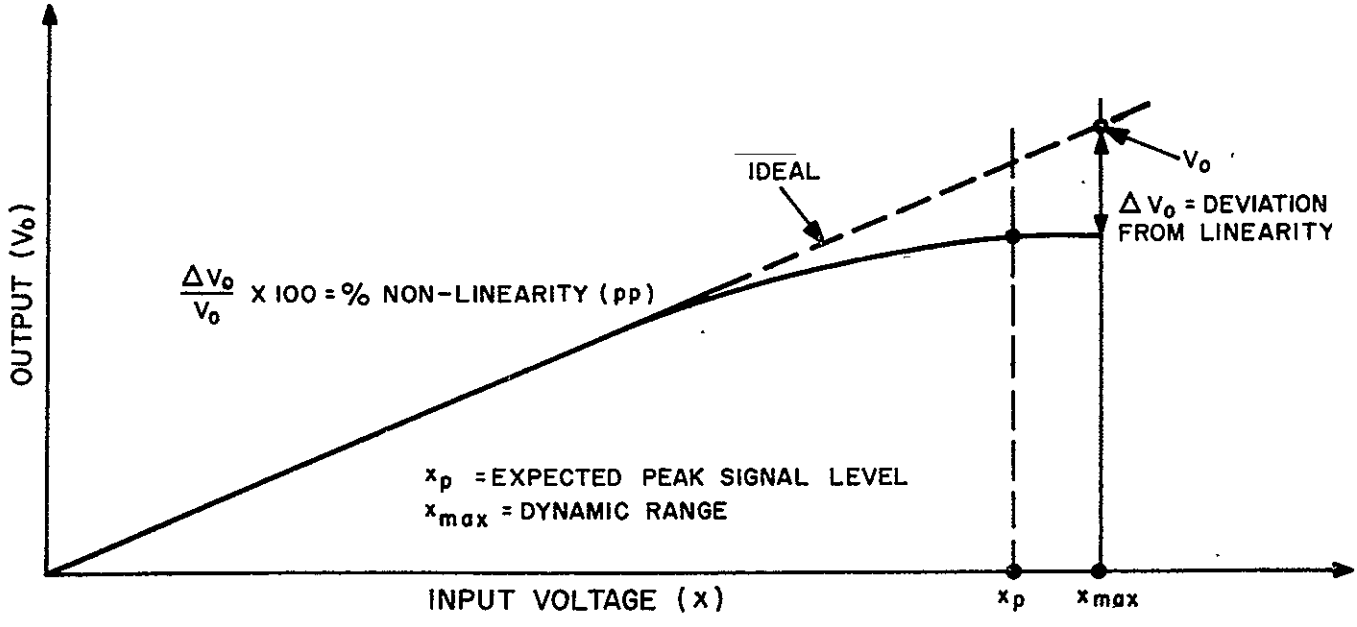

Figure I-2. Definition of Gain Non-Linearity

*H.S.E. Wang, "Distortion of FM Signals Caused by Channel Phase Non-Linearity and Amplitude Fluctuations" IEEE Transactions on Communication Technology, August 1966.

D. DISTORTION DUE TO PHASE NON-LINEARITY IN THE IF FILTER

1. General

Departure of IF filter response from linearity will produce signal distortion. The IF filter is a eighth order Butterworth with a geometric center frequency at 51.0 MHz and a 3 dB bandwidth at 3.4 MHz. Calculations, made with an RCA 601 computer, yielded the second and third order distortions due to phase non-linearity. The results are tabulated in Table I-1.

TABLE I-1. SIGNAL-TO-DISTORTION RATIO DUE TO IF PHASE NON-LINEARITY

Channel	Second Order (dB)	Third Order (dB)	Net Loss (dB rms/rms)
IRIS	50.6	42.8	42.1
VIP	48.9	40.4	39.8
IDCS	46.2	36.2	35.8
THIR	41.5	30.5	30.2
TC	44.2	33.1	32.8

2. Problem

An FM signal (e_1) is passed through an RF filter, an ideal discriminator and a modulation filter (see Figure I-3). The output (e_4) consists of the modulation plus phase distortion terms introduced by the RF filter. The problem is to find the power in the important phase distortion terms.

3. Analysis

A quasi-steady state analysis is used; the RF filter is assumed to operate on the instantaneous input frequency, i.e., $w_c + m$.* Therefore,

$$e_2 = |H(\omega)| \sin(\omega_c t + \int m dt + \Phi(\omega)|$$

where

$$\omega = \omega_c + m$$

*P.D. Shaft, "Distortion of Multitone FM Signals Due to Phase Non-Linearity," IEEE Transactions on Space Electronics and Telemetry.

RF FILTER CENTER FREQUENCY = ω_c

RF FILTER TRANSFER FUNCTION = $H(\omega) = |H(\omega)| \; e^{j\phi(\omega)}$

IDEAL DISCRIMINATOR CENTER FREQUENCY = ω_c .

IMPUT $e_1 = \text{SIN}\left(\omega_c t + \int m dt\right)$

WHERE m = MODULATION (GAUSSIAN DISTRIBUTED, ZERO MEAN VALUE)

$\omega_m = 2\pi$ BW OF RF FILTER (ONE SIDED BAND WIDTH)

$\omega_m = 2\pi$ BW OF MODULATION

Figure I-3. Equivalent Circuit for Phase Non-Linearity Analysis

The output of the discriminator is the time derivative of the phase angle of e_2 centered at w_c. Hence

$$e_3 = \frac{d}{dt}\left[\int m dt + \Phi(\omega_c + m)\right]$$

If the phase function $\Phi(\omega)$ is expanded about w_c, one gets

$$\Phi(\omega) = a_0 + a_1(\omega - \omega_c) + a_2(\omega - \omega_c)^2 + \ldots$$

If the carrier frequency (w_c) is much greater than the bandwidth of the RF filter (w_n), then the coefficients, a_i, in the above series are approximately equal to the coefficients in the expansion of the phase function $\Phi_L(\omega)$ of the equivalent low pass filter, i.e.

$$\Phi_L(\omega) = a_0 + a_1\omega + a_2\omega^2 + \ldots$$

where

$$H_L(\omega) = |H_L(\omega)| e^{j\Phi_L(\omega)} \doteq H(\omega - \omega_c), \quad |\omega - \omega_c| < \omega_n$$

Consequently, the discriminator output is

$$e_3 = m + \frac{d}{dt}\left[a_0 + a_1 m + a_2 m^2 + a_3 m^3 + \ldots\right]$$

Since the phase function is always an odd function, the even order coefficients are zero, i.e.,

$$a_0 = a_2 = a_4 = a_6 = \text{etc.} = 0$$

Thus,

$$e_3 = m + a_1 \dot{m} + \frac{d}{dt}\left[a_3 m^3 + a_5 m^5 + \ldots\right]$$

The first two terms of e_3 are linear functions of the modulation m. The remaining terms are non-linear functions of m; these are the distortion terms. Thus, the first distortion term is of third order. If the carrier frequency was not much greater than the RF filter bandwidth the even order coefficients would not be zero and the first distortion term would be of second order.

a. Autocorrelation Functions of the Phase Distortion Terms

The autocorrelation functions of the second and third order distortion terms will be calculated. In most cases, only the third order case will be needed.

(1) Second Order Case. - The autocorrelation function of the second order distortion term is given by

$$R_2(\tau) = E\left(\frac{d}{dt}\left[a_2 m^2(t)\right] \cdot \frac{d}{dt}\left[a_2 m^2\,(t+\tau)\right]\right)$$

$$R_2(\tau) = -a_2^2 \frac{d^2}{d\tau^2} E\left(m^2(t) m^2(t+\tau)\right)^*$$

Let

$$m(t) = m_1 \text{ and, } m(t+\tau) = m_2$$

---

*A. Papoulis, Probability, Random Variables, and Stochastic Processes, New York, McGraw-Hill, Co. Inc., 1965.

Then we have

$$R_2(\tau) = -a_2^2 \frac{d^2}{d\tau^2} E(m_1 m_1 m_2 m_2)$$

The technique for expanding $E(m_1\ m_1\ m_2\ m_2)$ and other similar forms, where m is gaussian distributed with zero mean value is in the Statistical Theory of Communications.* The result is

$$R_2(\tau) = -a_2^2 \frac{d^2}{d\tau^2} \left[E(m_1 m_1)\, E(m_2 m_2) + 2E(m_1 m_2)\, E(m_1 m_2) \right]$$

$$= -a_2^2 \frac{d^2}{d\tau^2} \left[R_m^2(0) + 2R_m^2(\tau) \right]$$

where

$$R_m(\tau) = E(m(t)\ m\ (t+\tau))$$

= autocorrelation function of the modulation

$R_m(0)$ = modulation power $= E(m^2(t))$

Since

$$\frac{d^2}{d\tau^2} R_m^2(0) = 0$$

$$R_2(\tau) = -2a_2^2 \frac{d^2}{d\tau^2} R_m^2(\tau)$$

*D. Middleton, Statistical Theory of Communications, New York, McGraw-Hill Book Co., Inc., page 343.

(2) Third-Order Case. - The autocorrelation function of the third order distortion term is given by

$$R_3(\tau) = E\left(\frac{d}{dt}\left[a_3 m^3(t)\right] \cdot \frac{d}{dt}\left[a_3 m^3(t+\tau)\right]\right)$$

$$= -a_3^2 \frac{d^2}{d\tau^2} E\left(m^3(t)\, m^3(t+\tau)\right)$$

$$= -a_3^2 \frac{d^2}{d\tau^2} E\left(m_1 m_1 m_1 m_2 m_2 m_2\right)$$

$$= -a_3^2 \frac{d^2}{d\tau^2} \left[\begin{array}{l} 2\,E(m_1 m_1)\; E(m_1 m_2 m_2 m_2) \\ +\,3\,E(m_1 m_2)\; E(m_1 m_1 m_2 m_2) \end{array}\right]$$

$$= -a_3^2 \frac{d^2}{d\tau^2} \left[\begin{array}{l} 2E(m_1 m_1)\;\left[3E(m_1 m_2)\; E(m_2 m_2)\right] \\ +\,3E(m_1 m_2)\left[\begin{array}{l} E(m_1 m_1)\; E(m_2 m_2) \\ +\,2\,E(m_1 m_2)\; E(m_1 m_2) \end{array}\right] \end{array}\right]$$

$$= -a_3^2 \frac{d^2}{d\tau^2} \left[\begin{array}{l} 9\,E(m_1 m_2)\; E(m_1 m_1)\; E(m_2 m_2) \\ +\,6\,E(m_1 m_2)\; E(m_1 m_2)\; E(m_1 m_2) \end{array}\right]$$

$$= -a_3^2 \frac{d^2}{d\tau^2} \left[9 R_m^2(0)\, R_m(\tau) + 6 R_m^3(\tau)\right]$$

Note that the term

$$-9 a_3^2 \frac{d^2}{d\tau^2} R_m^2(0)\, R_m(\tau)$$

is not a distortion term. It is the autocorrelation function of

$$3 a_3 R_m(0)\, \dot{m}$$

which is a linear function of m and should be added to the terms

$$m + a_1 \dot{m}$$

The autocorrelation function of the third order distortion term is

$$R_3'(\tau) = -6 a_3^2 \frac{d^2}{d\tau^2} R_m^3(\tau)$$

(The linear term has been removed.)

b. Spectra of the Phase Distortion Terms

The spectra of the phase distortion terms are found by taking the Fourier Transform (FT) of the autocorrelation functions. Thus

$$S_2(\omega) = FT(R_2(\tau)) = \text{double sided spectral density}$$

$$= 2 a_2^2 \omega^2 S_m(\omega) * S_m(\omega)$$

and

$$S_3(\omega) = FT(R_3'(\tau))$$

$$= 6 a_3^2 \omega^2 S_m(\omega) * S_m(\omega) * S_m(\omega)$$

where

$$S_m(\omega) = FT(R_m(\tau))$$

(The symbol * means convolution.)

c. Phase Distortion Power

The power due to the phase distortion terms at the output of the modulation filter (e_4) may be computed by using the following equation:

$$P_i = \frac{1}{2\pi} \int_{-\infty}^{+\infty} |H_m(\omega)|^2 S_i(\omega) \, d\omega$$

where Hm (W) is the transfer function of the modulation filter P_i is the i-th order distortion power

(1) Second Order Signal-To-Distortion Power Ratio, Rectangular Spectrum.- Let

$$S_m(\omega) = \begin{cases} \pi R_m(0)/\omega_m, & |\omega| < \omega_m \\ 0, & |\omega| > \omega_m \end{cases}$$

i.e., assume the modulation has a rectangular spectrum.

Then

$$S_m(\omega) * S_m(\omega) = \begin{cases} \frac{\pi R_m^2(0)}{\omega_m} \left[1 - \frac{|\omega|}{2\omega_m}\right], & |\omega| < 2\omega_m \\ 0 & |\omega| > 2\omega_m \end{cases}$$

and

$$S_2(\omega) = \begin{cases} \frac{2\pi a_2^2 R_m^2(0)}{\omega_m} \omega^2 \left[1 - \frac{|\omega|}{2\omega_m}\right], & |\omega| < 2\omega_m \\ 0, & |\omega| > 2\omega_m \end{cases}$$

The distortion-to-signal ratio at a frequency w is equal to

$$(D/S) = \frac{2\pi a_2^2 R_m^2(0) \omega^2 \left(1 - \frac{|\omega|}{2\omega_m}\right)}{\omega_m \left(\frac{\pi R_m(0)}{\omega_m}\right)}$$

$$(D/S) = 2 a_2^2 R_m(0) \omega_m^2 \left(\frac{\omega}{\omega_m}\right)^2 \left(1 - \frac{|\omega|}{2\omega_m}\right)$$

which agrees with equation (24) in the cited Text*.

The overall signal-to-distortion power ratio ($2DR_2$) at e_4 equals:

$$SDR_2 = \frac{R_m(0)}{\frac{1}{\pi}\int_0^{\omega_m} \frac{2\pi a_2^2 R_m(0)}{\omega_m}\left[\omega^2 - \frac{\omega^3}{2\omega_m}\right] d\omega}$$

$$SDR_2 = \frac{12}{5a_2^2 R_m(0)\,\omega_m^2}$$

(2) Second Order Signal-To-Distortion Power Ratio, Parabolic Spectrum.- Let

$$S_m(\omega) = \begin{cases} 3\pi R_m(0)\,\omega^2/\omega_m^3 & , \ |\omega| < \omega_m \\ 0 & , \ |\omega| > \omega_m \end{cases}$$

i.e., assume that the input modulation has a parabolic spectrum. Then

$$S_m(\omega) * S_m(\omega) = \begin{cases} \frac{9\pi R_m^2(0)}{2\omega_m}\left[\frac{2}{5} - \frac{\omega}{\omega_m} + \frac{2}{3}\left(\frac{\omega}{\omega_m}\right)^2 - \frac{1}{30}\left(\frac{\omega}{\omega_m}\right)^5\right], & |\omega| < 2\omega_m \\ 0 & |\omega| > 2\omega_m \end{cases}$$

*P. D. Shaft, "Distortion of Multitone FM Signals Due to Phase Non-Linearity," IEEE Transactions on Space Electronics and Telemetry.

The overall signal-to-distortion power ratio is

$$SDR_2 = \frac{R_m(0)}{\frac{1}{\pi}\int_0^{\omega_m} \frac{9\pi a_2^2 R_m^2(0)}{\omega_m}\left[\frac{2\omega^2}{5} - \frac{\omega^3}{\omega_m} + \frac{2\omega^4}{\omega_m^2} - \frac{\omega^7}{30\omega_m^5}\right] d\omega}$$

$$SDR_2 = \frac{28}{3 a_2^2 R_m(0) \omega_m^2}$$

Note that the SDR is larger for a parabolic modulation spectrum than a rectangular modulation spectrum by a factor of 3.89.

(3) Third Order Signal-To-Distortion Power Ratio, Rectangular Spectrum.- Let

$$S_m(\omega) = \begin{cases} \pi R_m(0)/\omega_m, & |\omega| < \omega_m \\ 0, & |\omega| > \omega_m \end{cases},$$

i.e., we again assume a rectangular modulation spectrum.

Then

$$S_m(\omega) * S_m(\omega) * S_m(\omega) = \frac{\pi R^3(0)}{4\omega_m}\left[3 - \frac{\omega^2}{\omega_m^2}\right]; \quad |\omega| < \omega_m$$

The overall signal-to-distortion power ratio is

$$SDR_3 = \frac{R_m(0)}{\frac{1}{\pi}\int_0^{\omega_m} \frac{6 a_3^2 \pi R_m^3(0)}{4\omega_m}\left[3\omega^2 - \frac{\omega^4}{\omega_m^2}\right] d\omega}$$

$$SDR_3 = 5/6\, a_3^2 R_m^2(0) \omega_m^2$$

(4) Third Order Signal-To-Distortion Power Ratio, Parabolic Spectrum. - Let

$$S_m(\omega) = \begin{cases} 3\pi R_m(0)\ \omega^2/\omega_m^3 & |\omega| < \omega_m \\ 0 & |\omega| > \omega_m \end{cases}$$

i.e., again the modulation has a parabolic spectrum. In order to calculate the distortion power (P) given by

$$P = \frac{6\,a_3^2}{2\pi} \int_{-\omega_m}^{+\omega_m} \omega^2\, S_m(\omega) * S_m(\omega) * S_m(\omega)\, d\omega$$

Let w = t and make use of the Laplace Transform (LT). Then

$$P = \frac{6\,a_3^2}{8\pi^3} \left[LT^{-1} \left[\frac{1}{S} \frac{d^2}{d^2} \left(LT\,(S_m(t)) \right)^3 \right] \right]_{-\omega_m}^{+\omega_m}$$

It is easily shown that

$$LT\left[S_m(t)\right] = \frac{3\pi R_m(0)}{\omega_m^3} \left[e^{s\omega_m} \left[\frac{\omega_m^2}{S} - \frac{2\omega_m}{S^2} + \frac{2}{S^3} \right] - e^{-s\omega_m} \left[\frac{\omega_m^2}{S} + \frac{2\omega_m}{S^2} + \frac{2}{S^3} \right] \right]$$

Substituting this in the equation for P and evaluating P, one finds that

$$P = 6\,a_3^2\, \frac{27\,R_m^3(0)}{8\,\omega_m^9} \cdot \frac{272}{3465}\,\omega_m^{11} = \frac{612}{385}\,a_3^2\,R_m^3(0)\,\omega_m^2$$

Consequently,

$$SDR_3 = \frac{R_m(0)}{\frac{612}{385} a_3^2 R_m^3(0) \omega_m^2} = \frac{385}{612 a_3^2 R_m^2(0) \omega_m^2}$$

Note that the signal-to-distortion ratio is higher for modulation with a rectangular spectrum than for modulation with a parabolic spectrum by a factor of 102/77 or 1.325 for the third order distortion case.

(5) Computer Calculation of the Signal-To-Distortion Power Ratio. Let m(t) be a frequency multiplexed signal, i.e., the spectrum of m(t) is as shown in Figure I-4. The modulation filters are located as shown in Figure I-5. The RF filter is such that the distortion is of the third order, therefore the equation

$$S_3(\omega) = 6 a_3^2 \omega^2 S_m(\omega) * S_m(\omega) * S_m(\omega)$$

applies. In order to obtain the distortion power in each frequency band, the spectrum of the modulation must be convolved with itself twice. This is best done on a digital computer by sampling $S_m(w)$ and convolving the sampled

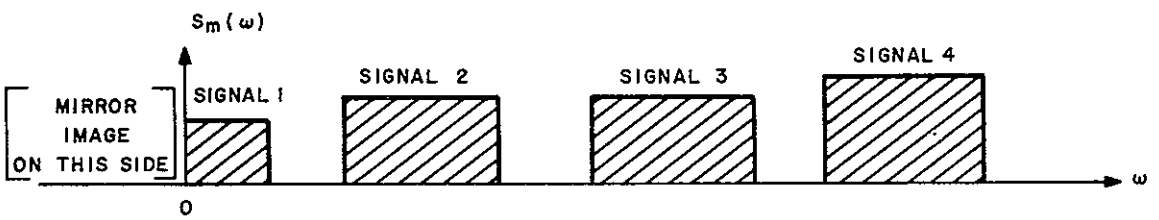

Figure I-4. Frequency Multiplexed Signal Spectrum

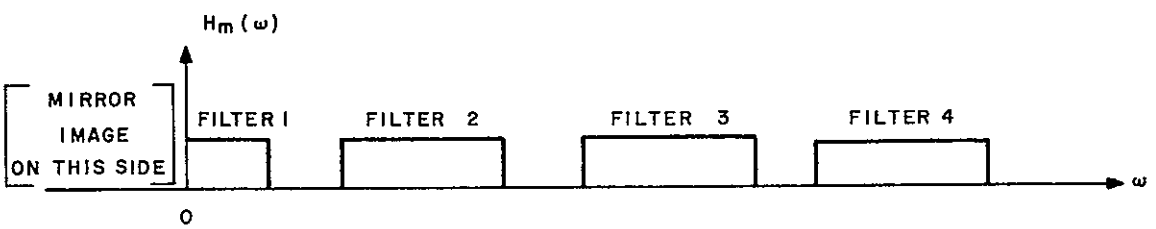

Figure I-5. Modulator Filter Spectrum

functions. The resulting sampled function is then weighted by $6 a_3^2 \omega^2$. By adding up the samples that fall within the various bands and multiplying by an appropriate constant, the distortion power in each band can be calculated.

(a) Calculation of a_3 For the Normalized Low Pass Filter. -

Let

$$H_L(S) = \frac{n_0 + n_1 s + n_2 s^2 + n_3 s^3 + \ldots}{d_0 + d_1 s + d_2 s^2 + d_3 s^3 + \ldots}$$

then

$$\Phi_L(\omega) = \tan^{-1} \frac{n_1\omega - n_3\omega^3 + \ldots}{n_0 - n_2\omega^2 + \ldots} - \tan^{-1} \frac{d_1\omega - d_3\omega^3 + \ldots}{d_0 - d_2\omega^2 + \ldots}$$

Since $\tan^{-1} x = x - \frac{x^3}{3} + \ldots$, we have

$$\Phi_L(\omega) = \omega \frac{n_1 - n_3\omega^2 + \ldots}{n_0 - n_2\omega^2 + \ldots} - \frac{\omega^3}{3}\left[\frac{n_1 - n_3\omega^2 + \ldots}{n_0 - n_2\omega^2 + \ldots}\right]^3 + \ldots$$

$$- \omega \frac{d_1 - d_3\omega^3 + \ldots}{d_0 - d_2\omega^2 + \ldots} + \frac{\omega^3}{3}\left[\frac{d_1 - d_3\omega^2 + \ldots}{d_0 - d_2\omega^2 + \ldots}\right] + \ldots$$

$$= \omega\left[\frac{n_1}{n_0} - \frac{d_1}{d_0}\right] + \omega^3 \left[\begin{array}{c} \frac{n_2 n_3 - n_0 n_4}{n_0^2} - \frac{n_2^3}{3n_0^3} \\ \frac{-d_2 d_3 \; d_0 d_4}{d_0^2} + \frac{d_2^3}{3d_0^3} \end{array}\right] + \ldots$$

Hence,

$$a_3 = \frac{n_2 n_3 - n_0 n_4}{n_0^2} - \frac{d_2 d_3 - d_0 d_4}{d_0^2} - \frac{n_2^3}{3n_0^3} + \frac{d_2^3}{3d_0^3}$$

This equation applies to a filter of unit bandwidth, i.e., $w_o = 1$. For a filter of bandwidth w_o, the above equation becomes

$$a_3 = \frac{1}{\omega_0^3}\left[\frac{n_2 n_3 - n_0 n_4}{n_o^2} - \frac{d_2 d_3 - d_0 d_4}{d_0^2} - \frac{n_2^3}{3 n_0^3} + \frac{d_2^3}{3 d_0^3}\right]$$

(b) Calculation Of The Second Order Distortion Coefficient. - If a bandpass filter with a bandwidth-to-center frequency which is not negligibly small is considered, then the even order coefficients in the expansion

$$\Phi(\omega) = a_0 + a_1 (\omega - \omega_c) + a_2 (\omega - \omega_c)^2 + \ldots$$

can be significant. To determine the value of a_2 the bandpass $\leftrightarrow$ low pass transformation is used, i.e.,

$$\frac{\omega}{\omega_0} \leftrightarrow \frac{1}{2\omega_0}\left[\omega - \frac{\omega_c^2}{\omega}\right], \quad \omega_c^2 = \omega_H \omega_L$$

ω_H = upper cutoff frequency

ω_L = lower cutoff frequency $\qquad \omega_H - \omega_L = 2\omega_0$

Expanding the right hand side about ω, we get

$$\frac{1}{2\omega_0}\left[\omega - \frac{\omega_c^2}{\omega}\right] = \frac{1}{\omega_0}\left[\Delta\omega - \frac{\Delta\omega^2}{2\omega_c} + \frac{\Delta\omega^3}{2\omega_c^2} - \ldots\right]$$

where $\Delta\omega = \omega - \omega_c$. This must be substituted in the phase expansion of a low pass filter of bandwidth ω_o, i.e.,

$$\Phi_L(\omega) = a_1 \frac{\omega}{\omega_0} + a_3 \left(\frac{\omega}{\omega_0}\right)^3 + a_5 \left(\frac{\omega}{\omega_0}\right)^5 + \ldots$$

The result is

$$\Phi(\omega) = a_1 \frac{1}{\omega_0}\left[\Delta\omega - \frac{\Delta\omega^2}{2\omega_c} + \ldots\right] + O(\Delta\omega^3)$$

Thus, the second order distortion coefficient is

$$a_2 = -\frac{a_1}{2\,\omega_0\,\omega_c}$$

From Paragraph (b) the coefficient a_1 for a normalized low pass filter is

$$a_1 = \left[\frac{n_1}{n_0} - \frac{d_1}{d_0}\right]$$

Hence

$$a_2 = \frac{1}{2\omega_0\omega_c}\left[\frac{d_1}{d_0} - \frac{n_1}{n_0}\right]$$

Note that the above equation for a_2 applies only if the bandpass filter is formed by resonating each reactive element of the equivalent low pass filter. Bandpass filters obtained by capacitively coupling tuned tank circuits (for example) do not obey the original bandpass - lowpass transformation. In such cases, the equation for a_2 above does not apply.

E. LINEAR CROSSTALK

Linear crosstalk was calculated with the frequency division multiplexed spectrum shown on Figure I-6 and the relative amplitudes of the subcarriers for the frequency deviations shown in Table I-2. For the calculations, the spectrum of each channel was simulated by a sinusoid. The final value of signal-to-crosstalk ratio includes the linear crosstalk and the contribution of the 40 dB signal-to-crosstalk ratio of the multiplexer. Table I-3 lists the signal-to-crosstalk results.

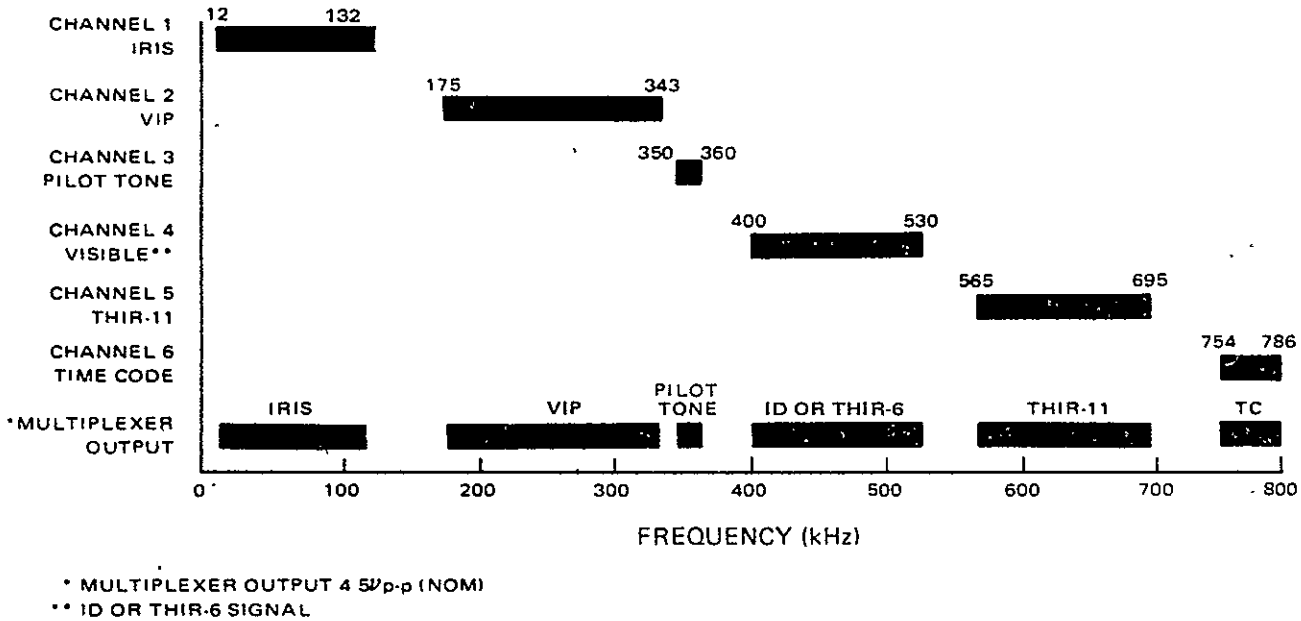

* MULTIPLEXER OUTPUT 4 5V p-p (NOM)
** ID OR THIR-6 SIGNAL

Figure I-6. Frequency Division Multiplexer Frequency Spectrum

TABLE I-2. FREQUENCY DEVIATIONS

Channel	Peak Frequency Deviation (kHz)
IRIS*	100
VIP	300
PT	44
ID	300
THIR	200
TC	300
	Total ±1244

* Expanded to 200 kHz Deviation by Contract Mod. No. 12 refer to Section 5, Par. A.1.

TABLE I-3. SIGNAL-TO-CROSSTALK RATIOS

Channel	Multiplexer SNR (dB rms/rms)	Demultiplexer Signal-To-Crosstalk -Linear- (dB rms/rms)	Net Signal-to-Crosstalk Ratio dB rms/rms
IRIS	40	29.3	28.9
VIP	40	48.5	39.4
PT	40	31.0	30.5
ID	40	39.7	36.8
THIR	40	35.7	34.3
TC	40	44.8	38.8

F. LIST OF REFERENCES

All the references cited in the text are tabulated in the order used in the text.

1. D. Middleton, Statistical Theory of Communications, New York, McGraw-Hill Book Co., Inc., 1960, p 343.
2. A. Papoulis, Probability, Random Variables, and Stochastic Processes, New York, McGraw-Hill Book Co., Inc. 1965.
3. H.S.E. Wang, Distortion of FM Signals Caused by Channel Phase Non-Linearity and Amplitude Fluctuations, IEEE Transactions on Communication Technology, August 1966.
4. P.D. Shaft, Distortion of Multitone FM Signals Due to Phase Non-Linearity, IEEE Transactions on Space Electronics and Telemetry.

APPENDIX II
LINK CALCULATIONS

The calculation for the carrier-to-noise-ratio of the RF link is shown in Table II-1.

TABLE II-1. CARRIER-TO-NOISE-RATIO CALCULATION FOR THE RF LINK

Parameter	Gain
Transmitter Power (5W)	+7.0 dBw
Spacecraft Cabling, etc.	-0.5 dB (assumed)
Spacecraft Antenna Gain	0.0 dB (at ±55°) *
Propagation	-167.6 dB (1840 NMat 1710 MHz, 5° elevation)
Polarization Loss	0.0 dB (assumed)
Ground Station Antenna	+47.7 dB **
Ground Station Cabling, etc.	-0.2 dB (assumed)
Performance Margin	-6.0 dB (assumed)
RECEIVER POWER	-119.6 dBw
NOISE POWER	-137.7 dBw (3 MHz BW, Noise Figure: 2.2 dB)*
CARRIER TO NOISE RATIO	+18.1 dB

*Noise figure measured as 2.2 dB; reported verbally by the RCA Service Company at GSFC, 3/1/65.

Particular attention should be drawn to the value given above for the spacecraft antenna gain: 0 dB at ±55°. The Nimbus Handbook for Experimenters (Nimbus B), dated October 1965, gives the spacecraft antenna gain as +6.5 dB with half power beam width of 90°. It is possible, therefore, that the gain of the antenna is several db higher, at ±55°, than the assumed value of 0 dB.

At greater elevation angles each of three factors improve the received CNR:

- shorter path length
- lower ground antenna temperature
- smaller angle (from axis) for spacecraft antenna.

*Stampfl, "The Nimbus Spacecraft and its Communication System as of September 1961, NASA Technical Note, D-1422, January 1963

**Paul A. Lenty, Handbook of NASA/GSFC Tracking, Data Acquisition, and Communication Antennas, GSFC, Greenbelt, Maryland.

APPENDIX III
COMPUTER SIMULATION OF VIP CHANNEL OUTPUT

A. INTRODUCTION

The results of the simulation of the VIP channel are presented in this appendix. The performance of channels with various bandwidths and phase equalizations is given.

B. CALCULATED WAVEFORMS FOR VIP CHANNEL

The simulation of the VIP channel was performed on an RCA-601 computer. The following approximations were used for the amplitude response and phase response:

1. Amplitude Response

The amplitude response was considered flat from d-c to the cutoff frequency fc.

2. Phase Response

The nonlinear portion of the phase response was approximated by

$$\Delta\phi\,(f) = -k \sin\left(\frac{\pi}{2} \cdot \frac{f}{f_c}\right) \qquad A-(1)$$

where

$\Delta\phi\,(f)$ is the nonlinear portion of the phase response, and
k is the peak phase distortion.

The corresponding time-delay distortion curve $\Delta t_d(f)$ is given by

$$\Delta t_d(f) = \frac{\Delta\phi\,(f)}{2\pi f} = -\frac{k}{2\pi f} \sin\left(\frac{\pi}{2} \cdot \frac{f}{f_c}\right) \qquad A-(2)$$

The peak-to-peak differential delay distortion (DTD) is

$$DTD = \frac{k}{2\pi f_c}\left(\frac{\pi}{2} - 1\right)$$

Figure 22 in the main body of this report shows how $\Delta t_d(f)$ is fitted to the specification limits. The corresponding value of k is 3.30 radians. Figures A-1, A-2, and A-3 show the computer waveforms in response to words A, B, and C when the specification for time-delay distortion is met. The normalized bandwidth is 1.4.

Figure A-4 is a plot of the single-pulse response of the system; it shows the skewness introduced by phase distortion. The plot is based on a square-pulse input having unit amplitude and a width equal to half a bit.

In order to verify the validity of the phase approximation, a computer run was performed for a value of peak phase distortion k corresponding to the differential time-delay distortion curve measured on the VIP Multiplexer/Demultiplexer (MUX/DEMUX) breadboard. This value of k was found to be approximately unity ($k \approx 1.0$). Figure A-5 is a plot of the calculated single-pulse response; it shows only slight distortion. The computer waveform in response to word C is shown in Figure A-6. The actual response to word C, as measured on the VIP breadboard, is shown in Figure A-7. A comparison of Figures A-6 and A-7 shows that the sinusoidal approximation of phase nonlinearity yields distortion that is greater than the actual phase distortion of the system.

For a more exact approximation of the VIP channel, the value of k should have been taken with a negative sign ($k \approx -1.0$). The minus sign is introduced because the single-sideband spectrum of the VIP subcarrier is the lower sideband spectrum. This phase sign is effectively reversed by the down-converting process in the demultiplexer. The sign reversal causes the distortion in the computer waveform to appear as a mirror image of the distortion in the actual channel.

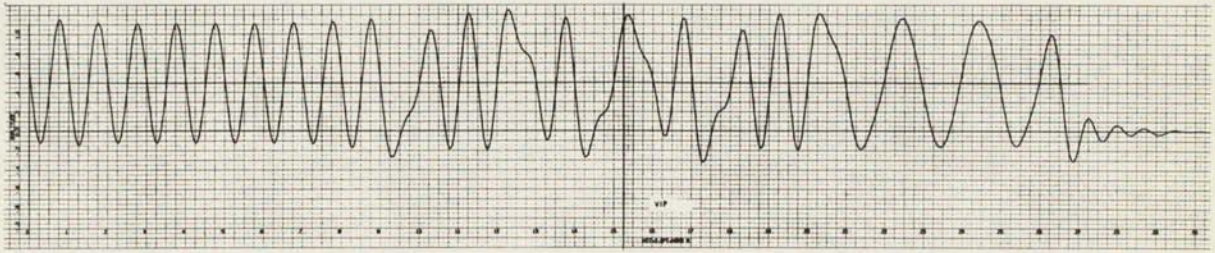

Figure A-1. Calculated VIP-Channel Response to Word A (Phase Nonlinearity: k = 3.30 radians; Normalized Bandwidth: 1.4)

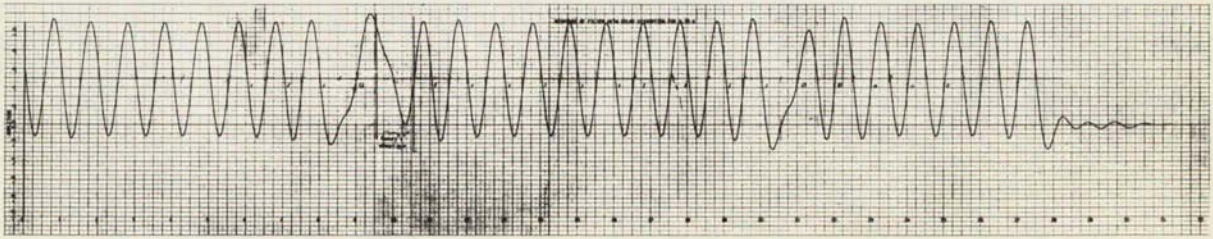

Figure A-2. Calculated VIP-Channel Response to Word B (Phase Nonlinearity: k = 3.30 radians; Normalized Bandwidth: 1.4)

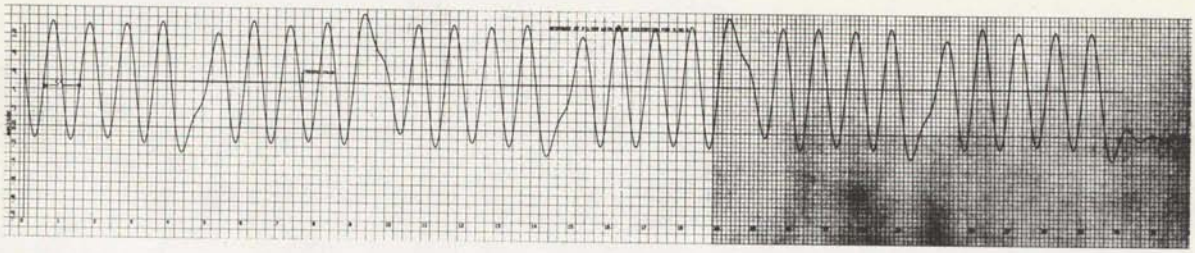

Figure A-3. Calculated VIP-Channel Response to Word C (Phase Nonlinearity: k = 3.30 radians; Normalized Bandwidth: 1.4)

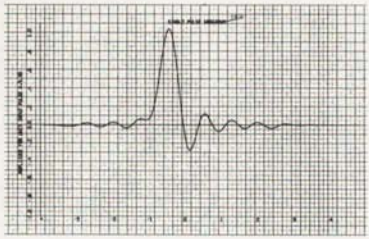

Figure A-4. Calculated Single-Pulse Response (Phase Nonlinearity: k = 3.30 radians)

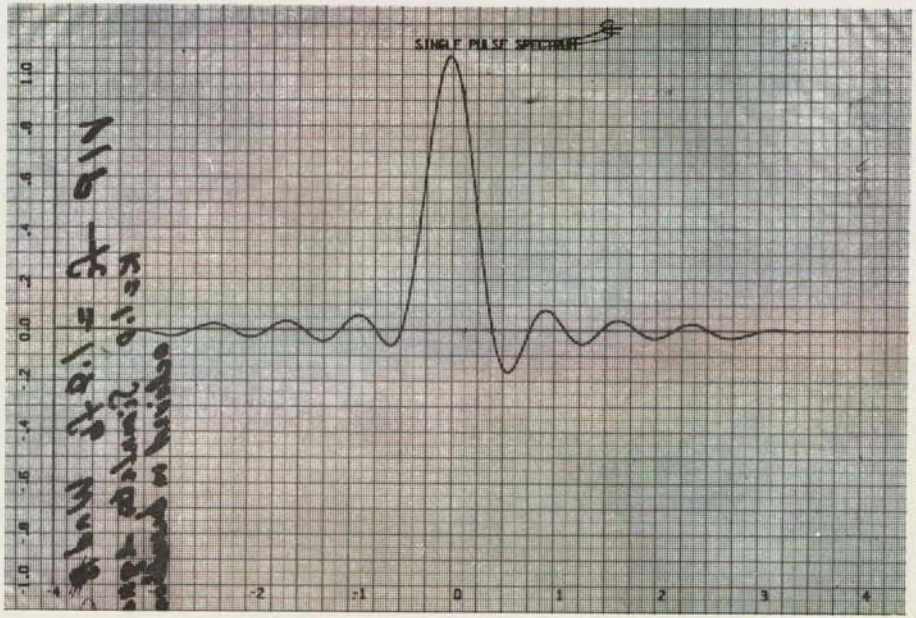

Figure A-5. Calculated Single-Pulse Response (Phase Nonlinearity: k = 1.00 radian)

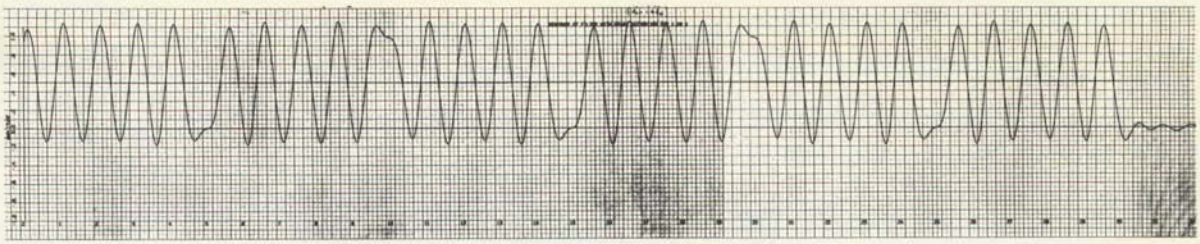

Figure A-6. Calculated VIP-Channel Response to Word C (Phase Nonlinearity: k = 1.00 radian; Normalized Bandwidth 1.4)

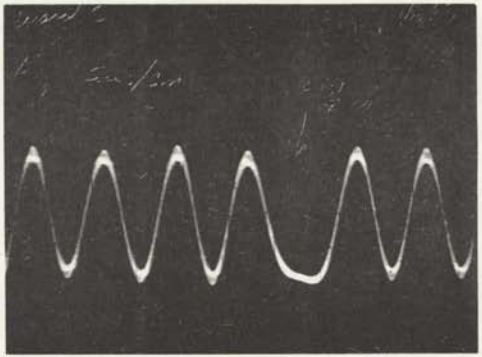

Figure A-7. VIP Breadboard Response to Word C (1 bit = 7.8 microseconds)

C. PAIRED-ECHO METHOD FOR CALCULATING DISTORTED WAVEFORMS

The computer waveforms were obtained by the paired-echo method described in references 1 and 2. In this method, the amplitude response of the channel is assumed to be flat from d-c to the cutoff frequency f_c. Because the response beyond f_c attenuates rapidly, it is approximated by an infinite attenuation slope.

The biphase signal is considered to be unipolar. Each bit has a duration T. A binary "one" is represented by a unity-amplitude pulse of duration T/2 occupying the first half of the bit and zero amplitude in the second half. Conversely, a binary "zero" is represented by zero amplitude in the first half of the bit and unity amplitude in the second half. Each unipolar waveform has a fixed average value of 0.5. This average value is subtracted from the output waveform in order to determine the zero-crossings.

Considering the signal as unipolar simplifies the calculations, since the response of the system need only be calculated for a single, unity-amplitude pulse. A "one" is distinguished from a "zero" by the position of the pulse in the bit cell. This feature is especially convenient for manual calculation of intersymbol interference.

The response of the perfectly equalized channel (linear phase) to a square pulse of unity amplitude and duration T/2 is

$$g_1(t) = \frac{1}{\pi}\left[S_i\omega_c\left(t+\frac{T}{4}\right) - S_i\omega_c\left(t-\frac{T}{4}\right)\right] \qquad \text{(A-3)}$$

or

$$g_1(t) = \frac{1}{\pi}\left[S_i 2\pi\left(f_c t+\frac{R}{4}\right) - S_i 2\pi\left(f_c t-\frac{R}{4}\right)\right] \qquad \text{(A-4)}$$

where $g_1(t)$ is the output function, and

$$S_i(x) = \int_0^x \frac{\sin t}{t}\,dt$$

$$R = f_c T$$

Figure A-8 shows a plot of $g_1(t)$ superimposed on the square-pulse biphase signal.

---

1) H.A. Wheeler, The Interpretation of Amplitude and Phase Distortion in Terms of Paired Echos. IRE, Volume 27, June 1939, p 359, 385.

2) Papoulis, The Fourier Integral and Its Applications, McGraw-Hill Co., Inc., 1962, p 115.

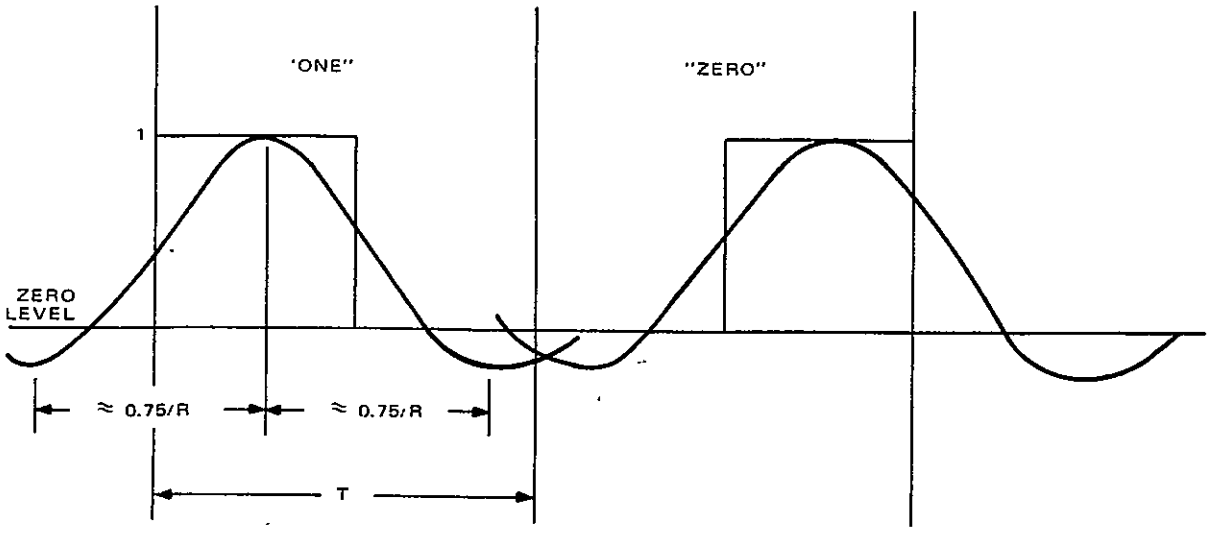

Figure A-8. Response of Perfectly Equalized Channel

The nonlinear phase component of the channel is approximated by

$$\Delta\phi = - k \sin\left(\frac{\pi}{2} \cdot \frac{f}{f_c}\right) \qquad \text{(A-5)}$$

The envelope delay curve $t_g(f)$ is given by

$$t_g(f) = \frac{\partial(\Delta\phi)}{\partial\omega} = - \frac{k}{4f_c} \cos\left(\frac{\pi}{2} \cdot \frac{f}{f_c}\right) \qquad \text{(A-6)}$$

The time-delay distortion curve $\Delta t_d(f)$ is given by

$$\Delta t_d(f) = \frac{\Delta\phi}{2\pi f} = - \frac{k}{2\pi f} \sin\left(\frac{\pi}{2} \cdot \frac{f}{f_c}\right) \qquad \text{(A-7)}$$

The sine-wave approximation of phase nonlinearity is fairly close to the phase nonlinearity of sharp-cutoff filters. The approximation is even better when the channel is phase equalized by an all-pass network.

The nonlinear phase component introduces some distortion in the original pulse $g_1(t)$ to produce the pulse $g_d(t)$. The main effect of the distortion is to skew the waveform; one undershoot lobe is attenuated with respect to the other and the waveform is no longer symmetrical. In addition, the peak value of the waveform is depressed. The distortion is caused by the dispersive channel producing echos that interfere with the original pulse $g_1(t)$. The distorted pulse waveform $g_d(t)$ is given by

$$g_d(t) = \sum_{n=-\infty}^{\infty} J_n(k)\, g_1\,(t + n\alpha) \qquad \text{(A-8)}$$

where

$J_n(k)$ is the ordinary Bessel function of the nth order; and

$$\alpha = \frac{1}{4f_c}$$

The expansion converges rapidly even for values of k as large as 6.0; therefore, a few terms are sufficient to obtain a very close approximation of $g_d(t)$.

Phase nonlinearity produces unsymmetrical intersymbol interference. This interference is stronger on one side of the bit, as is evident in Figure A-4. However, the greatest contributor to intersymbol interference is the first large undershoot. It is responsible, among other things, for large timing shifts in channels that have a bandwidth close to the bit-rate frequency. This effect can be avoided by employing sufficient bandwidth to allow occurrence of the large undershoot at a fairly remote position from the beginning or the middle of the next bit.

Figure A-9 shows the distorted pulses superimposed on the square pulses. The final waveform was obtained by adding the various contributions of the pulse tails into neighboring bits. This operation was performed easily by means of the digital computer.

D. INTERSYMBOL INTERFERENCE VERSUS BANDWIDTH AND PHASE DISTORTION

The computer simulation was performed for various values of bandwidth and phase distortion. The sinusoidal approximation of phase nonlinearity was used throughout. For convenience, the distortion due to phase nonlinearity is expressed as peak-to-peak group (envelope) delay distortion $t_g(p\text{-}p)$. The group delay distortion is related to the phase distortion k as follows:

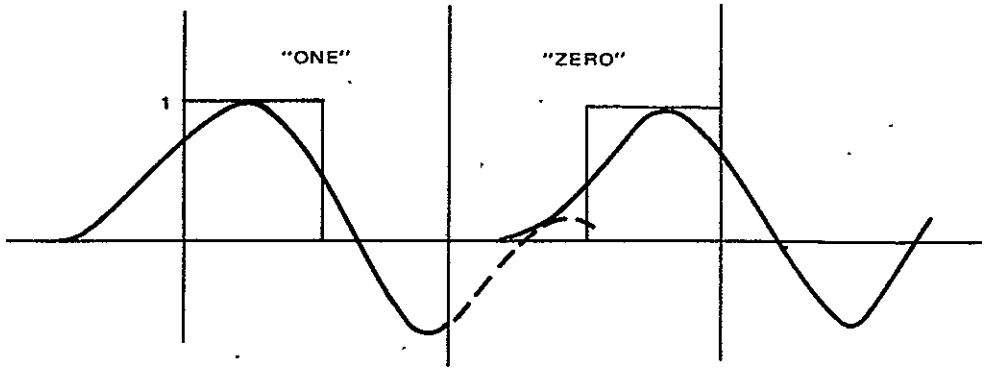

Figure A-9. Response of Unequalized Channel

$$t_g(p\text{-}p) = \frac{k}{4f_c} \qquad \text{(A-9)}$$

The group delay function $t_g(\omega)$ is defined as

$$t_g(\omega) = \frac{\partial \phi(\omega)}{\partial \omega} \qquad \text{(A-10)}$$

The results of the simulation are plotted in Figures A-10 through A-13. The effects of intersymbol interference are in the form of signal amplitude loss and timing shifts from the ideal location. The signal loss is calculated for a reset-integrator decoder such as the Dynatronics BSC-7B.

Such a decoder processes the signal in several steps*. The incoming filtered and noisy biphase data are synchronously demodulated; that is, multiplication by the extracted clock signal transforms the data back to NRZ bits. Each NRZ bit is integrated. The voltage level at the end of the integration time (one bit duration) triggers a threshold detector (Schmitt trigger), and a reconstituted NRZ signal is produced at the output.

*Refer to Appendix VII of this report.

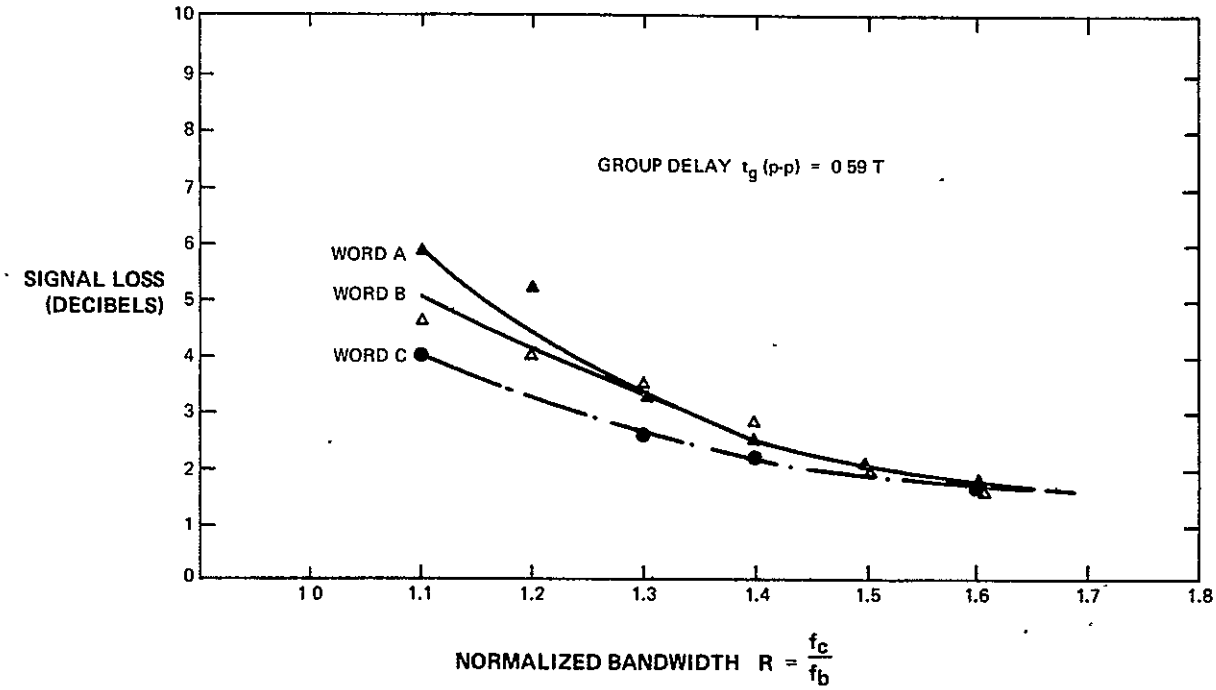

Figure A-10. Variation of Signal Degradation With Bandwidth (Fixed Group Delay Equalization)

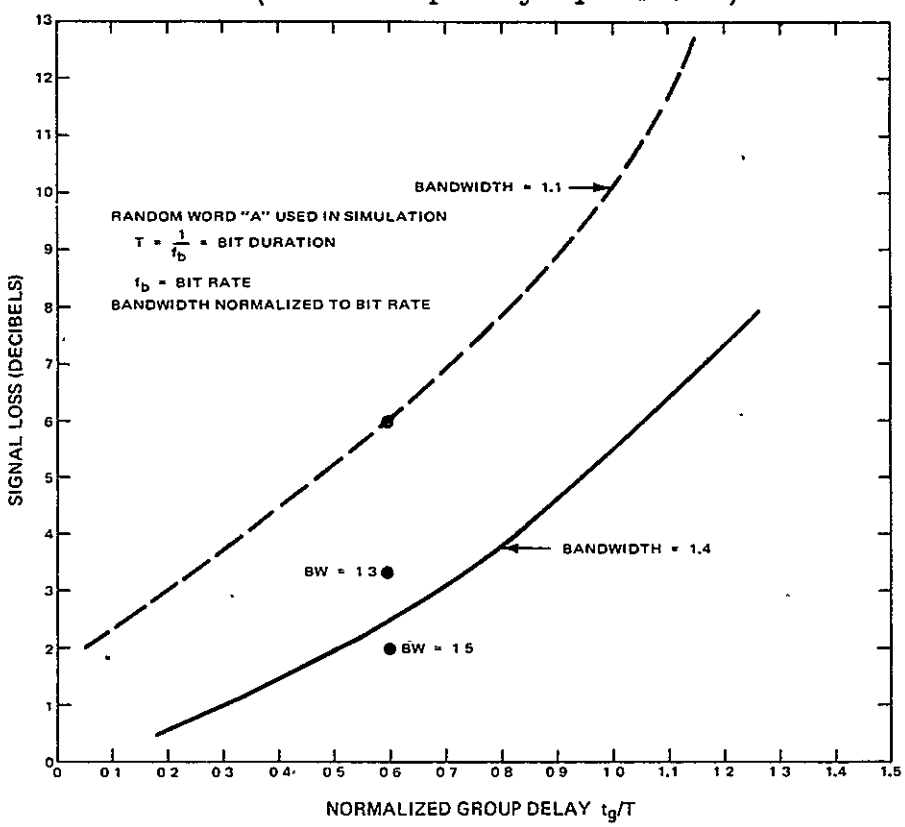

Figure A-11. Variation of Signal Loss With Group Delay and Bandwidth

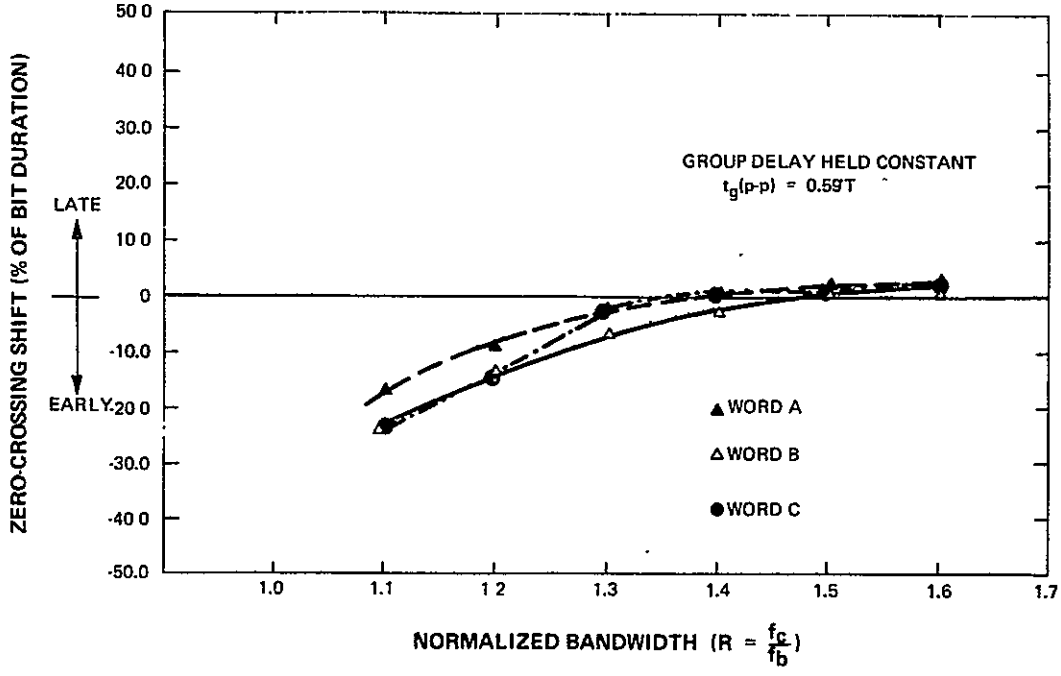

Figure A-12. Variation of Timing Error With Bandwidth

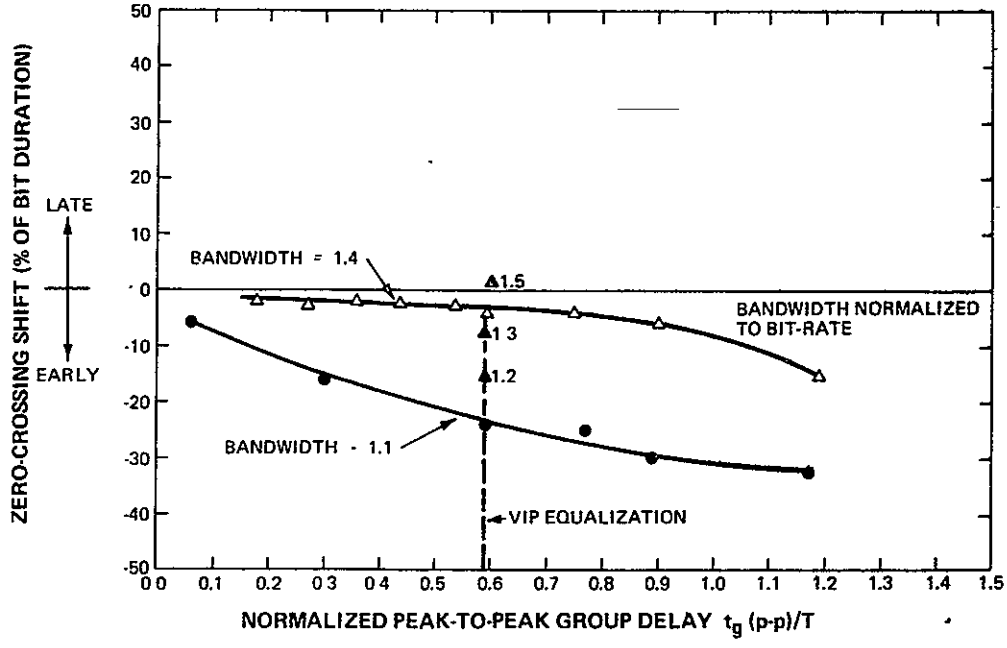

Figure A-13. Variation of Timing Error With Group Delay Distortion

APPENDIX IV
THEORY OF SSB-AM

A. INTRODUCTION

The VIP subcarrier spectrum is essentially single-sideband. A pilot tone, used as a reference subcarrier for the synchronous demodulation at the receiving station is extracted from the frequency division multiplexed spectrum by a phase-locked loop. A functional block diagram is shown on Figure IV-1.

B. ANALYSIS

1. Introduction

For simplification, the assumption that the bandpass filters reject the upper sidebands completely is made. The spectrum of the transmitted signal is a pure single side band. The output of the modulator (before filtering) is

$$v(t) = f(t) \times A \cos \omega_o t$$

The spectrum of v(t) is $V(\omega)$*

$$V(\omega) = A \frac{f(\omega) + \omega_o}{2} + A \frac{f(\omega - \omega_o)}{2}$$

where: $f(\omega)$ is the Fourier spectrum of f(t).

After filtering, the single sideband spectrum of g(t) is

$$G(\omega) = \frac{A}{2} F(\omega - \omega_o)$$

when the assumption is made that the banspass filter phase response is linear.

At the ground station, the signal g(t) is multiplied by the recovered subcarrier $B \cos(\omega_o t + \phi_o)$ and filtered in a low pass filter that eliminates the high product terms and passes the base band signals. The output of the demodulator is

$$Z(t) = B_g(t) \cos(\omega_o t + \phi_o)$$

---

* A. Papoulis, The Fourier Integral and its Applications, McGraw Hill Book Co., New York, 1962.

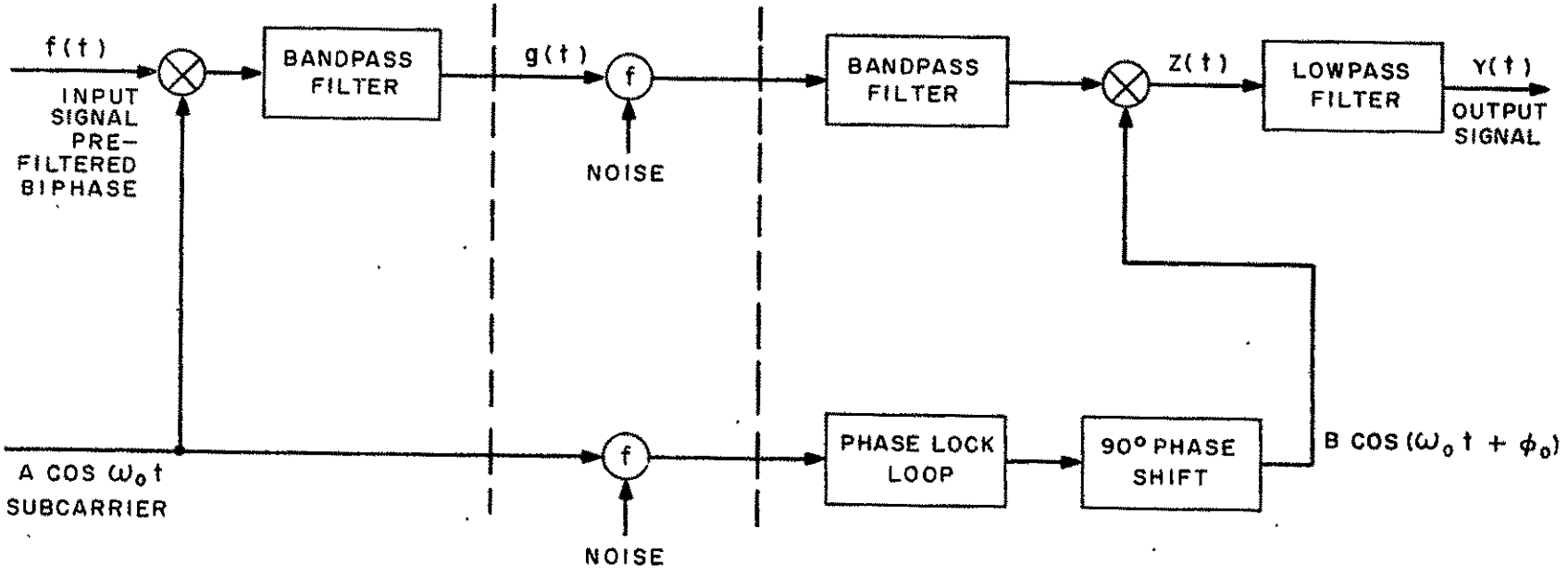

Figure IV-1. VIP Channel, Functional Block Diagram

2. No Phase Error

If the phase error ϕ is equal to zero, then

$$Z(t) = Bg(t) \cos \omega_o t,$$

$$Z(\omega) = \frac{B}{2} G(\omega - \omega_o) + \frac{B}{2} G(\omega + \omega_o)$$

$$\therefore Z(\omega) = \frac{B}{2} \times \frac{A}{2} F(\omega - 2\omega_o) + \frac{B}{2} \times \frac{A}{2} F(\omega)$$

The low pass filter eliminates the term $F(\omega - 2\omega_o)$ which is centered at twice the subcarrier frequency.

The output y(t) then has a Fourier spectrum $Y(\omega)$ equal to

$$Y(\omega) = \frac{B \times A}{4} F\omega) \text{ or}$$

$$y(t) = kf(t)$$

where k is a constant.

3. Phase Error Included

If the extracted subcarrier has a static phase error of ϕ_o radians, then

$$Z(t) = Bg(t) \cos \phi_o \cos \omega_o t - Bg(t) \sin \phi_o \sin \omega_o t$$

After filtering by the low pass filter, Y(t) equals the inphase term P(t) plus the quadrature term Q(t), where

$$P(t) = \frac{AB}{4} f(t) \cos \phi_o, \text{ and}$$

$$Q(t) = \frac{AB}{4} \hat{f}(t) \sin \phi_o$$

The term $\hat{f}(t)$ is the Hilbert transform* of (t). The Fourier spectrum of f (t) is related to the Fourier transform $F(\omega)$ of f(t) as follows:

$$\hat{F}(\omega) = \begin{cases} -j F(\omega) & \omega \geq 0 \\ +j F(\omega) & \omega < 0 \end{cases}$$

---

* M. Schuartz, W. L. Bennet, S. Stein, Communications Systems and Techniques", McGraw Hill Book Co. New York, 1966.

In other words $\hat{F}(\omega)$ is obtained from $F(\omega)$ by shifting all frequency components of $F(\omega)$ by -90°. This is illustrated in Figure IV-2. The term $\hat{f}(t)$ is also defined as

$$\hat{f}(t) = \frac{1}{\pi} \int_{-\infty}^{\infty} \frac{f(\tau)\, dt}{t - \tau}$$

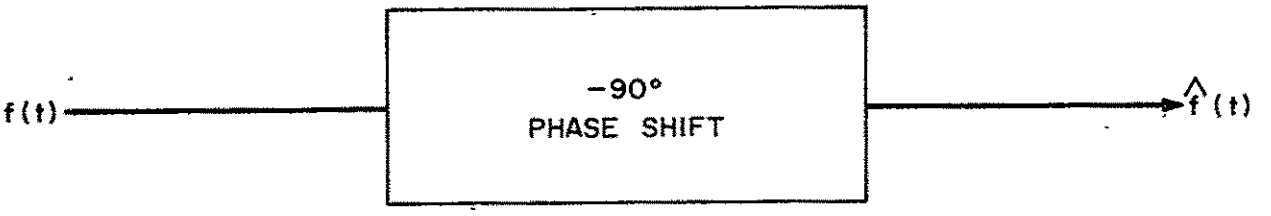

Figure IV-2. Phase Shift Diagram

In conclusion, the phase error (ϕ) depresses the useful signal by cos ϕ and introduces a quadrature (distortion term) proportional to $\hat{f}(t) \sin \phi_o$.

4. Effect of Phase Error On Overall Frequency Response

In general, the lowpass filter output

$$y(t) = k\ (f(t) \cos \phi_o + \hat{f}(t) \sin \phi_o).$$

For a sinewave test signal, $f(t) = C \sin \omega_i t$, and the output

$$y(t) = k \left[C_y \cos \phi_o \sin \omega_i t + C_y \sin \phi_o \sin (\omega_i t - 90^\circ) \right]$$

$$y(t) = kC\ (\cos \phi_o \sin \omega_i t + \sin \phi_o \cos \omega_i t)$$

$$y(t) = kC \sin (\omega_i t - \phi_o)$$

Consequently, the static phase error ϕ_o appears directly in the overall phase response of the system. If the system phase response with zero static phase error is as shown on Figure IV-3a, then with static phase error $+\phi_o$ the overall response will appear as shown on Figure IV-3b.

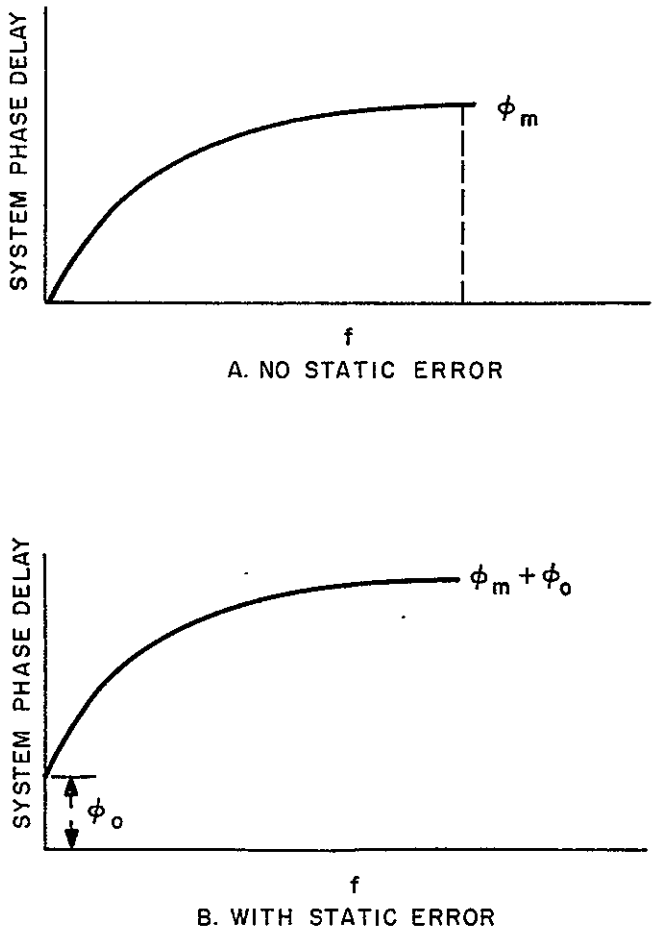

Figure IV-3. Effects of Static Phase Error

APPENDIX V
FREQUENCY SPECTRUM OF REPETITIVE BIPHASE WORDS

A. INTRODUCTION

The biphase signal is composed of m ones and one zero. The period of the repetitive word is then (m +1)T, where T is the duration of a single biphase bit. The square wave biphase spectrum is the product of the NRZ waveform by the square wave clock as shown in Figure V-1.

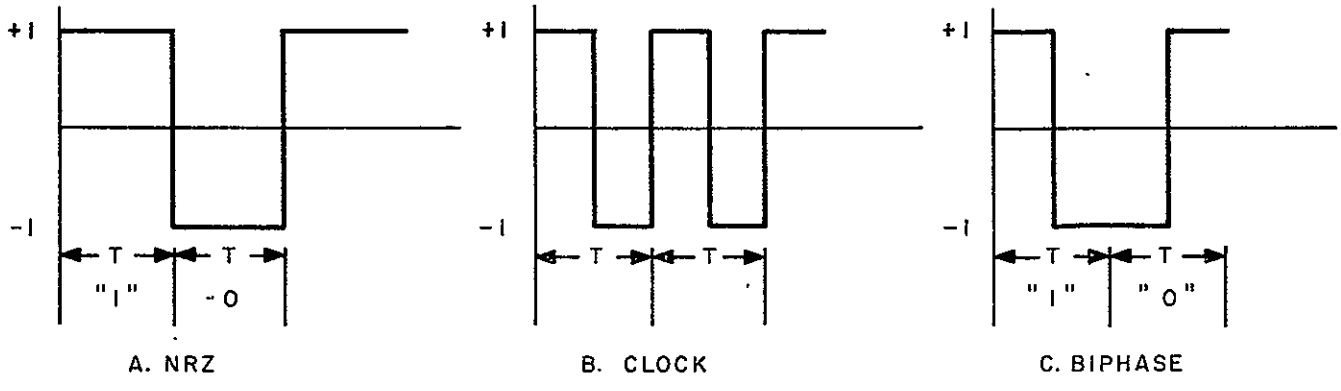

Figure V-1. Composition of Biphase Signal

B. ANALYSIS

With the NRZ and clock signals amplitude varying between +1 and -1, the clock square wave is expressed by the following Fourier Series.

$$f(t) = \frac{4}{\pi} \cos W_b t + \frac{4}{3\pi} \cos 3W_b t + \frac{4}{5\pi} \cos 5W_b t \ \ldots$$

where $W_b = 2\pi \times$ bit rate; $(f_b = \frac{1}{T})$.

The biphase spectrum is obtained by first deriving the spectrum of the NRZ word and translating it in frequency by f_b, $3f_b$ and $5f_b$ and comparing it by the

factors $4/\pi$, $/3\pi$, and $4/5\pi$, respectively. The spectrum of one NRZ pulse, shown on Figure V-2, is expressed as

$$X(w) = \frac{T \sin \frac{wt}{2}}{\frac{WT}{2}}$$

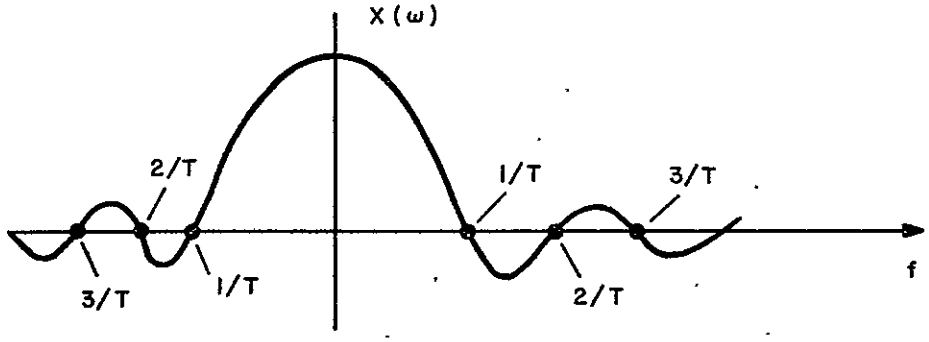

Figure V-2. Spectrum of a Single NRZ Pulse for Duration T and Amplitude of Plus One

Due to the tails in the spectrum of X(t), there will be a fold over after the frequency translations processes so that the spectrum will look skewed around dc. Neglecting the interference due to the tails of the spectrum centered at $3f_b$ and $5f_b$ into the first lobe centered around f_b, the approximate spectrum V(w) for frequency ranges less than $1.5f_b$ and a single biphase bit equals

$$V(d) = \frac{-T}{\pi \propto} \left[\cos (\propto \pi) -1 \right]$$

where $\propto = f/f_b$

1. Spectrum for Repetitive Biphase Bits

For a repetitive sequence of binary ones, the biphase signal consists of the clock with specular components centered at f_b, $3f_b$, and $5f_b$ with voltage amplitudes equal to $4/\pi$, $4/3\pi$, and $4/5\pi$, respectively.

2. Spectrum for m Ones, and One Zero

To obtain the spectrum for m ones and one zero, the signal is decomposed into a periodic of ones to which is added a repetitive sequence of waveforms representing the zero. The repetitive period is (m + 1) T. However, this

waveform is doubled in amplitude to cancel the extra one added previously. This is shown on Figure V-3. The line spectrum of the repetitive double zeros is given by

$$A\,(n\,\Delta\,\omega) = \frac{+4}{(n+1)T}\quad V\,(n\,\Delta\,\omega) \quad \text{or}$$

$$A\left(\frac{nf_b}{m+1}\right) = \frac{+4}{(m+1)\,T}\quad V\left(\frac{nf_b}{m+1}\right)$$

where n is the number of a particular component; for example

$$n = 0 \text{ at } d_c$$

$$n = 1 \text{ at } f = \frac{f_b}{m+1}$$

3. Final Expression for Spectrum of m Ones and One Zero

The voltage amplitude spectrum obtained by adding the spectra of para 1 and 2 is

$$G_1(\alpha) = \frac{4}{m+1} \times \frac{1}{\pi\alpha} \times \left[\cos(\alpha\pi) - 1\right]$$

where $\alpha = f/f_b$ $\qquad \alpha \neq 1$, $\alpha < 1.5$

At $\alpha = 1$

$$G_2(\alpha = 1) = \frac{4}{\pi} + G_1(\alpha = 1) = \frac{4}{\pi}\left(\frac{m-1}{m+1}\right)$$

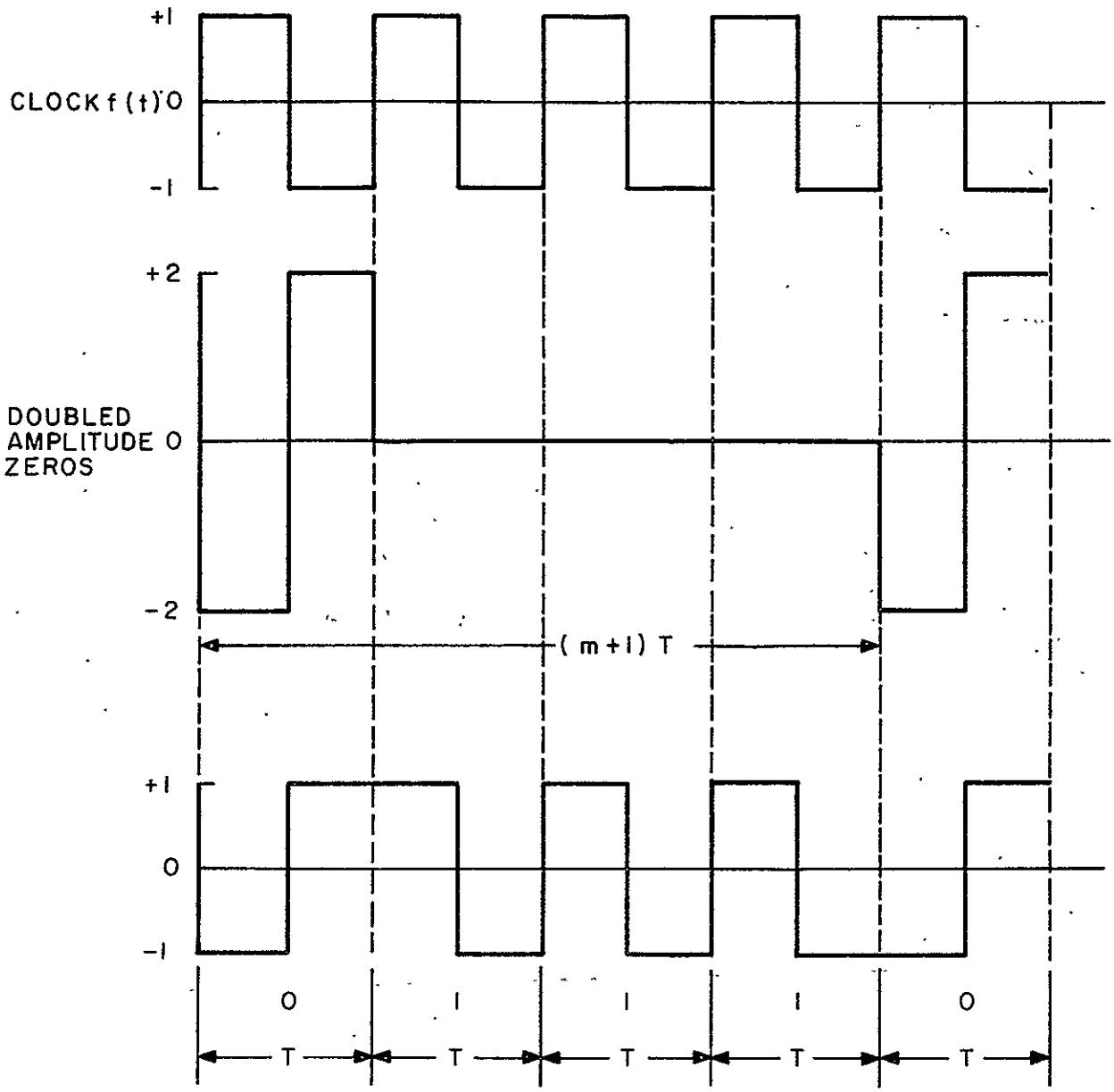

Figure V-3. Steps in Decomposing Waveform
Made up of Three Ones and a Zero

APPENDIX VI

INTERFACE SIGNAL VARIATIONS

Interface signal variations are due to the tolerances on the impedance values, voltage levels, and transmitter deviation sensitivity. The tolerances specified include long-term variations. An equivalent circuit is shown on Figure VI-1, and a variation of $\pm$ 10 percent on the deviation sensitivity of the FM transmitter is assumed. The multiplexer gain is adjusted to obtain a 3.36 $\pm$ 0.34 volt p-p open circuit voltage when the input voltage of 6.5 $\pm$ 0.01 volts p-p is applied to the input through a resistor of 10000 $\pm$ 10 ohms.

The nominal signal loss from the open circuit tape recorder to transmitter deviation is 0.250 K (voltage ratio), where K = the nominal multiplexer gain. The worst case loss:

$$L = \begin{pmatrix}\text{Tape Recorder}\\ \text{Voltage Level}\end{pmatrix} x \begin{pmatrix}\text{Tape Recorder/}\\ \text{Multiplexer}\\ \text{Interface Ratio}\end{pmatrix} x \begin{pmatrix}\text{Multiplexer/}\\ \text{Transmitter}\\ \text{Interface Ratio}\end{pmatrix} x \begin{pmatrix}\text{Multiplexer}\\ \text{Gain}\end{pmatrix} x \begin{pmatrix}\text{Transmitter}\\ \text{Sensitivity}\end{pmatrix}$$

$$= 0.90 \times \frac{950}{2000} \times \frac{540}{1080} \times 0.90\,K \times 0.90 = 0.173$$

$$\text{The worst case loss} = \frac{0.250}{0.173} = 3.2 \text{ db.}$$

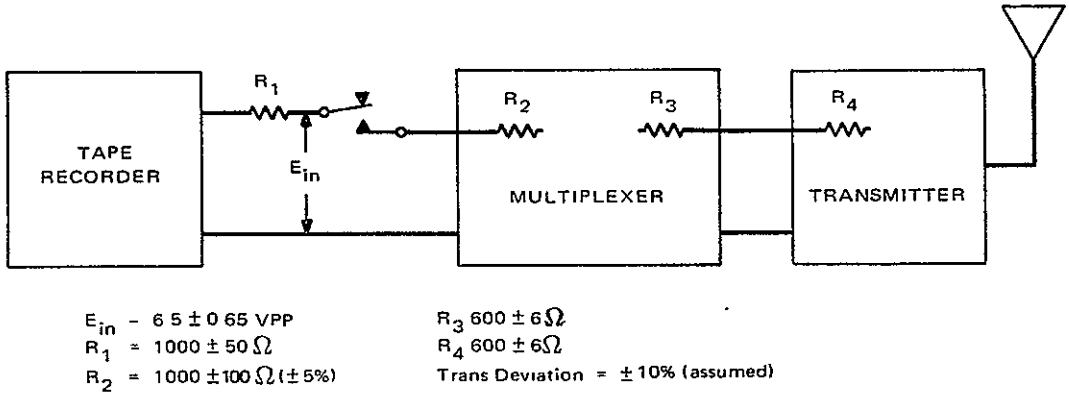

Figure VI-1. Block Diagram for Signal Variation Calculation

APPENDIX VII

SIGNAL-TO-NOISE RATIO REQUIREMENTS FOR RESET INTEGRATOR DECODER OPERATING ON BAND-LIMITED BIPHASE DATA

A. INTRODUCTION AND SUMMARY

This memorandum derives the signal-to-noise ratio degradation or improvement due to the processing of biphase digital data by a reset integrator decoder. The input SNR into the decoder is corrected by the amount of degradation or improvement to yield the SNR at the decision circuit. The probability of a bit-error is then given by the well-known complementary-error-function formula for bipolar PAM signals. The formulas given here apply only to sharp cut-off FM channels carrying biphase digital data and yield a conservative value of the degradation or improvement because they make use of the maximum value (unity) of the correlation function between the integrated noise processes in the two halves of the bit. The amount of margin is of the order of 1 or 2 db depending on the channel. The exact value of the correlation coefficient can be calculated by the formulas given in Appendix B for a more accurate determination of SNR requirements. Once the SNR degradation (or improvement) is obtained, the System Probability of Error versus SNR curve is obtained by shifting the curve characterizing the threshold detector to the right by the number of db of degradation (vice-versa for improvement). The SNR requirement for a desired System Probability of Error can then be read directly from the curve.

For user convenience, the formulas are presented below and on the following page; their derivation is given in the body of this memorandum.

Case I - Low-Pass Channel; Parabolic Noise:

$$\left(\frac{A^2}{N_1}\right) = \left\{ \frac{\left(\frac{\pi}{2}\right)^2 \times 24}{\omega_c^2 T^2} \left[1 - \left(\frac{2}{\omega_c T}\right) \sin \pi R \right] \right\} \left(\frac{S_p^2}{N_o}\right)$$

where

$\frac{A^2}{N_1} = \left(\frac{\text{Peak}}{\text{RMS}}\right)^2$ signal-to-noise ratio into decoder, in channel bandwidth,

$\frac{S_p^2}{N_o} = \left(\frac{\text{Peak}}{\text{RMS}}\right)^2$ signal-to-noise ratio at decision circuit,

$\omega_c = 2\pi f_c$,

f_c = channel bandwidth (sharp cut-off),

T = bit duration, and

$R = f_c T$.

Case II - Bandpass Channel; Parabolic Noise

$$\frac{A^2}{N_1} = \left(\frac{\pi}{2}\right)^2 \cdot 6 \left\{ 4\,\frac{(\omega_c/\omega_o)}{(\omega_o T)^2} - \frac{8 \sin \pi R}{(\omega_o T)^3} - \frac{8}{(\omega_o T)^2}\left[0.577 + \ln(\pi R) - Ci(\pi R)\right] + \frac{2}{\omega_o T}\left[\frac{\cos(\pi R) - 1}{\pi R} + Si(\pi R)\right] \right\} \frac{S_p^2}{N_o} \div \Delta$$

where

$$\Delta = \left(\frac{\omega_c}{\omega_o}\right)^3 - 3\left(\frac{\omega_c}{\omega_o}\right)^2 + 3\left(\frac{\omega_c}{\omega_o}\right),$$

$$Ci(x) = \int_{\infty}^{x} \frac{\cos v}{v}\, dv,$$

$\omega_o = 2\pi f_o$,

f_o = subcarrier frequency, and

f_c = bandwidth in subcarrier domain (ssb AM)

All other symbols are as defined for Case I.

B. BIPHASE CODING FORMAT

The biphase coding format considered here is defined in Figure 1. The biphase signal is the product-modulation of an NRZ data onto a squarewave subcarrier at the bit rate frequency. A binary "1" has a positive level in the first half of the bit and a negative level in the second half of the bit.

A binary "0" has a negative level in the first half of the bit and a positive level in the second half. A binary "0" is obtained from a binary "1" by 180° phase reversal of the squarewave carrier. The biphase format has a zero crossing in the middle of each bit. There is a strong clock frequency component which is easily extracted by a phase-locked loop after nonlinearity processing the input waveform through a zero-crossing detector.

C. OPERATION OF RESET INTEGRATOR DECODER FOR BIPHASE DATA

The reset integrator decoder (such as Dynatronics type BSC-7B) operates on the biphase data which is degraded by additive channel noise. The useful signal waveform is a quasi-sinusoidal waveform resulting from the effect of the channel

bandwidth limitation on the square input waveform. A typical filtered biphase (corresponding to the defined biphase format) signal is shown on Figure 2.

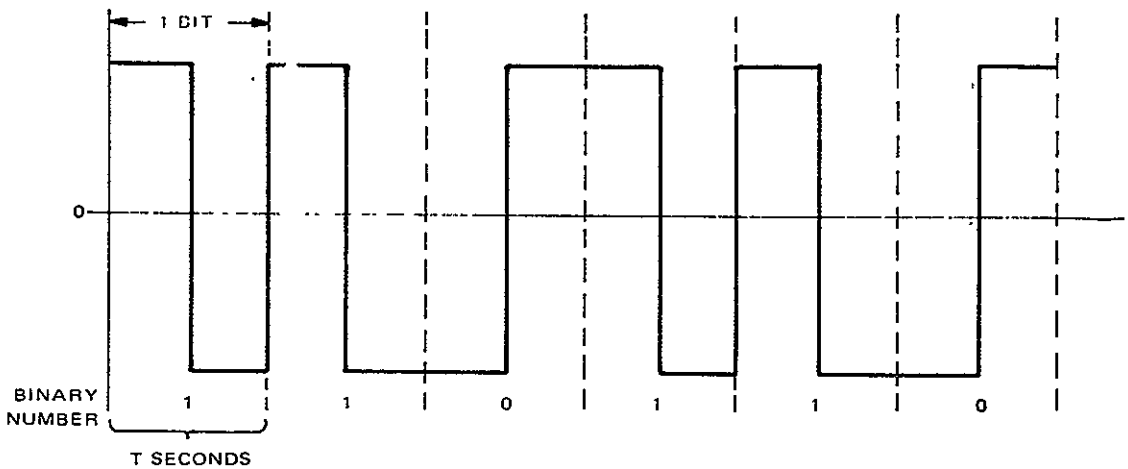

Figure 1. Definition of Biphase Format

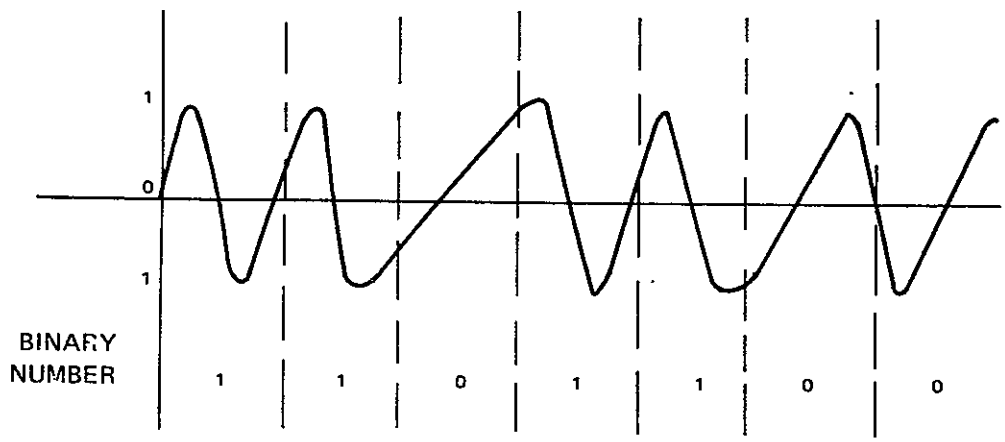

Figure 2. Typical Filtered Biphase System

In this analysis the signal is a sequence of binary "1's" (1111 ....) which yield a sinusoidal waveform at the bit-rate frequency (f_b). The channel strongly attenuates all frequencies above the cut-off frequency.

Figure 3 shows a simplified block diagram of a reset integrator decoder. The phase-locked loop extracts the timing signal from the incoming data. This timing signal is used to invert the second half of any bit before applying it to the reset integrator. In an actual decoder this inversion is accomplished by appropriately gating one of two data channels into the integrator. The data in both channels are identical except for a polarity change. During the time interval corresponding to the first half of the bit, the biphase data is connected to the

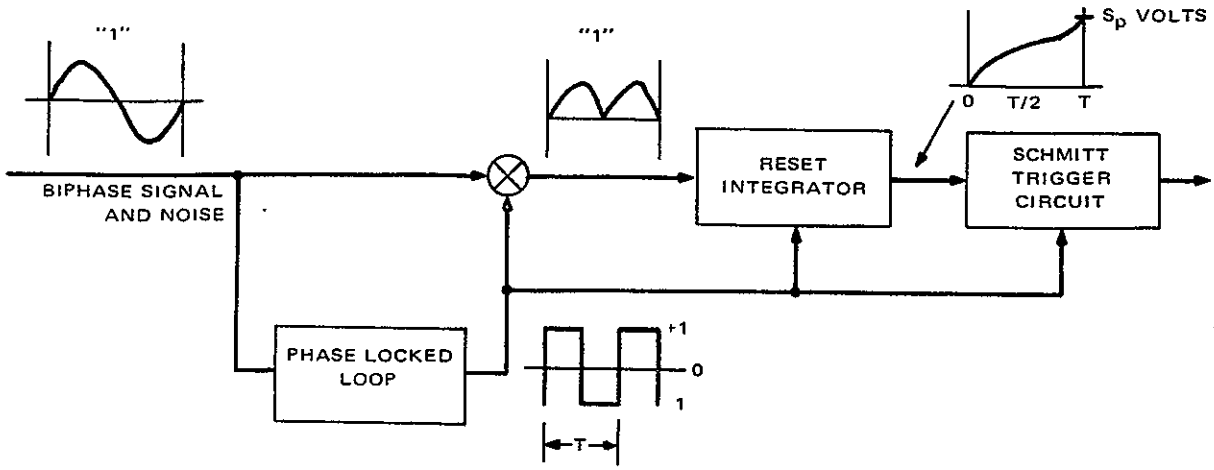

Figure 3. Simplified Block Diagram of Reset Integrator Decoder

integrator with no polarity inversion. During the second half of the bit the second channel carrying the inverted data is connected to the integrator. In Figure 3, this inverting operation is represented by a multiplication of the incoming data by the square-wave clock signal from the phase-locked loop. The filtered biphase "1" is shown as it appears at the decoder input and at the reset integrator. A biphase "0" would be treated the same but all waveforms along the decoder would have the opposite polarity.

D. SYSTEM CHARACTERISTICS

The two cases considered in this analysis are for two digital channels in a typical spacecraft-to-ground link. The cases are idealized in the sense that the only degrading factor taken into consideration is the link additive noise.

Figure 4 shows a simplified block diagram of the system. The tape recorder has two tracks of digital biphase data. The data from channel 1 is filtered and applied to the adder. The data from channel 2 is first up-converted in frequency by a local oscillator of frequency f_o and then filtered to eliminate the upper sideband. This signal is also applied to the adder, and the composite signal from the adder is applied to the frequency-modulated transmitter.

At the ground station, the FM signal is demodulated in a discriminator, and signals 1 and 2 are separated by appropriate sharp-cutoff bandpass and low-pass filters. Signal 2 is shifted to baseband by mixing with the pilot tone of frequency f_o.

The noise spectra are indicated on the diagram. The noise density at the receiver output is parabolic. This assumes that the channel noise is white.

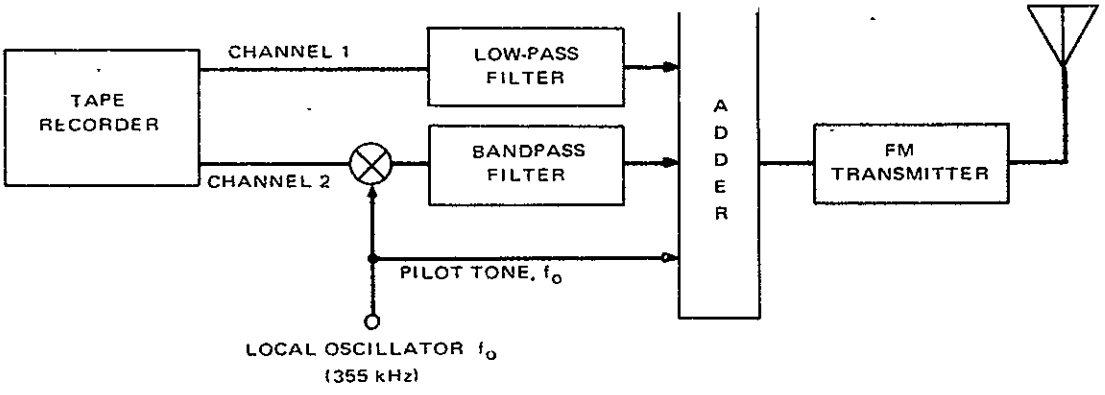

A. BLOCK DIAGRAM OF SPACECRAFT EQUIPMENT

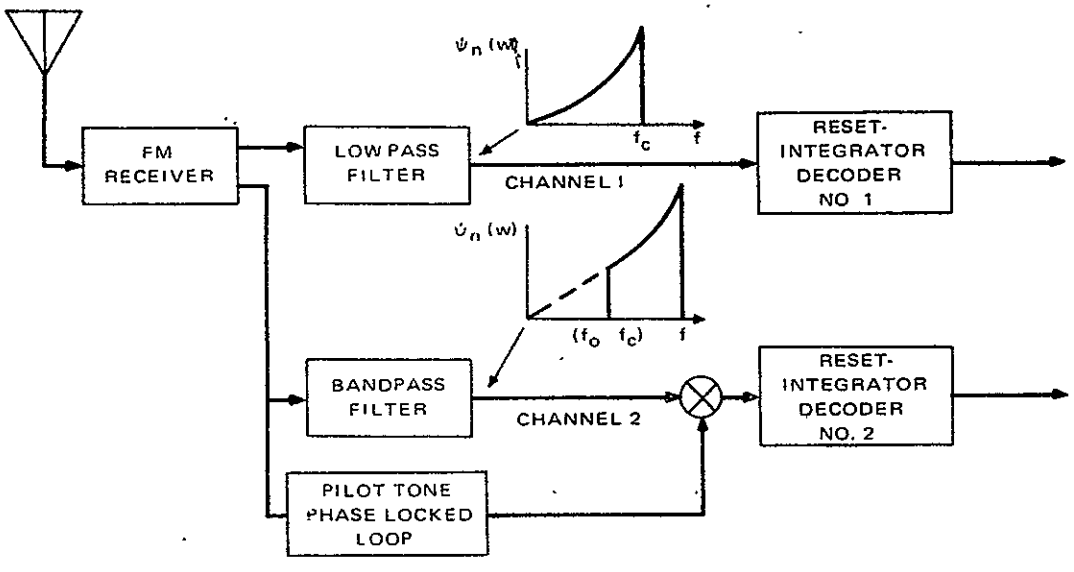

B. BLOCK DIAGRAM OF GROUND EQUIPMENT (SHOWING NOISE SPECTRA)

igure 4. Simplified System Block Diagram Showing the Two Digital Channels

E. SIGNAL LEVEL AT INTEGRATOR OUTPUT

The start of the integrator period is determined by the clock. For the periodic sequency of binary "ones" assumed in this analysis, the signal into the decoder is the sinewave function $f(t) = A \sin \omega t$. There is no timing error between the data and the clock. The sign of the second half of the bit is inverted before the integration.

At time $t = T$, the voltage level at the integrator output is*

$$S_p = 2 \int_0^{T/2} \left[A \sin \omega_b t \right] dt = 4A/\omega_b \qquad (1)$$

where A is the peak sinewave voltage at the decoder input. This voltage operates a Schmitt trigger circuit whose output is a binary "1" if S_p is positive or a binary "0" if S_p is negative. The operation of the Schmitt trigger circuit is inhibited until the decision time $t = T$ determined by the clock.

F. CALCULATION OF THE VARIANCE OF THE SIGNAL LEVEL AT THE INTEGRATOR OUTPUT

Due to the presence of noise, the integrator voltage at time T is a random variable whose mean is $S_p = 4A/\omega_b$. The variance of the random variable must be calculated. If the variance is denoted by N_o, then the probability of error is given by

$$P_e = \frac{1}{2} \operatorname{erfc} \left(S_p^2/2N_o \right)^{1/2} \qquad (2)$$

where erfc is the complementary error function**. This expression is based upon the assumption that the noise is Gaussian. At time $t = T^+$, the integrator is reset to zero (capacitor discharged), and the integration over the next bit begins.

---

* When there is intersymbol interference the integrated area is less than this value.

** $\operatorname{erf}(t) = \frac{2}{\sqrt{\pi}} \int_0^t \exp(-x^2)\, dx.$

The stationary noise process into the decoder is denoted by n(t). The noise output of the decoder at time t = T is

$$\hat{y} = S_p + \hat{v}_o$$

where

$$\hat{v}_o = \int_0^{T/2} \hat{n}(t)dt + \int_{T/2}^{T} \left[-\hat{n}(t)\right] dt \qquad (3)$$

since the sign of the noise process is also inverted over the second half of the bit.

The mean value of v_o is $E\left[\hat{v}_o\right] = 0$. The variance of $\hat{v}_o$ is

$$E\left[\hat{v}_o^2\right] = E\left[(\hat{v}_1 + \hat{v}_2)^2\right]$$

where

$E\left[(\hat{v}_1 + \hat{v}_2)^2\right]$ is the expected value of $\left[(\hat{v}_1 + \hat{v}_2)^2\right]$ (in the probabilistic sense),

$$\hat{v}_1 = \int_0^{T/2} \hat{n}(t)dt, \text{ and}$$

$$\hat{v}_2 = \int_{T/2}^{T} -\hat{n}(t)dt$$

Therefore

$$E\left[\hat{v}_o^2\right] = N_o = 2\sigma^2(1+\rho) \qquad (4)$$

where

$$\rho = \frac{E\left[\hat{v}_1 \hat{v}_2\right]}{\sigma_1 \sigma_2} \text{ (correlation function* of } \hat{v}_1 \text{ and } \hat{v}_2), \qquad (5)$$

---

* The value of the correlation function can be obtained by using the formulas developed in Appendix B. In all analyses performed here, the maximum value of the correlation function (unity) has been used.

$$\sigma_1^2 = E\left[\hat{v}_1^2\right],$$

$$\sigma_2^2 = E\left[\hat{v}_2^2\right], \text{ and}$$

$$\sigma_1^2 = \sigma_2^2 = \sigma^2$$

For worst case calculations, $\rho = 1$ and

$$N_o = 4\sigma^2 = 4E\left[\hat{v}_1^2\right] \tag{6}$$

It is shown in Appendix A that

$$E\left[\hat{v}_1^2\right] = \frac{1}{2\pi}\int_{-\infty}^{\infty} \left| H(\omega) \right|^2 \psi_n(\omega)\, d\omega \tag{7}$$

where $H(\omega)$ is the Fourier transform of the reset integrator impulse response and $\psi_n(\omega)$ is the noise power density (watts/Hz) at the decoder input. It should be noted that for the calculations produced in equation 3, only an integrator operating from 0 to T/2 has been considered*. The impulse response of the reset integrator over the period 0 to T/2 is shown in Figure 5.

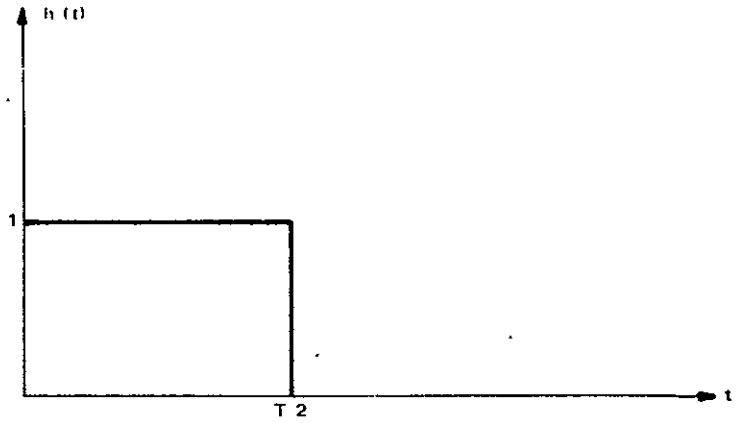

Figure 5. Impulse Response of Reset Integrator Over the Period from 0 to T/2

* The physical integrator operates over the period 0 to T, but due to the sign inversion in the second half of the bit, its action is equivalent to an integration over the period of 0 to T/2.

For an input function f(t), the output function g(t) is

$$g(t) = \int_{-\infty}^{\infty} f(\tau)h(t - \tau)d\tau = \int_{(t - T/2)}^{t} f(\tau)d\tau$$

$$g\left(\frac{T}{2}\right) = \int_{0}^{T/2} f(t)\,dt$$

Now

$$H(\omega) = \int_{0}^{T/2} e^{-j\omega t}\,dt = (1 - e^{-j\omega T/2})/j\omega$$

and

$$\left|H(\omega)\right|^2 = \left[\frac{2 \sin (\omega T/4)}{\omega}\right]^2 = \frac{T^2}{4} \cdot \frac{\sin^2 (\omega T/4)}{(\omega T/4)^2} \qquad (8)$$

Therefore, the variance N_0 is, in general

$$N_0 = 4E\left[\hat{v}_1^{\,2}\right] = \frac{T^2}{2\pi}\int_{-\infty}^{\infty} \left[\frac{\sin^2 (\omega T/4)}{(\omega T/4)^2}\right] \psi_n (\omega)\,d\omega \qquad (9)$$

In this equation $\psi_n(\omega)$ is double-sided, i.e., covers negative and positive frequencies, and has units of watts/Hz (assuming a 1-ohm load).

G. RESULTS FOR CASE I

The double-sided noise density is $\psi_n(\omega) = (k/2)\ \omega^2$. Alternately, the single-sided noise density is $\psi(\omega) = k\omega^2$. Let N_1 be the noise power (watts) in bandwidth f_c at the input to the decoder. The input signal is a sinewave of peak amplitude A volts and frequency f_b.

The noise power is

$$N_1 = \frac{1}{2\pi}\int_{0}^{\omega c} K\omega^2\,d\omega = K\omega_c{}^3/6\pi \qquad (10)$$

From equation 9, the noise variance at the threshold detector at time t = T is

$$N_0 = \frac{T^2}{2\pi}\int_{0}^{\omega c} \frac{K\omega^2 \sin^2\left(\frac{\omega T}{4}\right)}{(\omega T/4)^2}\,d\omega$$

Therefore

$$N_0 = \frac{8K}{2\pi}\left[\omega_c - \frac{2}{T}\sin \pi R\right] \qquad (11)$$

where $R = f_c/f_b$.

Combining equations 1, 10, and 11 one finds the general expression of decoder input signal-to-noise ratio in terms of the desired signal-to-noise ratio at the decision circuit (at time $t = T$) to be

$$\frac{A^2}{N_1} = \left(\frac{S_p^2}{N_0}\right)\cdot\left\{\frac{\left(\frac{\pi}{2}\right)^2 \times 24}{\omega_c^2 T^2}\left[1 - \left(\frac{2}{\omega_c T}\right)\sin \pi R\right]\right\} \qquad (12)$$

The quantity enclosed by the braces is the degradation or improvement.

For this particular application the system constraints and requirements are

$$P_e = 1 \times 10^{-6}$$

$$f_b = 120 \text{ kilobits/sec, and}$$

$$f_c/f_b = R = 1.1,$$

and the desired SNR at the threshold detector is

$$\frac{S_p^2}{N_0} = 13.5 \text{ db (peak/rms, see Figure 6).}$$

From equation (12) one finds a degradation of 1.3 db.

Therefore,

$$\left(\frac{A^2}{N_1}\right)_{db} = \left(\frac{S_p^2}{N_0}\right)_{db} + 1.3 \text{ db}$$

$$= 14.8 \text{ db (peak/rms)}$$

at the decoder input and in the bandwidth $f_c = 1.1\, f_b$.

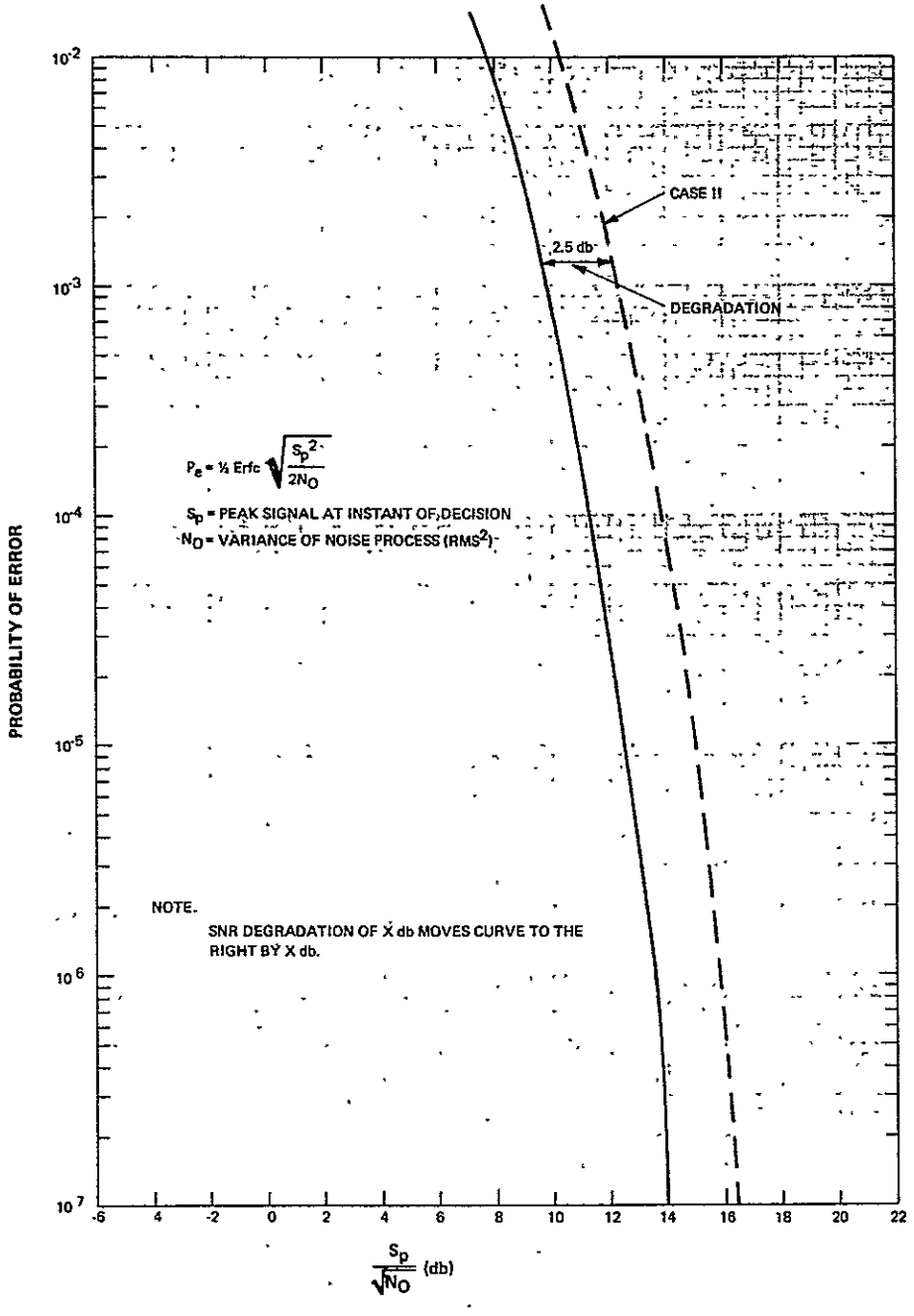

Figure 6. Probability of Error at a Threshold Detector (Bipolar Signal)

H. RESULTS FOR CASE II

The noise density shown on Figure 4 is given by $\psi_n(\omega) = K/2\ (\omega - |\omega_0|\ )^2$ for the double-sided case and $\psi(\omega) = K(\omega - |\omega_0|\ )^2$ for the single-sided case. The frequency $\omega_0 = 2\pi f_0$ is the local oscillator frequency.

The input noise power into the decoder is given by

$$N_1 = \frac{1}{2\pi}\int_0^{\omega_c} K(\omega_0 - \omega)^2\, d\omega = \frac{K}{2\pi \times 3}\left[(\omega_c - \omega_0)^3 + \omega_0^3\right]$$

$$= \frac{K}{6\pi}\left[\omega_c^3 - 3\omega_c^2\omega_0 + 3\omega_c\omega_0^2\right]$$

$$= \frac{K\omega_0^3}{6\pi}\left[\left(\frac{\omega_c}{\omega_0}\right)^3 - 3\left(\frac{\omega_c}{\omega_0}\right)^2 + 3\left(\frac{\omega_c}{\omega_0}\right)\right]$$

The noise power N_0 from equation 9 is:

$$N_0 = \frac{T^2}{2\pi}\int_0^{\omega_c} K(\omega - \omega_0)^2\, \frac{\sin^2(\omega T/4)\, d\omega}{(\omega T/4)^2}$$

The noise power is then expanded into three integrals, I_1, I_2, I_3 such that

$$N_0 = I_1 + I_2 + I_3$$

where

$$I_1 = \left(\frac{KT^2}{2\pi}\right)\int_0^{\omega_c} \frac{\omega^2 \sin^2 \omega T/4}{(\omega T/4)^2}\, d\omega = \frac{32K}{\pi T}\int_0^{\omega_c T/4} \sin^2 dx$$

$$I_2 = -\left(\frac{KT^2}{2\pi}\right)\ 2\omega_0\int_0^{\omega_c} \frac{\omega \sin^2(\omega T/4)\, d\omega}{(\omega T/4)^2}$$

$$= -\frac{16K\omega_0}{\pi}\int_0^{\omega_c T/4} \frac{\sin^2 x\, dx}{x}$$

$$I_3 = \left(\frac{KT^2}{2\pi}\right)\ \omega_0^2\int_0^{\omega_c} \frac{\sin^2(\omega T/4)}{(\omega T/4)^2}\, d\omega$$

$$= \frac{2KT\omega_0^2}{\pi}\int_0^{\omega_c T/4} \frac{\sin^2 dx}{x^2}$$

Integrating by parts we obtain

$$I_1 = \frac{8K}{2}\left[\omega_c - \frac{2}{T}\sin \pi R\right]$$

$$I_2 = -\frac{K\omega_0}{\pi} \times 16 \times \frac{1}{2}\left[0.577 + \ln\left(\frac{\omega_c T}{2}\right) - C_i\left(\frac{\omega_c T}{2}\right)\right] \quad * \qquad (14)$$

$$I_3 = \frac{2K\omega_0^2 T}{\pi}\left[\frac{1 - \cos\left(\frac{\omega_c T}{2}\right)}{\omega_c T/2} + S_i\left(\frac{\omega_c T}{2}\right)\right]$$

where

$$C_i(x) = \int_\infty^x \left(\frac{\cos v}{v}\right) dv, \text{ and}$$

$$S_i(x) = \int_0^x \left(\frac{\sin v}{v}\right) dv.$$

These functions are tabulated.

The ratio N_0/N_1 becomes:

$$\frac{6T^2\left\{\frac{4(\omega_c/\omega_0)}{(\omega_0 T)^2} - \frac{8\sin \pi R}{(\omega_0 T)^3} - \frac{8}{(\omega_0 T)^2}\left[0.577 + \ln(\pi R) - C_i(\pi R)\right] + \frac{2}{\omega_0 T}\left[\frac{\cos \pi R - 1}{\pi R} + S_i(\pi R)\right]\right\}}{\left(\frac{\omega_c}{\omega_0}\right)^3 - 3\left(\frac{\omega_c}{\omega_0}\right)^2 + 3\left(\frac{\omega_c}{\omega_0}\right)} \qquad (15)$$

where

f_c = low-pass cut-off frequency (Hz),

f_b = bit rate (bits per second),

f_0 = local oscillator frequency (Hz), and

$T = \frac{1}{f_b}$ = bit duration (seconds).

---

* J. D. Krauss, "Antennas", McGraw-Hill, 1950, Page 144.

The peak signal (volts) at the integrator output at time T is

$$S_p = \frac{2A}{\pi} T$$

where A = peak amplitude of sinusoidal input voltage.

Combining equations 1 and 15, one obtains for Case II:

$$\frac{A^2}{N_1} = \left[\left(\frac{\pi}{2}\right)^2 \left(\frac{1}{T}\right)^2 \left(\frac{N_0}{N_1}\right)\right] \frac{S_p^2}{N_0} \qquad (16)$$

As an example, calculations have been performed for the following parameters:

f_b = 128 kb/sec,

$R = f_c/f_b = 1.4$,

f_0 = 355 kHz

For these parameters, the ratio N_0/N_1 becomes

$$\frac{N_0}{N_1} = \frac{6T^2\left[4\frac{\omega_c}{\omega_0} \times \frac{1}{(\omega_0 T)^2} - \frac{8}{(\omega_0 T)^3} \operatorname{Sin}(1.4\pi) - \frac{17.9}{(\omega_0 T)^2} + \frac{2.76}{\omega_0 T}\right]}{\left(\frac{\omega_c}{\omega_0}\right)^3 - 3\left(\frac{\omega_c}{\omega_0}\right)^2 + 3\left(\frac{\omega_c}{\omega_0}\right)} = 0.73\,T^2 \qquad (17)$$

This yields a degradation of 2.5 db, therefore

$$\left(\frac{A^2}{N_1}\right)_{db} = 2.5 \text{ db} + \left(\frac{S_p^2}{N_0}\right)_{db}$$

N_1 is measured in the bandwidth $f_c = 1.4\, f_b$.

Note: The numerical values of integrals I_2 and I_3 were also evaluated graphically for this special case and agree very closely with the values obtained from equations 14. This ascertains the correctness of the rather cumbersome analytical expression for N_0/N_1.

From Figure 6 for a probability of error $P_e = 1 \times 10^{-6}$, $\frac{S_p^2}{N_0} \approx 13.5$ db $\left(\frac{\text{peak}}{\text{rms}}\right)$

Therefore,

$$\left(\frac{A^2}{N_1}\right)_{db} = 16.0 \text{ db (peak/rms)} \tag{18}$$

I. CONCLUSIONS

Formulas have been given for the calculation of signal-to-noise ratio requirements to achieve a given probability of error for a biphase decoder of the reset-integrator type in the presence of Gaussian noise. Intersymbol interference is not included in the formulas; the amount of intersymbol interference will vary with the channel bandwidth and phase equalization, and also with the particular binary word used. The degradation introduced has to be determined for each particular case by computer simulation or some other means and the link SNR given by the derived formulas increased accordingly. The formulas are valid for channel bandwidths smaller than three times the bit rate when a periodic sequence of binary "1's" or "0's" yield a sinewave at the bit rate frequency.

APPENDIX A

SIGNAL-TO-NOISE RATIO AT A RESET INTEGRATOR

A reset integrator integrating over a time interval $(0,\gamma)$ has an impulse response h(t) given by

$$\begin{aligned} &h(t) = 0 \text{ for } t < 0 \\ &h(t) = 0 \text{ for } t > \gamma \\ &h(t) = 1 \text{ for } 0 \leq t \leq \gamma \end{aligned} \qquad \text{(A-1)}$$

If the noise into the integrator is denoted by n(t) and if this noise process is Gaussian and stationary, then the noise level at time $t = \gamma$ is a random variable $\hat{v}_1$ whose variance σ_1^2 is given by:

$$\sigma_1^2 = E\left[\hat{v}_1^2\right] = E\left[\int_0^\gamma n(t)dt \int_0^\gamma n(\alpha)d\alpha\right] \qquad \text{(A-2)}$$

where $E\left[\ \right]$ is the expected value of the variable.

The mean of $\hat{v}_1$ is assumed zero, therefore

$$\sigma_1^2 = \int_0^\gamma \int_0^\gamma E\left[n(t)\,n(\alpha)\right]dtd\alpha \qquad \text{(A-3)}$$

$$\sigma_1^2 = \int_0^\gamma \int_0^\gamma R_n(t,\alpha)\,dtd\alpha \qquad \text{(A-4)}$$

where $R_n(t,\alpha)$ is the auto-correlation function of the noise n(t). Since n(t) is stationary, then

$$R_n(t,\alpha) = R_n(t-\alpha) \qquad \text{(A-5)}$$

and

$$\sigma_1^2 = \int_0^\gamma \int_0^\gamma R_n(t-\alpha)\,dtd\alpha$$

$$\sigma_1^2 = \int_0^\gamma d\lambda \int_{-\lambda}^{\gamma-\lambda} R_n(v)dv \qquad \text{(A-6)}$$

$$\sigma_1^2 = \int_{-\infty}^{\infty} h(\lambda)d\lambda \int_{-\infty}^{\infty} h(v+\lambda)\,R_n(v)\,dv$$

where

$$t - \alpha = v, \text{ and}$$

$$t = \lambda$$

If $\psi_n(\omega)$ is the double-sided power spectral density (watts/Hz) of the input noise n(t), then by definition

$$R_n(v) = \frac{1}{2\pi} \int_{-\infty}^{\infty} \psi_n(\omega) e^{j\omega v} d\omega$$

$$\sigma^2 = \frac{1}{2\pi} \int\int\int h(\lambda)h(v + \lambda)\psi_n(\omega)e^{j\omega v} d\omega dv d\lambda \qquad (A-7)$$

$$\sigma^2 = \frac{1}{2\pi} \int\int\int h(\lambda)h(\theta)\psi_n(\omega)e^{j\omega\theta}e^{-j\omega\lambda} d\omega d\lambda d\theta$$

where $v + \lambda = \theta$. Therefore, the variance can be expressed as

$$\sigma^2 = \frac{1}{2\pi} \int_{-\infty}^{\infty} H(\omega)H(-\omega)\psi_n(\omega) d\omega \qquad (A-8)$$

$$\sigma^2 = \frac{1}{2\pi} \int_{-\infty}^{\infty} |H(\omega)|^2 \psi_n(\omega) d\omega \qquad (A-9)$$

APPENDIX B

CALCULATION OF CORRELATION FUNCTION FOR CASE I

In the analysis, the required SNR was calculated for the worst case situation where the correlation function ρ is unity. However, for a proper comparison with experimental data, the actual values of ρ must be calculated.

The correlation function ρ is defined as

$$\rho \triangleq \frac{E[\hat{v}_1 \hat{v}_2]}{\sigma^2} \tag{B-1}$$

For Case I where the noise density is $\psi_n(\omega) = \frac{k\omega^2}{2}$, we have

$$\rho = \frac{-\int_{-\omega_c}^{\omega_c} \omega^2 |H(\omega)|^2 \cos\left(\frac{\omega T}{2}\right) d\omega}{\int_{-\omega_c}^{\omega_c} \omega^2 |H(\omega)|^2 d\omega} \tag{B-2}$$

where

$$|H(\omega)|^2 = \frac{T^2}{4} \frac{\sin^2\left(\frac{\omega T}{4}\right)}{\left(\frac{\omega T}{4}\right)^2}$$

is the magnitude squared of the Fourier transform of the impulse response of the reset integrator. Therefore,

$$\rho = \frac{\frac{\omega_c}{2} + \frac{1}{2T} \sin \omega_c T - \frac{2}{T} \sin\left(\frac{\omega_c T}{2}\right)}{\omega_c - \frac{2}{T} \sin \frac{\omega_c T}{2}} \tag{B-3}$$

where $\omega_c = 2\pi f_c$ is the low-pass bandwidth for Case I (d.c. to f_c), and T is the bit duration. For the particular example considered $f_c = 1.1\ f_b$; $f_b = 120$ kb/sec; and $T = 1/f_b$.

Thus, for this example $\rho = 0.57$ and the noise power N_0 of equation 4 becomes

$$N_0 = 2(1 + \rho)\sigma^2 = 2 \times 1.57 \times \sigma^2$$

The actual required input SNR to the decoder for a given bit-error probability is smaller than the worst case SNR by the factor 1.57/2.0 or -1.0db.

DERIVATION OF EQUATIONS B-2 AND B-3

With n(t) the noise process into the decoder, we have:

$$\hat{v}_1 = \int_0^{T/2} n(t)dt$$

$$\hat{v}_2 = \int_{T/2}^{T} -n(t)dt$$

$$E[\hat{v}_1\hat{v}_2] = E\left[\int_0^{T/2} n(\alpha)d\alpha \int_{T/2}^{T} -n(\gamma)d\gamma\right] \quad \text{(B-4)}$$

$$= -\int_0^{T/2}\int_{T/2}^{T} R_n(\alpha-\gamma)\,d\alpha d\gamma \quad \text{(B-5)}$$

where $R_n(z)$ the auto-correlation function of n(t) and is

$$R_n(z) = \frac{1}{2\pi}\int_{-\infty}^{\infty} \psi_n(\omega)e^{j\omega z}\,d\omega \quad \text{(B-6)}$$

With $\gamma = \frac{T}{2} + \beta$, we have

$$E\left[\hat{v}_1\hat{v}_2\right] = -\int_0^{T/2}\int_0^{T/2} R_n\left(\alpha - \beta - \frac{T}{2}\right)d\alpha d\beta \quad \text{(B-7)}$$

$$E\left[\hat{v}_1\hat{v}_2\right] = -\frac{1}{2\pi}\int_{-\infty}^{\infty}\int_{-\infty}^{\infty}\int_{-\infty}^{\infty} h(\alpha)h(\beta)\psi_n(\omega)e^{j\omega\alpha}e^{-j\omega\beta}e^{-j\omega T/2}d\alpha d\beta d\omega \quad \text{(B-8)}$$

The function h(t) is the impulse response at T/2 of the reset integrator (see Figure 4). This function is unity between 0 and T/2 and has zero value outside. Equations B-7 and B-8 are identical. By using h(t), the limits of integration are extended to $-\infty$ and $+\infty$ for mathematical convenience. The value of the integral is, of course, unchanged.

The transfer function $H(\omega)$ is the Fourier transform of h(t), i.e.:

$$H(\omega) = \int_{-\infty}^{\infty} h(t)e^{-j\omega t}\,dt$$

Consequently

$$E\left[\hat{v}_1\hat{v}_2\right] = -\frac{1}{2\pi}\int_{-\infty}^{\infty}\psi_n(\omega)\left|H(\omega)\right|^2\cos\left(\omega\frac{T}{2}\right)d\omega \qquad \text{(B-9)}$$

Equation B-9 results from the fact that only the even (real) part of $e^{-j\omega T/2}$ contributes to the integral since integration is carried over symmetrical limits and since both $\psi_n(\omega)$ and $|H(\omega)|^2$ are even functions of ω.

The variance σ^2 is given by:

$$\sigma^2 = E\left[\hat{v}_1^2\right] = E\left[\hat{v}_2^2\right]$$

$$\sigma^2 = \frac{1}{2\pi}\int_{-\infty}^{\infty}\left|H(\omega)\right|^2\psi_n(\omega)d\omega$$

Consequently,

$$\rho = \frac{E\left[\hat{v}_1\hat{v}_2\right]}{\sigma^2} = \frac{\int_{-\infty}^{\infty}\psi_{n1}(\omega)\left|H(\omega)\right|^2\cos\frac{\omega T}{2}\,d\omega}{\int_{-\infty}^{\infty}\psi_n(\omega)\left|H(\omega)\right|^2 d\omega} \qquad \text{(B-10)}$$

Expression B-10 is completely general. For Case I, it reduces to equation B-2 given previously.